Development and applications of density matrix functional theory of generalized Hubbard Models

von
Herrn **Matthieu Saubanère**
aus Dax, France

Dissertation zur Erlangung des akademischen Grades
eines Doktors der Naturwissenschaften (Dr. rer. nat.)

vorgelegt dem Fachbereich Mathematik und Naturwissenschaften
der Universität Kassel

Betreuer:
Prof. Dr. G. M. Pastor

Disputation am 26. August 2011

Development and applications of density matrix functional theory of generalized Hubbard Models

by
Matthieu Saubanère
born in Dax, France

A Thesis submitted to the Department of Mathematics and Natural Sciences in partial fulfillment of the requirements for the degree Doctor of Natural Sciences (Dr. rer. nat.)

Theoretical physics institute
University of Kassel

supervised by
Prof. Dr. G. M. Pastor

Examination on 26$^{\text{th}}$ August 2011

Mais la vérité vous le savez, c'est ce qui simplifie le monde et non ce qui crée le chaos. La vérité, c'est le langage qui dégage l'universel. Newton n'a point "découvert" une loi longtemps dissimulée à la façon d'une solution de rébus, Newton a effectué une opération créatrice. Il a fondé un langage d'homme qui pût exprimer à la fois la chute de la pomme dans un pré ou l'ascension du soleil. La vérité, ce n'est point ce qui se démontre, c'est ce qui simplifie.

Antoine de Saint-Exupéry,
Terre des hommes, Éditions Gallimard, 1939

Abstract

In this Thesis, we develop and apply an accurate method to determine the ground-state properties of strongly-correlated electrons in the framework of lattice model Hamiltonians. In lattice density-functional theory (LDFT) the basic variable is the one-particle density matrix γ. From a generalized HK theorem, the ground state energy $E_{gs}[\gamma_{gs}] = \min_\gamma E[\gamma]$ is obtained by minimizing the energy-functional $E[\gamma]$ over all the physical or representable γ. The energy functional can be divided into two contributions: the kinetic-energy functional $T[\gamma]$, which linear dependence on γ is exactly known, and the correlation-energy functional $W[\gamma]$, which dependence on γ is not explicitly known. Finding accurate approximations for $W[\gamma]$ constitutes the actual challenge of this thesis. Part of this work is based on previous studies which derive an approximation of $W[\gamma]$ for the Hubbard Hamiltonian based on scaling hypothesis and an exact analytical results for the Hubbard dimer. However, this approach is limited to spin independent and homogeneous systems. In order to extend the scope of LDFT, we have developed three different approaches to derive $W[\gamma]$ in order to study broken symmetry problems. First we extend the previous scaling functional to system having charge transfer. By a systematic study of the dependence of $W[\gamma]$ on the charge distribution we find similar scaling properties as for the homogeneous case. An extension to the Hubbard model on bipartite lattices is then derived and applied to finite and infinite systems with repulsive and attractive interactions. The high accuracy of this functional is demonstrated. Nevertheless, this approach is difficult to transfer to more complex systems, since the calculation of $W[\gamma]$ applies to the system as a whole. To overcome this problem, we derive another approximation based on local scaling properties. This functional is formulated on-site so that it can be applied to any ordered or disordered Hamiltonian with on-site interaction. As applications we study the metal-insulator transition in the ionic Hubbard model in one- and two-dimensions, as well as the one-dimensional Hubbard chain with first and second nearest neighbor hoppings. Finally, we develop a numerical approach of $W[\gamma]$, on the basis on exact diagonalizations of an effective many-body Hamiltonian corresponding to a cluster surrounded by an effective medium. This effective Hamiltonian depends on the density matrix γ and allows to derive approximation to $W[\gamma]$ which improve systematically with increasing cluster size. The formulation is spin-dependent and allows a straightforward generalization to multi-orbital correlated systems such *spd*-Hamiltonians. In addition it take into account the effects of short-range charge and spin fluctuations in the functional. The accuracy of the method is demonstrated for the Hubbard model by comparison with the Bethe-*Ansatz* solution (1D) and quantum Monte Carlo simulations (2D). Finally, an outlook or relevant future developments of the theory is provided.

Abstrakt

In dieser Doktorarbeit wird eine akkurate Methode zur Bestimmung von Grundzustandseigenschaften stark korrelierter Elektronen im Rahmen von Gittermodellen entwickelt und angewandt. In der Dichtematrix-Funktional-Theorie (LDFT, vom englischen *lattice density functional theory*) ist die Ein-Teilchen-Dichtematrix γ die fundamentale Variable. Auf der Basis eines verallgemeinerten Hohenberg-Kohn-Theorems ergibt sich die Grundzustandsenergie $E_{gs}[\gamma_{gs}] = \min_\gamma E[\gamma]$ durch die Minimierung des Energiefunktionals $E[\gamma]$ bezüglich aller physikalischer bzw. repräsentativer γ. Das Energiefunktional kann in zwei Beiträge aufgeteilt werden: Das Funktional der kinetischen Energie $T[\gamma]$, dessen lineare Abhängigkeit von γ genau bekannt ist, und das Funktional der Korrelationsenergie $W[\gamma]$, dessen Abhängigkeit von γ nicht explizit bekannt ist. Das Auffinden präziser Näherungen für $W[\gamma]$ stellt die tatsächliche Herausforderung dieser These dar. Einem Teil dieser Arbeit liegen vorausgegangene Studien zu Grunde, in denen eine Näherung des Funktionals $W[\gamma]$ für das Hubbardmodell, basierend auf Skalierungshypothesen und exakten analytischen Ergebnissen für das Dimer, hergeleitet wird. Jedoch ist dieser Ansatz begrenzt auf spin-unabhängige und homogene Systeme. Um den Anwendungsbereich von LDFT zu erweitern, entwickeln wir drei verschiedene Ansätze zur Herleitung von $W[\gamma]$, die das Studium von Systemen mit gebrochener Symmetrie ermöglichen. Zuerst wird das bisherige Skalierungsfunktional erweitert auf Systeme mit Ladungstransfer. Eine systematische Untersuchung der Abhängigkeit des Funktionals $W[\gamma]$ von der Ladungsverteilung ergibt ähnliche Skalierungseigenschaften wie für den homogenen Fall. Daraufhin wird eine Erweiterung auf das Hubbardmodell auf bipartiten Gittern hergeleitet und an sowohl endlichen als auch unendlichen Systemen mit repulsiver und attraktiver Wechselwirkung angewandt. Die hohe Genauigkeit dieses Funktionals wird aufgezeigt. Es erweist sich jedoch als schwierig, diesen Ansatz auf komplexere Systeme zu übertragen, da bei der Berechnung von $W[\gamma]$ das System als ganzes betrachtet wird. Um dieses Problem zu bewältigen, leiten wir eine weitere Näherung basierend auf lokalen Skalierungseigenschaften her. Dieses Funktional ist lokal bezüglich der Gitterplätze formuliert und ist daher anwendbar auf jede Art von geordneten oder ungeordneten Hamiltonoperatoren mit lokalen Wechselwirkungen. Als Anwendungen untersuchen wir den Metall-Isolator-Übergang sowohl im ionischen Hubbardmodell in einer und zwei Dimensionen als auch in eindimensionalen Hubbardketten mit nächsten und übernächsten Nachbarn. Schließlich entwickeln wir ein numerisches Verfahren zur Berechnung von $W[\gamma]$, basierend auf exakten Diagonalisierungen eines effektiven Vielteilchen-Hamilton-Operators, welcher einen von einem effektiven Medium umgebenen Cluster beschreibt. Dieser effektive Hamiltonoperator hängt von der Dichtematrix γ ab und erlaubt die Herleitung von Näherungen an $W[\gamma]$, dessen Qualität sich systematisch mit steigender Clustergröße verbessert. Die Formulierung ist spinabhängig und ermöglicht eine direkte Verallgemeinerung auf korrelierte Systeme mit mehreren Orbitalen, wie zum Beispiel auf den spd-Hamilton-Operator. Darüber hinaus berücksichtigt sie die Effekte kurzreichweitiger Ladungs- und Spinfluktuationen in dem Funktional. Für das Hubbardmodell wird die Genauigkeit der Methode durch Vergleich mit Bethe-Ansatz-Resultaten (1D) und Quanten-Monte-Carlo-Simulationen (2D) veranschaulicht. Zum Abschluss wird ein Ausblick auf relevante zukünftige Entwicklungen dieser Theorie gegeben.

Acknowledgments

First of all, I would like to thank my supervisor Prof. Dr. G. M. Pastor whose patience and help were very important during this work. I would not have achieve this thesis without his stimulating suggestions and encouragements.

Many thanks to Prof. Dr. Martin E. Garcia to accept to evaluate this manuscript in a very short time.

Special thanks to Prof. Dr. Harald O. Jeschke for his careful review of the manuscript.

I am grateful to Dr. M. B. Lepetit for my stay in Caen where I have learned the DMRG method.

I wish acknowlwdge Dr. J. L. Chávez, for teaching me the *ab-initio* code VASP and the fruitful collaboration on magnetic impurity in a one-dimentional metallic host.

I would like to express my gratitude to Prof. Dr. J. Dorantes for his valuable criticism and suggestions I got during the year he has spend at the university of Kassel.

Special thanks to Mouna Kebede, Lucila Juárez, Dr. Pedro Ruiz, Dr. Giulia Gualdi, for their essential help correcting my English and Waldemar Töws for the German translation of the abstract.

I am thankful to the Theoretical Physics members, and in particular the ones belonging to the Prof. Pastor's group, for the atmosphere and all the interesting conversations. Special thanks for Dr. Luis Díaz, Dr. Pedro Ruiz, and Lucila Juárez. Thanks also to the secretary Katarina Schmidt and Andrea Weacker for their great help solving any situation.

I would like to thank also the University of Kassel and the I.T. Service Zentrum for the computer facilities.

Many thank to all my former flatmate which have make me discover Kassel and Germany and to all my other friends in France.

Finally, I am grateful to my parents, my sister and Ela for their love and support.

Contents

Chapter 1

Introduction

State of the art condensed matter electronic theories are mostly based on two complementary approaches. One of them is density functional theory (DFT) [1] which replaces the wave function, which characterizes a quantum mechanical state completely, by the electronic density $\rho(\overrightarrow{r})$ as the fundamental variable of the many-body problem. In particular, the energy E of any electronic system is expressed as a functional of $\rho(\overrightarrow{r})$ by splitting it in two different terms. The first one depends explicitly on the system under study through the external potential $V_{\text{ext}}(\overrightarrow{r})$ acting on the electrons. This typically involves the ion-electron interaction and any other external fields. The second type of contributions describes intrinsic properties of the electronic system, namely, the kinetic energy $T[\rho]$ and the interaction energy $W[\rho]$. These are universal functionals of $\rho(\overrightarrow{r})$ in the sense that they are independent of the considered external potential describing a given specific system. The ground-state properties can then be found by implementing a variational procedure with respect to $\rho(\overrightarrow{r})$, for example, as in the Kohn-Sham scheme [2]. It is important to remark that in order to use DFT, one needs explicit forms of these two universal functionals. Since the beginning of DFT large number of studies have been devoted to deriving approximations for the challenging $T[\rho]$ and $W[\rho]$. In particular one should mention the local density approximation (LDA), [2] which is the simplest and probably most successful approximation and which takes the homogeneous electron gas as reference system. Further improvements have been done by considering, for example, the dependence of T and W on the gradient of the density. Nowadays many functionals of different types are available [3, 4, 5]. The most important of these approaches is the generalized gradient approximation (GGA) [6].
The DFT formulation is of general validity and has been successfully applied to a great variety of physical problems, well-beyond the initial scope of the inhomogeneous electrons gas. For example, it can be applied to obtain properties of atoms, molecules, periodic systems, metallic alloys, etc [3, 4, 7]. Among the consider properties one can mention the ground-state energy, spin and orbital moments, binding energy, phonon frequencies, magnetic anisotropies energy, etc. Nevertheless, it is also well known that the usual LDA and GGA approximations to the exchange and correlation energy-functional $E_{XC} = W+T-T_0$, which take into account all the correlation effects including the ones on the kinetic energy $T - T_0$ where T_0 is the kinetic energy of a non-correlated system, fail systematically to describe systems showing strong electron correlations in narrow bands [8, 9, 10, 11, 12, 13]. This is the case, for example, of problems involving a separation of charge and spin de-

grees of freedom, or the ones showing correlation-induced localizations [14, 15]. For the improvement of this theory, it is therefore important to understand the reasons behind these drawbacks. Among the prenomen of current interest one should stress the importance of the separation of charge and spin degrees of freedom and the development of insulating gap due to strong interaction, in order to extend its applicability, to more complex strongly interacting systems.

The second main approach to condensed matter electronic theory is based on many-body model Hamiltonians. In order to study more complex phenomena, such as strong electronic correlations, it is compulsory to reduce the number of degree of freedom. Notice that strong electronic correlations generate many interesting and important effects in condensed mater. Let us recall for example, magnetism, superconductivity, Mott insulators, mixed valence systems, topological effects, etc. which detailed understanding still remain a challenge. One of the most common and simple models to study these systems is the Hubbard model [16] which describes the interplay between electronic delocalization, charge redistribution and electronic correlations. From this model one can also derive, in the limit of strong correlations, spin Hamiltonians like Heisenberg or tJ models. In addition, from the Hubbard models related Hamiltonians is is possible to describe the effects of magnetic a impurity as the Anderson model and Kondo models [17]. In the past fifty years, an enormous research effort has been done to develop methods, both numerical and analytical, for solving these models and for understanding the rich variety of effects generated by the Coulomb interactions. However, there are few known exact results as the Bethe-*Ansatz* for the one-dimensional Hubbard chain [18], the Nagaoka theorem [19] for systems close to band filling at the atomic limit and the Lieb theorem [20] on the nature of the ground state for bipartite lattice at half-band filling. Another way to approach the solution to the Hubbard model is based on perturbation theory, such as the so called Hubbard I approximation [16], or the cluster perturbation theory [21]. Many mean-field approximations have also been developed, for example, the saddle-point slave boson theory [22] or the dynamical mean field theory (DMFT) [23]. Some accurate through very demanding numerical methods are also available, as for instance, the density matrix renormalization group (DMRG) method [24] for one-dimensional (1D) systems and quantum Monte Carlo (QMC) method [25].

Taking into account that only few studies have been done to render DFT applicable in the study of strongly correlated systems, as for instance the LDA+U [26] or LDA+DMFT [27] which combine *ab-initio* DFT calculations for the electronic structure with many-body technique to compute the correlation-energy functional. Therefore, the development of DFT for lattice models Hamiltonians is challenging for both sides. On one side, for density functional theory, which fails when electrons are strongly correlated, it would allow to extend its applicability to strongly correlated systems. In addition, the information inferred from DFT studies of lattice Hamiltonians could also provide new insights on the properties of the universal kinetic- and interaction-energy functionals and thus improve functionals used in *ab-initio* DFT codes. This would be helpful in order to improve methods as LDA+U or LDA+DMFT. On the other side, since DFT has an universal validity, it possible to apply it to model Hamiltonians. These new perspectives give us the opportunity to develop a new strategy to study systems involving strongly correlated electrons.

Recently, the application of DFT to lattice models was developed and applied to several strongly correlated systems yielding interesting results. For example, one can mention

the determination of band gaps in semiconductors [28], the study of the role of off-diagonal elements of the density matrix and the non-interacting v-representability in strongly correlated systems [29], and the development of energy functionals of the density matrix with applications to the Hubbard and Anderson models [30]. More recently, an exchange and correlation energy-functional of the site occupations has been derived on the basis of the Bethe-*Ansatz* to the one-dimensional (1D) Hubbard model [31]. Moreover, time dependent effects have also been investigated [32].
It is also in this context, that lattice density functional theory (LDFT) have been introduced, at the beginning of the new millennium [33, 34, 35]. One of the originalities of this approach relies on the use of the single-particle density matrix (SPDM) as the fundamental variable, instead of considering only the electronic density as in conventional DFT. This choice is motivated by the fact that for the lattice models it is the hopping term in the Hamiltonian (connectivity matrix) and the energy levels at each site (diagonal level) which determine the system under study: 1D, 2D, or 3D lattice, homogeneous or inhomogeneous system, magnetic field, etc. In addition, the energy associated to these single particle contribution is the convolution between the hopping and energy level matrix and the SPDM. Consequently, the SPDM imposes itself as the relevant variable to develop a DFT for model Hamiltonians. This can be also justified by the fact that non-correlated states and strongly correlated states often have the same charge distribution n_i (for example, homogeneous systems). Thus considering only electronic density is insufficient to characterize the system. In general, previous studies show that by considering only the local occupation n_i as variable yields to interaction functionals which depend non-linearly on the Coulomb and on the hopping integrals [31]. This is in contradiction with known general results such as the Levy and Lieb formulation of DFT, which implies that the correlation-energy functional depends linearly on the Coulomb integral and does not depend on the hopping integral.
As in the case of conventional DFT, the variational principle and the one-to-one correspondence theorem (generalization of Hohenberg-Kohn theorem for LDFT) are used to determine the ground-state energy and SPDM. In LDFT the dependence of one particle contribution on the SPDM is straightforward. The main challenge consists in having an explicit approximation of the correlation-energy functional (CEF).
Several systematic studies of the CEF for the homogeneous Hubbard models. It has been shown that W can be appropriately scaled as a function of $g_{12} = (\gamma_{12} - \gamma_{12}^{\infty})/(\gamma_{12}^{0} - \gamma_{12}^{\infty})$, where γ_{12}^{0} (γ_{12}^{∞}) refers to the limit of weak (strong) electronic correlations. In other words, the change in W associated to a given change in the degree of the NN charge transfer and electron delocalization can be regarded as nearly independent of the system under study [33, 34]). Consequently, an approximation of the CEF was introduced by taking as a reference the simple and analytical case (the Hubbard Dimer) and using the scaling properties with respect to the $v-$representability. Using this approximation, the model was applied to several homogeneous systems [33, 35, 36, 37]. All these studies have shown the relevance of this approach and, in particular obtain accurate results for ground states properties performing very simple analytic calculations. In addition, in a previous works, a new functional was derived in the context of LDFT for the Anderson impurity model [38]. An important limitation of these studies, refers to the non-local formulation of the CEF which excludes any problem involving symmetry-breaking (non-periodic clusters, charge density waves (CDWs), spin waves, inhomogeneities in general) in the range of applicability of LDFT. Theses problems play a major role in physics. For example, nano-particles

and in particular, magnetic nano-particles are one of the most challenging research subjects nowadays. Moreover, strong correlations can also be important in this subject and they could be studied in the framework of geometrically inhomogeneous Hubbard clusters [39]. Inhomogeneous potentials, can also drive the formation of CDWs, resulting in some exotic phase diagrams, for example, the metallic phase due to the interplay between the ionic potential and the Coulomb-interaction in the 2D square lattice ionic Hubbard model [40]. Inhomogeneity is also predominant to drive superconductivity in attractive Hubbard model, in particular in cuprates [41].
It is the goal of this thesis to extend the scope of LDFT, to problems where inhomogeneous chare distribution is important. In this work, we study systematically the dependence of the CEF of the charge distribution by numerical Lanczos diagonalization [42] in inhomogeneous periodic clusters. From this study, we derive further approximations for the correlation energy functional, which extend the scaling behavior already observed in the homogeneous case [34]. Moreover, we also focus on obtaining a local or on-site formulation of the CEF. Local formulations of a CEF provide a real advantages in order to study inhomogeneous systems, since they should be particularity easy to transfer to any on-site correlated systems. This implies, that the environment of a site is considered as a field parameter by the density-matrix. Finally, in order to formulate a more general and potentially more accurate approach we have developed a numerical method to approximate $W[\gamma]$. It involves the exact diagonalization of an effective many-body Hamiltonian of a cluster surrounded by an effective field. This effective Hamiltonian depends on the density matrix γ. We show in the case of the Hubbard model that this method increases systematically the accuracies of ground states properties (about 0.5% relative error on ground states energy for a nine sites cluster). By using a real space expansion, this method take into account short-range charge and spin fluctuations, which are playing a major role at the strongly correlated limit. This method is spin-dependent so that it can by applyed directly to spin polarized systems. In addition, it is possible to extend it straightforwardly to system having inter-site correlation. This provide an important step in order to study multi-band Hamiltonian which are compulsary in order to study reallistic systems, in particular those having $3d$- or $4f$-elements.

This thesis is organized as follows. In the first part, we briefly present the theoretical background. The chapter 2 is devoted to review the Hohenberg-Kohn-Sham DFT in the continuum. Chapter 3 presents the Hubbard model, its origin, some known exact results, simple mean field approximations, and related models. We also point out at the end of chapter 3 the possibility of using the Hubbard model within an attractive interaction. The chapter 4 focus on presenting the concept of density functional theory on a lattice. The second part focus on the dependence of the CEF on charge distribution and on methods to approximate it. The chapter 5 study systematically the properties of the CEF using numerical exact diagonalization. From the scaling properties, we derive a first approximation for the interaction energy for bipartite Hamiltonians. We apply this new formulation to finite size systems, as well as for the attractive Hubbard model. Our results are then compared with exact Lanczos diagonalization (cluster), Bethe-*Ansatz* and DMRG (one-dimensional systems). In chapter 6 we derive a local formulation of the correlation-energy functional and apply it to study the metal-insulator transition (band-insulator and Mott-insulator) in inhomogeneous systems and in the one-dimensional chain with next nearest neighbors. Finally, in Chapter 7 we develop the cluster expansion and prove that for the Hubbard model the accuracy is increased remarkably. Finally, we summarize

the conclusions of this work and point out its challenging perspectives conserning further development of LDFT.

Chapter 2

Fundamentals on density functional theory

Density functional theory (DFT) is one of the most popular and successful quantum mechanical approaches to condensed matter systems. Nowadays, it is routinely applied for calculating properties (e.g., binding energy in molecules, band structures of solids, magnetic moments in nanoparticles, etc.) with very good agreement with experiments. Moreover, there exist many different *ab-initio* DFT implemented codes in the market solving the Kohn-Sham equations with diverse characteristics (for example, by using the projector augmented wave (PAW) as the Vienna ab-initio simulation package (VASP), using Green's function (GF) methods like the GF Korringa Kohn and Rostoker (KKR) method, etc...). Historically, the first theory replacing the wave function $|\Psi\rangle$ by the electronic density $\rho(\vec{r})$ was developed in the 20's by Thomas and Fermi (TF) [43, 44]. The TF theory has been rapidly abandoned as soon as one could show, short after its formulation and application to atoms, that it could describe no molecular bonding. Until 1964, the density functional (DF) approach was not used very intensively and was more considered as model or approximation. From this perspective, the most important method is the Slater approach $X\alpha$ which was intend to simplify the cumbersome exchange interaction on Hartree-Fock (HF) calculations by a phenomenological functional depending on the local density. The situation changed drastically in 1964 with a publication by Hohenberg and Kohn (HK) [1]. In this paper, the authors proved two fundamental theorems establishing that for the ground-state energy, the Thomas-Fermi model can be consider as an approximation of an exact theory, the density functional theory. This so called HK theorem, proves the existence of a functional relation between the ground state energy $E_{\rm gs}[\rho(\vec{r})]$ and the electronic density $\rho(\vec{r})$. In addition, one can use the variational principle to determine $E_{\rm gs}$ and $\rho(\vec{r})$. However, DFT becomes really practical when it is formulated as an effective single-body theory, a breakthrough achieved by Kohn and Sham (KS) [2]. In KS theory, the problem is reduced to the solution of a one-particle electronic problem within an effective potential that is also a functional of the density. In this chapter, we present, first of all, DFT in its original version using the HK theorems but also a more modern version derived by Levy and Lieb [45]. In section 2.2 we present the Kohn-Sham scheme together with a simple but really successful approximation to the correlation-energy functional, the famous local density approximation (LDA).

2.1 DFT as a many-body theory

In this section we present the foundations of DFT in its original version by HK and a more general one following the Levy and Lieb procedure. These are central properties since they prove the validity of the theory, and its universality.

2.1.1 The Hohenberg-Kohn theorems

We start from the Schrödinger equation for a system of N interacting fermions in the Born-Oppenheimer approximation. The electronic Hamiltonian reads

$$\begin{aligned}\hat{H} &= \frac{-\hbar^2}{2m}\sum_{\sigma}\int d\vec{r}\,\hat{\psi}^{\dagger}_{\sigma}(\vec{r})\,\nabla^2\,\hat{\psi}_{\sigma}(\vec{r}) + \sum_{\sigma}\int d\vec{r}\,\hat{\psi}^{\dagger}_{\sigma}(\vec{r})\,V_{\text{ext}}(\vec{r})\,\hat{\psi}_{\sigma}(\vec{r}) \\ &\quad + \frac{1}{2}\sum_{\sigma,\sigma'}\int d\vec{r}\,d\vec{r'}\,\hat{\psi}^{\dagger}_{\sigma}(\vec{r})\,\hat{\psi}^{\dagger}_{\sigma'}(\vec{r'})\,w(\vec{r},\vec{r'})\,\hat{\psi}_{\sigma'}(\vec{r'})\,\hat{\psi}_{\sigma}(\vec{r}),\end{aligned} \tag{2.1}$$

where $\hat{\psi}^{\dagger}_{\sigma}$ ($\hat{\psi}_{\sigma}$) is a creation (annihilation) operator of a fermion with spin σ. These operators respect the Pauli principle by satisfying the anti-commutation law $\{\hat{\psi}^{\dagger}_{\sigma}(\vec{r}),\hat{\psi}_{\sigma'}(\vec{r'})\} = \delta(\vec{r}-\vec{r'})\delta_{\sigma,\sigma'}$. $V_{\text{ext}}(\vec{r})$ is a one-particle external potential describing the ionic potentials where the electrons are moving and/or any other external fields. Finally, $w(\vec{r},\vec{r'})$ is the electron-electron interaction (Coulomb repulsion, for example), which is independent of the specific system under study. Following the presentation of Dreizler and Gross [4], we define $\mathbf{V}$ as the ensemble of all local one-particle potentials such that $|\Psi_{\text{gs}}\rangle$ is the *non degenerate* ground-state of the eigenvalue problem

$$\begin{aligned}\hat{H}|\Psi\rangle = (\hat{T}+\hat{V}_{\text{ext}}+\hat{W})|\Psi\rangle = E|\Psi\rangle \\ \hat{H}|\Psi_{\text{gs}}\rangle = E_{\text{gs}}|\Psi_{\text{gs}}\rangle,\end{aligned} \tag{2.2}$$

with $\hat{V}_{\text{ext}} \in \mathbf{V}$. Defining by $\mathbf{\Psi}$ the ensemble of states $|\Psi_{\text{gs}}\rangle$, we can stablish a transformation between the ensemble of external potentials $\mathbf{V}$ and the ensemble of N-particle wave functions $\mathbf{\Psi}$ as

$$C : \mathbf{V} \longrightarrow \mathbf{\Psi}. \tag{2.3}$$

By construction, this transformation is surjective. In other words, each element of $\mathbf{\Psi}$ is mapped to at least one element of $\mathbf{V}$.
For all wave functions in $\mathbf{\Psi}$ we can compute the associated density

$$\rho(\vec{r}) = \langle\Psi|\sum_{\sigma}\hat{\psi}^{\dagger}_{\sigma}(\vec{r})\,\hat{\psi}_{\sigma}(\vec{r})|\Psi\rangle = N\sum_{\sigma}\int d\vec{x}_2 ... \int d\vec{x}_N |\Psi(\vec{r}\sigma,\vec{x}_2 ... \vec{x}_N)|^2, \tag{2.4}$$

where $\vec{x}_i = (\vec{r}_i,\sigma_i)$ refers to position and spin coordinates. If we now call $\mathbf{N}$ the ensemble of all densities derived from a non degenerate ground state, we can define another transformation

$$D : \mathbf{\Psi} \longrightarrow \mathbf{N}. \tag{2.5}$$

We are interested in establishing the inverse transformation of C and D. Assuming this inversion is possible, the knowledge of C^{-1} would allow us to know from a N-particle wave

function $|\Psi\rangle \in \mathbf{\Psi}$ the *unique* potential $\hat{V}_{\text{ext}} \in \mathbf{V}$ associated to $|\Psi\rangle$ and consequently the full Hamiltonian. On the other hand the knowledge of D^{-1} would establish the correspondence between a given electronic density $\rho(\vec{r}) \in \mathbf{N}$ and the associated ground-state wave function $|\Psi\rangle$. The combination $C^{-1}D^{-1}$ would associate directly an external potential $\hat{V}_{\text{ext}}$ to the electronic density of the ground state $\rho(\vec{r})$. In other words, if C^{-1} and D^{-1} exist, the ground-state energy of the Hamiltonian can be directly obtained as a functional of the electronic density.
We establish now the existence of the inverse of C and D. This is equivalent to proving that the transformation between $\mathbf{V}$ and $\mathbf{\Psi}$ is bijective. We focus first on the transformation C and show that two potentials $\hat{V}_{\text{ext}}$ and $\hat{V}'_{\text{ext}} \in \mathbf{V}$ yield two different ground states $|\Psi\rangle$ and $|\Psi'\rangle$, as soon as the $\hat{V}_{\text{ext}}$ and $\hat{V}'_{\text{ext}}$ differ by more than a constant [$\hat{V}_{\text{ext}}(\vec{r}) - \hat{V}'_{\text{ext}}(\vec{r}) \neq const.$].
From the Schrödinger equation, we have

$$\begin{aligned}(\hat{T} + \hat{W} + \hat{V}_{\text{ext}})|\Psi_{\text{gs}}\rangle &= E_{\text{gs}}|\Psi_{\text{gs}}\rangle \quad \text{and} \\ (\hat{T} + \hat{W} + \hat{V}'_{\text{ext}})|\Psi'_{\text{gs}}\rangle &= E'_{\text{gs}}|\Psi'_{\text{gs}}\rangle \end{aligned} \tag{2.6}$$

We follow the proof by reductio ad absurdum. Supposing that $|\Psi_{\text{gs}}\rangle = |\Psi'_{\text{gs}}\rangle$, then it follows that

$$(\hat{V}_{\text{ext}} - \hat{V}'_{\text{ext}})|\Psi_{\text{gs}}\rangle = (E_{\text{gs}} - E'_{\text{gs}})|\Psi_{\text{gs}}\rangle. \tag{2.7}$$

Since $\Psi(\vec{r}) = \langle\vec{r}|\Psi\rangle$ cannot be zero in a domain of finite measure and $V_{\text{ext}}(\vec{r})$ and $V'_{\text{ext}}(\vec{r})$ are well behaved it follows that $\hat{V}_{\text{ext}}(\vec{r}) - \hat{V}'_{\text{ext}}(\vec{r}) = (E_{\text{gs}} - E'_{\text{gs}}) \ \ \forall \vec{r} \in \mathbb{R}^3$, in contradiction with $\hat{V}_{\text{ext}}(\vec{r}) - \hat{V}'_{\text{ext}}(\vec{r}) \neq const.$ Consequently $|\Psi_{\text{gs}}\rangle \neq |\Psi'_{\text{gs}}\rangle$ if $\hat{V}_{\text{ext}} - \hat{V}'_{\text{ext}} \neq const$, showing that C is a bijection between $\mathbf{V}$ and $\mathbf{\Psi}$, implying the existence of C^{-1}.
We now consider the transformation D and show that if $|\Psi_{\text{gs}}\rangle \neq |\Psi'_{\text{gs}}\rangle$ then $\rho(\vec{r}) \neq \rho(\vec{r'})$. On one hand, from the Rayleigh-Ritz variational principle for $|\Psi_{\text{gs}}\rangle \neq |\Psi'_{\text{gs}}\rangle$ and $|\Psi_{\text{gs}}\rangle$ non-degenerate, we obtain

$$E_{\text{gs}} = \langle\Psi_{\text{gs}}|\hat{H}|\Psi_{\text{gs}}\rangle < \langle\Psi'_{\text{gs}}|\hat{H}|\Psi'_{\text{gs}}\rangle. \tag{2.8}$$

Moreover, we have

$$\begin{aligned}\langle\Psi'_{\text{gs}}|\hat{H}|\Psi'_{\text{gs}}\rangle &= \langle\Psi'_{\text{gs}}|(\hat{T} + \hat{W} + \hat{V}'_{\text{ext}} + \hat{V}_{\text{ext}} - \hat{V}'_{\text{ext}})|\Psi'_{\text{gs}}\rangle \\ &= E'_{\text{gs}} + \int d\vec{r}\, \rho'_{\text{gs}}(\vec{r})[v(\vec{r}) - v'(\vec{r})], \end{aligned} \tag{2.9}$$

where $\hat{V}_{\text{ext}} = \sum_{i=1}^{N} v_i(\vec{r}_i)$. Replacing Eq. (2.9) in Eq. (2.8) one obtains

$$E_{\text{gs}} < E'_{\text{gs}} + \int d\vec{r}\, \rho'_{\text{gs}}(\vec{r})[v(\vec{r}) - v'(\vec{r})]. \tag{2.10}$$

The same operation can be done beginning with $|\Psi'_{\text{gs}}\rangle$, i.e., replacing $|\Psi\rangle$ by $|\Psi'\rangle$. This leads to

$$E'_{\text{gs}} < E_{\text{gs}} + \int d\vec{r}\, \rho(\vec{r})[v'(\vec{r}) - v(\vec{r})]. \tag{2.11}$$

We use again a proof by reductio ad absurdum and we suppose that $\rho_{\text{gs}}(\vec{r}) = \rho'_{\text{gs}}(\vec{r})$ leading to the contradiction

$$E_{\text{gs}} + E'_{\text{gs}} < E_{\text{gs}} + E'_{\text{gs}}. \tag{2.12}$$

We conclude that D is a bijection, so that D^{-1} exists. Note that the rather restrictive assumption of non-degenerate ground-state is essential for the present proof. However, an extension to degenerate ground-state is available [3, 4]
The existence of C^{-1} and D^{-1} and the fact that they are bijective imply that to any electronic density $\rho(\vec{r})$ corresponds a unique ground-state wave function $|\Psi_{\rm gs}\rangle$. This leads to the HK theorems

HK theorem 1: *The ground-state expectation value of any observable $\hat{\mathcal{O}}$ is a unique functional of the exact ground-state density:*

$$\langle\Psi_{\rm gs}[\rho_{\rm gs}(\vec{r})]|\hat{\mathcal{O}}|\Psi_{\rm gs}[\rho_{\rm gs}(\vec{r})]\rangle = \mathcal{O}[\rho_{\rm gs}(\vec{r})]. \tag{2.13}$$

Proof: The full inverse map $C^{-1}D^{-1} : \rho_{\rm gs}(\vec{r}) \rightarrow v(\vec{r})$ tells us that in the case of a non-degenerate ground state, the knowledge of the ground-state density determines the external potential of the system besides an irrelevant constant. Thus the entire Hamiltonian is a functional of $\rho(\vec{r})$ since the kinetic and interaction energies are operators that are system independent.

HK theorem 2: *It establishes the variational character of the energy functional*

$$E_{\hat{V}_{\rm ext}}[\rho(\vec{r})] = \langle\Psi[\rho(\vec{r})]|\hat{T} + \hat{V}_{\rm ext} + \hat{W}|\Psi[\rho(\vec{r})]\rangle, \tag{2.14}$$

where $\hat{V}_{\rm ext}$ is the external potential of the system.
Proof: The states $|\Psi[\rho(\vec{r})]\rangle$ are generated via D^{-1} from the elements of $\mathbf{N}$ and from the variational principle

$$E_{\rm gs} < \langle\Psi[\rho(\vec{r})]|\hat{T} + \hat{V}_{\rm ext} + \hat{W}|\Psi[\rho(\vec{r})]\rangle = E_{\hat{V}_{\rm ext}}[\rho(\vec{r})]. \tag{2.15}$$

In other words, $E_{\hat{V}_{\rm ext}}[\rho(\vec{r})]$ is larger that $E_{\rm gs}$ if $\rho(\vec{r}) \neq \rho_{\rm gs}(\vec{r})$. Moreover, since D^{-1} is bijective we have

$$E_{\rm gs} = \langle\Psi_{\rm gs}[\rho_{\rm gs}(\vec{r})]|\hat{T} + \hat{V}_{\rm ext} + \hat{W}|\Psi_{\rm gs}[\rho_{\rm gs}(\vec{r})]\rangle = E_{\hat{V}_{\rm ext}}[\rho_{\rm gs}(\vec{r})]. \tag{2.16}$$

This proves the variational character of the functional $E_{\hat{V}_{\rm ext}}[\rho(\vec{r})]$.

2.1.2 Consequences of HK theorems and representability issues

Now that we have enunciated and proved the HK theorems we discuss their consequences as well as some issues related to the representability of electronic densities. These are the conditions for a density $\rho(\vec{r})$ to be included in $\mathbf{N}$.
A straightforward important consequence of the HK theorems is that the ground-state density $\rho_{\rm ext}(\vec{r})$ can be determined by the minimization of the functional $E_{\hat{V}_{\rm ext}}[\rho(\vec{r})]$:

$$E_{\rm gs} = \min_{\rho(\vec{r})\in\mathbf{N}} E_{\hat{V}_{\rm ext}}[\rho(\vec{r})] \tag{2.17}$$

Since D^{-1} does not depend on the external potential $\hat{V}_{\rm ext}$, we can rewrite the energy functional as

$$E_{\hat{V}_{\rm ext}}[\rho(\vec{r})] = F_{\rm HK}[\rho(\vec{r})] + \int d\vec{r}\, v_{\rm ext}(\vec{r})\rho(\vec{r}) \tag{2.18}$$

where we have introduced the Hohenberg and Kohn functional

$$F_{\mathrm{HK}}[\rho(\vec{r})] = \langle \Psi[\rho(\vec{r})] | \hat{T} + \hat{W} | \Psi[\rho(\vec{r})] \rangle. \tag{2.19}$$

Note that $F_{\mathrm{HK}}[\rho(\vec{r})]$ does not depend on the external potential. Therefore, it is a universal functional for every system. However, $F_{\mathrm{HK}}[\rho(\vec{r})]$ depends on the number of fermions in the system, on their mass, charge, and form of their interaction $\hat{W}$. Notice that the HK functional is defined only for densities belonging to **N**. In other words, for a density obtained from a non-degenerate ground state corresponding to some physical (well behaved) external potential $\hat{V}_{\mathrm{ext}}$ (transformation C). The condition that $\rho(\vec{r})$ derives from the ground-state of an external potential $\hat{V}_{\mathrm{ext}}$ is known as the v-representability condition [3, 4]. The functional F_{HK} as well as $E_{\hat{V}_{\mathrm{ext}}}$ are defined only for densities associated with pure v-representable states, i.e., the densities resulting from states $|\Psi\rangle$ that are eigenvector of the eigenvalue problem (2.2). This condition limits seriously the practical application of F_{HK}. Unfortunately, the majority of wave functions $|\Psi\rangle$ are not v-representable states and consequently one cannot use the HK theorems under this condition. For example, Levy and Lieb [46] have proven that the density obtained from a mixed ensemble of q degenerate wave functions cannot be associated with an external potential. In order to prove this statement, they considered the density matrix

$$\hat{D} = \sum_{i=1}^{q} w_i |\Psi_i\rangle\langle\Psi_i| \tag{2.20}$$

with $w_i \geq 0$ and $\sum_{i=1}^{q} w_i = 1$. From $\hat{D}$ they compute the electronic density

$$\rho_D(\vec{r}) = \sum_{i=1}^{q} w_i \rho_i(\vec{r}) \quad \text{where} \quad \rho_i(\vec{r}) = \langle \Psi_i | \hat{\rho} | \Psi_i \rangle. \tag{2.21}$$

They showed that $\rho_D(\vec{r})$ cannot be obtained from a pure v-representable wave function despite the fact that by construction $\rho_D(\vec{r})$ is associated to an external potential. This class of wave functions are called ensemble v-representable. They are obtained as an incoherent superposition of pure state v-representable wave functions. Note that Englisch and Englisch have proven that these well behaves functions $\rho_D(\vec{r})$ are not the ground-state of any external potential. Therefore, it is not true that all well-behaved functions are pure state or even ensemble v-representable [47]. These formal problems of the HK functional may render its application unpractical. An extension of the domain of definition of the functional F_{HK} to any non negative density $\rho(\vec{r})$ whose integration gives the particle number N is most desirable.

2.1.3 Levi-Lieb functional

Levy and Lieb (LL) were the first to make the extention of the domain of F_{HK} [46]. They proposed as an extension the definition of a new functional

$$F_{\mathrm{LL}}[\rho(\vec{r})] = \min_{|\Psi\rangle \to \rho(\vec{r})} \langle \Psi | \hat{T} + \hat{W} | \Psi \rangle \tag{2.22}$$

where the minimization is done over all the fermion wave functions $|\Psi\rangle$ that give the same electronic density $\rho(\vec{r})$. In other words, one selects the $|\Psi\rangle$ that gives the minimum sum

of the of kinetic and correlation energy under the constraint of having a given $\rho(\vec{r})$. Note that $F_{\rm LL}[\rho(\vec{r})]$ is independent to the external potential which defines the problem.
In order for $F_{\rm LL}[\rho(\vec{r})]$ to be a universal functional, independent of the external potential, and that the minimization of the total energy

$$E[\rho(\vec{r})] = F_{\rm LL}[\rho(\vec{r})] + \int d\vec{r} v(\vec{r})\rho(\vec{r}) \tag{2.23}$$

to give the ground state energy, we need to prove the following two simple but important theorems.

Levy's theorem 1: *To any density $\rho(\vec{r})$ associated with a N-particle wave function $|\Psi\rangle$ corresponds a energy $E[\rho(\vec{r})]$ higher or equal to the ground-state energy $E_{\rm gs}$*

$$E[\rho(\vec{r})] = F_{\rm LL}[\rho(\vec{r})] + \int d\vec{r}\, v(\vec{r})\, \rho(\vec{r}) \geq E_{\rm gs} \tag{2.24}$$

Levy's theorem 2: *The ground-state energy $E_{\rm gs}$ is obtained for the ground-state density $\rho_{\rm gs}(\vec{r})$ as*

$$E[\rho_{\rm gs}(\vec{r})] = F_{\rm LL}[\rho({}_{\rm gs}\vec{r})] + \int d\vec{r} v(\vec{r})\rho_{\rm gs}(\vec{r}) = E_{\rm gs} \tag{2.25}$$

Notice that it is not necessary to impose the non-degeneracy of the wave function $|\Psi\rangle$. In this approach, the minimization runs over all densities $\rho(\vec{r})$ obtained from any N-particle wave function $|\Psi\rangle$. This ensemble of densities is N-representable.
Before the proof of these two theorems, it useful to introduce some extra definition. In this sense, we mean by $|\Psi_{\rm min}^{\rho(\vec{r})}\rangle$ the wave function which realizes the minimum on the right hand side of Eq. (2.22), i.e.,

$$F_{\rm LL}[\rho(\vec{r})] = \langle\Psi_{\rm min}^{\rho(\vec{r})}|\hat{T} + \hat{W}|\Psi_{\rm min}^{\rho(\vec{r})}\rangle. \tag{2.26}$$

$|\Psi_{\rm min}^{\rho(\vec{r})}\rangle$ is the wave function that minimizes $F_{\rm LL}$ among all $|\Psi\rangle$ which give the density $\rho(\vec{r})$. Finally, we denote by $\Psi_{\rm min}^{\rho_{\rm gs}(\vec{r})}$ the wave function which minimizes $F_{\rm LL}$ over all wave functions $|\Psi\rangle$ giving the ground-state density $\rho_{\rm gs}(\vec{r})$.

$$F_{\rm LL}[\rho_{\rm gs}(\vec{r})] = \langle\Psi_{\rm min}^{\rho_{\rm gs}(\vec{r})}|\hat{T} + \hat{W}|\Psi_{\rm min}^{\rho_{\rm gs}(\vec{r})}\rangle. \tag{2.27}$$

Proof of Levy's theorem 1:
Using Eq. (2.26) one obtains

$$\int d\vec{r}\, v(\vec{r})\, \rho(\vec{r}) + F_{\rm LL}[\rho(\vec{r})] = \int d\vec{r}\, v(\vec{r})\, \rho(\vec{r}) + \langle\Psi_{\rm min}^{\rho(\vec{r})}|\hat{T} + \hat{W}|\Psi_{\rm min}^{\rho(\vec{r})}\rangle \tag{2.28}$$

with $\hat{V}_{\rm ext} = \sum_{i=1}^{N} v_i(\vec{r}_i)$. It follows that

$$\int d\vec{r}\, v(\vec{r})\rho(\vec{r}) + F_{\rm LL}[\rho(\vec{r})] = \langle\Psi_{\rm min}^{\rho(\vec{r})}|\hat{T} + \hat{W} + \hat{V}_{\rm ext}|\Psi_{\rm min}^{\rho(\vec{r})}\rangle. \tag{2.29}$$

Then, the variational principle implies

$$\langle \Psi_{\rm min}^{\rho(\vec{r})} | \hat{T} + \hat{W} + \hat{V}_{\rm ext} | \Psi_{\rm min}^{\rho(\vec{r})} \rangle \geq E_{\rm gs}, \tag{2.30}$$

from which we deduce that

$$\int d\vec{r}\, v(\vec{r})\rho(\vec{r}) + F_{\rm LL}[\rho(\vec{r})] \geq E_{\rm gs}. \tag{2.31}$$

This proves Levy's theorem 1.

Proof of Levy's theorem 2:
Again, the variational principle imposes that

$$E_{\rm gs} \leq \langle \Psi_{\rm min}^{\rho_{\rm gs}(\vec{r})} | \hat{T} + \hat{W} + \hat{V}_{\rm ext} | \Psi_{\rm min}^{\rho_{\rm gs}(\vec{r})} \rangle. \tag{2.32}$$

In other words,

$$\langle \Psi_{\rm gs} | \hat{T} + \hat{W} + \hat{V}_{\rm ext} | \Psi_{\rm gs} \rangle \geq \langle \Psi_{\rm min}^{\rho_{\rm gs}(\vec{r})} | \hat{T} + \hat{W} + \hat{V}_{\rm ext} | \Psi_{\rm min}^{\rho_{\rm gs}(\vec{r})} \rangle. \tag{2.33}$$

We now separate the contributions that depend on the external potential from those which are independent of it:

$$\int d\vec{r}\, v(\vec{r})\rho_{\rm gs}(\vec{r}) + \langle \Psi_{\rm gs} | \hat{T} + \hat{W} | \Psi_{\rm gs} \rangle \leq \int d\vec{r}\, v(\vec{r})\rho_{\rm gs}(\vec{r}) + \langle \Psi_{\rm min}^{\rho_{\rm gs}(\vec{r})} | \hat{T} + \hat{W} | \Psi_{\rm min}^{\rho_{\rm gs}(\vec{r})} \rangle. \tag{2.34}$$

Consequently,

$$\langle \Psi_{\rm gs} | \hat{T} + \hat{W} | \Psi_{\rm gs} \rangle \leq \langle \Psi_{\rm min}^{\rho_{\rm gs}(\vec{r})} | \hat{T} + \hat{W} | \Psi_{\rm min}^{\rho_{\rm gs}(\vec{r})} \rangle. \tag{2.35}$$

Moreover, from the definition we have

$$\langle \Psi_{\rm gs} | \hat{T} + \hat{W} | \Psi_{\rm gs} \rangle \geq \langle \Psi_{\rm min}^{\rho_{\rm gs}(\vec{r})} | \hat{T} + \hat{W} | \Psi_{\rm min}^{\rho_{\rm gs}(\vec{r})} \rangle. \tag{2.36}$$

Eq. (2.35) and (2.36) impose that

$$\langle \Psi_{\rm gs} | \hat{T} + \hat{W} | \Psi_{\rm gs} \rangle = \langle \Psi_{\rm min}^{\rho_{\rm gs}(\vec{r})} | \hat{T} + \hat{W} | \Psi_{\rm min}^{\rho_{\rm gs}(\vec{r})} \rangle. \tag{2.37}$$

Using Eq. (2.27) we arrive to

$$\langle \Psi_{\rm gs} | \hat{T} + \hat{W} | \Psi_{\rm gs} \rangle = F_{\rm LL}[\rho_{\rm gs}(\vec{r})]. \tag{2.38}$$

Finally, by adding the term involving the external potential we obtain

$$F_{\rm LL}[\rho_{\rm gs}(\vec{r})] + \int d\vec{r} v(\vec{r})\rho_{\rm gs}(\vec{r}) = E_{\rm gs}. \tag{2.39}$$

This proves Levy's theorem 2.

It is important to recall that the Levy-Lieb variational scheme is not limited to non-degenerate systems. It is defined for any N-representable density $\rho(\vec{r})$, i.e. from any $\rho(\vec{r})$ which can be associated with the N-particle wave function. In fact, it is this formulation which is used to derive LDFT, as will be shown in Chapter 4.

2.2 DFT as an exact effective single-body theory

The variational principle of HK allows the determination of the exact ground-state density of any N-particle system. The advantages of a replacement of the direct variation with respect to the density by the intermediary orbital picture was first emphasized by Kohn and Sham (KS) [2]. This results in a self-consistent scheme, which is nowadays used for practical application of DFT. Many *ab-initio* computer codes solving the selfconsistent KS equations are available. In section 2.2.1 we present the KS equations following the book of Dreizler and Gross [4]. In particular, we show that this approach is exact by considering that the exact ground-state density of a correlated system can be reproduced by an auxiliary one-particle potential. Although the KS equations are exact, they include a highly non trivial unknown, the exchange and correlation (XC) potential, for which approximation have to be made. The most simple and famous approach is the local density approximations (LDA), which we present in Sec. 2.2.2. This *Ansatz* is derived from a reference system: the homogeneous interacting electron gas. Although LDA is a first hand approximation for inhomogeneous system (for example, molecules, crystalline solid alloys, etc.) it has been incredibly successful for predicting the ground-state properties of these systems [7].

2.2.1 The Kohn-Sham equations

Following Kohn and Sham, one can transform a many-body particle system into a non-interacting particle problem in a self-consistent field. The main idea behind of this transformation is in the assumption that the ground-state density of the many-body interacting system can be reproduced by an auxiliary potential $\hat{V}_{\rm S}$.[1] We consider an auxiliary N-particle non-interacting $\hat{H}_{\rm S} = \hat{T}_{\rm S} + \hat{V}_{\rm S}$ system described by the Hamiltonian

$$\hat{H}_{\rm S} = \hat{T}_{\rm S} + \hat{V}_{\rm S} \tag{2.40}$$

where $\hat{T}_{\rm S}$ is the kinetic operator and $\hat{V}_{\rm S}$ the auxiliary potential. The HK theorems state that there is a functional energy

$$\begin{aligned} E_{\rm S}[\rho(\vec{r})] &= T_{\rm S}[\rho(\vec{r})] + V_{\rm S}[\rho(\vec{r})] \\ &= T_{\rm S}[\rho(\vec{r})] + \int d\vec{r}\, v_{\rm S}(\vec{r})\, \rho(\vec{r}), \end{aligned} \tag{2.41}$$

for which the variational equation $\delta E_{\rm S}[\rho(\vec{r})] = 0$ gives the ground-state energy of $\hat{H}_{\rm S}$. The main hypothesis of the KS scheme is that there exists a one-particle potential associated to the same electronic density as the interacting system:

$$\rho(\vec{r}) = \rho_{\rm S}(\vec{r}) \tag{2.42}$$

In other words, the density of the interacting system has to be v-representable with and without interactions. If the ground state of $\hat{H}_{\rm S}$ is not degenerated, its density $\rho_{\rm S}(\vec{r})$ has a unique representation in terms of N one-particle orbitals:

$$\rho_{\rm S}(\vec{r}) = \sum_{i=1}^{N} |\varphi_i(\vec{r})|^2 \,. \tag{2.43}$$

[1] The subscript S in this subsection is used to point out a single-particle system

By hypothesis $\rho_{\rm S}(\vec{r}) = \rho(\vec{r})$. These orbitals have an energy ε_i and can be obtained by solving the Schrödinger equation

$$\left[\frac{-\hbar^2}{2m}\nabla^2 + \hat{V}_{\rm S}(\vec{r})\right]\varphi_i(\vec{r}) = \varepsilon_i\varphi_i(\vec{r});\;\; \varepsilon_1 \leq \varepsilon_2 \leq ... \leq \varepsilon_N. \tag{2.44}$$

The existence of the potential $\hat{V}_{\rm S}$ that generates the given density is an assumption, which for the moment does not have a strict justification. However, the uniqueness of $\hat{V}_{\rm S}$ results from HK theorems which of course applies to a non-interacting system ($\hat{W} = 0$). This implies that the one-particle orbitals $\varphi_i(\vec{r})$ are unique functionals of $\rho(\vec{r})$, i.e.,

$$\varphi_i(\vec{r}) = \varphi_i([\rho(\vec{r})]; \vec{r}). \tag{2.45}$$

The same holds for the non-interacting kinetic energy

$$T_{\rm S}[\rho(\vec{r})] = \sum_{i=1}^{N}\int d\vec{r}\,\varphi_i(\vec{r})\,\left(\frac{-\hbar^2}{2m}\nabla^2\right)\,\varphi_i(\vec{r}). \tag{2.46}$$

Now, we want to describe the system with N interacting electrons in an external potential $\hat{V}_{\rm ext}$ using an auxiliary potential $\hat{V}_{\rm S,ext}$ leading to the same ground-state density $\rho_{\rm gs}(\vec{r})$. We then write

$$\rho_{\rm gs}(\vec{r}) = \sum_{i=1}^{N}|\varphi_i(\vec{r})|^2, \tag{2.47}$$

where

$$\left[\frac{-\hbar^2}{2m}\nabla^2 + \hat{V}_{\rm S,ext}(\vec{r})\right]\varphi_i(\vec{r}) = \varepsilon_i\varphi_i(\vec{r});\;\; \varepsilon_1 \leq \varepsilon_2 \leq ... \leq \varepsilon_N. \tag{2.48}$$

These equations indicate how to pass formally from the interacting problem to a non-interacting system in an effective external field $\hat{V}_{\rm S,ext}$. The key point now is to find the form of $\hat{V}_{\rm S,ext}$ as a functional of $\rho(\vec{r})$.
In order to do that, we rewrite the functional energy $E_{\hat{V}_{\rm ext}}[\rho(\vec{r})]$ as a sum of different contributions, whose functional forms are explicitly known, and a term called exchange and correlation (XC) potential, whose functional dependence is challenging. In the KS scheme the kinetic contribution is divided into two parts. The first one, denoted by $T_{\rm S}[\rho(\vec{r})]$ corresponds to the kinetic energy of the non-interacting system. The remaining kinetic-energy contribution, reflecting the correlation effects, will be included in the XC energy. In the case of the Coulomb interaction energy, we separate the Hartree energy, which is given by the classical interaction of the electronic density $\rho(\vec{r})$ with itself. The remaining exchange and correlation contributions of the interactions are included in the XC energy $E_{\rm XC}[\rho(\vec{r})]$. Rewritten in this form, one needs to impose that $E_{\hat{V}_{\rm ext}}[\rho(\vec{r})]$ is stationary under small variations of $\rho(\vec{r})$ around the ground state $\rho_{\rm gs}(\vec{r})$ (stationarity condition). Then the energy functional $E_{\hat{V}_{\rm ext}}[\rho(\vec{r})]$ is written as

$$\begin{aligned} E_{\hat{V}_{\rm ext}}[\rho(\vec{r})] \;\; &= \;\; T_{\rm S}[\rho(\vec{r})] + \int d\vec{r}\,v_{\rm ext}(\vec{r})\,\rho(\vec{r}) \\ &\quad + \frac{1}{2}\int\int d\vec{r}\,d\vec{r'}\,\rho(\vec{r})\,\rho(\vec{r'})w(\vec{r},\vec{r'}) + E_{\rm XC}[\rho(\vec{r})], \end{aligned} \tag{2.49}$$

where the XC contribution is given by

$$E_{\rm XC}[\rho(\vec{r})] = F_{\rm HK}[\rho(\vec{r})] - \frac{1}{2}\int\int d\vec{r}\, d\vec{r'}\, \rho(\vec{r})\,\rho(\vec{r'})w(\vec{r},\vec{r'}) - T_{\rm S}[\rho(\vec{r})]. \tag{2.50}$$

The variational principle implies that $E_{\hat{V}_{\rm ext}}[\rho(\vec{r})]$ has a stationary point for the ground-state density $\rho_{\rm gs}(\vec{r})$, which gives the minimum energy, i.e.,

$$0 = \delta E_{\hat{V}_{\rm ext}}[\rho_{\rm gs}(\vec{r})] = E_{\hat{V}_{\rm ext}}[\rho_{\rm gs}(\vec{r}) + \delta\rho(\vec{r})] - E_{\hat{V}_{\rm ext}}[\rho_{\rm gs}(\vec{r})]. \tag{2.51}$$

Simple calculus of variations yields

$$\begin{aligned}\delta E_{\hat{V}_{\rm ext}}[\rho_{\rm gs}(\vec{r})] &= \delta T_{\rm S}[\rho_{\rm gs}(\vec{r})] + \int d\vec{r}\, V_{\rm ext}(\vec{r})\,\delta\rho(\vec{r}) \\ &\quad + \int\int d\vec{r}\, d\vec{r'}\,\delta\rho(\vec{r})\,\rho_{\rm gs}(\vec{r'})\,w(\vec{r},\vec{r'}) + \int d\vec{r}\,\frac{\delta E_{\rm XC}}{\delta\rho(\vec{r})}\delta\rho(\vec{r}),\end{aligned} \tag{2.52}$$

and

$$\delta E_{\hat{V}_{\rm ext}}[\rho(\vec{r})] = \delta T_{\rm S}[\rho(\vec{r})] + \int d\vec{r}\,\delta\rho(\vec{r})\left[V_{\rm ext}(\vec{r}) + \int d\vec{r'}\, w(\vec{r},\vec{r'})\rho(\vec{r'}) + v_{\rm XC}(\vec{r'})\right], \tag{2.53}$$

where we have introduced the XC potential $v_{\rm XC}(\vec{r}) = \delta E_{\rm XC}/\delta\rho(\vec{r})$. Let us recall that $F_{\rm HK}[\rho(\vec{r})]$ is defined only for v-representable densities with or without interaction. Consequently, the variations of the density should be restricted to v-representable functions. The variation of $T_{\rm S}[\rho(\vec{r})]$ is given by

$$\begin{aligned}\delta T_{\rm S}[\rho_{\rm gs}(\vec{r})] &= \sum_{i=1}^{N}\int d\vec{r}\,\left[\delta\varphi_i^*(\vec{r})\left(-\frac{\hbar^2}{2m}\nabla^2\right)\varphi_{i,\rm gs}(\vec{r}) + \varphi_{i,\rm gs}^*(\vec{r})\left(-\frac{\hbar^2}{2m}\nabla^2\right)\delta\varphi_i(\vec{r})\right] \\ &= \sum_{i=1}^{N}\int d\vec{r}\,\left[\delta\varphi_i^*(\vec{r})\left(-\frac{\hbar^2}{2m}\nabla^2\right)\varphi_{i,\rm gs}(\vec{r}) + \delta\varphi_i(\vec{r})\left(-\frac{\hbar^2}{2m}\nabla^2\right)\varphi_{i,\rm gs}^*(\vec{r})\right].\end{aligned} \tag{2.54}$$

Here, in the last equation we have used Green's theorem.[2]
From Eq. (2.47) we also know that,

$$\left[-\frac{\hbar^2}{2m}\nabla^2 + \hat{V}_{\rm S,ext}(\vec{r})\right]\varphi_i(\vec{r}) = \varepsilon_i\varphi_i(\vec{r}),$$

or equivalently

$$-\frac{\hbar^2}{2m}\nabla^2\varphi_i(\vec{r}) = [\varepsilon_i - \hat{V}_{\rm S,ext}(\vec{r})]\,\varphi_i(\vec{r}). \tag{2.55}$$

Replacing Eq. (2.55) in Eq. (2.54) gives

$$\delta T_{\rm S}[\rho_{\rm gs}(\vec{r})] = \sum_{i=1}^{N}\int d\vec{r}\,\left[\delta\varphi_i^*(\vec{r})[\varepsilon_i - \hat{V}_{\rm S,ext}(\vec{r})]\varphi_{i,\rm gs}(\vec{r}) + \varphi_{i,\rm gs}^*(\vec{r})[\varepsilon_i - \hat{V}_{\rm S,ext}(\vec{r})]\delta\varphi_i(\vec{r})\right]. \tag{2.56}$$

[2] $\int_V d\vec{r}[\phi\nabla.\nabla\psi - \psi\nabla.\nabla\phi] = \int_S d\vec{\sigma}.[\phi\nabla\psi - \psi\nabla\phi]$

Recalling that

$$\delta|\varphi_i(\vec{r})|^2 = |\varphi_i(\vec{r}) + \delta\varphi_i(\vec{r})|^2 = \varphi_i^*(\vec{r})\,\delta\varphi_i(\vec{r}) + \varphi_i(\vec{r})\,\delta\varphi_i^*(\vec{r}) \tag{2.57}$$

one obtains

$$\delta T_{\rm S} = \sum_{i=1}^{N} \varepsilon_i \int d\vec{r}\,\delta|\varphi_i(\vec{r})|^2 - \sum_{i=1}^{N} \int d\vec{r}\,\hat{V}_{\rm S,ext}(\vec{r})\,\delta|\varphi_i(\vec{r})|^2\,. \tag{2.58}$$

The normalization of $\varphi_i(\vec{r}) + \delta\varphi_i(\vec{r})$ implies

$$\delta T_{\rm S} = -\int d\vec{r}\,\hat{V}_{\rm S,ext}(\vec{r})\,\delta\rho(\vec{r}) \tag{2.59}$$

Replacing Eq. (2.59) in Eq. (2.52) and requiring $\delta E_{\hat{V}_{\rm ext}} = 0$ we obtain using the final equation of the auxiliary potential

$$\hat{V}_{\rm S,ext}(\vec{r}) = \hat{V}_{\rm ext}(\vec{r}) + \int d\vec{r'}\,w(\vec{r},\vec{r'})\,\rho_{\rm gs}(\vec{r'}) + v_{\rm XC}([\rho_{\rm gs}(\vec{r})],\vec{r}). \tag{2.60}$$

The auxiliary potential $\hat{V}_{\rm S,ext}(\vec{r})$ is central to the KS formulation. It contains the unknown XC contribution. In practice, one needs an approximation to $v_{\rm XC}$ in order to be able to apply the KS scheme. The goal of the next section is to present such an approximation.

2.2.2 Local density approximation (LDA)

The purpose of this subsection is to recall the local density approximation (LDA) to the XC potential [see Eq. (2.60)]. This approximation was originally introduced by Kohn and Sham who have taken the homogeneous electron gas as a reference system [2]. We will see that the analytic form of $v_{\rm XC}([\rho_{\rm gs}(\vec{r})],\vec{r})$ is unknown, even for the homogeneous electron gas. Therefore, the LDA requires introduction of a parameterization for different regimes [4, 48, 49, 50].
The LDA approximation is obtained directly from the energy of the homogeneous electron gas

$$e^{\rm LDA}[\rho(\vec{r})] = \frac{E^{\rm LDA}[\rho(\vec{r})]}{N} = e^{\rm hom}[\rho_{\rm gs}(\vec{r})]|_{\rho_{\rm gs}(\vec{r})\to\rho(\vec{r})}. \tag{2.61}$$

In the spin-polarized case or local spin density approximation (LSDA) the functional depends on both up and down densities $\rho_\uparrow(\vec{r})$ and $\rho_\downarrow(\vec{r})$, or equivalently, on

$$\rho(\vec{r}) = \rho_\uparrow(\vec{r}) + \rho_\downarrow(\vec{r}) \tag{2.62}$$

and

$$\zeta(\vec{r}) = \frac{1}{\rho(\vec{r})}(\rho_\uparrow(\vec{r}) - \rho_\downarrow(\vec{r})), \tag{2.63}$$

where $\zeta(\vec{r})$ represents the relative magnetization at the point $\vec{r}$.
The Hartree Fock approximation of the homogeneous electron gas yields directly the non-interacting kinetic energy $T_{\rm S}$ and the exchange energy $E_{\rm X}$ (see for instance, Eqs. (6.103) and (6.104) in Ref [4]). However, the dependence of the correlation energy $E_{\rm C}$ as a functional of the density is unknown analytically. In general, one uses some parameterization of $e_{\rm C} = E_{\rm C}/N$ for different density regimes. In order to use DFT, it is very useful to get

a parameterization of $v_{\mathrm{XC}}(\vec{r})$ since it provides an analytical expression of the exchange and correlation potential. Hedin and Lundqvist have proposed a formulation using two parameters that is written as follows [48]:

$$\tilde{e}_{\mathrm{C}}[\rho(\vec{r})] = \frac{e_{\mathrm{C}}[\rho(\vec{r})]}{\rho(\vec{r})} = -C\left\{(1+x^3)\ln\left(1+\frac{1}{x}\right)+\frac{x}{2}-x^2-\frac{1}{3}\right\}, \tag{2.64}$$

where $x = r_s/A$ and

$$r_s = \frac{1}{a_0}\left[\frac{3}{4\pi\rho(\vec{r})}\right]^{1/3} \tag{2.65}$$

is the Wigner-Seitz radius in units of the Bohr radius a_0. The parameters $C = 0.225[e^2/a_0]$ and $A = 21$ give the results of Singwi [49], which are considered to be reliable in a density interval $1 \leq r_s \leq 6$. For spin-polarized systems, von Bart and Hedin have proposed an approximation, which is obtained by interpolation of the paramagnetic and ferromagnetic limits [50]. This reads

$$\tilde{e}_i[\rho(\vec{r}),\zeta(\vec{r}] = \tilde{e}_i[\rho,\zeta=0] + (\tilde{e}_i[\rho,\zeta=1] - \tilde{e}_i[\rho,\zeta=0])f(\zeta(\vec{r})), \tag{2.66}$$

where $i \equiv$ X (C) for the exchange (correlation) contribution. The interpolation function

$$f(\zeta(\vec{r})) = \frac{(1+\zeta(\vec{r}))^{4/3}+(1-\zeta(\vec{r}))^{4/3}-2}{2(2^{1/3}-1)} \tag{2.67}$$

is chosen to reproduce the exact dependence of the exchange contribution of the homogeneous gas. The exchange energy for $\zeta = 0$ and $\zeta = 1$ of the paramagnetic and ferromagnetic cases are given by

$$\begin{aligned} \tilde{e}_X(\rho(\vec{r}),\zeta=0) &= -\frac{3e^2}{4}\left[\frac{3\rho(\vec{r})}{\pi}\right] \\ &\text{and} \\ \tilde{e}_X(\rho(\vec{r}),\zeta=1) &= 2^{1/3}\tilde{e}_X(\rho(\vec{r}),\zeta=0). \end{aligned} \tag{2.68}$$

These limiting cases are also parameterized by using the Hedin and Lundqvist parameters,

$$\begin{aligned} C(\zeta=0) = 0.0225[e^2/a_0] \quad &\text{and} \quad A(\zeta=0)=30, \\ &\text{and} \\ C(\zeta=1) = 0.0127[e^2/a_0] \quad &\text{and} \quad A(\zeta=1)=75. \end{aligned} \tag{2.69}$$

Using this parameterization of $\tilde{e}_{\mathrm{XC}} = \tilde{e}_{\mathrm{X}} + \tilde{e}_{\mathrm{C}}$ one obtains an analytic expression for the potential $v_{\mathrm{XC}} = \delta\tilde{e}_{\mathrm{XC}}/\delta\rho(\vec{r})$, namely

$$\begin{aligned} v_{\mathrm{XC}}^{\uparrow/\downarrow} &= \frac{\partial}{\partial\rho(\vec{r})}\{\rho(\vec{r})\tilde{e}_{\mathrm{XC}}[\rho(\vec{r}),\zeta(\vec{r}]\} \\ &= \tilde{e}_{\mathrm{XC}} + \rho\frac{\partial\zeta}{\partial\rho} \pm (1\mp\zeta)\frac{\partial\zeta}{\partial\rho}. \end{aligned} \tag{2.70}$$

It is worth to stressing that, despite its simplicity, the LDA approximation has been applied successfully for many physical problems [7]. However, multiple failures of this

approach have also been observed. Let us mention the semiconductor gap, for example in silicium, whose experimentally observed value is largely underestimated by using DFT within the LDA [8]. In this case, the error has been attributed to a discontinuity in the exchange and correlation potential with the number of particles rather than to the LDA itself [9, 10]. Systems with van der Waals interactions, which result from density fluctuations are also beyond the scope of the LDA [7]. Another example where the LDA as well as more advanced approximations such as the generalized gradient approximation (GGA) fails concern calculations of band-gaps in strongly correlated systems, for instance in transition metal, oxides, where the band-gaps are strongly underestimated [11, 12]. In this case, one of the explanations of this error, as given in the literature, is that the mechanism of localization of LDA is given by a Stoner-like parameter, which is too small to provide a good description of the gap [13].
Despite some attempts to describe properties of strongly correlated systems by using improved local density approaches [51, 52, 53, 54], it is clear that this approximation remains inadequate for these systems. Even though improvements have been achieved, for example within the GGA approximation [6], which takes into account the gradient of the density, or with hybrid approaches that combine the LDA with many-body techniques such as the dynamical mean field theory, it is still true that dealing properly with strong correlated materials remains a serious theoretical challenge. A profound improvement of density functionals that are enables them to handle strong electron correlations is therefore worthwhile.
Finally, to conclude this section, we would like to stress the universal character of DFT and of the Hohenberg-Kohn-Sham formulation, which imposes no restriction at all on the type of Hamiltonian. It is this universality of DFT, which opens the way to applications to model Hamiltonians, as it will be shown in chapter 4. However, before coming to this we shall review some of the main properties of many-body models taking the Hubbard model as a particularly relevant example.

Chapter 3

The Hubbard model

Electronic interactions play a major role in condensed matter physics. In general, for metals having no open d or f shell, (Cu, Au, Ag, ...) a free electron-like picture is rather accurate for the low lying excitations (Fermi-liquid theory). This is mainly due to the fact that s and p orbitals are rather delocalized, so that the electrons are weakly coupled near the Fermi energy due to the screening and the fermionic character of the electron. These orbitals are generally responsible for chemical bonding and metallic behavior. However, in transition-metals, where the d-shell is not filled, the situation is more complicated. The d orbitals are rather localized around the atoms, implying that the Coulomb repulsion is no longer negligible. On the other hand, these orbitals are in general also hybridized in the bulk. In this case, the free electron gas does not provide any more a good starting model to describe these systems. It is important in order to understand the physics of transition-metal systems, to have a theory that takes into account correlation effects in d-bands and to determine the interplay between electronic interactions and hybridizations. It is in this context that J. Hubbard, M. C. Gutzwiller and J. Kanamori derived a model Hamiltonian, usually known as Hubbard model, that is intended to capture the physics of the competition between delocalization, driven by hybridization, and localization of electrons driven by the electronic interaction [16, 55, 56]. For simplicity, they proposed a theory considering only a single orbital per atom having of course its two spin states. Although it is clear that some important aspects of real d-electrons are lost with this modeling, it is also reasonable to expect that the main physics of this interplay is captured in this theory. In the first section of this chapter we describe a way to pass from an interacting gas of electrons to the discrete Hubbard model on a lattice [16]. In section 3.2 we recall some cases where exact solutions are available: the dimer model, the one-dimensional Bethe-*Ansatz*, and the Nagaoka theorem near the atomic limit close to half-band filling. The section 3.3 concerns two basic mean-field treatments of the model, namely the Hartree-Fock approximation and the slave-boson theory. In section 3.4 we discuss other models related to the Hubbard Hamiltonians, in particular the tJ model and the Heisenberg model. Finally, in the last section of the chapter, we discuss the relevance of the Hubbard model for treating attractive electronic interactions and present a first hand approximation that is similar to the Bardeen-Cooper-Schrieffer (BCS) theory of superconductivity.

3.1 From the interacting electron gas to the discrete Hubbard Hamiltonian on a lattice

We consider a system composed by a narrow band containing n electrons. The case of a single band is considered for simplicity although the actual motivation are narrow d or f bands. We call $\psi_{\mathbf{k}}$ the Bloch function of the system which has an energy $\epsilon_{\mathbf{k}}$ where $\mathbf{k}$ is the wave vector. The actual choice of the basis wave function $\psi_{\mathbf{k}}$ is not decisive. For example, we may assume that these wave functions are obtained from a spin independent effective DFT or Hartree-Fock potential.
In order to write down the Hamiltonian of this problem, we denote as $\hat{c}^{\dagger}_{\mathbf{k},\sigma}$ ($\hat{c}_{\mathbf{k},\sigma}$) the creation (destruction) operator acting on an electron in the Bloch state $(\mathbf{k},\sigma)$, where $\sigma =\uparrow$ or $\downarrow$ is the spin label. Then we have

$$\begin{aligned} H &= \sum_{\mathbf{k},\sigma} \epsilon_{\mathbf{k}} \hat{c}^{\dagger}_{\mathbf{k},\sigma}\hat{c}_{\mathbf{k},\sigma} + \frac{1}{2}\sum_{\mathbf{k_1},\mathbf{k_2},\mathbf{k'_1},\mathbf{k'_2}} \sum_{\sigma_1,\sigma_2} \langle \mathbf{k_1},\mathbf{k_2}|\frac{1}{r}|\mathbf{k'_1},\mathbf{k'_2}\rangle\, \hat{c}^{\dagger}_{\mathbf{k_1},\sigma_1}\hat{c}^{\dagger}_{\mathbf{k_2},\sigma_2}\hat{c}_{\mathbf{k'_2},\sigma_2}\hat{c}_{\mathbf{k'_1},\sigma_1} \\ &\quad - \sum_{\mathbf{k},\mathbf{k'}}\sum_{\sigma}\left\{2\langle \mathbf{k},\mathbf{k'}|\frac{1}{r}|\mathbf{k},\mathbf{k'}\rangle - \langle \mathbf{k},\mathbf{k'}|\frac{1}{r}|\mathbf{k'},\mathbf{k}\rangle\right\}\nu_{\mathbf{k'}}\hat{c}^{\dagger}_{\mathbf{k},\sigma}\hat{c}_{\mathbf{k},\sigma}, \end{aligned} \tag{3.1}$$

where the sum runs over all $\mathbf{k}$ vectors in the first Brillouin zone and

$$\langle \mathbf{k_1},\mathbf{k_2}|\frac{1}{r}|\mathbf{k'_1},\mathbf{k'_2}\rangle = e^2\int d\mathbf{r}\, d\mathbf{r'}\frac{\psi^*_{\mathbf{k_1}}(\mathbf{r})\,\psi_{\mathbf{k'_1}}(\mathbf{r})\,\psi^*_{\mathbf{k_2}}(\mathbf{r'})\,\psi_{\mathbf{k'_2}}(\mathbf{r'})}{|\mathbf{r}-\mathbf{r'}|} \tag{3.2}$$

The first term of Eq. (3.1) represents the band energies of the electrons, the second their interaction and finally the last one subtracts the potential energy of the electrons in that part of the Hartree-Fock field arising from the electrons of the s-band itself. Notice that $\psi_{\mathbf{k}}$ could also be the Kohn-Sham orbitals obtained from a DFT $ab-initio$ calculation. In this case the last term of Eq. (3.1) should be replaced by the subtraction of electronic correlations obtained with the exchange-correlation potential. This term has to be subtracted in order to avoid double counting of the interaction. $\nu_{\mathbf{k}}$ are the occupation numbers of the bands in the Hartree-Fock calculation.
As the bands are considered to be narrow, it is convenient to change the basis since the Bloch wave functions are delocalized. In this sense, we introduce a basis set of Wannier functions, where the states are centered around the atomic position $\mathbf{R}_i$

$$\phi(\mathbf{x}) = \frac{1}{\sqrt{N}}\sum_{\mathbf{k}}\psi_{\mathbf{k}}(\mathbf{x}), \tag{3.3}$$

where N is the number of atoms. One can also write

$$\psi(\mathbf{x})_{\mathbf{k}} = \frac{1}{\sqrt{N}}\sum_{i} e^{\imath\mathbf{k}.\mathbf{R}_i}\phi(\mathbf{x}-\mathbf{R}_i), \tag{3.4}$$

where the sum runs over all atomic positions $\mathbf{R}_i$. It is also useful to introduce creation and annihilation operators on the new basis of Wannier function as

$$\hat{c}_{\mathbf{k},\sigma} = \frac{1}{\sqrt{N}}\sum_{i} e^{-\imath\mathbf{k}.\mathbf{R}_i}\hat{c}_{i,\sigma} \quad \hat{c}^{\dagger}_{\mathbf{k},\sigma} = \frac{1}{\sqrt{N}}\sum_{i} e^{\imath\mathbf{k}.\mathbf{R}_i}\hat{c}^{\dagger}_{i,\sigma}. \tag{3.5}$$

Notice that the set of Wannier functions is a full orthogonal basis set, and that they vanish for $|\mathbf{r}-\mathbf{R}_i| \to \infty$.
It is now suitable to rewrite the Hamiltonian (3.1) in the new basis,

$$\begin{aligned} H &= \sum_{i,j}\sum_{\sigma} t_{ij}\,\hat{c}^{\dagger}_{i,\sigma}\hat{c}_{j,\sigma} + \frac{1}{2}\sum_{i,j,k,l}\sum_{\sigma,\sigma'}\langle ij|\frac{1}{r}|kl\rangle\,\hat{c}^{\dagger}_{i,\sigma}\hat{c}^{\dagger}_{j,\sigma'}\hat{c}_{l,\sigma'}\hat{c}_{k,\sigma} \\ &\quad - \sum_{i,j,k,l}\sum_{\sigma}\left\{2\langle ij|\frac{1}{r}|kl\rangle - \langle ij|\frac{1}{r}|lk\rangle\right\}\nu_{jl}\,\hat{c}^{\dagger}_{i,\sigma}\hat{c}_{k,\sigma}, \end{aligned} \tag{3.6}$$

where

$$t_{ij} = \frac{1}{N}\sum_{\mathbf{k}} \epsilon_{\mathbf{k}} e^{\imath\mathbf{k}.(\mathbf{R}_i-\mathbf{R}_j)} \tag{3.7}$$

is the definition of the hopping integrals. Also,

$$\langle ij|\frac{1}{r}|kl\rangle = e^2\int d\mathbf{x}\,d\mathbf{x}'\frac{\phi^*(\mathbf{x}-\mathbf{R}_i)\,\phi(\mathbf{x}'-\mathbf{R}_j)\,\phi^*(\mathbf{x}-\mathbf{R}_k)\,\phi(\mathbf{x}'-\mathbf{R}_l)}{|\mathbf{x}-\mathbf{x}'|}, \tag{3.8}$$

and finally

$$\nu_{jl} = \frac{1}{N}\sum_{\mathbf{k}} \nu_{\mathbf{k}} e^{\imath\mathbf{k}.(\mathbf{R}_i-\mathbf{R}_j)}. \tag{3.9}$$

Since we are dealing with narrow bands, the Wannier orbitals are quite localized around the atoms. In these circumstances, it is a reasonable first approximation to neglect all integrals that are not intra-atomic since these dominate. We limit the integrals in Eq. (3.8) to the only intra-atomic orbital term $U = \frac{1}{2}\langle ii|\frac{1}{r}|ii\rangle$. The other contributions are neglected. Within this approximation, Eq (3.6) becomes

$$H^{Hubbard} = \sum_{i,j,\sigma} t_{ij}\hat{c}^{\dagger}_{i,\sigma}\hat{c}_{j,\sigma} + U\sum_{i}\hat{n}_{i,\sigma}\hat{n}_{i,\bar{\sigma}} - 2U\sum_{i,\sigma}\nu_i\hat{n}_{i,\sigma} \tag{3.10}$$

where $\hat{n}_i = \hat{c}^{\dagger}_{i,\sigma}\hat{c}_{i,\sigma}$ and $\nu_i = \frac{1}{N}\sum_{\mathbf{k}}\nu_{\mathbf{k}} = n/2$, implying that the last term of Eq. (3.10) is a constant and can be dropped.
Eq. (3.10) is called Hubbard Hamiltonian. Many extended versions of this Hamiltonian can be found in the literature, considering for example, inter-orbital interactions in order to be more realistic. Nevertheless, in general this model is a good starting point in order to investigate the effects of electronic interactions in narrow-band systems.

3.2 Exact results

Despite the apparent simplicity of the Hubbard model, there are actually only few exact results concerning the model. In this section we focus on some of them, which will be referred to later on in this thesis. We focus first on the Hubbard dimer, for which the size of the basis is small enough to allow us to diagonalize the Hamiltonian analytically. Later on, we present the solution for the one-dimensional Hubbard model derived originally by E. H. Lieb an F. Y. Wu [18]. Finally, near half-band filling and in the strongly interacting limit $U \to \infty$ the Nagaoka's theorem [19] and its later extension by H. Tasaki [57] gives us information about the stability of ferromagnetic ground states.

3.2.1 The inhomogeneous Hubbard dimer

We focus first on the simplest system, the inhomogeneous dimer at half-band filling and $S_z = 0$. The dimer is composed of two sites numbered by $i = 1$ and 2 with different energy levels ε_i and different on-site Coulomb repulsion $U_i = U + (-1)^i \Delta U$. Since its Hilbert space is composed of only four 2-body states, one can diagonalize the Hamiltonian easily and obtain an analytic relation in particular for the dependence of the Coulomb energy as a function of the density matrix. The Hamiltonian reads

$$\hat{H}^{dim} = -t \sum_{\sigma} \hat{c}^{\dagger}_{1,\sigma} \hat{c}_{2,\sigma} - t \sum_{\sigma} \hat{c}^{\dagger}_{2,\sigma} \hat{c}_{1,\sigma} + \frac{\varepsilon}{2} \sum_{\sigma} \hat{n}_{1,\sigma} - \frac{\varepsilon}{2} \sum_{\sigma} \hat{n}_{2,\sigma} + \sum_{i=1,}^{2} U_i \hat{n}_{i,\uparrow} \hat{n}_{i,\downarrow}. \quad (3.11)$$

The elements of the basis are

$$\begin{aligned} |1\rangle &= \hat{c}^{\dagger}_{1,\uparrow} \hat{c}^{\dagger}_{1,\downarrow} |0\rangle \qquad |2\rangle = \hat{c}^{\dagger}_{2,\uparrow} \hat{c}^{\dagger}_{2,\downarrow} |0\rangle \\ |3\rangle &= \hat{c}^{\dagger}_{1,\uparrow} \hat{c}^{\dagger}_{2,\downarrow} |0\rangle \qquad |4\rangle = \hat{c}^{\dagger}_{2,\uparrow} \hat{c}^{\dagger}_{1,\downarrow} |0\rangle. \end{aligned} \quad (3.12)$$

And the matrix-form of the Hamiltonian (3.11) becomes

$$\hat{H}^{dim} = \begin{pmatrix} U + \Delta U + \varepsilon & 0 & -t & -t \\ 0 & U - \Delta U - \varepsilon & -t & -t \\ -t & -t & 0 & 0 \\ -t & -t & 0 & 0 \end{pmatrix}. \quad (3.13)$$

For the homogeneous case ($\varepsilon = 0$ and $\Delta U = 0$) and $U > 0$ (repulsive interaction) the ground state energy is given by

$$E_{\rm gs} = \frac{U}{2} \left(1 - \sqrt{1 + \frac{16t^2}{U^2}} \right) \quad (3.14)$$

and the exited states have energies

$$E = 0, \;\; U, \;\; \text{and} \;\; \frac{U}{2} \left(1 + \sqrt{1 + \frac{16t^2}{U^2}} \right) \quad (3.15)$$

Figure 3.1 displays the eigenenergies of the inhomogeneous Hubbard dimer for representative cases as a function of the strength of the Coulomb repulsion. One observes the well known decrease of the ground state energy when U/t increases. It reaches its minimum value $E_{\rm gs} = 0$ for $U/t \to \infty$, when the electrons are fully and homogeneously localized.
The one-particle density matrix of the ground states $\gamma = \sum_{\sigma} \langle \Psi_{\rm gs} | \hat{c}^{\dagger}_{i,\sigma} \hat{c}_{j,\sigma} | \Psi_{\rm gs} \rangle$ is given in terms of the coefficients of the ground-state wave function $|\Psi_{\rm gs}\rangle = \sum_{i=1}^{4} \alpha_i |i\rangle$ as

$$\gamma = \begin{pmatrix} 2\alpha_1^2 + \alpha_3^2 + \alpha_4^2 & 2\alpha_3(\alpha_1 + \alpha_2) \\ 2\alpha_3(\alpha_1 + \alpha_2) & 2\alpha_2^2 + \alpha_3^2 + \alpha_4^2 \end{pmatrix} \quad (3.16)$$

Without Coulomb interaction ($U_i = 0$), the ground-state energy is the result of the interplay between the electron delocalization and the charge-transfer energy between the

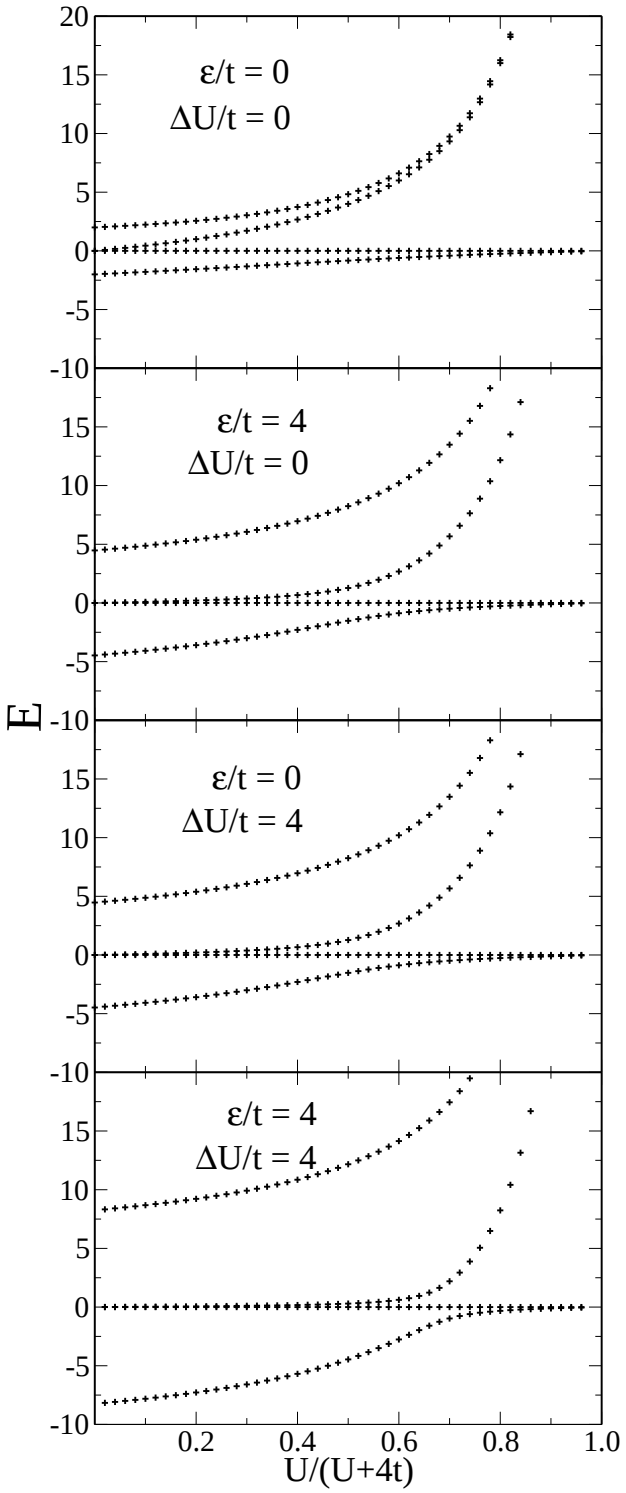

Figure 3.1: Eigenenergies of the inhomogeneous Hubbard dimer for representative values of the energy level shift ε/t and of the difference ΔU between the on-site Coulomb repulsions, as a function of the strength of the Coulomb repulsion U/t.

two sites. The charge transfer between the two sites induced by the inhomogeneity is $\Delta n = \gamma_{22} - \gamma_{11} = 2(\alpha_2^2 - \alpha_1^2)$. For a finite value of ε/t the ground state is a charge density wave, since one site contains more electrons that the other. Increasing the strength of the Coulomb repulsion tends to localize the electrons and to cancel the kinetic energy for $U/t \to \infty$, since the probability amplitude of states $|1\rangle$ and $|2\rangle$ is suppressed. This also renders the charge distribution progressively very homogeneous ($\Delta n \to 0$). Using Eq. (3.16) and the normalization condition of the basis set $\left(\sum_{i=1}^{4} \alpha_i^2 = 1\right)$ we can compute the average number of double occupations per site $\omega_1 = \alpha_1^2$ and $\omega_2 = \alpha_2^2$ as a function of the density matrix. Thus, one finds

$$\omega_i = \frac{\gamma_{ii}}{2} - \frac{\gamma_{12}^2}{4}\left(\frac{1 + \sqrt{1 - (\Delta n/2)^2 - \gamma_{12}^2}}{\gamma_{12}^2 + (\Delta n/2)^2}\right) \tag{3.17}$$

Notice that if one knows the ground-state density matrix, the Coulomb repulsion energy can be directly obtained.
In the case of an attractive electronic interaction ($U < 0$) the same calculations can be done. For example, one gets for the ground state energy of the homogeneous case

$$E_{\mathrm{gs}} = \frac{U}{2}\left(1 + \sqrt{1 + \frac{16t^2}{U^2}}\right). \tag{3.18}$$

In this case the process of localization is totally different. In fact, by increasing the strength of the interaction, the amplitude of the neutral states $|3\rangle$ and $|4\rangle$ is suppressed. The kinetic energy is then also reduced, but the nature of the ground state, where all electrons are paired is totally different in comparison to the repulsive interaction case.

3.2.2 Exact solution for the 1D Hubbard model: The Bethe *Ansatz*

Even though the diagonalization can be solved analytically for the Hubbard dimer, dealing with bigger systems is still a challenge. Due to the electronic interaction, one has to consider the full N-body basis set to diagonalize the Hubbard Hamiltonian. The problem lies in the fact that the size of this basis increases exponentially as a function of the size of the system as is shown in Fig. 3.2. It is possible to diagonalize numerically the Hamiltonian by using recursive methods (for instance the Lanczos method [42]) only for small clusters (up to 16 sites). However, there is in general no exact solution for bigger systems. A known solution is available in the case of one-dimensional homogeneous systems with NN hopping. The method, named the *Bethe Ansatz*, was proved by Lieb and Wu [18]. It takes the name from a similar method to solve the Heisenberg model in one dimension introduced by Bethe [58].
In the following, we present just the results obtained by Lieb and Wu [18], as one can find the complete demonstration in the literature [59]. Note that an investigation using the Bethe *Ansatz* and LDFT has also been performed in Ref. [33].

At the thermodynamic limit, $N_a \to \infty$, at fixed band filling N_e/N_a and a magnetization M/N_a, one obtains,

$$2\pi\rho(k) = 1 + \cos(k)\int_{-B}^{B} \frac{8U\sigma(\Lambda)d\Lambda}{U^2 + 16(\sin k - \Lambda)^2} \tag{3.19}$$

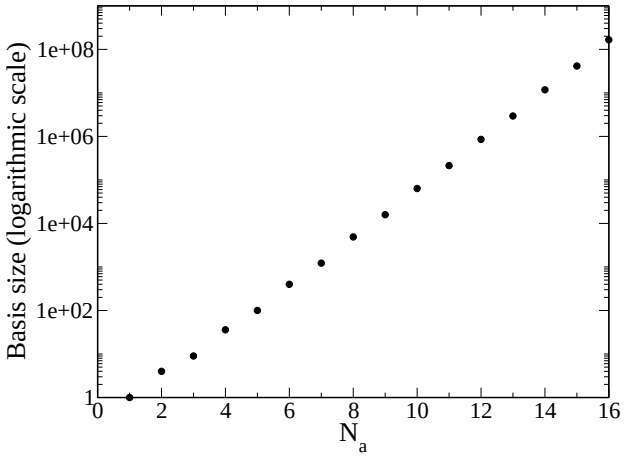

Figure 3.2: Size of the N-body basis as a function of the size of the system N_a at half-band filling and $S_z = 0$.

and

$$\int_{-Q}^{Q} \frac{8U\rho(k)dk}{U^2 + 16(\sin k - \Lambda)^2} = 2\pi\sigma(\Lambda) + \int_{-B}^{B} \frac{8U\sigma(\Lambda')d\Lambda'}{U^2 + 4(\Lambda - \Lambda')^2}, \tag{3.20}$$

where the real number k and Λ are distributed continuously between $-Q$ and $Q \leq \pi$ and $-B$ and $B \leq \infty$, with density function $\rho(k)$ and $\sigma(\Lambda)$ respectively. Q and B are determined by the conditions

$$\int_{-Q}^{Q} \rho(k)dk = \frac{N_e}{N_a} \quad \text{and} \quad \int_{-B}^{B} \sigma(\Lambda)d\Lambda = \frac{M}{N_a}. \tag{3.21}$$

Finally, the ground state energy is

$$E_{\text{gs}} = -2N_a t \int_{-Q}^{Q} \rho(k)\, \cos(k)\, dk. \tag{3.22}$$

The ground-state energy, the chemical potential, and the charge gap can be determined by solving the equations (3.19), (3.20) and (3.21) with an iterative method. This was done by Shiba [60]. In Fig 3.3 we show the results of the Bethe *Ansatz* for the ground state energy of an infinite homogeneous chain as a function of the band filling $n = N_e/N_a$. Representative values of the Coulomb repulsion are considered as shown in the figure. One observes that for low band filling ($n \leq 0.4$) the correlation effects are weak, since the electrons do not "see" each other. In contrast, the effect of correlations is really important near half-band filling. These lead to a drastic reduction of the kinetic energy in order to avoid double occupations. At the strongly correlated limit, the system becomes more localized. Near half-band filling the model is then equivalent to the tJ model of localized spins with hole conduction, as will be shown later on. It is also relevant to compute chemical potentials at half-band filling $\mu_+ = E(M+1, M, U) - E(M, M, U)$ and $\mu_- = E(M, M, U) - E(M-1, M, U)$, where $E(N_{e,\uparrow}, N_{e,\downarrow}, U)$ is the energy of the chain for a given Coulomb integral U, number of up electrons $N_{e,\uparrow}$ and down electrons $N_{e,\downarrow}$. Lieb

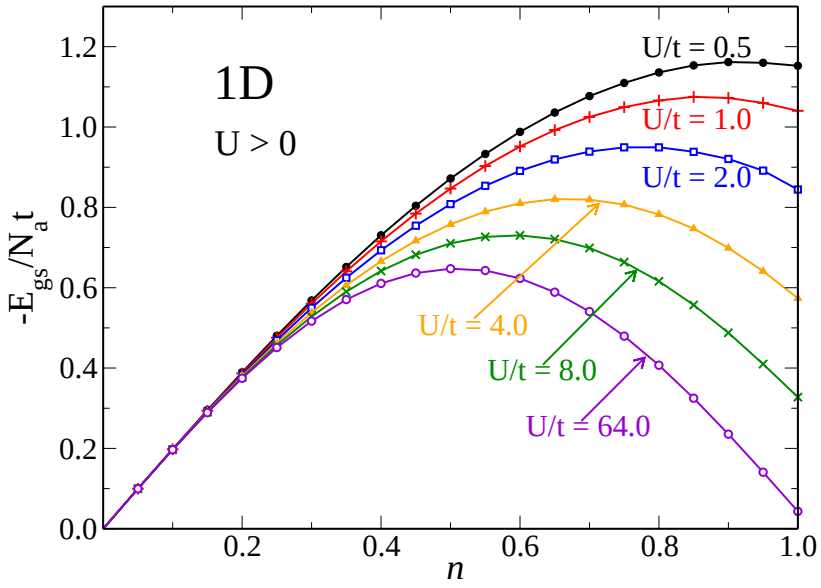

Figure 3.3: Ground state energy per site $E_{\rm gs}$ of an infinite homogeneous Hubbard chain as a function of the band filling $n = N_e/N_a$. Representative values of the strength of the Coulomb repulsion are considered.

and Wu have shown that at half-band filling for an arbitrary small value of U the charge gap $\Delta E_c = \mu_+ - \mu_-$ is always strictly positive. This result proves that for any $U \neq 0$ the system is an insulator and that the 1D Hubbard chains do not have a Mott-transition at finite U.

3.2.3 The Nagaoka theorem

In this section we present two theorems, originally proven by Nagaoka [19] which concern the atomic limit of the Hubbard models near half band filling. Even though these two theorems do not present a general solution for the Hubbard model, they give us a good idea of the nature of the ground state at this limit. We will use these theorems to approximate the strongly correlated limit of the density matrix for some implementations of our method [61]. In order to present it, we follow the more general formulation by Tasaki [57]. Let us consider a lattice Λ of N_a sites enumerated from $i = 1, ..., N_a$. The Hubbard Hamiltonian is given by

$$\hat{H} = \sum_{i,j,\sigma} t_{ij} \hat{c}^{\dagger}_{i,\sigma} \hat{c}_{j,\sigma} + V(\hat{n}_{i,\uparrow} + \hat{n}_{i,\downarrow}) + U \sum_{i} \hat{n}_{i,\sigma} \hat{n}_{i,\bar{\sigma}}, \tag{3.23}$$

where

$$V(\hat{n}_{i,\uparrow} + \hat{n}_{i,\downarrow}) = \sum_{i,\sigma} \varepsilon_i \, \hat{n}_{i,\sigma} + \frac{1}{2} \sum_{i,j,\sigma} W_{ij} (\hat{n}_{i,\sigma} + \hat{n}_{i,\bar{\sigma}})(\hat{n}_{j,\sigma} + \hat{n}_{j,\bar{\sigma}}) \tag{3.24}$$

and ε_i, and W_{ij} are arbitrary parameters. Furthermore, we assume that the Coulomb repulsion U is infinitely large, so that each site is occupied by at most one electron. Let

us recall the form of the spin operators by

$$\begin{aligned} \hat{S}_+ &= (\hat{S}_-)^\dagger = \sum_i \hat{c}^\dagger_{i,\uparrow}\hat{c}_{i,\downarrow}, \\ \hat{S}_z &= \frac{1}{2}\sum_i (\hat{n}_{i,\uparrow} - \hat{n}_{i,\downarrow}), \end{aligned} \tag{3.25}$$

and

$$\hat{\mathbf{S}}^2 = {S_z}^2 + \frac{1}{2}(S_+S_- + S_-S_+). \tag{3.26}$$

It is easy to see that $\hat{\mathbf{S}}^2$ commutes with $\hat{H}$. As usual, the eigenvalue of $\hat{\mathbf{S}}^2$ are denoted by $S(S+1)$. The conditions for the validity of the theorems are the following:

(i) All hopping matrix elements t_{ij} are non-negative.

(ii) The band filling is such that there is just one hole with respect to half filling, i.e., $N_e = N_a - 1$. Electron-hole symmetry, if available will allow us to apply the theorem also for $N_e = N_a + 1$.

(iii) The Coulomb repulsion integral U is infinitely large, i.e., $U \to \infty$.

(iv) The many-body Hilbert space of the model is connected. This condition, which is specified later on in more detail, requires that all many-body configurations are connected by the Hamiltonian operator. It is satisfied, for example, when the hopping matrix connects all the lattice (e.g., for $t_{ij} = -t$ for nearest neighbors (NN) ij).
Then, one can show the following theorem:

Nagaoka Theorem : Given the Hubbard Hamiltonian [Eq. (3.23)] with the conditions *(i)* to *(iii)* there exist at least $2S + 1 = N_a$ states with $S = S_{max} \equiv (N_a - 1)/2$ and $S_z = -S, ..., S$ among the ground states of the model.

Tasaki's extension (uniqueness): If, in addition, the condition *(iv)* is fulfilled, the ground state having $S = S_{max} \equiv (N_a - 1)/2$ is unique, besides the $2S + 1$ spin rotational degeneracy.

We specify now the connectivity condition *(iv)* and prepare the proof. For $N_e = N_a - 1$ a complete set of basis states of the model can be defined as

$$|i, \sigma\rangle = (-1)^i \hat{c}^\dagger_{1,\sigma_1}\hat{c}^\dagger_{2,\sigma_2}...\hat{c}^\dagger_{i-1,\sigma_{i-1}}\hat{c}^\dagger_{i+1,\sigma_{i+1}}...\hat{c}^\dagger_{N_a,\sigma_{N_a}}|0\rangle \tag{3.27}$$

where i denotes the position of the unique hole and $\sigma = \{\sigma_j\}_{j\neq i}$ is a multi-index defining the S_z projector of the spin of each electron. One says that two states $|i, \sigma\rangle$ and $|j, \tau\rangle$ of the basis are directly connected to each other if

$$\langle j, \tau|t_{ij}(\hat{c}^\dagger_{i,\sigma}\hat{c}_{j,\sigma} + \hat{c}^\dagger_{j,\sigma}\hat{c}_{i,\sigma})|i, \sigma\rangle = -t_{ij} \neq 0 \tag{3.28}$$

This is usually denoted by $|i, \sigma\rangle \leftrightarrow |j, \tau\rangle$. We also define that a lattice Λ satisfies the connectivity condition *(iv)* if all states $|i, \sigma\rangle$ with the same value of S_z are connected to each other in the formentioned sense.
Note that for finite systems it is obvious, that the statement of the theorem is also true for finite but sufficiently large U when the conditions of the Tasaki extension are satisfied,

except for condition *(iii)*. However there is no information about how U large should be.

Proof of Nagaoka's theorem: Let $|\Psi\rangle = \sum_{(i,\sigma)} \psi_{i,\sigma}|i,\sigma\rangle$ be an arbitrary normalized state. We define a state $|\Phi\rangle$, having $S = S_{max}$, as $|\Phi\rangle = \sum_i \phi_i |i,\{\uparrow\}\rangle$ where $\phi_i = \left(\sum_\sigma |\psi_{i,\sigma}|^2\right)^{1/2}$. The multi-index $\{\uparrow\}$ represents that all electrons have up spin (i.e, $\sigma_i = \uparrow,\ \forall i$). It follows

$$\begin{aligned}\langle\Psi|V(\hat{n}_{i,\uparrow}+\hat{n}_{i,\downarrow})|\Psi\rangle &= \sum_{(i,\sigma)} |\phi_{i,\sigma}|^2 \langle i,\sigma|V|i,\sigma\rangle = \sum_{(i,\sigma)} |\psi_{i,\sigma}|^2 \langle i,\{\uparrow\}|V|i,\{\uparrow\}\rangle \\ &= \langle\Phi|V(\hat{n}_{i,\uparrow}+\hat{n}_{i,\downarrow})|\Phi\rangle \end{aligned} \tag{3.29}$$

Using the Schwartz inequality, one obtains

$$\begin{aligned}\langle\Psi|t_{ij}(\hat{c}^\dagger_{i,\sigma}\hat{c}_{j,\sigma}+\hat{c}^\dagger_{j,\sigma}\hat{c}_{i,\sigma})|\Psi\rangle &= \sum_{\langle\sigma,\tau\rangle}(-t_{ij})\psi^*_{j,\tau}\psi_{i,\sigma} \geq (-t_{ij})\phi^*_j\phi_i \\ &\geq \langle\Phi|t_{ij}(\hat{c}^\dagger_{i,\sigma}\hat{c}_{j,\sigma}+\hat{c}^\dagger_{j,\sigma}\hat{c}_{i,\sigma})|\Phi\rangle \end{aligned} \tag{3.30}$$

where the sum in Eq. (3.30) runs over all pairs of spin configurations σ,τ such that $|i,\sigma\rangle \leftrightarrow |j,\tau\rangle$. This relation implies that the energy corresponding to the state $|\Phi\rangle$ is alway smaller or equal than the energy of the original state $|\Psi\rangle$. Then the proof of the theorem is completed by considering that $|\Psi\rangle$ is one of the ground states and using the SU(2) symmetry of the model (i.e., the spin rotational symmetry following from $[\vec{S},\hat{H}]=0$).

Proof of Tasaki's extension: To establish this theorem we use the Perron-Frobenius theorem.[1] The off-diagonal matrix element $\langle j,\tau|\hat{H}|i,\sigma\rangle = t_{ij}$ are non-vanishing when $|i,\sigma\rangle \leftrightarrow |j,\tau\rangle$. Also, the connectivity condition ensures that in any subspace with fixed S_z the matrix $\langle j,\tau|\hat{H}|i,\sigma\rangle$ is irreducible. Then by taking $\mathbf{M} = -\hat{H}$, the Perron-Frobenius theorem implies, that in each sector with fixed S_z the state with minimum energy is unique. Since the ground state is known to have $S = S_{max}$ and the system has SU(2) symmetry, the extension of Nagaoka's theorem follows.

3.3 Mean field theories

As was already pointed out in the previous section, only few special cases of the Hubbard model have an exact solution. A lot of approximations exist to approach the problem. For example the Hubbard I approximation [16] using perturbation theory around the atomic limit ($t = 0$). Many other approximations were developed later as for example the dynamical mean-field theory (DMFT) [23] or numerical methods such as the density matrix renormalization group [24]. In the following we present two mean field approximations. The first one, is the most basic Hartree-Fock approximation. The main purpose here is to demonstrate that the effects of correlation are very important and that simple mean-field approximation fails to reproduce the physics of correlated materials. The second example is the slave-boson theory in the saddle point approximation. Here, additional

[1] Let $\mathbf{M} = \{M_{ij}\}$ be a $N_a \times N_a$ matrix with positive matrix elements ($M_{ij} \geq 0\ \ i \neq j$). $\mathbf{M}$ is assumed to be indecomposable in the sense that, for any i,j there is a sequence $\{i_1, i_2, ...i_K\}$ with $i = i_1$ and $j = i_K$, and $M_{i_k i_{k+1}} \neq 0\ \ \forall k < K$. Then the eigenstate of $\mathbf{M}$ with maximum eigenvalue is unique (up to normalization), and give a linear combination of all the basis vectors with strictly positive coefficients.

boson operators are introduced in order to trace back the many-body configurations of the systems from a local perspective. The saddle point or mean field approximation applies to these additional degrees of freedom. Both methods will be used later on in this thesis for the sake of comparison.

3.3.1 Hartree-Fock approximation

For the sake of comparison, it is first convenient, to approach the problem within a simple approximation. In this sense it is justified to present the Hartree-Fock approximation. This approximation is well known and it is presented in many books of solid state physics [see for example [14, 16]]. Unfortunately, this simple scheme fails to reproduce most of the properties of this Hamiltonian as discussed at the end of the section.
One may obtain the effective one-particle Hartree-Fock Hamiltonian either by making an ad hoc mean-field approximation or by applying the Wick theorem to a single Slater determinant *Ansatz* wave function. $\hat{n}_{i,\sigma}\hat{n}_{i,\bar{\sigma}} = \langle\hat{n}_{i,\sigma}\rangle\hat{n}_{i,\bar{\sigma}} + \langle\hat{n}_{i,\bar{\sigma}}\rangle\hat{n}_{i,\sigma}$. Then the Hamiltonian Eq. (3.10) becomes

$$H^{HF} = \sum_{i,j,\sigma} t_{ij}\hat{c}^{\dagger}_{i,\sigma}\hat{c}_{j,\sigma} + U\sum_{i,\sigma}\langle\hat{n}_{i,\bar{\sigma}}\rangle\hat{n}_{i,\sigma}. \tag{3.31}$$

Performing a Fourier transform to reciprocal space in the homogeneous case ($\langle\hat{n}_{i,\sigma}\rangle = n_{\sigma}\ \ ,\forall i$) we obtain

$$H^{HF} = \sum_{\mathbf{k},\sigma}\left(\epsilon_{\mathbf{k}} + Un_{\bar{\sigma}}\right)\hat{c}^{\dagger}_{\mathbf{k},\sigma}\hat{c}_{\mathbf{k},\sigma}. \tag{3.32}$$

This mean-field Hamiltonian describes a collection of non-interacting particle with a modified band structure. The eigenvalues of a $(\mathbf{k},\sigma)$ state are shifted to $\epsilon_{\mathbf{k}} + Un_{\bar{\sigma}}$ and the density of states $\rho_{\sigma}(E)$ is equal to

$$\rho_{\sigma}(E) = \rho_0(E - Un_{\bar{\sigma}}) = \rho_0(E - Un + Un_{\sigma}) \tag{3.33}$$

where ρ_0 is the density of states for the non interacting case. The number of particles must be conserved, which requires

$$n_{\uparrow} + n_{\downarrow} = n. \tag{3.34}$$

The self-consistency implied by the saddle-point or minimum energy condition is obtained by calculating the number of electrons from the modified band structure:

$$n_{\sigma} = \int_{-\infty}^{\mu} dE\ \rho_0(E - Un + Un_{\sigma}). \tag{3.35}$$

Solving selfconsistent Eqs. (3.34) and (3.35) give the solution of the Hartree-Fock approximation.
Notice that the Hubbard Hamiltonian defined in Eq. (3.10) has the $SU(2)$ symmetry, which means that it is spin rotation invariant. Without the presence of a magnetic field, the solution should be non-magnetic ($n_{\uparrow} = n_{\downarrow} = n/2$). However, for large U it is possible to find a ferromagnetic solution which is energetically more stable. The condition of ferromagnetism can be found from Eq. (3.33) as

$$1 = U\rho_0(\mu - Un/2). \tag{3.36}$$

In fact, if the condition $U\rho_0(E) > 1$ is fulfilled for E equal to the paramagnetic Fermi energy the Hartree-Fock approximation predicts a ferromagnetic state. This implies breaking the spin-rotational symmetry. Another drawback of this approximation concerns the charge gap. It can be shown that the charge gap always vanishes in the paramagnetic phase using Hartree-Fock approximation. This would mean that the system remains metallic, even in the strongly correlated limit.

3.3.2 Slave-boson approximation

The slave-boson theory [22] was originally proposed in order to extend the original Fock space of a Hubbard or Anderson Hamiltonian by introducing auxiliary bosons. Within a saddle-point approximation, one gets an approximation of the problem which provides an alternative interesting perspective. At zero temperature it leads to the results derived from the Gutzwiller variational wave function [55].
For the Hubbard model, we enlarge the Fock space using for each site four bosons represented by the creation (annihilation) operators $\hat{e}_i^\dagger$ ($\hat{e}_i$) if the site i is empty, $\hat{p}_{i,\sigma}^\dagger$ ($\hat{p}_{i,\sigma}$) if the site i contains one electron with spin σ, and finally $\hat{d}_i^\dagger$ ($\hat{d}_i$) if the site is doubly occupied. For each site these bosons fullfil the normalization condition,

$$\sum_\sigma \hat{p}_{i,\sigma}^\dagger \hat{p}_{i,\sigma} + \hat{e}_i^\dagger \hat{e}_i + \hat{d}_i^\dagger \hat{d}_i = 1, \tag{3.37}$$

which should be regarded as a operator identity. Moreover they have to respect the electronic occupation on each site as given by the Fermion number operator.

$$\hat{c}_{i,\sigma}^\dagger \hat{c}_{i,\sigma} = \hat{p}_{i,\sigma}^\dagger \hat{p}_{i,\sigma} + \hat{d}_i^\dagger \hat{d}_i. \tag{3.38}$$

In the physical subspace defined by Eqs. (3.37) and (3.38) the Hamiltonian can be written by using both Fermion and Boson operators as

$$\tilde{H} = \sum_{i,j,\sigma} t_{ij} z_{i,\sigma}^\dagger z_{j,\sigma} \hat{c}_{i,\sigma}^\dagger \hat{c}_{j,\sigma} + U \sum_i \hat{d}_i^\dagger \hat{d}_i \tag{3.39}$$

with

$$\hat{z}_{i,\sigma} = \hat{e}_i^\dagger \hat{p}_{i,\sigma} + \hat{p}_{i,\bar{\sigma}}^\dagger \hat{d}_i. \tag{3.40}$$

$\tilde{H}$ has the same matrix elements as the Hubbard model [Eq. (3.10)] in the original purely fermionic Hilbert space.
In the following we focus on the homogeneous case (all sites are equivalent) at $T = 0$. In order to calculate the ground-state properties we perform a saddle point approximation in which the degrees of freedom of the bosons are treated as scalar fields. It is important to note that at the non-interacting limit ($U = 0$) this approximation leads to incorrect results, since the operator constraints (3.37) and (3.38) are only satisfied on average, i.e., not explicitly for each many-body configuration. For $U = 0$, the four bosonic degrees of freedom have same probability ($e^2 = d^2 = p_\sigma^2 = 1/4$) and

$$\langle \hat{z}_{i,\sigma}^\dagger \hat{z}_{j,\sigma} \rangle = e^2 p_\sigma^2 + d^2 p_{\bar{\sigma}}^2 + 2edp_\sigma p_{\bar{\sigma}} = 1/4 \tag{3.41}$$

rather than the unity as it should be for the non-interacting case where no renormalization of the hopping integral is expected. Nevertheless, this problem can be solved by

realizing that $z_{i,\sigma}$ can be consider as scalar product between vectors operator $(\hat{e}_i^\dagger, \hat{p}_{i,\bar{\sigma}}^\dagger)$ and $(\hat{p}_{i,\sigma}, \hat{d}_i)$. In order that the scalar product yield 1, when the vectors are parallel, i.e., in the uncorrelated limit, they must be properly renormalized. This is achieved by dividing them by their respective norm. This implies that the hopping renormalization operator $z_{i,\sigma}$ becomes

$$\tilde{z}_{i,\sigma} = \left(\hat{e}_i^\dagger \hat{e}_i^\dagger + \hat{p}_{i,\bar{\sigma}}^\dagger \hat{p}_{i,\bar{\sigma}}\right)^{1/2} \hat{z}_{i,\sigma} \left(\hat{d}_i^\dagger \hat{d}_i^\dagger + \hat{p}_{i,\sigma}^\dagger \hat{p}_{i,\sigma}\right)^{1/2}, \tag{3.42}$$

which satisfies the expected behavior $\langle \tilde{z}_{i,\sigma}^\dagger \tilde{z}_{j,\sigma} \rangle = 1$ in the $U = 0$ limit. Notice that in the physical space $\tilde{z}_{i,\sigma}$ has the same matrix elements as the more intuitive $\hat{z}_{i,\sigma}$.
The resulting saddle-point energy obtained from the Hamiltonian (3.39) reads

$$\varepsilon = Ud^2 + 2\int_{-\infty}^{+\mu} d\xi \rho_0(\xi) q\xi, \tag{3.43}$$

where $q = \langle \tilde{z}_{i,\sigma}^\dagger \tilde{z}_{j,\sigma} \rangle$, $\rho_0(\xi)$ is the single-particle density of states and μ the chemical potential. Eq. (3.43) has to be solve together with the constraint

$$n_\sigma = \int_{-\infty}^{+\mu} d\xi \, \rho(\xi). \tag{3.44}$$

derived from Eq. (3.38). The set of equations (3.43) and (3.44) define the solution of the slave-boson mean-field approximation for a homogeneous lattice at $T = 0$.
In order to illustrate this approach, we follow Ref. [22] and consider a system with a symmetric density of states at half filling ($n = 1$). In this case $\mu = U/2$ and $q = 8d^2(1-2d^2)$. ε is minimized by $d^2 = 1/4(1 - U/U_c)$ with $U_c = 16\int_0^{+\infty} d\xi \rho(\xi)\xi$ proportional to the energy of the non-interacting case. For $U = U_c$ the average number of double occupations is zero as well as the kinetic energy ($q = 0$). This indicates that the system becomes an insulator as a result of electron-electron interaction, which is usually denoted as Mott insulator.
Thus, the approximation is able to describe quanlitatively the metal-insulating transition driven by correlations. For $U < U_c$ the system is metallic but for $U \geq U_c$ it becomes insulator. It should be recalled that for some systems a finite gap opens in the low-energy spectrum already for arbitrary small U, for example, in the 1D and 2D homogeneous Hubbard model. Obviously, the paramagnetic or spin restricted slave boson theory provides an upper estimate of the value of this critical U_c.

3.4 Related models: tJ and Heisenberg models

Besides the Hubbard model, other simple many body Hamiltonians have been proposed to study the low energy electronic properties of strongly correlated materials. For example, the tJ and Heisenberg Hamiltonians. The tJ and Heisenberg models, which can be derived perturbatively from the atomic limit of the Hubbard model, focuses on different magnetic orders of system with localized magnetic moments. In this section, we present a short introduction of these models, focusing on the link with the Hubbard Hamiltonian. It is also possible to find more detailed studies about the physics of these systems in the literature [14, 17, 38, 62].

Even though this thesis does not focus on such models, it is useful to give a general idea of the physics of these two Hamiltonians. In particular, it is instructive to show the direct

relation with the Hubbard model at the atomic limit. Both the tJ and the Heisenberg model are devoted to studying the magnetic properties of a system with localized spins. In addition, the tJ model describes the interplay between the electronic interactions, responsible for antiferromagnetic order at half band filling and the delocalization of an extra electron or hole (kinetic energy).
These systems consider a ensemble of ions or atoms from which the low-energy states are described by the spin operator $\vec{S}_i$ for each site. The Hamiltonian of these two models are given by

$$\hat{H}^{tJ} = t\sum_{i,j,\sigma}(1-\hat{n}_{i,\bar{\sigma}})\hat{c}^{\dagger}_{i,\sigma}\hat{c}_{j,\sigma}(1-\hat{n}_{j,\bar{\sigma}}) + \sum_{i,j} J_{ij}\left(\vec{S}_i.\vec{S}_j - \frac{1}{4}\right) \tag{3.45}$$

$$\hat{H}^{H} = \sum_{i,j} J_{ij}\left(\vec{S}_i.\vec{S}_j - \frac{1}{4}\right) \tag{3.46}$$

The Heisenberg Hamiltonian has been very important to understand finite temperature properties of magnetic materials. On the other hand, it is well justified from a microscopic point of view when the magnetic moments are localized such as is the case for rare earth elements. However, it is not appropriate for describing systems with itinerant electrons, like for example transition metals, in particular for their metallic character. However, this can be treated using the tJ model which includes the kinetic energy of holes.
Historically, the Heisenberg model has been proposed before the Hubbard model on simple symmetry arguments. We propose here to use the Schrieffer-Wolf transformations (originally introduced in the context of the Kondo problem) [62] in order to derive the tJ and Heisenberg Hamiltonians from the Hubbard model [63]. Starting from the Hubbard Hamiltonian for a homogeneous system with NN hopping

$$H = t\sum_{i,j,\sigma}\hat{c}^{\dagger}_{i,\sigma}\hat{c}_{j,\sigma} + U\sum_{i}\hat{n}_{i,\sigma}\hat{n}_{i,\bar{\sigma}} \tag{3.47}$$

we focus on the limit where $U/t >> 1$ is large enough (but not infinite) at half filling or near to half-band filling. In this limit, the kinetic term can be treated as a perturbation. Two terms contribute to order t or t^2/U to the energy. The first one is the hopping term associated to the motion of holes which is proportional to t, i.e., independent of U. This energy vanishes at half-band filling $n = 1$ since there is one electron on each site. The second contribution is the contribution of *virtual* hopping involving the creation and the annihilation of a hole or electron-pair by NN hopping. The other processes are negligible, since they contribute with an energy of order U. Taking into account these considerations we transform the Hubbard model Eq. (3.47) to an effective Hamiltonian which describes these processes. In order to do that we need, first of all, to divide the kinetic part of the

Hamiltonian into various contributions:

$$\begin{aligned} H^{Hubbard} &= T_h + T_d + T_{mix} + V \quad \text{where,} \\ T_h &= t\sum_{i,j,\sigma}(1-\hat{n}_{i,\bar{\sigma}})\hat{c}^{\dagger}_{i,\sigma}\hat{c}_{j,\sigma}(1-\hat{n}_{j,\bar{\sigma}})\,, \\ T_d &= t\sum_{i,j,\sigma}\hat{n}_{i,\bar{\sigma}}\hat{c}^{\dagger}_{i,\sigma}\hat{c}_{j,\sigma}\hat{n}_{j,\bar{\sigma}}\,, \\ T_{mix} &= t\sum_{i,j,\sigma}(1-\hat{n}_{i,\bar{\sigma}})\hat{c}^{\dagger}_{i,\sigma}\hat{c}_{j,\sigma}\hat{n}_{j,\bar{\sigma}} + \sum_{i,j,\sigma}\hat{n}_{i,\bar{\sigma}}\hat{c}^{\dagger}_{i,\sigma}\hat{c}_{j,\sigma}(1-\hat{n}_{j,\bar{\sigma}}) \quad \text{and,} \\ V &= U\sum_{i}\hat{n}_{i,\sigma}\hat{n}_{i,\bar{\sigma}} \end{aligned} \tag{3.48}$$

T_h describes the transport of a hole, T_d the transport of double occupancy and finally T_{mix} the hopping term involving a creation (or destruction) of a hole or electron double occupancies. Notice that T_h and T_d do not connect different Hubbard bands in contrast to T_{mix}.
In the limit of large U/t and near the half-band filling, the term to be considered as perturbative is T_{mix}, since it involves the creation (or destruction) of a *virtual* electron-hole pair as well as a double occupation. We now apply a canonical transformation

$$\tilde{H} = e^{S}He^{-S} = H_0 + [S, T_{mix}] + ... \tag{3.49}$$

where $H_0 = T_h + T_d + V$ and $\tilde{H}$ has no term which is first order in T_{mix}. This implies that

$$[H_0, S] = T_{mix}. \tag{3.50}$$

From Eq. (3.50) one can deduce the generator S as

$$S = \frac{t}{U}\left(\sum_{i,j,\sigma}\hat{n}_{i,\bar{\sigma}}\hat{c}^{\dagger}_{i,\sigma}\hat{c}_{j,\sigma}(1-\hat{n}_{j,\bar{\sigma}}) - \sum_{i,j,\sigma}(1-\hat{n}_{i,\bar{\sigma}})\hat{c}^{\dagger}_{i,\sigma}\hat{c}_{j,\sigma}\hat{n}_{j,\bar{\sigma}}\right) \tag{3.51}$$

Using this transformation, one finds that

$$\tilde{H} = T_h + T_d + V + H_U + H_{ex} + H_{pair} + \mathcal{O}(t^3/U) \tag{3.52}$$

with

$$H_U = \frac{t^2}{U}\sum_{i,j,\sigma}(\hat{n}_{i,\sigma}\hat{n}_{i,\bar{\sigma}} + \hat{n}_{j,\sigma}\hat{n}_{j,\bar{\sigma}}) \tag{3.53}$$

$$H_{ex} = \frac{t^2}{U}\left(\sum_{i,j,\sigma}(\hat{n}_{i,\sigma}\hat{n}_{j,\bar{\sigma}} + \hat{n}_{j,\sigma}\hat{n}_{i,\bar{\sigma}}) - \frac{1}{2}\sum_{i,j,\sigma}\left(\hat{c}^{\dagger}_{i,\sigma}\hat{c}_{i,\bar{\sigma}}\right)\left(\hat{c}^{\dagger}_{j,\bar{\sigma}}\hat{c}_{j,\sigma}\right)\right) \tag{3.54}$$

and

$$H_{pair} = \frac{2t^2}{U}\sum_{i,j,\sigma}\hat{c}^{\dagger}_{i,\sigma}\hat{c}^{\dagger}_{i,\bar{\sigma}}\hat{c}_{j,\sigma}\hat{c}_{j,\bar{\sigma}} \tag{3.55}$$

The effective Hamiltonian can be then deduced by neglecting some less important contributions. In fact, at large U/t and near the half filling the system has no double occupation. One can then neglect T_d, which represents the hopping of double occupations. For the same reason, one can neglect H_U [see Eq. (3.53)] and H_{pair} [see Eq. (3.55)] which implies that double occupations do not contribute either. Then, one deduces the tJ model as the effective Hamiltonian

$$H_{\text{eff}} = T_h + H_{ex} = t\sum_{i,j,\sigma}(1-\hat{n}_{i,\bar{\sigma}})\hat{c}^{\dagger}_{i,\sigma}\hat{c}_{j,\sigma}(1-\hat{n}_{j,\bar{\sigma}}) + \sum_{i,j} J_{ij}\left(\vec{S}_i.\vec{S}_j - \frac{1}{4}\right) \tag{3.56}$$

Whith $J = 4t^2/U$, which is valid in the large U/t limit and near half-band filling.
The Heisenberg model [see Eq. 3.46] is then obtained by considering the half filling case where H_h does not contribute.
In conclusion, the strongly correlated limit of the Hubbard model is equivalent to a system of localized spins interacting with an exchange coupling $J = 4t^2/U$. This previous knowledge is central to our understanding of the subtle $U/t >> 1$ limit. Moreover, it sets the challenge for our theoretical investigation, namely, describing this limit with the concepts of DFT.

3.5 Attractive electronic interaction

In this section we focus on the case of an attractive electronic interaction ($U < 0$). This model was proposed in literature to explain exotic properties of the normal states and the superconductor states of correlated Fermions [64, 65]. In the first section 3.5.1 we explain quanlitatively that an electron-phonon interaction can lead to an effective attractive electron-electron interaction which drives the formation of Cooper pairs between electrons and superconducting properties. In the second section we recall the BCS approximation, which gives a first approximation of properties of such correlated systems. Later-on we will use this approximation to compare our own results for the attractive Hubbard model [64, 65].

3.5.1 Attractive electron-electron interaction mediated by phonons

A common simplification in the condensed matter problem consists of separating the movement of nuclei and electrons (Born-Oppenheimer approximation). This separation finds its justification in the difference between the mass of nuclei and electrons. For example, for the hydrogen atom the mass of the proton is 10^3 bigger than the mass of the electron. Consequently, the time scale of the electronic motion is also around 10^3 smaller than the one of the motion of the ion. This quantitative argument justifies the fact that the electrons are nearly moving in a constant ionic potential and the Born-Oppenheimer approximation. However, this approximation is actually far too simple, since the electron motion couples with the lattice vibrations (phonon modes). This coupling, known as electron-phonon interaction, can lead to an effective attractive electron-electron interaction that we show in this sub-section.
Consider a simplified model for a solid formed by atomic nuclei and electrons. The total system is described by the Hamiltonian

$$\hat{H} = \hat{H}_{\text{nuclei}} + \hat{H}_{\text{el}} + \hat{H}_{\text{el-ph}}, \tag{3.57}$$

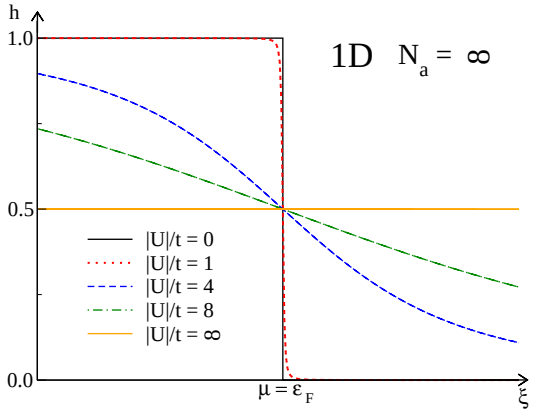

Figure 3.4: BCS electron distribution function $h_{\mathbf{k}}$ [see Eq. (3.68)] as a function of $\xi_{\mathbf{k}} = \epsilon_{\mathbf{k}} - \tilde{\mu}$, the energy of the k state shifted by the chemical potential for a 1D infinite chain at half-band filling and for different strengths of the attractive interaction $|U|/t$.

where $\hat{H}_{\text{nuclei}}$ is the Hamiltonian of the nuclei, $\hat{H}_{\text{el}}$ is the Hamiltonian of electrons containing their kinetic energy and interaction and $\hat{H}_{\text{el-ph}}$ is the effective interaction between electrons mediated by the phonons. The latter is normally written in the form [66]

$$\hat{H}_{\text{el-ph}} = \frac{1}{2} \sum_{\mathbf{k},\mathbf{k}',\mathbf{q},\sigma,\sigma'} \left[\frac{|g_{\mathbf{k}-\mathbf{k}'}|^2 \, \hbar \, \omega_{\mathbf{k}-\mathbf{k}'}}{(\epsilon_{\mathbf{k}} - \epsilon_{\mathbf{k}'})^2 - (\hbar\omega_{\mathbf{k}-\mathbf{k}'})^2} \right] \hat{c}^{\dagger}_{\mathbf{k}',\sigma} \hat{c}^{\dagger}_{\mathbf{k}+\mathbf{q},\sigma'} \hat{c}_{\mathbf{k}'+\mathbf{q},\sigma'} \hat{c}_{\mathbf{k},\sigma} \tag{3.58}$$

where $\hat{c}^{\dagger}_{\mathbf{k},\sigma}$ ($\hat{c}_{\mathbf{k},\sigma}$) are the usual creation (annihilation) operators of an electron with spin σ in a Bloch state with wave vector $\mathbf{k}$ associated with a single particle energy $\epsilon_{\mathbf{k}}$. The interaction Eq. (3.58) is attractive for small $\epsilon_{\mathbf{k}} - \epsilon_{\mathbf{k}'}$ and generally believed to be responsible for superconductivity. Cooper has shown that, neglecting the Coulomb interaction, and when the interaction Eq. (3.58) is attractive, this leads to the formation of electron pairs and superconductivity.

3.5.2 BCS approach for the Hubbard Hamiltonian

An alternative pairing mechanism is provided by the attractive Hubbard model. In this section we recall briefly the BCS theory [67] introduced to understand the superconductivity in presence of an attractive interaction. We follow the grand canonical formulation for a discrete lattice presented by K. Tanaka and F. Marsiglio [68] which is also described in many books [69]. For simplicity we constrain ourselves to the case of nearest neighbor hopping. With this condition, the Fourier transform in the $\mathbf{k}$ space of the Hubbard Hamiltonian reads

$$H = \sum_{\mathbf{k},\sigma} \epsilon_{\mathbf{k}} \hat{c}^{\dagger}_{\mathbf{k},\sigma} \hat{c}_{\mathbf{k},\sigma} - \frac{|U|}{N} \sum_{\mathbf{k},\mathbf{k}',q} \hat{c}^{\dagger}_{\mathbf{k},\uparrow} \hat{c}^{\dagger}_{-\mathbf{k}+\mathbf{q},\downarrow} \hat{c}_{-\mathbf{k}'+\mathbf{q},\downarrow} \hat{c}_{\mathbf{k}',\uparrow}. \tag{3.59}$$

Here we consider a lattice with periodic boundary conditions in each dimension for N sites. As usual, $\hat{c}_{\mathbf{k},\sigma}$ ($\hat{c}^{\dagger}_{\mathbf{k},\sigma}$) are the annihilation (creation) operators in the reciprocal space

and $\epsilon_{\mathbf{k}} = 2t\cos(\mathbf{k}.\mathbf{l})$ is the one-particle contribution ($\mathbf{l}$ is the lattice vector).
The BCS theory is based on a variational principle using an *Ansatz* wave function for a given number of pairs ν of electrons. The BCS wave function is a superposition of states with all the possible number of pairs $\{\nu\}$:

$$|BCS\rangle = c\prod_{\mathbf{k}}(1 + g_{\mathbf{k}}\hat{c}^{\dagger}_{\mathbf{k},\uparrow}\hat{c}^{\dagger}_{-\mathbf{k},\downarrow})|0\rangle, \tag{3.60}$$

where $|0\rangle$ denotes the Fermi sea and the coefficient c normalizes the wave function properly. This approximation do not conserve the particle number. Note that this formulation contrarily as the usual presentation has only the variational parameter $g_{\mathbf{k}}$ (and not the usual $u_{\mathbf{k}}$ and $v_{\mathbf{k}}$). Then we apply the variational principle to minimize the energy of the Hamiltonian Eq. (3.59) with the BCS wave function Eq. (3.60). This can be done by using the Lagrange constrained minimization and it can be read

$$\begin{aligned}
\mathcal{L} &= \frac{\langle BCS|H - \mu N|BCS\rangle}{\langle BCS|BCS\rangle} \\
&= 2\sum_{\mathbf{k}}(\epsilon_{\mathbf{k}} - \mu)\frac{g^2_{\mathbf{k}}}{1+g^2_{\mathbf{k}}} - \frac{|U|}{N}\sum_{\mathbf{k}}\frac{g^2_{\mathbf{k}}}{1+g^2_{\mathbf{k}}} \\
&\quad -\frac{|U|}{N}\sum_{\mathbf{k},\mathbf{k}'}\frac{g_{\mathbf{k}}}{1+g^2_{\mathbf{k}}}\frac{g_{\mathbf{k}'}}{1+g^2_{\mathbf{k}'}} - \frac{|U|}{N}\sum_{\mathbf{k}\neq\mathbf{k}'}\frac{g^2_{\mathbf{k}}}{1+g^2_{\mathbf{k}}}\frac{g^2_{\mathbf{k}'}}{1+g^2_{\mathbf{k}'}}
\end{aligned} \tag{3.61}$$

where μ is the chemical potential (Lagrange multipliers which ensure the conservation of the particle number). The first term of the precedent equation is the kinetic energy, the following two term come from the Cooper pair scattering ($q = 0$) and the last term is the Hartree term (scattering with $q \neq 0$). The *reduced* BCS Hamiltonian ($q = 0$ scattering only) not take into account this last term since is generally only shift the real part of the pole of Hamiltonian. However, it is important to keep it when one wants to compare BCS theory with exact or approximate solution of the attractive Hubbard model.
The next step is to carry out the variation with respect to the $g_{\mathbf{k}}$. It reads

$$2(\epsilon_{\mathbf{k}} - \tilde{\mu})g_{\mathbf{k}} = \Delta_{BCS}[1 - g^2_{\mathbf{k}}] \tag{3.62}$$

where

$$\tilde{\mu} = \mu + \frac{|U|}{N}\sum_{\mathbf{k}}\frac{g^2_{\mathbf{k}}}{1+g^2_{\mathbf{k}}} \tag{3.63}$$

and

$$\Delta_{BCS} = \frac{|U|}{N}\sum_{\mathbf{k}}\frac{g_{\mathbf{k}}}{1+g^2_{\mathbf{k}}}. \tag{3.64}$$

Which solution is

$$g_{\mathbf{k}} = \frac{E_{\mathbf{k}} - (\epsilon_{\mathbf{k}} - \tilde{\mu})}{\Delta_{BCS}} \tag{3.65}$$

where $E_{\mathbf{k}} = \sqrt{(\epsilon_{\mathbf{k}} - \tilde{\mu})^2 + \Delta^2_{BCS}}$ is the quasi-particle energy. It appears that Δ_{BCS} is shifting the quasi-particle energy (for $\Delta_{BCS} = 0$ the quasi-particles have the same energy that the eigenvectors of the normal state) and play the role of minimum energy gap induce

by the attractive interaction. Since Δ_{BCS} depends also of $g_{\mathbf{k}}$ this solution is only implicit and has to be determined by numerical iteration. The chemical potential is determined by using the number equation as

$$n = \frac{N_e}{N} = 1 - \frac{1}{N}\sum_{\mathbf{k}} \frac{\epsilon_{\mathbf{k}} - \tilde{\mu}}{E_{\mathbf{k}}}. \tag{3.66}$$

Finally the total energy of the system $E = \langle H \rangle = \langle \mathcal{L} + \mu N_e \rangle$ is given by

$$\frac{E}{N} = \frac{1}{N}\sum_{\mathbf{k}} \epsilon_{\mathbf{k}} \left(1 - \frac{\epsilon_{\mathbf{k}} - \tilde{\mu}}{E_{\mathbf{k}}}\right) - |U| \left(\frac{n}{2}\right)^2 - \frac{\Delta_{BCS}}{|U|} \tag{3.67}$$

The function

$$h_{\mathbf{k}} = \frac{1}{2}\left(1 - \frac{\epsilon_{\mathbf{k}} - \tilde{\mu}}{(\epsilon_{\mathbf{k}} - \tilde{\mu})^2 + \Delta_{BCS}^2}\right) \tag{3.68}$$

corresponds to the distribution of the electrons in the $\mathbf{k}$ space. If Fig. (3.4) we present h_k as the function $\xi_k = 2\cos(k) - \tilde{\mu}$, the energy of the k vector shifted by the chemical potential (equal to the Fermi energy) for an infinite one dimensional chain and for different value of the strength attractive interaction U. At the non-interactive limit (black full line) one recognize the characteristic step function since only the k states having an energy lower the Fermi level are occupied. For a small value of U/t (e.g $|U|/t = 1$, red dotted curve), only the k states near the Fermi surface are interacting, lowering (increasing) the occupancy of the states $k < k_F$ ($k > k_F$). As increasing $|U|/t$ more k states are interacting until the strong-interacting limit where all electrons are paired (full orange line) and all k states are half occupied.

The BCS approach have been the first successful approach to explain superconductivity and in particular the ground states energy of systems with attractive interaction. However, it have been show that for some properties such as the energy gap or correlators are not well reproduced [70].

Chapter 4

Density functional theory on a lattice

After having presented the generalities about DFT in continuum and about model Hamiltonians in the two previous chapters, we would like to recall the theoretical background concerning LDFT. A general formulation of the approach presented by R. López-Sandoval and G. M. Pastor [33, 34]. In Sec. 4.1 we summarize and discuss this formalism, given special emphasis to the case of the inhomogeneous Hubbard Hamiltonians. In the section 4.2 we present the method for computing the interaction-energy functional $W[\gamma_{ij}]$ numerically, which will be used at several stages throughout this thesis. Previous studies to N-representable density matrices have shown that is Kohn-Sham-like variational scheme in LDFT involves in general non integer eigenvalues of the density matrix. We recall this important results in the section 4.4. As in conventional DFT, the representability issues, in LDFT is an important non trivial problem. For this reason and in order to clarify the situation, we discuss the condition of representabilies by presenting numerical results. Since minimizing the energy functional with respect to the full density matrix is not evident in practice, we present a formal way to reduce the number of variables by introducing a physically motivated degree of electronic delocalization.

4.1 Density-functional theory of model Hamiltonians

In order to be explicit we focus on the inhomogeneous Hubbard model which is expected to capture the main interplay between electronic correlations and charge-density redistributions. The Hamiltonian is given by

$$\hat{H} = \sum_{i,\sigma} \varepsilon_i \, \hat{n}_{i\sigma} + \sum_{\langle i,j\rangle\sigma} t_{ij} \hat{c}^{\dagger}_{i\sigma} \hat{c}_{j\sigma} + U \sum_{i} \hat{n}_{i\downarrow} \hat{n}_{i\uparrow}, \tag{4.1}$$

where ε_i denotes the site-dependent energy levels, t_{ij} the nearest neighbor (NN) hopping integrals, and U the on-site interaction[1] [16]. As usual $\hat{c}^{\dagger}_{i\sigma}$ ($\hat{c}_{i\sigma}$) stands for the creation

[1] The LDFT formalism can be easily extended to arbitrary interactions $H_I = (1/2)\sum V_{ijkl} \hat{c}^{\dagger}_{i\sigma} \hat{c}^{\dagger}_{k\sigma'} \hat{c}_{l\sigma'} \hat{c}_{j\sigma}$, by replacing $U \sum_i \hat{n}_{i\uparrow} \hat{n}_{i\downarrow}$ by H_I in the expressions for the interaction-energy functional $W[\gamma]$. However, note that the functional dependence of W on γ is crucially sensitive to the form of V_{ijkl}. See also Refs. [34] and [36].

(annihilation) operator for an electron with spin σ at site i ($\hat{n}_{i\sigma} = \hat{c}^{\dagger}_{i\sigma}\hat{c}_{i\sigma}$). The values of ε_i and t_{ij} define the distribution of different elements in the lattice, its dimensionality and structure, and the range of the single-particle hybridizations (typically, $t_{ij} = -t < 0$ for NN ij). They specify the system under study and thus play the role given in conventional DFT to the external potential $v_{ext}(\vec{r})$. Consequently, the basic variable in LDFT is the single-particle density matrix γ_{ij} with respect to the sites i and j. The situation is similar to the density-matrix functional theory proposed by Gilbert for the study of nonlocal pseudopotentials [71], since the hoppings are nonlocal in the sites.

The ground-state energy E_{gs} and density-matrix γ^{gs}_{ij} are determined by minimizing the energy functional

$$E[\gamma] = E_K[\gamma] + W[\gamma] \tag{4.2}$$

with respect to γ_{ij}. $E[\gamma]$ is defined for all density matrices that derive from a physical state, i.e., that can be written as

$$\gamma_{ij} = \sum_{\sigma} \gamma_{ij\sigma} = \sum_{\sigma} \langle \Psi | \hat{c}^{\dagger}_{i\sigma} \hat{c}_{j\sigma} | \Psi \rangle \ , \tag{4.3}$$

where $|\Psi\rangle$ is an N-particle state. Such γ_{ij} are said to be pure-state N-representable. In some cases it is also useful to distinguish the subset of so-called pure-state interacting v-representable γ_{ij}, or simply v-representable γ_{ij}, which are those that can be derived from a ground-state of Eq. (4.1), i.e., $\gamma_{ij} = \gamma^{gs}_{ij}$ for some values of ε_i, t_{ij} and U. An extension of the definition domain of $E[\gamma]$ to ensemble-representable density matrices

$$\Gamma_{ij} = \sum_{n} w_n \langle \Psi_n | \sum_{\sigma} \hat{c}^{\dagger}_{i\sigma} \hat{c}_{j\sigma} | \Psi_n \rangle \, , \tag{4.4}$$

with $w_n \geq 0$ and $\sum_n w_n = 1$, is straightforward following the work of Valone [72].

The first term in Eq. (4.2) is given by

$$E_K[\gamma] = \sum_{i} \varepsilon_i \gamma_{ii} + \sum_{i \neq j} t_{ij} \gamma_{ij} \ . \tag{4.5}$$

It includes all single-particle contributions, namely, the crystal-field energy and the kinetic energy associated with the electron delocalization. Notice that both the diagonal and off-diagonal parts of γ are taken into account exactly [34].

The second term in Eq. (4.2) is the interaction-energy functional

$$W[\gamma] = \min_{\Psi \to \gamma} \left[U \sum_{i} \langle \Psi[\gamma] | \hat{n}_{i\uparrow} \hat{n}_{i\downarrow} | \Psi[\gamma] \rangle \right] \ , \tag{4.6}$$

which is given by Levy's constrained search minimization [45]. Here the optimization runs over all N-particles states $|\Psi[\gamma]\rangle$ that satisfy

$$\langle \Psi[\gamma] | \sum_{\sigma} \hat{c}^{\dagger}_{i\sigma} \hat{c}_{j\sigma} \, | \Psi[\gamma] \rangle = \gamma_{ij} \tag{4.7}$$

for all i and j. Thus, $W[\gamma]$ represents the minimum possible value of the interaction energy that is compatible with a given density matrix γ_{ij}, i.e., with a given charge distribution

and degree of electron delocalization. W is a universal functional of γ_{ij} in the sense that it is independent of the external parameters ε_i and t_{ij}, i.e., it is independent of the system under study. However, $W[\gamma]$ depends on the number of electrons N_e, on the internal structure of the many-body Hilbert space, as given by N_e and the number of orbitals or sites N_a, and on the kind of the many-body interactions, in the present case Hubbard's on-site form [16]. It is often convenient to express W in terms of the Hartree-Fock energy E_{HF} and the correlation energy E_c as $W = E_{HF} + E_c$. Notice that, in contrast to the KS approach, the expression for the kinetic, crystal-field, and exchange energies are exact, so that E_c includes only the Coulomb correlation contributions.

Finally, the variational principle for the ground-state density matrix γ_{ij}^{gs} follows from the relations [45]

$$E_{gs} \leq E[\gamma] = E_K[\gamma] + W[\gamma] \tag{4.8}$$

for all pure-state N-representable γ_{ij} and

$$E_{gs} = E_K[\gamma^{gs}] + W[\gamma^{gs}] \,, \tag{4.9}$$

where $E_{gs} = \langle \Psi_{gs} | \hat{H} | \Psi_{gs} \rangle$ refers to the ground-state energy.
It is interesting to analyze the dependence of $W[\gamma]$ on the interaction parameter U, since this reveals rigorous constraints to be satisfied by any explicit approximation. Once the sign of U is defined, it is clear that the minimization in Eq. (4.6) and the representability constraints (4.7) are independent of U. Therefore, we may write

$$W[\gamma] = U \min_{\Psi \to \gamma} \left[\sum_i \langle \Psi[\gamma] | \hat{n}_{i\uparrow} \hat{n}_{i\downarrow} | \Psi[\gamma] \rangle \right] \tag{4.10}$$

for all $U > 0$. The strict linearity of $W[\gamma]$ with respect to U is an important non trivial property that should be fulfilled by any approximation. It is a consequence of the fact that the density matrix γ univocally defines all single-particle contributions. The situation is different in the DFT of the continuum, since the electronic density $n(\overrightarrow{r})$ is not enough to define the kinetic energy unambiguously. Therefore the Hohenberg-Kohn or Levy-Lieb functionals are the results of the compromise of minimizing the sum of kinetic plus Coulomb interaction terms $T + W$ for a given $n(\overrightarrow{r})$. In the context of lattice models (in particular for the Hubbard model) there have been attempts to describe the many-body problem in terms of the orbital occupation $n_i = \langle \hat{n}_i \rangle = \gamma_{ii}$ alone, in the spirit of continuum DFT [28, 31]. In this case a non-linear dependence of the exchange correlation (XC) energy as a function of U/t needs to be assumed, since the kinetic energy is implicitly added to the interaction term when constructing the XC functional. It should be moreover noted that the kinetic energy of electrons in a lattice is not well-defined by the diagonal γ_{ii}. For example γ_{ii} alone, which is independent of i in an homogeneous system does not allow one to discern between weakly and strongly correlated states. While such occupation-number approaches are formally correct, the resulting functionals are intrinsically non-universal. They should not be transferred among different lattices (e.g., 1D, 2D and 3D) since the corresponding kinetic-energy operators are different.

Once the minimization Eq. (4.6) is done, one can write

$$W[\gamma] = \sum_i U_i \langle \Psi_{LL}[\gamma] | \hat{n}_{i\uparrow} \hat{n}_{i\downarrow} | \Psi_{LL}[\gamma] \rangle \tag{4.11}$$

where $|\Psi_{LL}[\gamma]\rangle$ denote the state yielding the minimum in Eq. (4.6). From the precedent equation it is possible to extract a rigorous formulation of the local average of double occupancy per site ω_i:

$$\omega_i = \frac{\partial W}{\partial U_i} \, . \tag{4.12}$$

In this way in possible to write the total correlation energy functional as a sum of local contribution:

$$W[\gamma] = \sum_i U_i \, \omega_i \tag{4.13}$$

This expression will be used in the following section in order to derive the functional dependence of ω_i from analytical calculations on simple systems. Notice that the formalism is the same considering an spin-symmetry braking by introducing an external magnetic field $h_i(\hat{n}_{i,\uparrow} - \hat{n}_{i,\downarrow})$ instead of the diagonal disorder.

4.2 Computing the exact interaction-energy functional

In order to determine $W[\gamma]$ we seek the extremes of

$$\begin{aligned} F &= U \sum_l \Big(\langle \Psi | \hat{n}_{l\uparrow} \hat{n}_{l\downarrow} | \Psi \rangle \Big) \; + \; \varepsilon \Big(1 - \langle \Psi | \Psi \rangle \Big) \\ &+ \sum_{i,j} \lambda_{ij} \Big(\langle \Psi | \sum_\sigma \hat{c}^\dagger_{i\sigma} \hat{c}_{j\sigma} | \Psi \rangle - \gamma_{ij} \Big) \end{aligned} \tag{4.14}$$

with respect to $|\Psi\rangle$. Lagrange multipliers ε and λ_{ij} have been introduced to enforce the normalization of $|\Psi\rangle$ and the representability of γ_{ij}. Derivation with respect to $\langle\Psi|$, ε and λ_{ij} yields the eigenvalue equations

$$\sum_{\substack{\langle ij \rangle \\ \sigma}} \lambda_{ij} \; \hat{c}^\dagger_{i\sigma} \hat{c}_{j\sigma} \; |\Psi\rangle \; + \; U \sum_i \hat{n}_{i\uparrow} \hat{n}_{i\downarrow} \; |\Psi\rangle = \varepsilon \; |\Psi\rangle \; . \tag{4.15}$$

and the auxiliary conditions $\langle\Psi|\Psi\rangle = 1$ and $\gamma_{ij} = \langle\Psi| \sum_\sigma \hat{c}^\dagger_{i\sigma} \hat{c}_{j\sigma} |\Psi\rangle$. The Lagrange multipliers λ_{ij} play the role of energy levels ($i = j$) and hopping integrals ($i \neq j$) to be chosen in order that $|\Psi\rangle$ yields the given γ_{ij}. The pure-state representability of γ_{ij} ensures that there is always a solution.

In practice, one usually varies λ_{ij} systematically in order to scan the full domain of representability of γ_{ij}. For given λ_{ij}, the eigenstate $|\Psi_0\rangle$ corresponding to the lowest eigenvalue of Eq. (4.15) yields the minimum $W[\gamma]$. Any other $|\Psi\rangle$ satisfying $\gamma_{ij} = \langle\Psi| \sum_\sigma \hat{c}^\dagger_{i\sigma} \hat{c}_{j\sigma} |\Psi\rangle$ would have higher ε and higher W, since γ_{ij} and E_K are fixed. These are the so-called interacting v-representable γ_{ij}, which can be derived from a ground-state of Eq. (4.15) or (4.1). They are the physically relevant ones, since they necessarily include the absolute minimum γ^{gs}_{ij} of $E[\gamma]$. However, one also finds pure-state representable γ_{ij}, which correspond to excited states or to linear combinations of eigenstates of Eq. (4.15). Therefore, the domains of v- and N-representability are in general different, as it will be discussed below.

Equation (4.15) can be solved numerically for finite lattices with different structures, boundary conditions, and band fillings. In this case we expand $|\Psi[\gamma_{ij}]\rangle$ in a complete set

of basis states $|\Phi_m\rangle$ which have definite occupation numbers $\nu_{i\sigma}^m$ at all orbitals $i\sigma$, i.e., $\hat{n}_{i\sigma}|\Phi_m\rangle = \nu_{i\sigma}^m|\Phi_m\rangle$ with $\nu_{i\sigma}^m = 0$ or 1. The values of $\nu_{i\sigma}^m$ satisfy the usual conservation of the number of electrons $N_e = N_{e\uparrow} + N_{e\downarrow}$ and of the z component of the total spin $S_z = (N_{e\uparrow} - N_{e\downarrow})/2$, where $N_{e\sigma} = \sum_i \nu_{i\sigma}^m$. For not too large clusters, the ground state $|\Psi_0[\gamma_{ij}]\rangle$ of Eq. (4.15) can be determined by sparse-matrix diagonalization procedures, for example, by using the Lanczos iterative method [42]. In practice we usually calculate $|\Psi_0[\gamma_{ij}]\rangle$ in the subspace of minimal S_z, since this ensures that there are no *a priori* restrictions on the total spin S. In addition, spin-projector operators may be used to investigate the dependence of $W[\gamma]$ on S [73].

Interesting examples of non-v-representable γ_{ij} are found when there is a discontinuous change in the nature of the ground state as a function of external or interaction parameters. Consider for instance the Hubbard model on a bipartite finite ring with $N_a = 4k$ sites (k a positive integer) and sub-lattices energy levels ε_1 and ε_2 [see Eq. (4.1)]. In the homogeneous case ($\Delta\varepsilon = \varepsilon_2 - \varepsilon_1 = 0$) the Fermi energy corresponding to half-band filling is degenerate ($n = 1$). This degeneracy is removed for arbitrary small values of U or $\Delta\varepsilon$. However, the nature of the ground state is completely different for $U > 0$ ($\Delta\varepsilon = 0$) and $\Delta\varepsilon > 0$ ($U = 0$). In the first case the charge distribution remains homogeneous for all $U > 0$, while in the second case a CDW state sets in, with a finite amplitude Δn^0 even for arbitrary small $\Delta\varepsilon$. As a result, the density matrices having $0 < \gamma_{11} - \gamma_{22} < \Delta n^0$ and off-diagonal γ_{12} close to the uncorrelated limit γ_{12}^0 are not pure state v-representable. Consequently, the domain of v-representability is concave. In fact, for the examples to be discussed in Sec. 4.3 it is not simply connected, since the level crossing occurs even for $U/t \to +\infty$. Notice, however, that this is a finite size effect which tends to disappear as the length $N_a = 4k$ of the ring increases. For large N_a the contribution of the Fermi level to γ_{ij} and to its discontinuity becomes negligible. This last case will be more extensively discussed in the next section.

In the non-v-representable domain of values of γ_{ij} Levy's constrained-search minimum $|\Psi_0[\gamma_{ij}]\rangle$ is given by a linear combination $|\Psi\rangle = a|\alpha\rangle + b|\beta\rangle$ of the two ground states which level crossing is at the origin of the discontinuity of γ_{ij}^{gs} ($\langle\alpha|\beta\rangle = 0$). The coefficients $a > 0$ and $b = \sqrt{1-a^2}e^{i\varphi}$ are obtained by minimizing $W[\gamma]$ under the constraint $\langle\Psi|\hat{c}_{i\sigma}^\dagger\hat{c}_{j\sigma} + \hat{c}_{j\sigma}^\dagger\hat{c}_{i\sigma}|\Psi\rangle = \gamma_{ij\sigma} + \gamma_{ji\sigma}$. Without loss of generality we assume that the hopping integrals are always real so that the energy functionals depends only on the sum of γ_{ij} and γ_{ji} ($t_{ij} = t_{ji}$). It is easy to see that any intermediate γ_{ij} is not pure-state v-representable but that it can be derived from a ket of the form $|\Psi\rangle = a|\alpha\rangle + i\sqrt{1-a^2}|\beta\rangle$. In this range the density matrix has the form $\gamma_{ij} = a^2\gamma_{ij}^\alpha + (1-a^2)\gamma_{ij}^\beta$, where γ_{ij}^α and γ_{ij}^β are the density matrices corresponding to $|\alpha\rangle$ and $|\beta\rangle$. The interaction energy associated to $|\Psi\rangle$ is $W = a^2W^\alpha + (1-a^2)W^\beta$. It necessarily yields the minimum of Levy's constrained search, since $|\Psi\rangle$ is one of the ground states of the Hubbard model. Any other state representing the same γ_{ij} would have the same kinetic energy and therefore an equal or higher W. This shows that the N-representability domain is convex, even if the v-representability domain is concave. This simple result is of crucial importance for practical applications, in which a minimization in the respect to γ needs to be performed.

4.3 Representability of the density matrix

Representability is a fundamental property of any SPDM. For a given γ it tells us if there is an associated pure ground-state wave-function (v-representability), an pure oth-

erwise arbitrary eigen-wave function (N-representability), or an incoherent mixed state (ensemble N-representability). The type of state from which γ is derived plays a role in determining which mathematical domain is relevant to prossed the minimization of SPDM. Unfortunately, to our knowledge, there is no necessary and sufisant condition (NASC) for characterizing N-representability. However, there is a well-known NASC for ensemble representability [33]:

If the eigenvalues η_k of a density matrix γ such as $0 \leq \eta_k \leq 1$ and $\sum_k \eta_k = N_e$, then this γ is ensemble N-representable.

In order to illustrate the problem of representability, we present in the following a numerical study of the representability domain of inhomogeneous Hubbard rings. For simplicity, we focus on bipartite lattices consisting of a sub-lattice $\mathcal{S}_1$, where the energy levels $\varepsilon_i = \varepsilon_1 = \varepsilon/2$, and a sub-lattice $\mathcal{S}_2$, where $\varepsilon_i = \varepsilon_2 = -\varepsilon/2$. Moreover we choose $\gamma_{12} > 0$ and $t_{ij} = -t < 0$ for NN ij. Non-bipartite lattices can be treated analogously by considering positive and negative domains of γ_{12} separately. Positive (negative) values of γ_{12} are relevant for negative (positive) hopping integrals. As shown in Ref. [34] for homogeneous density distributions, non-bipartite lattices show scaling properties of $W[\gamma]$ that are similar to the bipartite case. In Figs. 4.1 and 4.2 the NN density matrix element γ_{12} of the ground state of the inhomogeneous Hubbard model is shown as a function of the electron density γ_{11} at one of the sub-lattices. Fig. 4.1 shows the representability-domain as a function of the size N_a of 1D and 2D Hubbard clusters having periodic boundary conditions, from sizes $N_a = 2$ to $N_a = 16$ sites, and half band filling $n = N_e/N_a = 1$. In Fig. 4.2 the band-filling dependence for a bipartite ring having $N_a = 14$ sites is presented. They were obtained from Lanczos exact diagonalization for representative values of the Coulomb repulsion strength $U/t > 0$ by varying systematically the difference $\Delta\varepsilon = \varepsilon_1 - \varepsilon_2 > 0$ between the energy levels of the sub-lattices. The curves, given only for $0 \leq \gamma_{11} \leq 1$, are symmetric with respect to the homogeneous case $\gamma_{11} = 1$ $[(\gamma_{11} + \gamma_{22})/2 = n = 1]$. They display the correlation between diagonal and off-diagonal elements of the density matrices γ_{ij}, as derived from the ground state of the model for different values of the parameters that define the system (i.e., the energy level difference $\Delta\varepsilon$ and the NN hopping t). These density matrices are referred to as pure-state interacting v-representable, or simply v-representable, by analogy with the DFT of the inhomogeneous electron gas. In the continuum theory the electron densities $\rho(\vec{r})$ derived from exact ground states are called interacting v-representable, since they stay in one-to-one correspondence with an external potential $v_{ext}(\vec{r})$ [1, 3, 4]. While the v-representable domain contains all the ground state γ_{ij}^{gs}, it is also important to investigate the properties of the more general N-representable γ_{ij}, which constitute the domain of definition of the Levy-Lieb functional $W[\gamma]$.

For each γ_{11}, or charge transfer $\Delta n = \gamma_{22} - \gamma_{11}$, the upper bound γ_{12}^0 for the NN γ_{12} corresponds to the largest possible value of the kinetic energy, which is achieved by the uncorrelated ground-state for the given Δn. Since the underlying electronic state is a single Slater determinant, the interaction energy is given by the Hartree-Fock value $W^0 = W[\gamma^0] = UN_a(\gamma_{11}^2 + \gamma_{22}^2)/8$, except eventually in special cases with unusual degeneracies in the single-particle spectrum (e.g., $N_a = N_e = 4$ and $\Delta n = 0$). The uncorrelated γ_{12}^0 is largest for an homogeneous density distribution ($\Delta n = 0$) and decreases monotonically as the charge transfer increases. It vanishes in the limit where only one sub-lattice is occupied (see Fig. 4.1). This can be understood by recalling that in an uncorrelated state an increase of Δn is the result of an increasing difference $\Delta\varepsilon$ in the energy levels of the

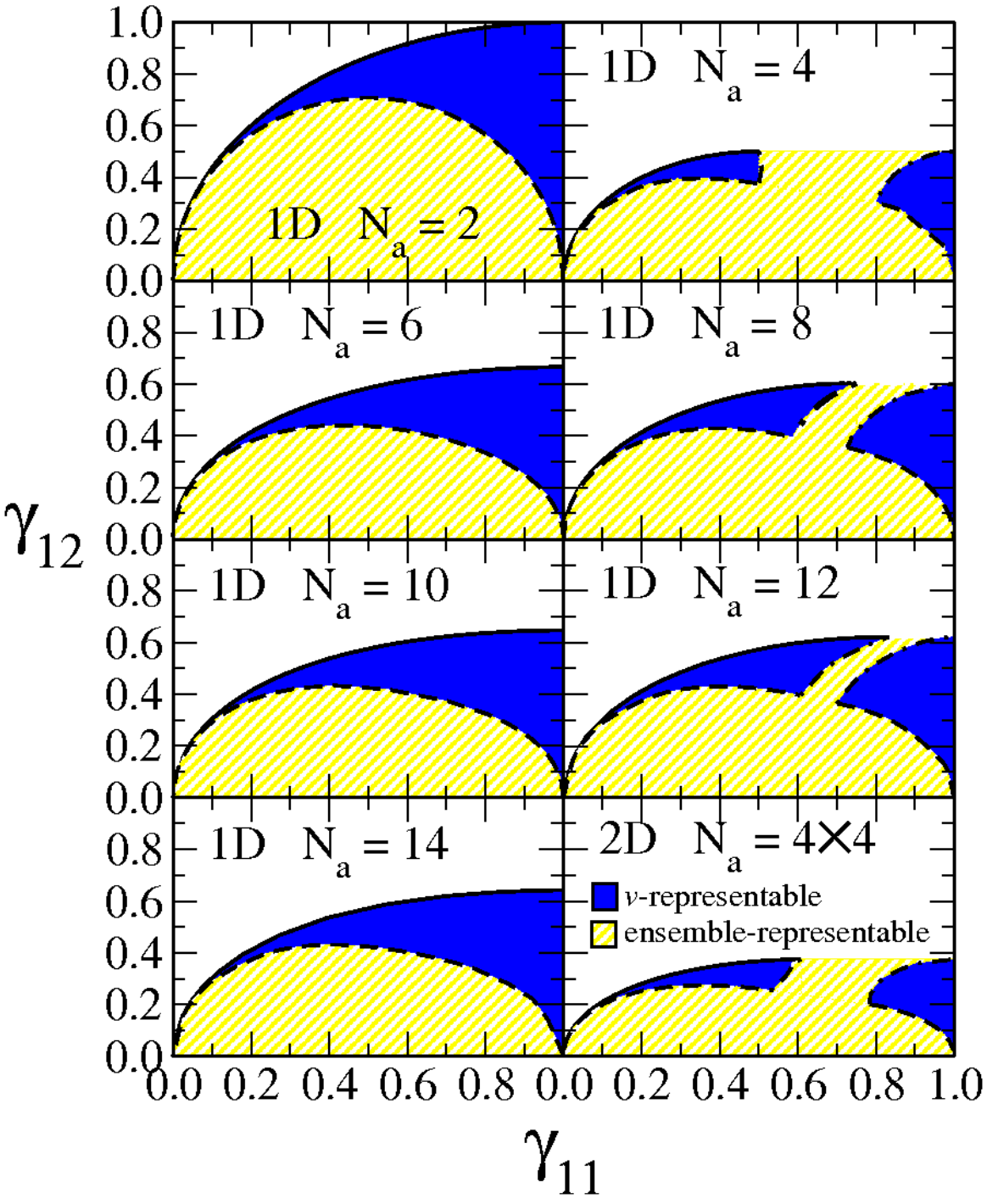

Figure 4.1: NN bond order γ_{12} between the two sub-lattices as a function of the charge density γ_{11} on the sub-lattice $\mathcal{S}_1$ delimiting the representability domain of bipartite Hubbard clusters at half band fillings. The solid (dashed) black line refers to the non-correlated (strong correlated) limits. The blue solid (yellow dashed) zone corresponds to the v-representable (ensemble-representable) domains. One dimensional wires and 2D square lattices of various number of atoms N_a are considered.

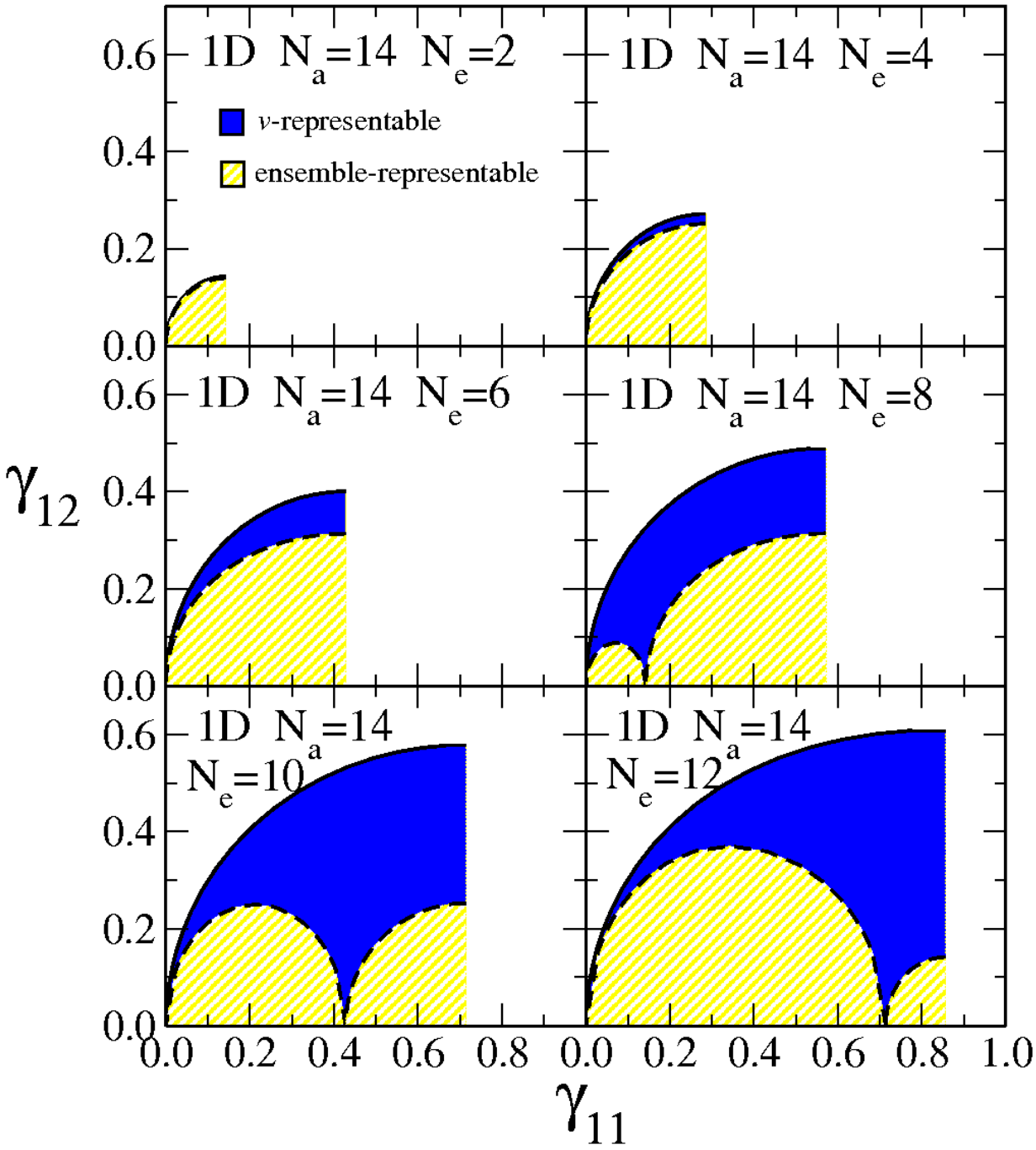

Figure 4.2: NN bond order γ_{12} between the two sub-lattices as a function of the charge density γ_{11} on the sub-lattice $\mathcal{S}_1$ delimiting the representability domain of 1D bipartite Hubbard rings having $N_a = 14$ sites and different band fillings. The solid (dashed) black line refers to the non-correlated (strong correlated) limits. The blue solid (yellow dashed) zone corresponds to the v-representable (ensemble-representable) domains.

sub-lattices, which reduces the possibility for the electrons to delocalize. In the limit of complete charge transfer ($\gamma_{11} \to 0$) no charge fluctuations at all are possible.

For $\gamma_{12} < \gamma_{12}^0$, and a given Δn, the number of linearly independent many-body states yielding the given γ_{ij} is larger. Therefore the electrons can reduce the optimum value of the interaction W, for a fixed γ_{ij}, by reducing the number of double occupations ($U > 0$). The minimum value of the interaction energy per site is $W^\infty = U(1-\gamma_{11})/2$ for $n = 1$ and $\gamma_{11} \leq 1$. We shall denote by γ_{12}^∞ the largest possible value of γ_{12} compatible with the minimum number of double occupations W^∞/U. γ_{12}^∞ defines the lower bound for the v-representable γ_{ij} and corresponds to the the ground state of the model for $U \to +\infty$ [$W(\gamma_{12}^\infty) = W^\infty$, see Fig. 4.1]. Smaller values of γ_{12} are still pure-state N-representable. To show this one may consider a linear combination of two states having the same γ_{11} and opposite γ_{12}^∞. One of them is the ground state yielding γ_{12}^∞ for negative t_{ij} and the other for positive t_{ij} ($U \to +\infty$). It is easy to see that these states have all the same minimal interaction energy W^∞. Therefore, W is independent of γ_{12} and equal to W^∞ for $|\gamma_{12}| \leq \gamma_{12}^\infty$. Although they are pure-state representable, these γ_{ij} can never match a ground state, since there are states having the same Δn and W but larger γ_{12}.

In the absence of charge transfer ($\gamma_{11} = \gamma_{22} = 1$) the minimum $W^\infty = 0$ can only be achieved by any of the 2^{N_a} fully localized states for which $\gamma_{12}^\infty = 0$ spin degeneracy. This corresponds to the well-known Heisenberg limit of the homogeneous Hubbard model. However, as charge transfer increases it is possible to delocalize part of the electrons, even in the limit of strong correlations (i.e., $W = W^\infty$). Therefore, $\gamma_{12}^\infty > 0$ for $0 < \gamma_{11} < 1$. Although the details of the strongly correlated ground state are quite complex, one can easily estimate that γ_{12}^∞ should be larger than the γ_{12} of a Slater determinant having one localized (e.g., up) electron in the sites of the sub-lattice 2 ($\gamma_{22} > 1$), while the remaining (e.g., down) electrons occupy delocalized states following an average occupation $\gamma_{22} - 1$ on sub-lattice 2 and γ_{11} on sub-lattice 1. Consequently, γ_{12}^∞ should be largest for intermediate values of the number of delocalized electrons per site. This corresponds roughly to a half-filled delocalized subband ($\gamma_{11} = \gamma_{22} - 1 \sim 1/2$ and $\Delta\varepsilon/U \sim 1$). The resulting γ_{12}^∞ presents therefore a maximum as a function of γ_{11}, vanishing only for $\Delta n = 1$ and $\Delta n = 0$, where the number of delocalized electrons or holes is zero (see Fig. 4.1). Notice that the actual maximum of γ_{12}^∞ is found for $\gamma_{11} < 1/2$.

Fig. 4.1 shows 1D chains ($N_a = 4,\ 8,\ 12$) and are interesting example of a disconnected domain of v-representability. These correspond to the result of the crossing between the two lowest $S = 0$ levels. One of them favors a strong CDW state and is the ground state for large Δn, while the other yields a rather uniform density distribution and dominates for γ_{11} close to 1. The ground-state density matrix γ_{ij}^{gs} is discontinuous at the level crossing, as indicated by the dashed lines in Fig. 4.1(a). For $U = 0$ the discontinuity appears for an arbitrary small Δn. As $U > 0$ increases, γ_{12}^{gs} decreases and the transition from an homogeneous to an inhomogeneous density distribution shifts to a finite increasing $\Delta\varepsilon$. In contrast, the discontinuity in γ_{11} remains approximately constant, even for $U \to +\infty$ [see Fig. 4.1(a)]. This leads to a whole range of γ_{ij} that cannot be attained by the ground state of the Hubbard model. Therefore, the domain of pure-state v-representability is not simply connected. In this intermediate region, γ_{ij} can be represented by a linear combination of the two orthogonal degenerate ground-states at the origin of the level crossing. As discussed in Sec. 4.1, Levy's constrained search functional W corresponds here to the interpolation of the interaction energies in the two degenerate states as given by the straight dashed curves in Fig. 4.1(a).

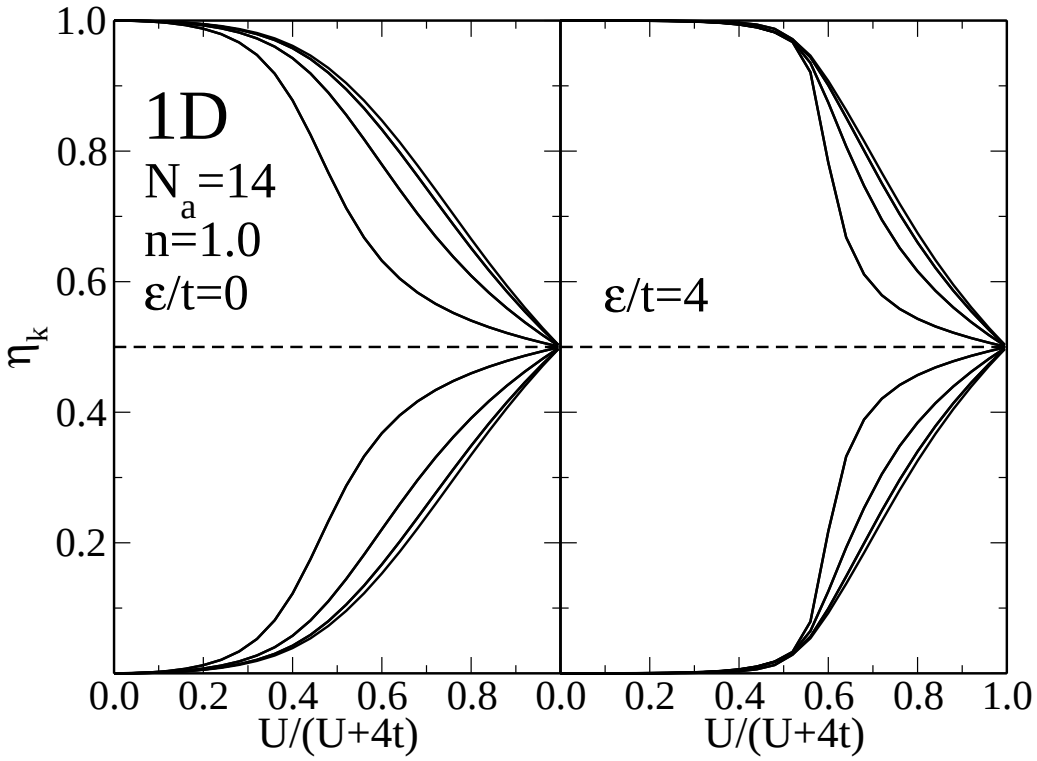

Figure 4.3: Occupation numbers η_k ($k = 1, .., 14$), as a function of the strength of the Coulomb interaction in the ground state of a bipartite Hubbard ring having $N_a = 14$ sites and half band filling ($n = 1$). Results are presented for two representative values of the energy level shift $\varepsilon/t = 0$ (left) and $\varepsilon/t = 4$ (right). For symmetry reason, only 8 of the 14 eigenvalues are different. Spin up and spin down occupations are the same in the singlet ground state ($\eta_k = \eta_{k,\uparrow} = \eta_{k,\downarrow}$).

4.4 Variational equations

The previously presented Levy-Lieb formulation proves the existence of a functional relation between the ground-state energy of a many-particle system E_{gs} and the density matrix γ. In this section we show that one needs to satisfy specific condition in order to derive variational relations, which are analogous to the Kohn-Sham equations in conventional DFT. We follow the presentation made by R. López-Sandoval and G. M. Pastor for N-representable density matrix [33].
The variational principle can be implemented by using Lagrange multipliers. One considers the auxiliary function

$$\mathcal{L} = E[\gamma] - \mu \left(\sum_{k,\sigma} \eta_{k,\sigma} - N_e \right) - \sum_{k,\sigma} \varepsilon_{k,\sigma} \left(\sum_i \mid u_{ik,\sigma} \mid^2 -1 \right) \tag{4.16}$$

where

$$\begin{aligned} \gamma_{ij,\sigma} &= \sum_{k=1}^{N} u^*_{ik,\sigma}\eta_{k,\sigma}u_{jk,\sigma}, \\ 0 \leq \eta_{k,\sigma} &\leq 1, \\ \sum_{k=1}^{N} \mid u_{ik,\sigma} \mid^2 &= 1 \end{aligned} \tag{4.17}$$

The matrix γ is characterized by its eigenvalues $\eta_{k,\sigma}$ and its eigenvectors $u_{ik,\sigma}$, also known as the natural orbitals. The function $\mathcal{L}$ is composed, from left to right, by the energy $E[\gamma]$ for the N-representable SPDM, the constraint of the number of particle for the SPDM, and the normalization of the natural orbitals for SPDM.

Differentiation of $\mathcal{L}$ with respect to $u^*_{ik,\sigma}$ yields the saddle point condition

$$\frac{\partial \mathcal{L}}{\partial u^*_{ik,\sigma}} = \sum_{i'j\sigma'} \frac{\partial E}{\partial \gamma_{i'j\sigma'}} \frac{\partial \gamma_{i'j\sigma'}}{\partial u^*_{ik,\sigma}} - \varepsilon_k u_{ik,\sigma} = 0. \tag{4.18}$$

Using that

$$\frac{\partial \gamma_{i'j\sigma'}}{\partial u^*_{ik,\sigma}} = \eta_{k,\sigma} u_{jk,\sigma} \delta_{ii'} \delta_{\sigma\sigma'} \tag{4.19}$$

one obtains

$$\sum_j \left(\frac{\partial E}{\partial \gamma_{ij\sigma}} - \lambda_{k,\sigma}\delta_{ij} \right) u_{jk,\sigma} = 0, \qquad \lambda_{k,\sigma} = \frac{\varepsilon_k}{\eta_{k,\sigma}}. \tag{4.20}$$

This is an eigenvalue equation equivalent to a one-particle effective Hamiltonian $\hat{H}_{\text{eff}}$ with eigenenergy $\lambda_{k,\sigma}$.
Differentiation of $\mathcal{L}$ with respect to $\eta_{k,\sigma}$ yields the condition

$$\frac{\partial \mathcal{L}}{\partial \eta_{k,\sigma}} = \sum_{i'j\sigma'} \frac{\partial E}{\partial \gamma_{i'j\sigma'}} \frac{\partial \gamma_{i'j\sigma'}}{\partial \eta_{k,\sigma}} - \mu = 0 \tag{4.21}$$

at the saddle point, which is equivalent to

$$\sum_i \left(\sum_j \frac{\partial E}{\partial \gamma_{ij\sigma}} u_{jk,\sigma} \right) u^*_{ik,\sigma} = \mu. \tag{4.22}$$

Finally, using Eq. (4.20), we obtain

$$\lambda_{k,\sigma} = \mu. \tag{4.23}$$

This previous result could seem surprising since it means that all eigenvalue $\lambda_{k,\sigma}$ of the effective Hamiltonian $\hat{H}_{\text{eff}}$ are degenerated (see Eq. 4.23) and associated with a fractional occupation number $\eta_{k,\sigma}$ for the eigenvalue problem associated to the N-representable matrix γ. This is different from the usual KS approach which describes the electronic density with auxiliary orbitals having integer occupation numbers. However, also in KS theory the eigenvalues $\varepsilon_k = \mu$ for all k having $0 < \eta_k < 1$, as shown by Janak [4]. In

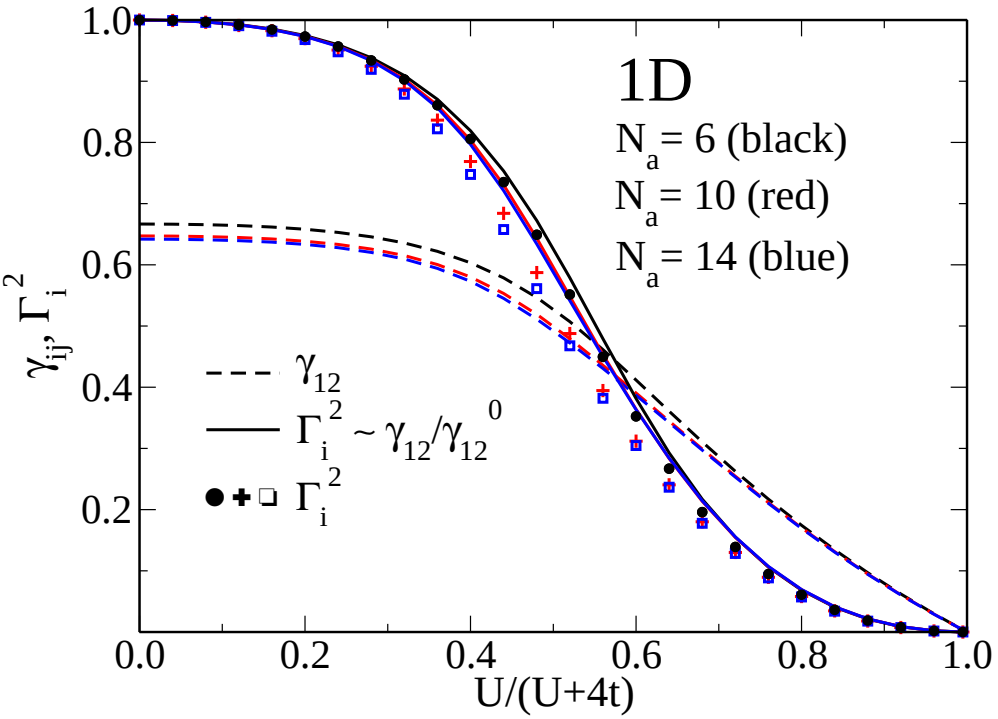

Figure 4.4: NN bond order γ_{12} and degree of delocalization Γ_i^2 as a function of the strength of the Coulomb interaction U/t in homogeneous Hubbard rings having $N_a = 6$ (black), $N_a = 10$ (red) and $N_a = 14$ sites (blue). The dashed line refers to γ_{12}, the full-line to the approximation of Γ_i^2: Eq. (4.26) and symbol to the exact Γ_i^2.

LDFT the degeneracy of $\lambda_{k,\sigma}$ is a direct consequence of the electronic correlation. That the eigenvalues are equal to the chemical potential is formally correct when the occupation numbers are fractional. This behavior is shown in Fig 4.3 where we show the occupation number $\eta_k = \eta_{k,\uparrow} = \eta_{k,\downarrow}$ in the ground state of a 14 sites Hubbard ring at half band filling $S = 0$. One observes that an arbitrary small value of U/t is enough for all the η_k to become fractional, independently of the energy level shift ε/t between the two sub-lattices.

4.5 Relevant part of the density matrix, degree of electronic delocalization

As we have presented above, the energy is a functional of the SPDM. However, minimizing over all the elements of the SPDM, appears to be a complicated numerical problem. It would be therefore useful if one could define a variable common of any system which is able to describe how much the system is delocalized without the need of the full density matrix. To approach this problem, we present a dimensionless variable derived from the ensemble N-representable NASC (see Sec. 4.3), which is bounded between zero and one, and which can be useful to describe the degree of electronic delocalization. Starting from the NASC for the ensemble N-representability, in [38] it has been shown that

If a density matrix γ is N-ensemble-representable then

$$0 \leq \Gamma^2_{i,\sigma} \leq 1 \ , \quad \text{with} \quad \Gamma^2_{i,\sigma} = \frac{\sum_{j\neq i} \mid \gamma_{ij,\sigma} \mid^2}{\gamma_{ii,\sigma}(1-\gamma_{ii,\sigma})}. \tag{4.24}$$

Proof: If γ is N-ensemble-representable then all its eigenvalues $\eta_{k,\sigma} \in [0,1]$. Since $\eta_{k,\sigma} \leq 1$ then $1-\gamma_\sigma$ is also positive definite and its eigenvalues are also less or equal to 1. Then we have that $\gamma(1-\gamma)$ is also positive definite and

$$\langle i \mid \gamma_\sigma - \gamma^2_\sigma \mid i \rangle \geq 0 \tag{4.25}$$

From this inequality it follows that:

$$\begin{aligned} \langle i \mid \gamma_\sigma - \gamma^2_\sigma \mid i \rangle &\geq 0 \\ \gamma_{ii,\sigma} - \textstyle\sum_j \gamma_{ij,\sigma}\gamma_{ji,\sigma} &\geq 0 \\ \gamma_{ii,\sigma} - \gamma^2_{ii,\sigma} - \textstyle\sum_{j\neq i} \gamma_{ij,\sigma}\gamma_{ji,\sigma} &\geq 0 \\ \gamma_{ii,\sigma}(1-\gamma_{ii,\sigma}) &\geq \textstyle\sum_{j\neq i} \mid \gamma_{ij,\sigma} \mid^2 \quad \Rightarrow \quad \Gamma^2_{i,\sigma} \leq 1. \end{aligned}$$

The fact that $\Gamma^2_{i,\sigma} \geq 0$ is obvious.
Note that unless some model parameter diverges $\gamma_{ii,\sigma}$ is never strictly zero or one in a connected quantum mechanical system. Another properties of $\Gamma^2_{i,\sigma}$ can be mentioned. At the non-correlated limit the occupations number η_k of γ are zero or one. Then $\gamma = \gamma^2$ and all $\Gamma^2_{i,\sigma} = 1$. In contrast, $\Gamma^2_{i,\sigma} = 0$ when there is no electronic delocalization $\gamma_{i\neq j,\sigma} = 0 \quad \forall i,j,\sigma$. i.e., these two properties are valid for any system at any band filling. Moreover, starting from the non-correlated limit having $\Gamma^2_{i,\sigma} = 1$, by increasing the Coulomb interaction, $\Gamma^2_{i,\sigma}$ decreases until it reaches its minimum value for $U \to \infty$. However, $\Gamma^2_{i,\sigma} > 0$ except for some system at half-band filling for which $\Gamma^2_{i,\sigma} = 0$ for $U \to \infty$, e.g, square lattice. $\Gamma^2_{i,\sigma}$ could be use to describe the degree of electronic delocalization of a system since for $\Gamma^2_{i,\sigma} = 1 \quad (\Gamma^2_{i,\sigma} = 0)$ the systems is fully delocalized (localized). Intermediate values of $\Gamma^2_{i,\sigma}$ correspond to the interplay between localization induced by the Coulomb repulsion, and delocalization.
In the case of infinite dimensions and for the dimer, $\Gamma^2_{i,\sigma} = \frac{\gamma_{i,j,\sigma,ijNN}}{\gamma^0_{i,j,\sigma,ijNN}}$ where $\gamma^0_{i,j,\sigma,ijNN}$ is the electronic delocalization between two NN at the non-correlated limit. However we show that for other system, considering only the NN bond order in the calcul of $\Gamma^2_{i,\sigma}$ is a good approximation.
In Fig 4.4 we are showing the NN bond order γ_{ij} and $\Gamma_i = \sum_\sigma \Gamma_{i,\sigma}$ for the ground state of homogeneous 1D Hubbard chains having $N_a = 6, 10$, and 14 as a function of the strength of the Coulomb repulsion U/t. The exact results (symbols) of γ_{ij} as well as its approximation taking only into account the NN bond order

$$\Gamma^2_{i,\sigma} \simeq \frac{\gamma^2_{12,\sigma}}{\gamma^{0\ 2}_{12,\sigma}} \tag{4.26}$$

are bounded between zero and one. This is not the case of $\gamma_{i,j}$ which is system dependent. One sees also in this figure that Γ^2_i is nearly independent of the system size, so that it can be a good approximation for a degree of delocalization. In addition, by considering only

the first NN in its calculation one obtains quantitatively its value. The scalability of Γ_i^2 will be studied later on in this work. It is also very important to be able to define a variable which can describe the degree of delocalization or localization for any system. In this sense, these previous results are promising concerning $\Gamma_{i,\sigma}^2$, since it has been shown that it can be reduce to only the NN contribution without lost of much information. This is a useful property since for a large system, minimizing the energy-functional over all the element of the density matrix can be difficult in practice. With $\Gamma_{i,\sigma}^2$ we have defined a convenient variable, describing the degree of electronic delocalization of any systems ($\Gamma_{i,\sigma}^2 = 1$ fully delocalized, $\Gamma_{i,\sigma}^2 = 0$ fully localized). In addition, we have shown that knowing only the NN bond order and its non-correlated limit, one can give a good approximation of $\Gamma_{i,\sigma}^2$ and of the degree of delocalization.

Chapter 5

Scaling approximation for bipartite systems

Once the LDFT formalism has been presented, we focus now on the main challenge of the problem: the derivation of an accurate approximation to the correlation-energy functional (CEF) for inhomogeneous system. In a previous work on homogeneous systems, it is shown that the CEF admits several scaling properties from which simple and quite accurate approximations to the CEF can be inferred [33, 34, 35, 36, 37] . Following this phylosophy we show that theses properties are also present in inhomogeneous system having charge transfert between sites. In order to simplify the problem, we focus on the bipartite Hubbard model. In the first section, we make a systematic study of the CEF in finite systems in order to extract the scaling properties. Then we propose an extention of the scaling approximation based on the inhomogeneous Hubbard dimer. Finally, we apply the *Ansatz* and compare our results with other available methods for representative examples.

5.1 Exact numerical studying of the correlation-energy functional $W[\gamma]$

Before developing an approximation to the CEF $W[\gamma]$, it is very useful to study its properties as obtained from exact diagonalizations following the method described in Sec. 4.2. As already mentioned, for homogeneous systems the CEF presents quite remarkable scaling properties which are suitable for introducing simple and efficient approximations. In this section we study the effect of a bipartite diagonal potential on the scaling properties of $W[\gamma]$, a systemactic study on finite bipartite lattices.

Let us first discuss exact results for $W[\gamma]$ in the 1D Hubbard rings, which were obtained from Lanczos diagonalizations by varying systematically γ_{ij}, the band filling n, and the number of sites N_a. In Fig. 5.1 W is shown as a function of γ_{12} for representative values of $\Delta n = \gamma_{22} - \gamma_{11}$. Despite the strong dependence of W on Δn the are several important qualitative properties shared by all the curves:
(i) As already discussed, the domain of N representability of γ_{12} is bounded by the bond order γ_{12}^0 in the uncorrelated limit. γ_{12}^0 decreases monotonously as Δn increases vanishing for $\Delta n = 2$. This is an important contribution to the Δn dependence of W which reflects

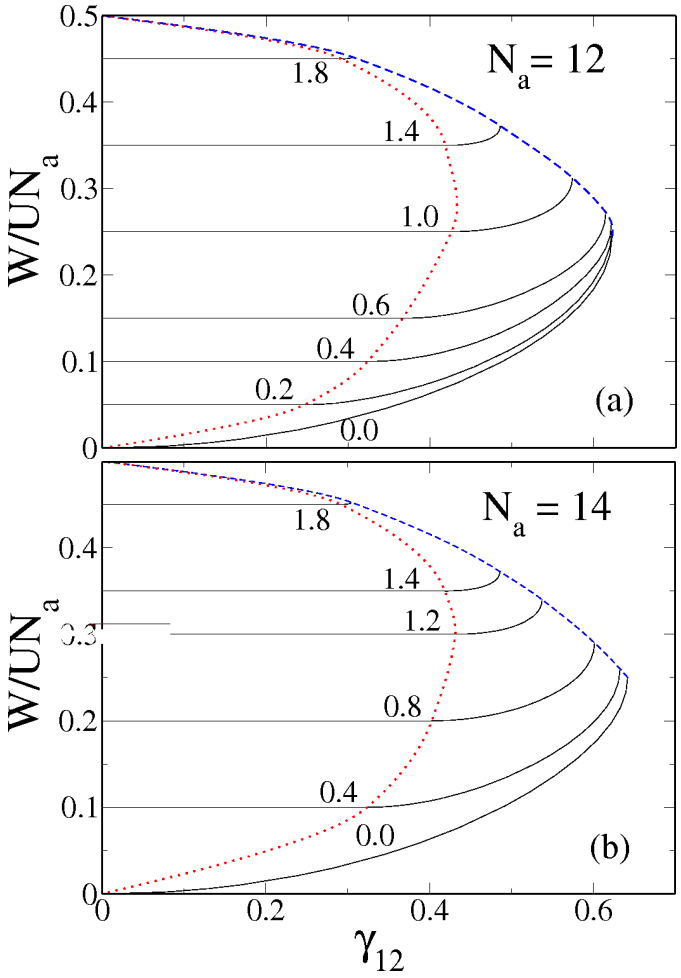

Figure 5.1: Interaction energy W of the Hubbard model on 1D rings as a function of NN density-matrix element γ_{12}: (a) $N_a = 12$ and (b) $N_a = 14$ sites at half-band filling $n = 1$. The different charge transfers $\Delta n = \gamma_{22} - \gamma_{11}$, are indicated by the numbers labelling the curves. The dashed curve (blue) shows the Hartree-Fock upper bound $E_{HF} = W^0 = UN_a[n^2 + (\Delta n/2)^2]/4$. The dotted curve (red) corresponds to the strongly correlated limit where $\gamma_{12} = \gamma_{12}^{\infty}$ and $W = W^{\infty} = UN_a\Delta n/4$ for $n = 1$. Notice that W is constant for $0 \leq \gamma_{12} \leq \gamma_{12}^{\infty}$.

the interplay between charge transfer and electron delocalization.
(ii) In the delocalized limit, $W(\gamma_{12}^0, \Delta n) = W^0 = E_{HF}$ for all Δn, since the electronic state yielding the largest γ_{12} is a single Slater determinant. Moreover, one observes that $\partial W/\gamma_{12}$ diverges at $\gamma_{12} = \gamma_{12}^0$. This is a necessary condition in order that the ground-state density matrix satisfies $\gamma_{12}^{gs} < \gamma_{12}^0$ for arbitrary small $U > 0$, as expected from perturbation theory.
(iii) Starting from γ_{12}^0, W decreases with decreasing γ_{12}, reaching its lowest possible value $W^\infty = UN_a(\gamma_{22} - 1)/2$ for $\gamma_{12} = \gamma_{12}^\infty$ ($W^\infty = UN_a\Delta n/4$ for $n = 1$). The decrease of W with decreasing γ_{12} means that the reduction of the Coulomb energy due to correlations is done at the expense of kinetic energy or electron delocalization. Reducing γ_{12} beyond γ_{12}^∞ cannot lead any further reduction of W for the given Δn.
(iv) The strongly correlated γ_{12}^∞ is in general finite showing a non-monotonous dependence on Δn. It vanishes only for $\Delta n = 0$, where the electrons are localized evenly at all sites keeping just their spin degree of freedom. It also vanishes for $\Delta n = 2$, where all the electrons form localized pairs on one sublattice. In the latter case both γ_{12}^∞ and γ_{12}^0 are zero.
(v) In the limit of small $\gamma_{12} - \gamma_{12}^\infty > 0$, one observes that $W \propto U(\gamma_{12} - \gamma_{12}^\infty)^2$. Therefore, for $U/t \gg 1$, $(\gamma_{12}^{gs} - \gamma_{12}^\infty) \propto t/U$ and $E_{gs} - W^\infty \propto t^2/U$, a result expected from perturbation theory and which corresponds to the Heisenberg or t-J limit of the homogeneous Hubbard model [14].

In order to compare the functional dependence of W for different Δn and to analyze its scaling behavior we focus on the v representable domain $\gamma_{12}^\infty \leq \gamma_{12} \leq \gamma_{12}^0$ where W is not trivially constant. To this aim it is useful to bring the domains of representability for different N_a to a common range and to scale W with respect to the Hartree-Fock and strongly correlated values. We therefore consider $(W - W^\infty)/(W^0 - W^\infty)$ as a function of $g_{12} = (\gamma_{12} - \gamma_{12}^\infty)/(\gamma_{12}^0 - \gamma_{12}^\infty)$ as displayed in Fig. 5.2 ($W^0 = E_{HF}$). In this form the results for different N_a appear as remarkably similar, showing that the largest part of the dependence of W on γ_{12} and Δn comes from the domain of representability of γ_{ij} and the limiting values for weak and strong correlations. An analogous scaling behavior has been found in previous numerical studies of W for an homogeneous charge distribution [34]. In this case one also observes that $W(g_{12})$ depends weakly on system size N_a provided it is measured in units of the Hartree-Fock energy E_{HF} and if γ_{12} is scaled within the relevant domain of representability $[\gamma_{12}^\infty, \gamma_{12}^0]$. In the present context, Fig. 5.2 implies that the change in W associated to a given change in the degree of delocalization g_{12} can be regarded as nearly independent of system size.

The very good scalability of W as a function of g_{12} for different system sizes is not obvious. In fact, if one considers $W(g_{12})$ for different charge transfers Δn, one observes much more significant deviations. This is demonstrated in Fig. 5.3 where the results for a 1D ring with $N_a = 14$ sites are compared for different Δn. Qualitatively, the dependence of W on the degree of delocalization g_{12} is similar for different Δn. Notice, for instance, the behavior for weak and strong correlations ($g_{12} \approx 0$ or 1) and the overall shape in the crossover region. This shows that the scaling hypothesis works satisfactorily even for different Δn. However, the quantitative differences between the scaled W for various Δn are more significant than those found for different sizes (see Figs. 5.2 and 5.3). This is actually not very surprising, since the nature of the electronic correlations are expected to evolve as we move from purely metallic to strongly ionic-like bonds. It is therefore important to investigate systematically the functional dependence of W for different Δn

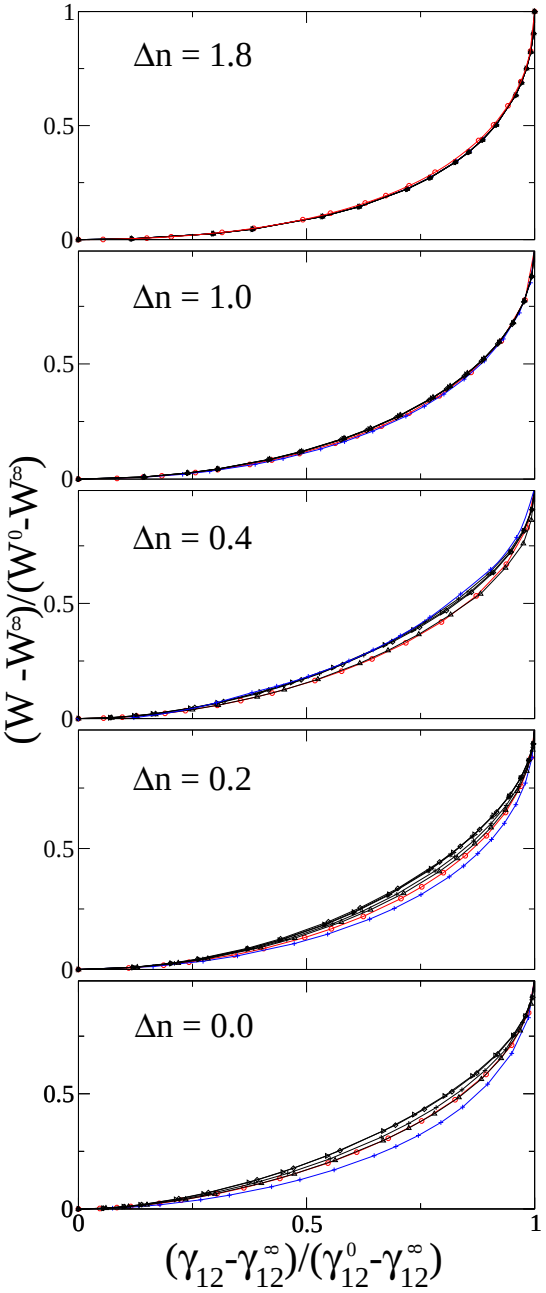

Figure 5.2: Scaled interaction energy W of the 1D Hubbard model as a function of the degree of electron delocalization $g_{12} = (\gamma_{12} - \gamma_{12}^{\infty})/(\gamma_{12}^{0} - \gamma_{12}^{\infty})$. $W^0 = E_{HF}$ and γ_{12}^{0} refer to the uncorrelated limit ($U = 0$) while W^{∞} and γ_{12}^{∞} to the strongly correlated limit ($U/t \to +\infty$). Results are given for band filling $n = 1$, all even numbers of sites $N_a = 2$–14, and different charge transfers Δn. Open circles (red) correspond to $N_a = 2$ and crosses (blue) to $N_a = 4$. The other sizes are very difficult to tell apart.

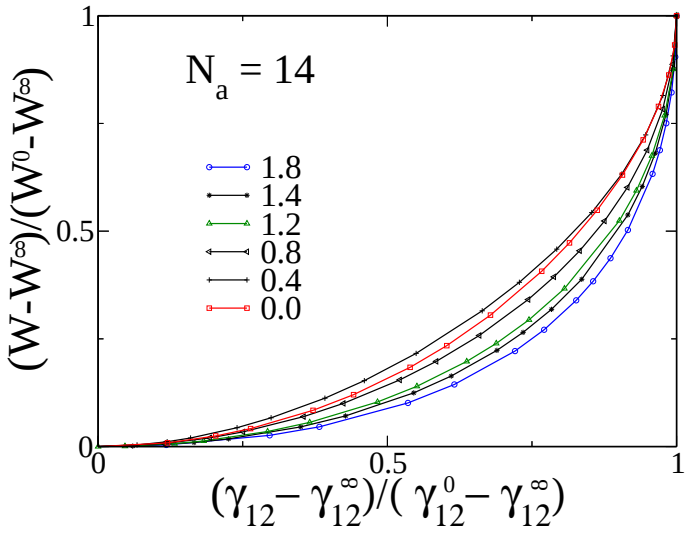

Figure 5.3: Charge transfer dependence of the the scaled interaction-energy functional W of the 1D Hubbard model. Results are given as a function of the degree of electron delocalization $g_{12} = (\gamma_{12} - \gamma_{12}^{\infty})/(\gamma_{12}^{0} - \gamma_{12}^{\infty})$ for $N_a = 14$, $n = 1$ and different charge transfers $\Delta n = 0.0$–1.8.

in order to elucidate its scaling behavior and evaluate the possibilities of transferring it from simple to complex many-body problems.

In Fig. 5.4 the band-filling dependence of W in a $N_a = 10$ site Hubbard ring is shown for $N_e \leq N_a$ and $\gamma_{12} \geq 0$. The same functional dependence is obtained for $N_e > N_a$ or $\gamma_{12} < 0$ due to electron-hole symmetry and the bipartite symmetry of the lattice $[W(\gamma_{12}, \Delta n) = W(\pm\gamma_{12}, \pm\Delta n)]$. While $W(\gamma_{12})$ depends strongly on n and Δn, several qualitative features are common to all the curves:
(i) As in the half-filled band case, the domain of v-representability of γ_{12} is limited by the bond orders in the uncorrelated and strongly-correlated limits: $\gamma_{12}^{0} \leq \gamma_{12} \leq \gamma_{12}^{\infty}$, where γ_{12}^{0} (γ_{12}^{∞}) corresponds to the ground state of the model for $U = 0$ ($U \to +\infty$). Notice that γ_{12}^{0} increases monotonously with N_e as the single-particle band is filled up. In contrast the behavior of γ_{12}^{∞} is more complex, showing either a monotonous increase with n for $\Delta n \geq 1$ or non-monotonous band-filling dependence for $\Delta n < 1$ (see Fig. 5.4). As already discussed, the dependence of γ_{12}^{0} and γ_{12}^{∞} on n and Δn are of central importance to the band-filling dependence of W.
(ii) In the weakly correlated limit, $W(\gamma_{12}^{0}, \Delta n) = W^{0}$ is given by the Hartree-Fock energy $E_{HF}/N_a = U(n^2 + \Delta n^2/4)/2$, since the underlying state is a single Slater determinant[1]. Moreover, the divergence of $\partial E_{\mathrm{C}}/\partial\gamma_{12}$ for $\gamma_{12} = \gamma_{12}^{0}$ shows that $\gamma_{12}^{gs} < \gamma_{12}^{0}$ for arbitrary small $U > 0$, as expected from perturbation theory.
(iii) Starting from $\gamma_{12} = \gamma_{12}^{0}$, W decreases monotonously with decreasing γ_{12} reaching its lowest possible value $W^{\infty} = UN_a \max\{0, n - 1 + \Delta n/2\}/2$ for $\gamma_{12} = \gamma_{12}^{\infty}$. As already dis-

[1]In the presence of degeneracies in the single-particle spectrum one may find that Levy's minimum W does not derive from a single Slater determinant and that $W^{0} < E_{\mathrm{HF}}$. However, this is a finite-size effect which importance decreases with increasing N_a.

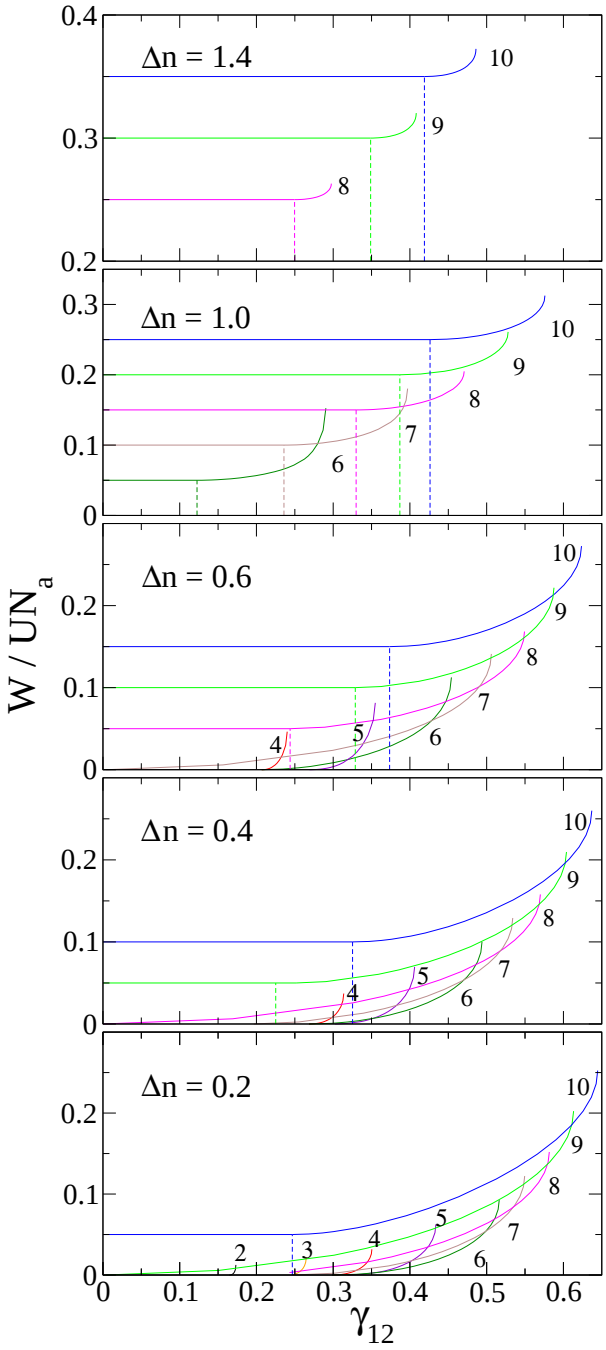

Figure 5.4: Interaction energy W of the 1D Hubbard model as a function of NN density-matrix element γ_{12} for representative charge transfers $\Delta n = \gamma_{22} - \gamma_{11}$. Results are given for $N_a = 10$ sites and different band fillings $n = N_e/N_a$. The numbers indicate the number of electrons N_e corresponding to each curve and the vertical dash lines the value of γ_{12}^{∞} below which $W = W^{\infty}$ remains constant.

cussed for $n = 1$, γ_{12}^{∞} defines the lower bound of the domain of v-representability. Smaller γ_{12} are still pure-state representable but $W = W^{\infty}$ is constant in this range. For the sake of clarity, the values of γ_{12}^{∞} are indicated by vertical dashed lines. Notice that W^{∞} vanishes for small electron density, provided that the charge transfer is not very strong (i.e., $n + \Delta n/2 = \gamma_{22} \leq 1$). The decrease of W with decreasing γ_{12} illustrates, once more, how the correlation-induced reduction of the Coulomb energy occurs at the expense of kinetic energy or electron delocalization.
(iv) γ_{12}^{∞} always represents the largest NN bond order that can be achieved under the constraint of minimal Coulomb repulsion energy. As the uncorrelated γ_{12}^{0}, γ_{12}^{∞} vanishes when the occupation of one the sublattices is either 0 or 2 (i.e., $\gamma_{11} = 0$ under the assumption $\gamma_{11} < \gamma_{22}$ and $n \leq 1$). However, in the strongly correlated limit, γ_{12}^{∞} also vanishes when the occupation of one the sublattices is strictly 1, since this leaves no possibility for the electrons or holes to delocalize without involving charge fluctuations (bipartite lattice). This is of course only possible for $n \geq 1/2$. One therefore finds, assuming $\gamma_{11} < \gamma_{22}$, that $\gamma_{12}^{\infty} = 0$ for $\gamma_{22} = n + \Delta n/2 = 1$.
(v) For small n or Δn, where both γ_{11} and γ_{22} are smaller than 1, it is possible to approximate the strongly correlated state (minimal W) by a fully-polarized Nagaoka state, as in the homogeneous case [35]. Here γ_{12}^{∞} is largest for $\Delta n = 0$, decreasing monotonously with increasing Δn, and vanishing for $\gamma_{11} = 0$ ($\Delta n = n$) or $\gamma_{22} = 1$ [$\Delta n = 2(1 - n)$] whatever occurs first. This explains the non-monotonous dependence of γ_{12}^{∞} as a function of n with a maximum for $n = 1/2$ for $\Delta n < 1$ (i.e., nearly half-filled fully-polarized-spin band).
(vi) In the other regime, for $\Delta n > 1$ [$1/2 < n < 1$ and $\gamma_{22} = (n + \Delta n/2) > 1$] one can obtain a lower bound for γ_{12}^{∞} by assuming localized electrons in sublattice 2, for instance with spin up, so that γ_{12} is given by the remaining $N_e - N_a/2$ down electrons. While this *Ansatz* neglects spin fluctuations and is therefore rather poor quantitatively, it explains the monotonous increase of γ_{12}^{∞} with increasing n for fixed $\Delta n > 1$ as the down band is filled up (see Fig. 5.4). The approximation remains qualitatively correct provided that $\gamma_{22} = (n + \Delta n/2) > 1$. In particular it explains that γ_{12}^{∞} vanishes for $\gamma_{11} = 0$ and $\gamma_{22} = 1$, and that, for a given n, it shows a local maximum for Δn not far from 1 [$2(1 - n) \leq \Delta n \leq 2n$], i.e., for $\gamma_{11} \simeq \gamma_{22} - 1$, when the delocalized electrons are evenly distributed among the two sublattices (see Fig. 5.4, for example, for $N_e = 8$).

The results for different band fillings are compared in Fig. 5.5 by considering the scaled interaction energy $(W - W^{\infty})/(W^{0} - W^{\infty})$ as a function of $g_{12} = (\gamma_{12} - \gamma_{12}^{\infty})/(\gamma_{12}^{0} - \gamma_{12}^{\infty})$. Once the relevant v-representable domains are brought to a common range, one observes a remarkably similar behavior for all band-fillings. Fig. 5.5 shows that the largest part of the band-filling dependence of W in the inhomogeneous Hubbard model comes from its limiting values $W^{0} = E_{\mathrm{HF}} = UN_a(n^2 + \Delta n^2/4)/2$ and $W^{\infty} = UN_a \max\{0, n - 1 + \Delta n/2\}/2$, and on the corresponding bounds γ_{12}^{0} and γ_{12}^{∞} of the domain of representability. Similar conclusions are inferred from calculations for other sizes and lattice structures. Notice that the strongest dependence of the scaled interaction on n is found for a nearly homogeneous charge density (small Δn) and for intermediate values of g_{12}. As we approach the strongly correlated limit ($g_{12} \leq 0.4$) the dependence of n is relatively weak even for $\Delta n \simeq 0$ One concludes that a properly scaled interaction energy follows approximately a universal behavior.

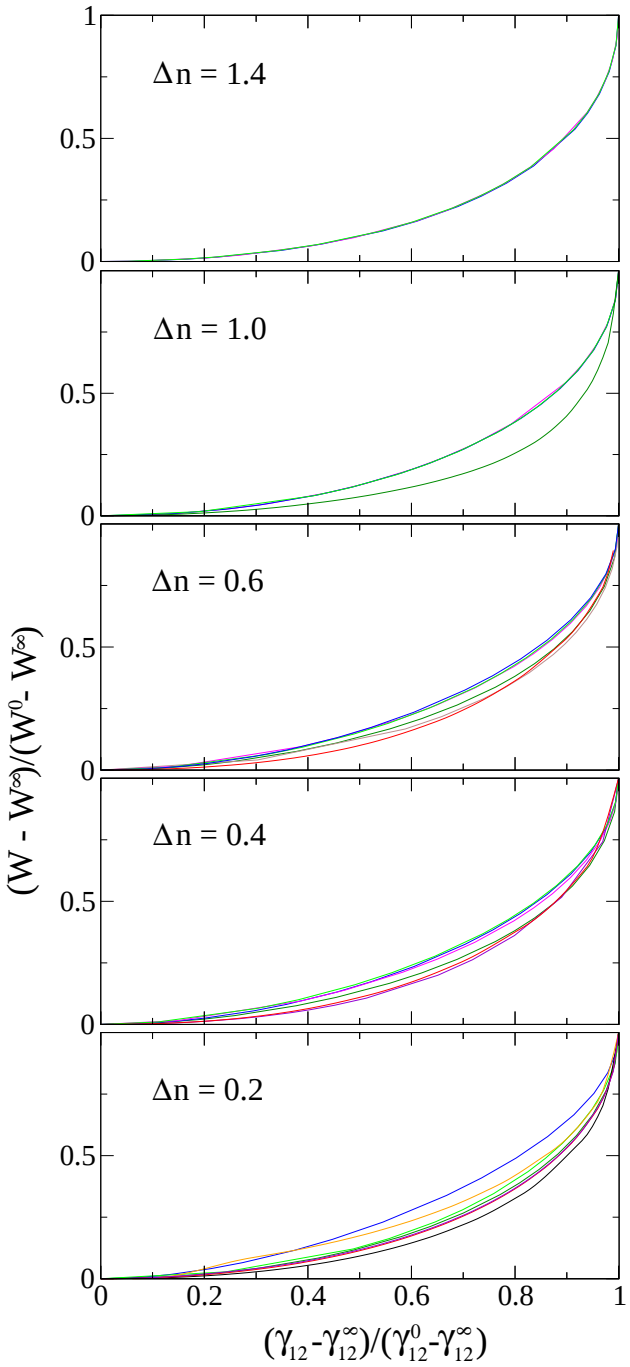

Figure 5.5: Scaled interaction energy of the 1D Hubbard model for $N_a = 10$ sites as a function of $g_{12} = (\gamma_{12} - \gamma_{12}^{\infty})/(\gamma_{12}^{0} - \gamma_{12}^{\infty})$. For each charge transfer Δn results are given for different band fillings $n = N_e/N_a$ as in Fig. 5.4.

5.2 Scaling *Ansatz* for $W[\gamma]$

The challenge now is to exploit the scaling properties shown in the previous section. The above study revealed that the dependence of W as a function of the NN bond order γ_{12} can be considered to be approximately independent of the system size, lattice dimension and band filling n, provided that two simple scaling conditions are taken into account. First, $W(\gamma_{12})$ must be scaled between the limit of weak correlation $W^0 = \sum_i \gamma_{ii\uparrow}\gamma_{ii\downarrow}$ and the limit of strong correlation $W^\infty = \sum_i \max[\gamma_{ii} - 1, 0]$, corresponding to the given charge distribution γ_{ii}. Second, γ_{12} must be scaled accordingly in the range $\gamma_{12}^\infty < \gamma_{12} < \gamma_{12}^0$ between the strongly correlated limit γ_{12}^∞ and the weakly correlated limit γ_{12}^0. This range represents the domain of v-representability of γ. Mathematically, this means that for a given density distribution $\{\gamma_{ii}\}$ it is a good approximation to regard

$$\mathrm{w} = \frac{W - W^\infty}{W^0 - W^\infty} \tag{5.1}$$

as a function of the degree of electron delocalization

$$g_{12} = \frac{\gamma_{12} - \gamma_{12}^\infty}{\gamma_{12}^0 - \gamma_{12}^\infty}. \tag{5.2}$$

In other words, the relative change in W associated to a change in the degree of electron delocalization g_{12} can be considered as nearly independent of the system under study. This extends the conclusions of previous investigations on the homogeneous Hubbard model to the inhomogeneous case [34]. Notice, however, that the relation between w and g_{12} does depend on γ_{ii}, and in particular on the charge transfer $\Delta n = \gamma_{22} - \gamma_{11}$ between the sub-lattices of a bipartite structure[2]. Consequently, a sound general approximation to W can be obtained by scaling the functional dependence of W on γ_{ij} corresponding to a simple reference system, which already contains the fundamental interplay between delocalization, charge transfer, and correlations.

The Hubbard dimer is the smallest and simplest system that fulfills these conditions. We therefore propose the scaled dimer approximation W_{sc}, which is given by

$$\frac{W_{\mathrm{sc}} - W^\infty}{W^0 - W^\infty} = \frac{W_2 - W_2^\infty}{W_2^0 - W_2^\infty}, \tag{5.3}$$

where the subindex 2 refers to the dimer. Using the definition of w [Eq.(5.1)] one may write Eq. (5.3) in a compact form as $\mathrm{w}_{\mathrm{sc}}(g_{12}, \Delta n) = \mathrm{w}_2(g_{12}, \Delta n)$, which implies

$$W_{\mathrm{sc}} = W^\infty + (W^0 - W^\infty)\frac{W_2 - W_2^\infty}{W_2^0 - W_2^\infty}. \tag{5.4}$$

Notice that all the terms on the right-hand side of Eq. (5.4) are simple functions of γ_{ij}. The uncorrelated and strongly correlated bounds in the dimer ($N_{\mathrm{e}} = N_{\mathrm{a}} = 2$) are given by $W_2^0 = [1 + (\Delta n/2)^2]/4$ and $W_2^\infty = \Delta n/4$. For an arbitrary system, these bounds are given by $W^0 = \sum_i \gamma_{ii\uparrow}\gamma_{ii\downarrow}$ (Hartree-Fock limit) and $W^\infty = \sum_i \max[\gamma_{ii} - 1, 0]$ (minimal

[2]Numerical results reported in Sec. 5.1 show that the dependence of W on Δn is not very strong in general, always much weaker than the dependence on g_{12}.

double occupations).[3] Finally, the exact dimer interaction-energy functional for $N_e = 2$ is given by

$$\frac{W_2}{UN_a} = \begin{cases} 1 - \frac{\gamma_{12}^2}{2} \frac{1+\sqrt{1-(\Delta n/2)^2-\gamma_{12}^2}}{(\Delta n/2)^2+\gamma_{12}^2}, & \text{if } \gamma_{12}^{\infty} < \gamma_{12} < \gamma_{12}^0 \\ \Delta n/4, & \text{if } |\gamma_{12}| < \gamma_{12}^{\infty}. \end{cases} \tag{5.5}$$

Despite its simplicity, Eqs. (5.4) and (5.5) reproduce several important exact properties that are common to all systems:
(i) The definition of $W[\gamma]$ is conditioned by the domain of v representability of the NN bond order γ_{12}, which is given by $\gamma_{12}^{\infty} \leq \gamma_{12} \leq \gamma_{12}^0$. The lower bound γ_{12}^{∞} corresponds to the strongly correlated limit and represents the maximum electron delocalization under the constraint of minimal double occupations. The upper bound γ_{12}^0 is the non-interacting limit of γ_{12} yielding the maximum degree of delocalization, irrespectively of the value of the double occupations. Notice that both γ_{12}^{∞} and γ_{12}^0 depend on the band filling n, on the charge transfer Δn, and on the NN connectivity of the specific lattice under study. For the half-filled dimer ($n = 1$) we have $\gamma_{12}^{\infty} = \sqrt{\Delta n(2-\Delta n)/2}$ and $\gamma_{12}^0 = \sqrt{1-(\Delta n/2)^2}$.
(ii) At the non-correlated limit, the underlying electronic state $\Psi[\gamma_{12}^0]$ is a single Slater determinant and $W(\gamma_{12}^0) = W^{\mathrm{HF}} = UN_a[n^2 + (\Delta n/2)^2]/4$. Moreover, $\partial W/\partial\gamma_{12}$ diverges for $\gamma_{12} = \gamma_{12}^0$. This is a necessary condition in order that an arbitrary small U yields a non-vanishing change in the ground-state density matrix $\gamma_{12}^{\mathrm{gs}}$, which is expected from perturbation theory.
(iii) For any fixed charge distribution $\{\gamma_{ii}\}$, W decreases with decreasing γ_{12}, reaching its lowest possible value $W^{\infty} = UN_a(\max[n - \Delta n/2 - 1, 0] + \max[n + \Delta n/2 - 1, 0])/2$ for $\gamma_{12} = \gamma_{12}^{\infty}$. The monotonic decrease in W upon decreasing γ_{12} means that any reduction in the Coulomb energy resulting from correlations is achieved at the expense of kinetic energy or electron delocalization. Notice that in most cases $\gamma_{12}^{\infty} > 0$. Reducing γ_{12} beyond γ_{12}^{∞} cannot lead to any further decrease in W for the given $\{\gamma_{ii}\}$. Therefore, W is constant, equal to W^{∞} in the range of $|\gamma_{12}| \leq \gamma_{12}^{\infty}$.
(iv) The strongly correlated γ_{12}^{∞} shows a non-monotonous dependence on charge transfer Δn. On a bipartite lattice γ_{12}^{∞} vanishes for $\Delta n = 2 - 2n$ if $n \geq 1/2$. In this case, all sites of one sub-lattice contain strictly one electron, while the sites of the other sub-lattice contain $2n - 1$ electrons ($\gamma_{22} = 1$ and $\gamma_{11} = 2n - 1$). Since the occupation of one of the sub-lattices is equal to one, no electronic hopping can occur in the strongly correlated limit. In addition, γ_{12}^{∞} also vanishes for extreme charge transfers, where one of the sub-lattices is completely empty ($\gamma_{22} = 2n$, $\gamma_{11} = 0$ and $\Delta n = 2n$, for $n \leq 1$) or completely full ($\gamma_{22} = 2$, $\gamma_{11} = 2n - 2$ and $\Delta n = 4 - 2n$, for $n \geq 1$). In this case the uncorrelated γ_{12}^0 also vanishes.

The general validity of these properties relies on the universality and transferability of the interaction-energy functional. In order to exemplify the previous general trends we present in Fig. 5.6 results for W_{sc} as a function of g_{12} for different representative values of Δn. To evaluate the accuracy of the scaled dimer approximation these results are compared with the exact Levy-Lieb functional $W_{\mathrm{ex}}[\gamma]$, which was calculated by performing the minimization in Eq. (4.6) for a finite ring having $N_a = 10$ sites and different numbers of electrons N_e. The constraints on $|\Psi\rangle$ given by Eq. (4.7) are imposed for $i = j$ ($\gamma_{11} + \gamma_{22} = 2n$ and $\gamma_{22} - \gamma_{11} = \Delta n$) and for NN ij along a periodic ring ($\gamma_{ij} = \gamma_{12}$) by using the method

[3] In case of degeneracies at the Fermi energy of the single-particle spectrum in a finite system, W^0 can be calculated by applying degenerate perturbation theory ($W^0 < W^{\mathrm{HF}}$).

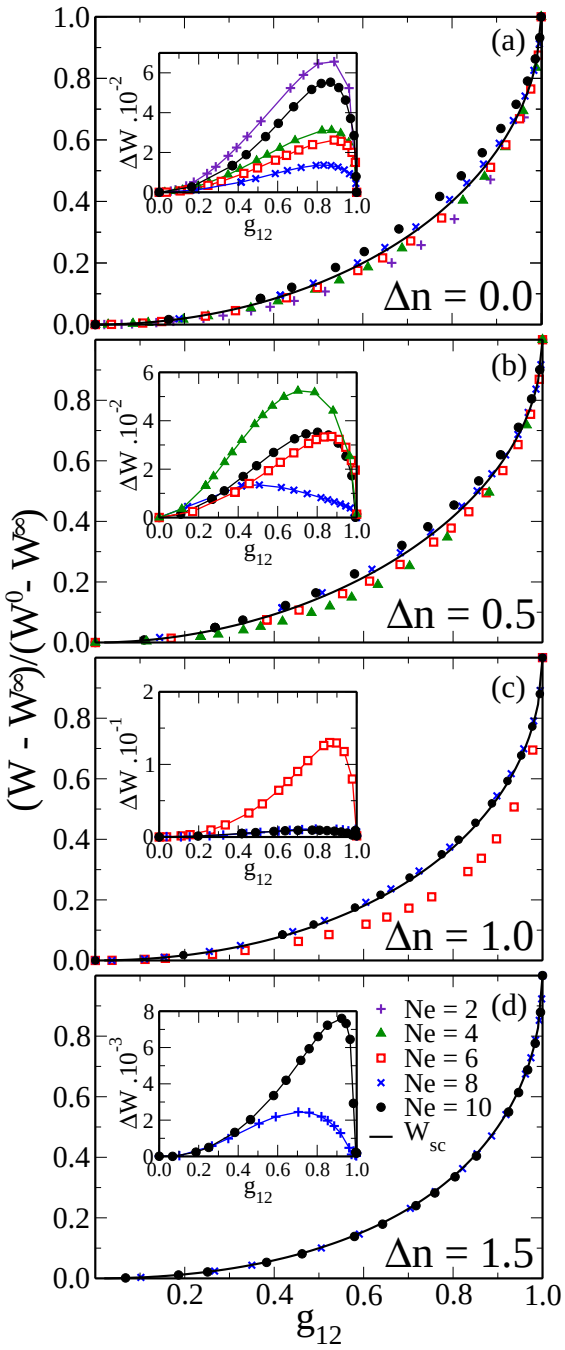

Figure 5.6: Comparison between the scaled dimer functional $W_{\rm sc}[\gamma]$ as a function of the degree of electron delocalization $g_{12} = (\gamma_{12} - \gamma_{12}^{\infty})/(\gamma_{12}^{0} - \gamma_{12}^{\infty})$ [solid curves, Eq. (5.4)] and the exact functional $W_{\rm ex}$ derived from Lanczos diagonalization (symbols). Results are shown for a 1D bipartite ring having $N_{\rm a} = 10$ sites, different band fillings $n = N_{\rm e}/N_{\rm a}$ and representative charge transfers $\Delta n = \gamma_{22} - \gamma_{11}$. The inset figures display the corresponding relative errors $\Delta W = (W_{\rm sc} - W_{\rm ex})/(W^{0} - W^{\infty})$.

of Lagrange multipliers. In this way the constrained minimization amounts to computing the ground state of an effective Hubbard model, which has been done numerically by means of the Lanczos method [34, 74]. The calculations demonstrate the above discussed trends *(i)–(iv)*. In addition, one observes that the proposed approximation $W_{\rm sc}$ follows quite closely the exact functional $W_{\rm ex}$ all along the crossover from weak to strong correlations (see Fig. 5.6). This is quite remarkable taking into account the strong dependence of the boundary values W^0, W^∞, γ_{12}^0 and γ_{12}^∞ on band filling n and charge transfer Δn. The quantitative discrepancies are in general small [i.e., $|W_{\rm sc}-W_{\rm ex}|/(W^0-W^\infty) \simeq 0.008$–$0.06$] except for $N_{\rm e}=6$ and $\Delta n=1$, where $|W_{\rm sc}-W_{\rm ex}|/(W^0-W^\infty) \simeq 0.1$). Moreover, the largest deviations between $W_{\rm sc}$ and $W_{\rm ex}$ occur for rather large values of γ_{12} ($g_{12} \simeq 0.8$–0.9) which concern mainly the weakly correlated regime where the kinetic energy dominates. Consequently, a good general performance of the method can be expected. Although the dependence of W on the degree of delocalization g_{12} is similar for different Δn, one observes significant differences between Figs. 5.6 (a)–(d), which reflect the changes in the nature of the electronic correlations as we move from purely metallic to strongly ionic like bonds. These are well reproduced by the scaling *Ansatz* $W_{\rm sc}$. In the following section several applications of LDFT are presented by using $W_{\rm sc}$ as approximation to the interaction-energy functional.

5.3 Applications to bipartite clusters

For the applications of the theory we consider the inhomogeneous Hubbard model on bipartite 1D and 2D clusters consisting of a sub-lattice $\mathcal{S}_1$, where the energy levels $\varepsilon_i = \varepsilon_1 = \varepsilon/2$, and a sub-lattice $\mathcal{S}_2$, where $\varepsilon_i = \varepsilon_2 = -\varepsilon/2$ [see Eq. (4.1)]. Besides the band-filling $n = N_{\rm e}/N_{\rm a}$, the system is characterized by two dimensionless parameters: the bipartite potential ε/t, which controls the degree of charge transfer $\Delta n = \gamma_{22}-\gamma_{11}$ between the sub-lattices, and the Coulomb repulsion strength U/t, which measures the importance of correlations. The ground-state properties of the model are the result of a subtle interplay between the kinetic energy associated to electronic hopping and delocalization, which is proportional to $t\gamma_{12}$, the charge-transfer energy $\Delta E_{\rm CT} = -\varepsilon\Delta n/2$, and Coulomb-repulsion energy W. Bipartite clusters with periodic boundary conditions (PBC) are interesting to study for two reason. First, the finite size of these system allow us to compare our method with exact diagonalization results (for clusters having $N_a \leq 16$) in order to validate our theory before applying it to more challenging infinite systems. Second, they present non-trivial finite-size effects also due to their hight symmetry, which lead to degeneracies having often huge consequences on the properties. As an example, we display in Fig. 5.7 the non-correlated one-particle spectra of some representative 1D and 2D bipartite clusters for different values of the energy level shift ε/t. The ground state of an homogeneous non-correlated cluster with PBC is a Slater determinant and its eigenstates are plane waves with wave number $k_n = 2\pi n/N_a$. The translation symmetry imposes that $E(k) = E(-k)$ leading to a highly degeneracy spectrum. One can clearly see, the high degeneracy of these spectra and the future consequence on the charge gap calculation. For example, at half band filling, the $N_a = 12$ site ring with $\varepsilon/t = 0$ has a charge gap $\Delta E_{\rm c}/t = 0$, while it is finite and equal $\Delta E_{\rm c}/t = 0.88$ for $N_a = 14$. Another interesting point is that the energy level shift ε/t not break the degeneracy in the 1D case. It only breaks some part of the degeneracies in the 2D case. The reason is that the bipartite potential does not break the

inversion symmetry and consequently the states having k and $-k$ stay degenerate.

The physical behavior of bipartite cluster is analyzed from the homogeneous to the strongly ionic regimes, as well as from weak to strong correlations, by computing the ground-state energy $E_{\rm gs}$, the NN bond order γ_{12}, the charge transfer Δn, the average number of double occupations per site $W/UN_{\rm a}$ and the charge gap $\Delta E_{\rm c}$. The accuracy of the scaled dimer approximation is quantified by systematically comparing the LDFT results with exact Lanczos diagonalization [42] on finite 1D rings or 2D squares with periodic boundary conditions. These systems also provide an interesting opportunity to assess the ability of LDFT to deal with discrete single-particle spectra and with possible degeneracies at the Fermi energy, which often leads to non-trivial charge transfers as a function of the model parameters.

Figure 5.8 shows the ground-state properties of a 1D ring having $N_{\rm a} = 14$ sites as a function of the Coulomb repulsion strength U/t. Different values of the energy level shift ε/t are considered at half band filling $n = 1$. First of all, for the homogeneous case ($\varepsilon/t = 0$ and $\Delta n = 0$) one observes the well-known monotonous increase of $E_{\rm gs}$ with increasing U/t, reaching $E_{\rm gs} = 0$ for $U/t \to \infty$, where both electronic hopping and double occupations vanish. At the same time γ_{12} and W decrease monotonously with U/t [see sub-figures (b) and (d)]. A number of new features appear when the bipartite level shift ε is finite. In this case, as we go from weak to strong correlations, the system undergoes a qualitative change from a delocalized charge-density-wave (CDW) state ($\Delta n \simeq 0.9$–1.6 and $\gamma_{12} \simeq 0.3$–0.6) to a nearly localized state having an homogeneous charge distribution ($\Delta n < 0.01$ and $\gamma_{12} < 0.1$). Starting from the weakly correlated CDW state and increasing U/t, one observes a decrease in Δn, since inhomogeneous charge distributions necessarily imply larger average double occupations [see sub-figures (c) and (d)]. Nevertheless, a nearly homogeneous charge distribution is only reached for $U \gg \varepsilon$.

An interesting effect, which becomes more distinctive as ε/t increases, is the non-monotonous dependence of the kinetic energy and bond order γ_{12} as a function of U/t. Notice that the maximum in γ_{12} does not correspond to the non-interacting limit but to a finite value of U/t [see sub-figure (b)]. In fact, for $U \simeq \varepsilon$ the Coulomb repulsion on the doubly occupied sites on sub-lattice $\mathcal{S}_2$ compensates the energy difference between the two sub-lattices ($\varepsilon_1 = \varepsilon/2 = -\varepsilon_2 > 0$). This allows a nearly free-like motion of the γ_{11} electrons occupying sub-lattice $\mathcal{S}_1$, together with the extra $\gamma_{22} - 1$ electrons on sub-lattice $\mathcal{S}_2$ ($\gamma_{11} < \gamma_{22}$ for $\varepsilon > 0$). Consequently, the delocalization of the electrons is enhanced for $U \simeq \varepsilon$, yielding a maximum in γ_{12}. The effect is more pronounced for $\varepsilon/t \gg 1$, since this implies a stronger CDW at $U = 0$ and a larger crossover value of $U = \varepsilon$. Moreover, it is interesting to observe that for large ε the maximum in γ_{12} corresponds to $\Delta n = 1$ [compare sub-figures (b) and (c)]. Indeed, for $U/t \simeq \varepsilon/t \gg 1$ (in practice $U/t \simeq \varepsilon/t \geq 4$) one electron is essentially locked in the sub-lattice $\mathcal{S}_2$, and the remainder electron in the unit cell is evenly distributed among the two sub-lattices.

For $n = 1$ this implies $\gamma_{11} \simeq 1/2$ and $\gamma_{22} \simeq 3/2$, or equivalently, $\Delta n = 1$. Concerning the comparison between LDFT and exact results one observes that all the considered ground-state properties are very well reproduced by the scaled dimer *Ansatz*. This holds for all values of the energy level shift between the sub-lattices, not only close to the weak and strongly correlated limits but also in the intermediate interaction region. Moreover, the fact that γ_{12}, Δn and W are all obtained with a high level of precision shows that the results for $E_{\rm gs}$ are not the consequence of a strong compensation of errors. It is also interesting to note that the accuracy actually improves as the charge distribution

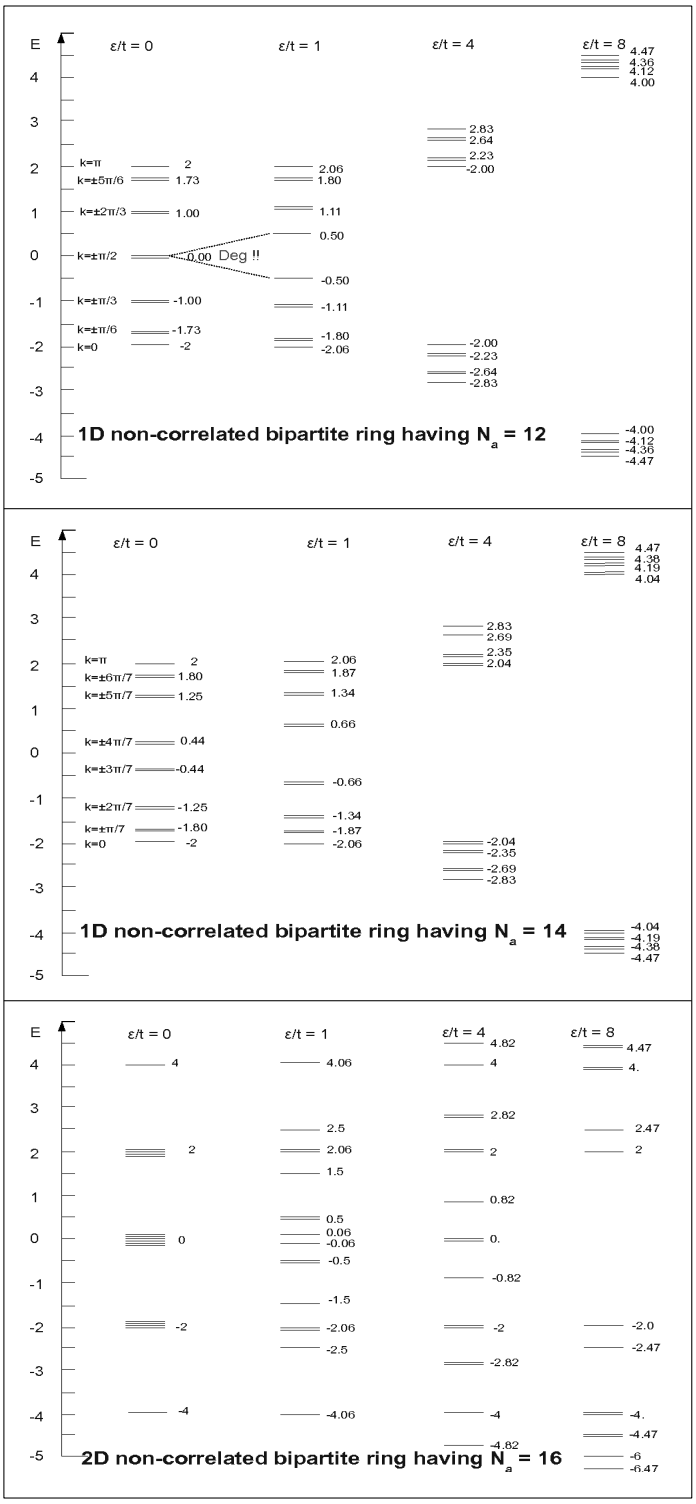

Figure 5.7: One-particle spectra at $U/t = 0$ for Hubbard bipartite rings having $N_a = 12$ and 14 sites and for a 4×4 cluster with periodic boundary conditions ($N_a = 16$ sites). Representative values of the energy level shift ε/t are considered.

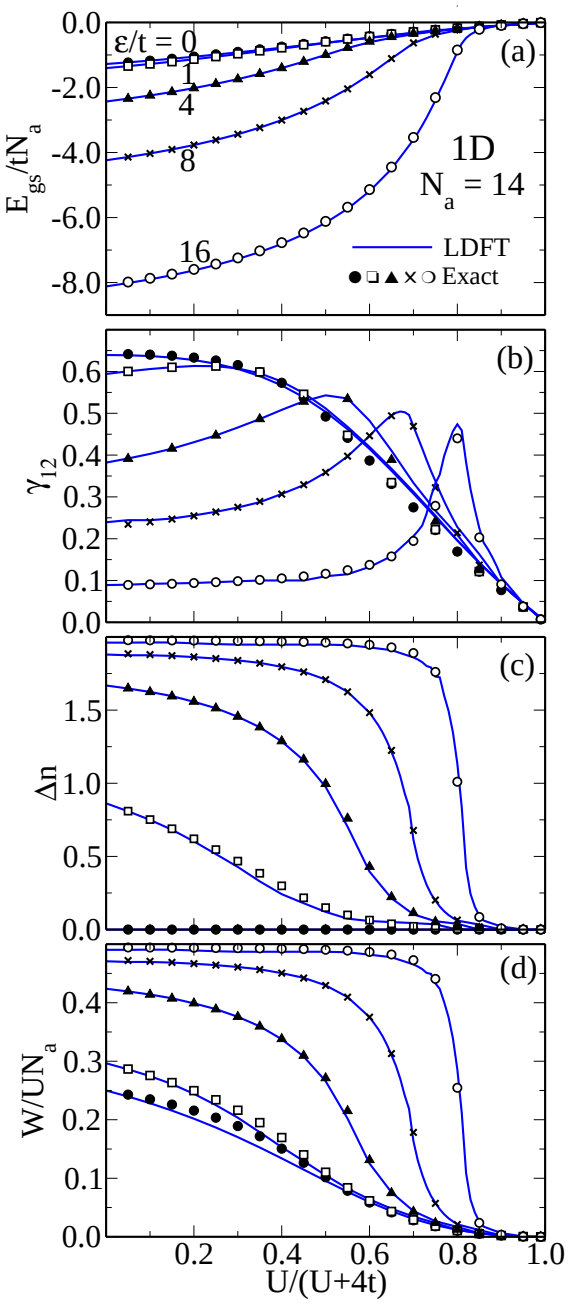

Figure 5.8: Ground-state properties of bipartite Hubbard rings having $N_\mathrm{a} = 14$ sites and half band filling $n = 1$ as a function of the Coulomb repulsion strength U/t. Different values of the energy level shift ε between the sub-lattices are considered as indicated in (a). Results are given for (a) ground-state energy E_gs, (b) NN bond order γ_{12}, (c) charge transfer $\Delta n = \gamma_{22} - \gamma_{11}$ and (d) average number of double occupations per site W/UN_a. The solid curves refer to LDFT using the scaling approximation W_sc [see Eq. (5.4)] while the symbols are the results of exact Lanczos diagonalization.

becomes more inhomogeneous, i.e., as ε/t and the CDW are stronger. In other words, the homogeneous case, which was investigated in detail in Refs. [34] and [35], is the most difficult one. This seems reasonable, since large values of ε enhance the importance of single particle contributions to the energy and somehow tend to decouple the 1D chain in dimers, within which correlations are taken into account exactly. A similar improvement of the accuracy of the scaled dimer functional has already been observed in dimerized chains with homogeneous charge density [36]. One concludes that LDFT, combined with Eqs. (5.4) and (5.5) for $W[\gamma]$, provides a very good description of electron correlations and of the resulting interplay between kinetic, charge-transfer and Coulomb energies in 1D lattices.

In Fig. 5.9 the band-filling dependence of $E_{\rm gs}$ is shown for a 1D ring having $N_{\rm a} = 14$ sites and representative values of the Coulomb repulsion U/t and of the energy level shift ε/t. For low electron densities, up to quarter filling $n = 1/2$, one observes that $E_{\rm gs}$ decreases for all U/t as the band is filled up. Notice in particular the weak dependence of $E_{\rm gs}$ on the Coulomb repulsion strength, even for $U/t \gg 1$. This implies that for low carrier densities charge fluctuations are very efficiently suppressed by correlations. Consequently, the kinetic and crystal-field energies dominate over the Coulomb energy ($n \leq 1/2$). This is quite remarkable, since ignoring correlations would have lead to a quadratic increase in the Coulomb energy ($E_{\rm HF} \propto Un^2$). Comparing different crystal fields ε/t, one notes that the role of electron interactions is most important in the homogeneous case, where our results coincide with previous calculations [35]. As ε/t increases the electrons tend to be localized on one sub-lattice in order to take advantage of the crystal field, thereby reducing the importance of both kinetic and Coulomb contributions. Consequently, $E_{\rm gs}$ is nearly independent U/t ($\varepsilon/t \geq 4$ and $n \leq 1/2$). Beyond quarter filling the n dependence of $E_{\rm gs}$ changes qualitatively, since double occupations become unavoidable, not only for delocalize electronic states but also for ionic states with significant charge transfer to the most stable sub lattice. In this case ($n \geq 1/2$) $E_{\rm gs}$ continues to decrease with increasing n only if the Coulomb interactions are weak ($U/t < 4$). Otherwise, for $U/t > 4$, $E_{\rm gs}$ goes first over a minimum at $n = 1/2$, where the decrease in kinetic and crystal-field energies is approximately canceled by the increase in Coulomb energy. Then, it increases with n as we move to even higher densities ($n > 1/2$). These trends are qualitatively similar for all values of the bipartite potential. However, the crossover from low- to high-density behavior becomes more abrupt as ε/t increases [compare Figs. 5.8 (a)–(d)]. As in Fig. 5.8 the agreement between the LDFT results (solid curves) and the Lanczos diagonalization (symbols) is most satisfying for all values of n, U and ε. The scaling approximation reproduces all the previous trends very accurately. Moreover, as already mentioned in the context of Fig. 5.8, the quality of the results for $E_{\rm gs}$ is not the consequence of a compensation of errors on different contributions (i.e., $E_{\rm CD}$, $E_{\rm K}$ and W). This is probably the reason behind the favorable outcome for all band fillings and interaction parameters.

The charge excitation gap

$$\Delta E_{\rm c} = E(N_{\rm e} + 1) + E(N_{\rm e} - 1) - 2E(N_{\rm e}) \tag{5.6}$$

is a property of considerable interest in strongly correlated systems, which measures the insulating or metallic character of the electronic spectrum as a function of ε/t, U/t and n. It can be directly related to the discontinuities in the derivatives of the single-particle and correlation energies per site with respect to the electron density n. Therefore, the

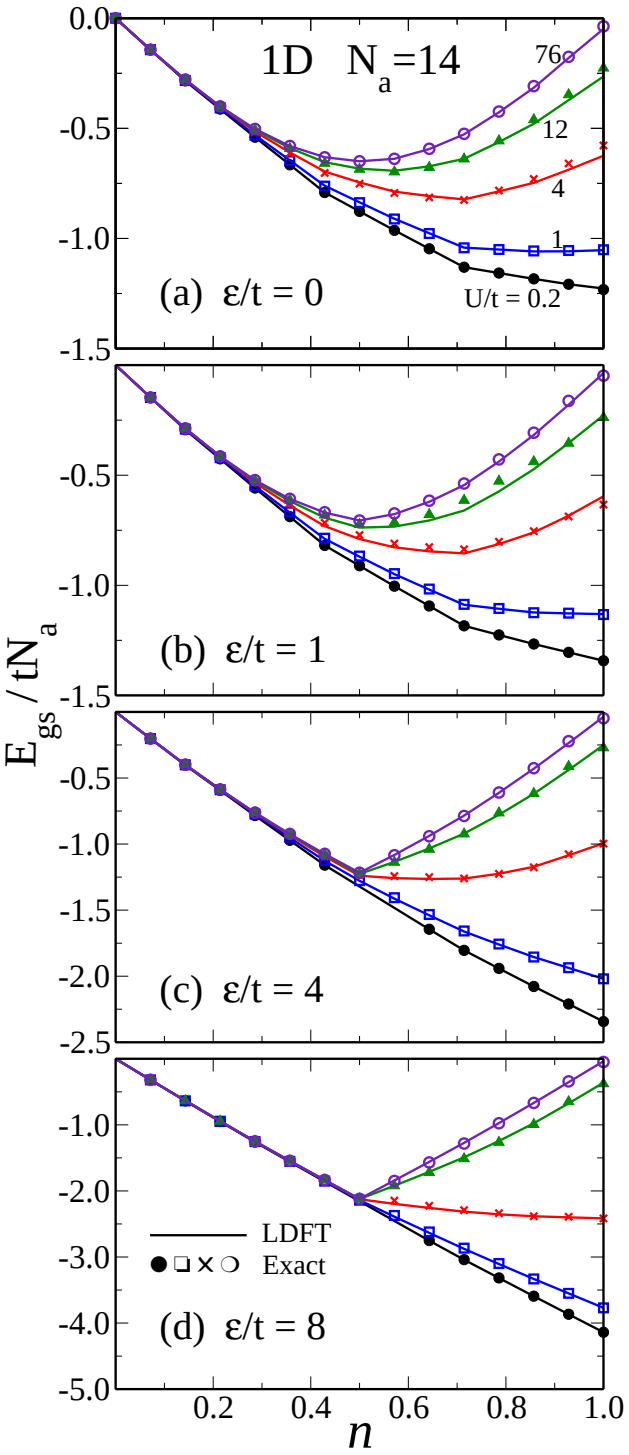

Figure 5.9: Band-filling dependence of the ground-state energy of 1D Hubbard rings having $N_\mathrm{a} = 14$ sites and different bipartite potentials ε. The solid curves refer to LDFT with the scaled dimer functional W_sc, and the symbols to exact numerical results. Representatives values of the Coulomb repulsion strength U/t are considered as indicated in (a).

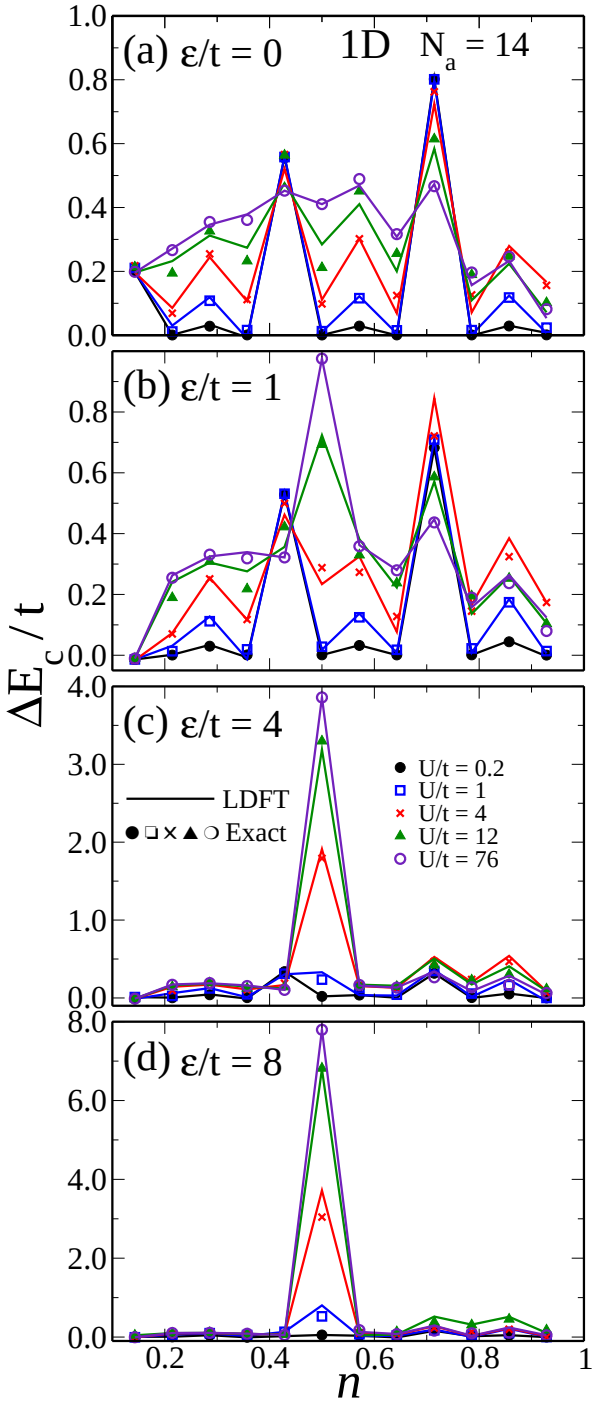

Figure 5.10: Charge gap $\Delta E_{\rm c} = E(N_{\rm e}+1) + E(N_{\rm e}-1) - 2E(N_{\rm e})$ as a function of band filling n in 1D Hubbard rings having $N_{\rm a} = 14$ sites and different bipartite potentials ε. The solid lines connecting discrete points refer to LDFT with the scaled dimer functional and the symbols to exact Lanczos diagonalization. Representative values of the Coulomb repulsion strength U/t are considered as indicated in (c). Results for $n = 1$ are given in Fig. 5.13.

calculation of $\Delta E_{\rm c}$ constitutes a more serious challenge than the calculation of $E_{\rm gs}$, particularly in the framework of a density-functional approach. In Fig. 5.10 results are given for $\Delta E_{\rm c}$ as a function of band filling $n < 1$, which correspond to a 1D Hubbard rings having $N_{\rm a} = 14$ sites and different ε/t and U/t. The half-filled-band case deserves special attention and is considered in Fig. 5.13.

Finite bipartite rings have a discrete single-particle energy spectrum, which is conditioned by the two important inversion and electron-hole symmetries. The former requires $\varepsilon_\alpha(k) = \varepsilon_\alpha(-k)$, where $\alpha = 1, 2$ refers to the two bands of the unit cell, and the latter implies that for each eigenenergy $\varepsilon_\alpha(k)$ the inverse $-\varepsilon_\alpha(k)$ is also an eigenvalue. In the following we restrict ourselves to $N_{\rm a}$ even, as imposed by the periodic boundary conditions. In the homogeneous case ($\varepsilon = 0$) we have one atom per unit cell and $-\pi/a \leq k \leq \pi/a$. The single-particle energies are given by $\varepsilon_k = -2t\cos(ka)$, where $k = 0$, $k = \pm\nu\pi/aN_{\rm a}$ with $\nu = 1, \ldots (N_{\rm a}-1)$, and $k = \pi/a$. For $N_{\rm a}/2$ even, this yields a doubly degenerate level in the middle of the band corresponding to $k = \pm\pi/2a$, while for $N_{\rm a}/2$ odd $k = \pm\pi/2a$ is not allowed and there is a gap in the middle of the band between two doubly degenerate states ($k = \pm 4\pi/7a$ and $k = \pm 5\pi/7a$ for $N_{\rm a} = 14$). For $N_{\rm a}/2$ even, the alternating bipartite potential ($\varepsilon \neq 0$) couples the states having $k = \pm\pi/2a$ and opens a gap ε at half band filling ($n = 1$), while for $N_{\rm a}/2$ odd, one observes simply an enhancement of the existing gap between doubly degenerate states. The results for $\Delta E_{\rm c}$ in the non-interacting limit ($U/t \ll 1$) can be interpreted in terms of the single-particle spectrum. In particular for $N_{\rm a} = 14$ one finds that for $U = 0$ the charge gap $\Delta E_{\rm c} = 0$ for $N_{\rm e} = 3$–5, 7–9 and 11–13 due to the presence of double degenerate states. Any small Coulomb interaction $U \neq 0$ removes the double degeneracy yielding a finite $\Delta E_{\rm c}$ for $N_{\rm e} = 4$, 8 and 10. This explains the even-odd alternations as a function of $N_{\rm e}$ for small U/t [see Figs. 5.10 (a) and (b)].

For strong interactions ($U/t > 4$) the single-particle picture breaks down and simple detailed interpretations seem difficult. One may however observe that for low carrier density ($n < 1/2$) the gap tends to decrease as ε/t increases, even for large U/t, since the two sub-lattices progressively decouple from each other. In contrast, an increasingly important gap develops for large U/t at $n = 1/2$, which tends to $\Delta E_{\rm c} = \varepsilon$ for $U/t \to +\infty$. This contrasts with the corresponding gap in the weakly correlated limit, which vanishes for $N_{\rm a}/2$ odd and is finite (of the order of $t/N_{\rm a}$) for $N_{\rm a}/2$ even. The origin of the finite charge gap for large U/t is the energy difference between adding an electron in the sub-lattice $\mathcal{S}_1$ (having $\varepsilon_1 = \varepsilon/2$) and removing an electron in the sub-lattice $\mathcal{S}_2$ (having $\varepsilon_2 = -\varepsilon/2$). In fact, for $U/t \gg 1$ the kinetic energy is very weak, $E_{\rm CD}$ dominates over $E_{\rm K}$, and therefore the sub-lattice $\mathcal{S}_1$ is essentially empty in the strongly correlated ground state ($n \leq 1/2$). Notice that a finite $\Delta E_{\rm c} \simeq \varepsilon$ for $n = 1/2$ and large U/t is also found in the thermodynamic limit, as well as for finite $N_{\rm a}$ with $N_{\rm a}/2$ even.

As for any excitation, obtaining accurate results for $\Delta E_{\rm c}$ within a density functional approach is more delicate than for the ground-state properties. Nevertheless, it seems fair to say that LDFT with the present approximation to W performs quite well quantitatively, except for intermediate values of ε/t and U/t [see, for example, $\varepsilon/t = 1$ and $U/t = 12$ in Fig. 5.10(b)]. In particular the removal of degeneracies due to the interactions and the resulting even-odd oscillations, the crossover from weak to strong correlations, and the development of a finite gap $\Delta E_{\rm c} \simeq \varepsilon$ at quarter filling for $U/t \gg 1$ are very well reproduced. As we have seen, an important gap opens at quarter band filling with increasing the strength of the Coulomb repulsion. This phenomena is studied in particular in Fig 5.11 where we present the charge gap $\Delta E_{\rm c}/t$ at quarter filling ($n = 1/2$) as predicted by LDFT

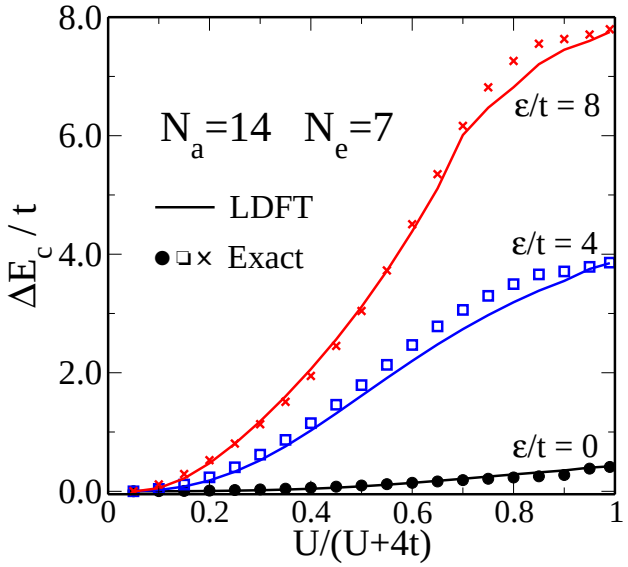

Figure 5.11: (Color online) Charge gap $\Delta E_c/t$ as a function of the Coulomb repulsion strength U/t in 1D Hubbard rings having a $N_a = 14$ sites, quarter filling $n = 1/2$, and representative values of the bipartite potential ε. The curves refer to LDFT with the scaled dimer functional W_{sc} and the symbols to exact diagonalization.

within the scaling approximation (solid curves) and by exact diagonalizations (symbols). Different values of the energy level shift are considered as indicated in the figure. Besides the very good agreement between LDFT and exact diagonalizations, one observes the increase of the gap as a function of U/t particularly for finite values of ε/t. In the non correlated case, the gap is $\Delta E_c/t = 0$, since the degeneracies of the spectrum is not broken by the bipartite potential (see Fig. 5.7). For the homogeneous case ($\varepsilon/t = 0$) a gap opens as U/t increases (reaching $\Delta E_c/t = 0.5$ for $U \to \infty$). In contrast the thermodynamic limit presents a metallic behavior. This is a finite size effect due to the Coulomb repulsion which break the degeneracy k, $-k$ and opens a gap between these two states. For a finite value of ε/t and as the Coulomb interaction increases the gap increases reaching $\Delta E_c/t = \varepsilon/t$ for $U \to \infty$. Starting from the non-correlated case where the gap in zero and the ground states is a CDW, increasing the Coulomb repulsion enhances the stability of the less energetic sub-lattice. At $U \to \infty$ all the electrons are localized on the most favorable sub-lattice. An additional electron on the system will be necessary on the higher energy sub-lattice, since double occupation are not allowed. Consequently, adding this electron implies an energy increase of about ε/t.

The charge gap at half band filling has the specificity of involving an extra double occupation for $N_e = N_a + 1$, which is unavoidable even in a strongly correlated state, in contrast to any smaller band filling $N_e \leq N_a$. This implies that a contribution of the order of U to ΔE_c must be taken for granted. It is therefore more meaningful to consider $(\Delta E_c - U)/t$ as reported in Fig. 5.12 and 5.13, which represents the nontrivial kinetic and correlation contributions.

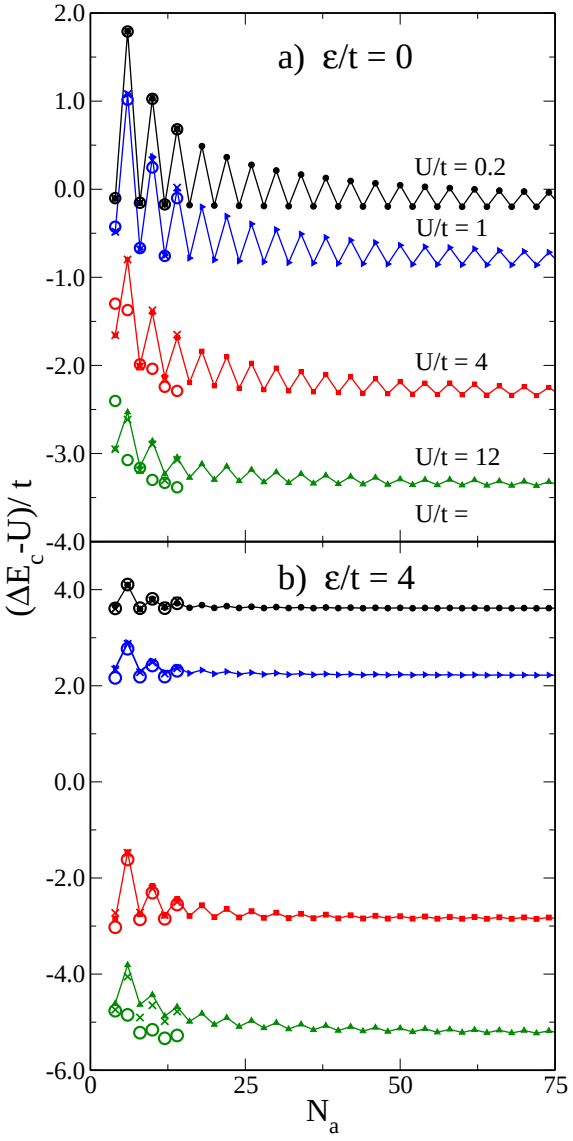

Figure 5.12: Non trivial part of the charge gap $(\Delta E_{\rm c} - U)/t$ as a function of the size of the 1D Hubbard bipartite ring at half band filling $n = 1$. Representative values of the bipartite potential ε and the Coulomb integral U are considered. The symbols connected by solid lines refer to LDFT with the scaled dimer functional $W_{\rm sc}$ and an approximation of γ_{12}^{∞}, The crosses are obtained with the same dimer functional $W_{\rm sc}$ but using exact value of γ_{12}^{∞}. Finally the open circles correspond to exact diagonalization.

In Fig 5.12 we present the size dependence of the non trivial part $\Delta E_{\rm c} - U$ of the charge gap for representative values of U/t and ε/t for 1D Hubbard chain with periodic boundary conditions and half band filling. These calculation allow us to study the transition from finite size objects to the thermodynamic limit. We observe first of all for $\varepsilon/t = 0$ super-even oscillations, which come from the properties on the one-particle spectrum which is degenerate at the Fermi level for $N_a = 4n$, n integer $n \geq 1$. In this case the degeneracy at the Fermi level implies that the charge gap is zero at the non correlated limit where in the other case the charge gap is finite. As the size increase, the value of the charge gap converge to the infinite chain limit since the discrete spectrum becomes continuous ($\Delta E_{\rm c} = 0$ for $U = 0$). As the strength of the Coulomb repulsion increases the oscillatory behavior disappears, as shown by the exact diagonalization results ($N_a \leq 14$, big circles). Since our scaling *Ansatz* use the scaling properties of the v-representability domain, the correlation-energy functional is strongly affected by the oscillations of the limits of the v-representability domain. Consequently, even for strong correlations, LDFT gives an oscillatory behavior for the charge gap. Nevertheless, the results are qualitatively comparable, and seem to converge at infinite-size limit to an underestimation of the charge gap. For $\varepsilon/t = 4$ and at weak correlation ($U/t \leq 1$) the oscillations are weaker due to the important charge transfer Δn between the two sub-lattices ($\Delta n \simeq 1.6$). At the non-correlated limit, the energy level shift breaks the degeneracies and increasing the charge gap as ε/t increases. The convergence to the infinite-size limit is faster. The case $U = \varepsilon = 4$ is interesting since there is again an important oscillatory behavior. In this case, the charge transfer energy compensate the Coulomb repulsion ($\Delta n \simeq 0.5$) and consequently the kinetic energy which induces the oscillatory behavior play an important role. As for the homogeneous case, at the strongly correlated limit, LDFT preserves the oscillatory behavior, and gives qualitative good results, underestimating the charge gap. Notice that the LDFT results obtain within the exact γ_{ij}^{∞} and the approximation of γ_{ij}^{∞} [61] are quantitatively comparable. At the strongly correlated limit, and near to half band filling, the electronic density is nearly homogeneous since $U >> \varepsilon$. In this case the approximation of γ_{ij}^{∞} is very good. The largest error made by our approximation of γ_{ij}^{∞} occurs for $\Delta n \simeq 1.0$ near to half band filling. This would require $\varepsilon \simeq U/t \rightarrow /t\infty$ which is physically unrealistic.

In Fig. 5.13 we present the non trivial part of the charge gap $\Delta E_{\rm c}$ as a function of the Coulomb repulsion strength. We present results for 1D systems having $N_a = 12$, 14 sites and at the thermodynamic limit ($N_a \rightarrow \infty$). Are also considered representative value of the energy level shift ε/t. In the homogeneous case without interactions ($\varepsilon = 0$ and $U = 0$) the gap vanishes for $N_{\rm a}/2$ even, while it remains of the order of $t/N_{\rm a}$ for $N_{\rm a}/2$ odd. $\Delta E_{\rm c} - U$ decreases monotonously as U/t increases, reaching a common limit $\Delta E_{\rm c} = U - 2w_b$ for all $N_{\rm a}$, where w_b represents the kinetic energy gained through the delocalization of the extra electron or hole. In the homogeneous case $w_b = 2t$ coincides with the single-particle band width, since the ground-state for $N_{\rm e} = N_{\rm a} \pm 1$ is the fully-polarized ferromagnetic Nagaoka state [19]. The structureless shape of $\Delta E_{\rm c}$ as a function of U/t hides a profound change in the nature of the underlying charge excitation along the crossover from weak to strong interactions, namely, from a single-particle electron-hole excitation to a strongly-correlated low-spin to high-spin excitation [18, 19, 75]. The simplicity $\Delta E_{\rm c}$ versus U/t should not understate the merit of the LDFT results in comparison to exact diagonalization ($N_{\rm a} = 12$ and 14).

For non-vanishing bipartite potential and $U = 0$ the charge gap is positive, equal

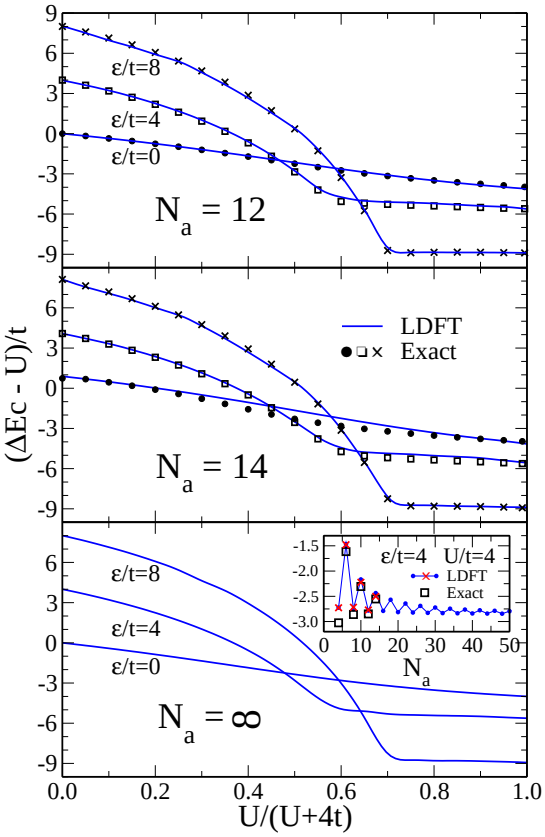

Figure 5.13: Charge gap $\Delta E_{\rm c} = E(N_{\rm e}+1) + E(N_{\rm e}-1) - 2E(N_{\rm e})$ as a function of the Coulomb repulsion strength U/t in 1D Hubbard rings having a band filling $n = 1$, representative values of the bipartite potential ε, and (a) $N_{\rm a} = 12$, (b) $N_{\rm a} = 14$ and (c) $N_{\rm a} = \infty$ sites. The curves refer to LDFT with the scaled dimer functional $W_{\rm sc}$ and the symbols to exact diagonalization. In the inset figure the ring-length dependence of $\Delta E_{\rm c} - U/t$ is shown for $\varepsilon/t = 4$ and $U/t = 4$.

to ε for $N_{\rm a}/2$ even, and slightly larger than ε for $N_{\rm a}/2$ odd (for example for $N_{\rm a} = 14$, $\Delta E_{\rm c}/t = 1.32$, 4.08 and 8.08 for $\varepsilon/t = 1$, 4 and 8, respectively). The underlying excitation involves the promotion of an electron across the single-particle gap opened by the bipartite potential. This corresponds to a delocalized electron-hole excitations between CDW states, which are more or less strong depending on the value of ε/t. As U/t increases $\Delta E_{\rm c} - U$ decreases and eventually changes sign, since the Coulomb repulsion brings the energy of the states with doubly-occupied configurations on sub-lattice $\mathcal{S}_2$ closer to the energy of singly-occupied configurations on sub-lattice $\mathcal{S}_1$ ($\varepsilon_1 = -\varepsilon_2 = \varepsilon/2 > 0$). For $U > \varepsilon$ the system undergoes a transition to an homogeneous state, after which the gap becomes essentially linear in U. In the strongly correlated limit $\Delta E_{\rm c} = U - 2w_b$ for all $N_{\rm a}$, where, as in the homogeneous case, w_b represents the energy gained through the addition of the extra electron or hole. These are the same due to the electron-hole symmetry of the bipartite lattice. In the homogeneous case, the extra electron occupies the $k = 0$ state of

the minority-spin band, while the majority band is full (Nagaoka state) [19]. Therefore, $w_b = 2t$ coincides with the single-particle band width. In the presence of a finite bipartite potential the situation is similar, since an extension of Nagaoka's theorem also holds in the presence of inhomogeneous energy levels ε_i [57]. However, notice that the bipartite potential introduces a shift of the energy ε_0 of the $k = 0$ single-particle state, which stabilizes the system with $N_e = N_a \pm 1$ electrons relative to the half-filled case ($N_e = N_a$). For example, $\varepsilon_0/t = -2.83$ for $\varepsilon/t = 4$ and $\varepsilon_0/t = -4.47$ for $\varepsilon/t = 8$. Consequently, the strongly correlated limit of $(\Delta E_c - U)/t$ decreases with increasing ε/t.

The comparison between LDFT and exact diagonalization shows a very good agreement. This confirms the previously observed trend to a slight improvement of accuracy as the strength of the bipartite potential ε/t increases. Fig. 5.13 also reports LDFT results for the charge gap in the thermodynamic limit. In this case γ_{12}^{∞} is obtained from a Nagaoka-like variational state in which the spin-up orbitals of sub-lattice $\mathcal{S}_2$ are occupied ($\gamma_{22} > \gamma_{11}$) and the remaining $\gamma_{11} + \gamma_{22} - 1$ spin-down electrons are delocalized throughout the entire lattice [61]. The trends observed for $N_a = \infty$ are essentially the same as for $N_a = 12$ or 14. The dependence of ΔE_c on the chain length is given in the inset of Fig. 5.13 (c). The accuracy of the LDFT calculations for different N_a is quantified by comparison with exact results.

Figure 5.14 shows the ground-state properties of the 2D Hubbard model on a square cluster having $N_a = 16$ sites and periodic boundary conditions. The results are given as a function of the Coulomb repulsion strength U/t for different values of the energy level shift ε/t at half band filling $n = 1$. First of all, one observes a number of qualitative similarities with the ground-state properties of 1D rings presented in Fig. 5.8. Among these let us mention the monotonous increase of E_{gs} with increasing U/t, the stabilization associated with the bipartite potential ε, and the convergence of all E_{gs} curves to the $\varepsilon = 0$ case when $U \gtrsim \varepsilon$ [see Fig. 5.14(a)]. The convergence of E_{gs} to the homogeneous limit occurs for U/t larger than the value at which the NN bond order γ_{12} is maximal, once the charge transfer $\Delta n = \gamma_{22} - \gamma_{11}$ and the interaction energy W drop. These features are comparable to the behavior observed in the 1D case and can be understood in similar terms. They reflect the change form a weakly correlated CDW state to a strongly correlated nearly homogeneous state as the strength of the Coulomb interactions is increased. However, in the present 2D periodic cluster one observes distinctive discontinuities in γ_{12}, Δn and W as a function of U/t, that are absent in the 1D results for $N_a = 14$ (compare Figs. 5.8 and 5.14). These discontinuities are a finite-size effect resulting from the six-fold degeneracy of the single-particle spectrum at the Fermi energy ε_F. They are not specific to the 2D geometry, since similar effects are also found in finite 1D chains with periodic boundary conditions. In the present case, four of the degenerate states at ε_F admit a charge transfer of one electron between the sub-lattices [$\vec{k} = (\pm\pi/2a, \pm\pi/2a)$], while the two others show an homogeneous charge distribution [$\vec{k} = (\pi/a, 0)$ and $\vec{k} = (0, \pi/a)$]. Two of the former CDW states are stabilized by the bipartite potential, although they involve a higher average number of double occupations than the latter. The number of electrons at half band filling is such that only three of the six degenerate states are occupied for both spin directions ($U = 0$). In the weakly correlated limit and for $\varepsilon \neq 0$ two of the states with strong charge transfer are occupied. Thus, the ground state corresponds to a CDW state. This configuration remains stable for rather large values of U/t, until U becomes larger than ε. At this point a sharp transition to a nearly homogeneous state takes place. Short before the discontinuities occur γ_{12} goes over a maximum, as the energy to transfer an electron from

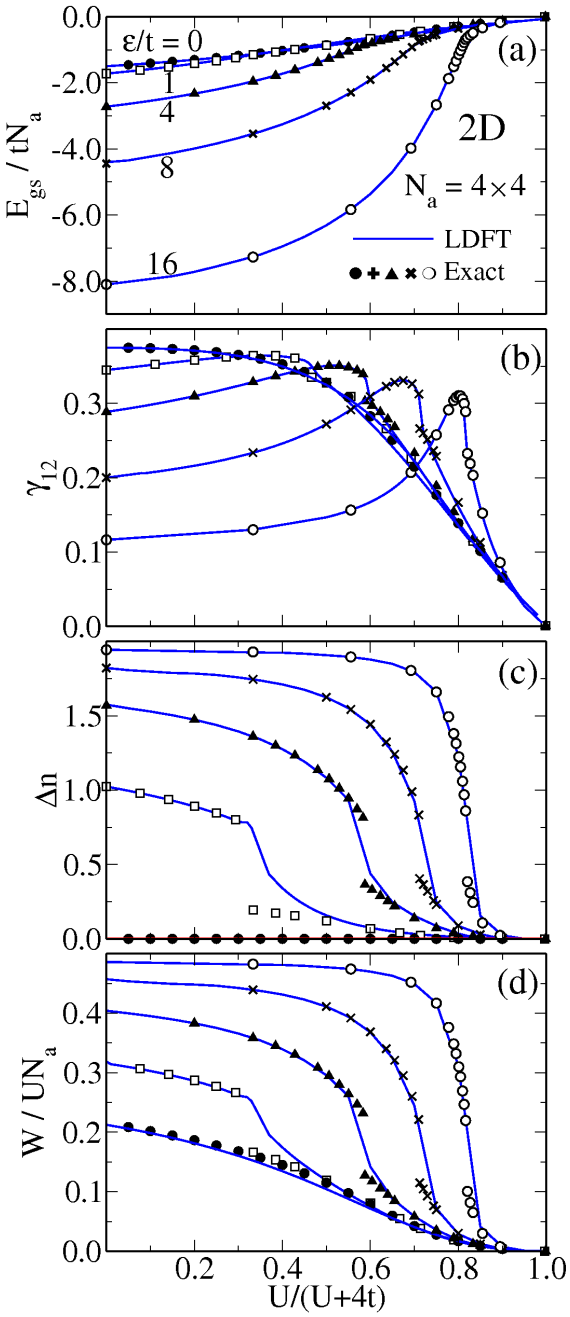

Figure 5.14: Ground-state properties of the half-filled Hubbard model on a 2D square cluster having $N_\mathrm{a} = 4 \times 4$ sites and periodic boundary conditions ($n = N_\mathrm{e}/N_\mathrm{a} = 1$). Results are given for (a) ground-state energy E_gs, (b) NN bond order γ_{12}, (c) charge transfer $\Delta n = \gamma_{22} - \gamma_{11}$, and (d) interaction energy W. LDFT (solid curves) and exact diagonalization (symbols) are compared as a function of the Coulomb repulsion strength U/t for representative values of the energy level shift ε between the sub-lattices, as indicated in (a). The discontinuities in the exact results for γ_{12}, Δn and W are a consequence of the degeneracy of the single-particle spectrum and the finite cluster size.

a doubly occupied site of sub-lattice $\mathcal{S}_2$ to an empty site on sub-lattice $\mathcal{S}_1$ vanishes. It is worth noting that such discontinuous jumps only take place for specific band fillings which match the degeneracies of the single-particle spectrum. They are not observed for other band fillings or in the thermodynamic limit. For example, for $N_\mathrm{e} = 10$, no discontinuities in the ground-state properties are observed, since the Fermi level is not degenerate. The importance of this finite-size effect decreases with increasing system size typically proportional to $1/N_\mathrm{a}$. In the present case the change in Δn resulting directly from the changes of occupation among the degenerate levels is 0.5, which corresponds to the transfer of two electrons per spin in an $N_\mathrm{a} = 16$ cluster.

Comparison with exact diagonalization shows that LDFT with the scaled dimer approximation yields quantitatively good results both for U significantly smaller and larger than ε. However, the approximation fails to reproduce the sharp transition. Instead, a continuous crossover is predicted, which becomes sharper and thus more accurate as ε/t increases (see Fig. 5.14). The shortcomings of the scaling approximation can be traced back to the particular form of the pure-state v-representability domain of the density matrix in the square 4×4 cluster, which is composed of two disjoint regions as a function of γ_{11} and γ_{12} for $\gamma_{11} + \gamma_{22} = 2$. In other words, the pure-state representability domain is neither convex nor simply-connected at half band filling. It is therefore not surprising that the scaling approximation yields a continuous crossover, since the scaling hypothesis implicitly assumes a convex or at least path-connected representability domain. Nevertheless, aside from this restriction, the overall predictions of LDFT always remain correct. Moreover, in the absence of degeneracies at ε_F (e.g., for $N_\mathrm{e} = 12$ and $N_\mathrm{a} = 16$ in 2D) LDFT recovers its usual performance for all model parameters. A more detailed discussion of the effects of degeneracies on the representability of the density matrix may be found in Ref. [74].

Finally, it is worth noting that the LDFT results for E_gs are invariably very accurate, even close to the transition and in spite of the discontinuities observed in other exact calculated properties. This is in fact the result of a compensation of errors between the charge-density energy $E_\mathrm{CD} = -\varepsilon\Delta n/2$ and the interaction energy W. Indeed, in the transition region the scaling *Ansatz* overestimates both Δn and W. In contrast, the bond order and thus the kinetic energy are obtained quite precisely [see Figs. 5.14 (b)–(d)].

It would be also interesting to investigate the site dependence of the on-site Coulomb repulsion integrals in order to achieve a more realistic modeling of some transition-metal oxides. However the most fundamental and straightforward consequence of the inhomogeneity of a system is the lack of translational invariance of the associated single-particle potential. This is described by the so-called external potential $v(\vec{r})$ of density-functional theory in the continuum and by the site-dependence of the energy levels ε_i in lattice models. It is for this reason that our attention has been focused on the effect of the site-dependence of ε_i until now. In any case, it is important to stress that neither the formulation of LDFT nor the derivation of an accurate approximation to the interaction-energy functional W are conditioned by the simplifying assumption that U is independent of the site. The fact that U can be factored out of W reduces the number of parameters of the model but is not at all essential. Since the formulation of LDFT (see Sec. 4.1) is formally correct for systems with inhomogeneous Coulomb integrals the challenge consists of in finding an accurate corelation energy functional. For bipartite systems the global scaling correlation functional can be straightforwardly extended considering a dimer within $U_1 \neq U_2$. The results shown in Fig. 5.15 were obtained by using such a scaled dimer approximation, which generalizes the case considered previously. This generalization at half band filling is

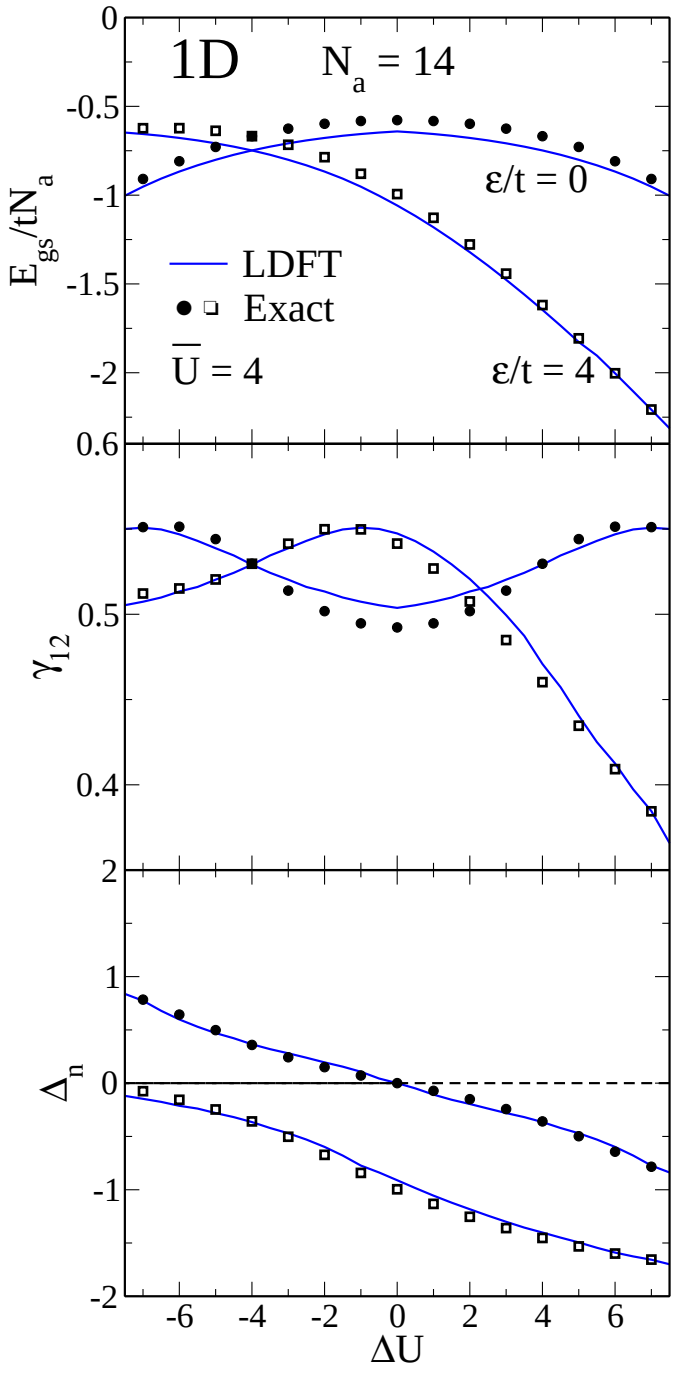

Figure 5.15: Ground-state energy $E_{\rm gs}$, NN bound order γ_{12} and charge transfer $\Delta n = \gamma_{22} - \gamma_{11}$ in a Hubbard ring having $N_{\rm a} = 14$ sites, half band filling $n = 1$, alternating energy levels $\varepsilon_i = \pm\varepsilon/2$, and alternating on-site Coulomb repulsions $U_1 = \overline{U} + \Delta U/2$ and $U_2 = \overline{U} - \Delta U/2$. The considered values of $\overline{U}$, ΔU and ε are indicated. The blue solid curves refer to LDFT within a generalized scaled-dimer approximation while the symbols are the results of exact Lanczos diagonalization.

based on the exact analytical solution of the interaction-energy functional for the Hubbard dimer with different Coulomb repulsions U_1 and U_2. In this case the equation (5.5) has to be replace by a more general one:

$$\frac{W_2}{N_a} = \begin{cases} \frac{\Delta n}{4}(U_2 - U_1) + (U_2 + U_1)\left[\frac{1}{2} - \frac{\gamma_{12}^2}{4}\left(\frac{1+\sqrt{1-(\Delta n/2)^2-\gamma_{12}^2}}{(\Delta n/2)^2+\gamma_{12}^2}\right)\right] & \text{if } \gamma_{12}^{\infty} < \gamma_{12} < \gamma_{12}^{0} \\ U_1 \Delta n/4, & \text{if } |\gamma_{12}| < \gamma_{12}^{\infty},\ \gamma_{11} > \gamma_{22} \\ U_2 \Delta n/4, & \text{if } |\gamma_{12}| < \gamma_{12}^{\infty},\ \gamma_{11} < \gamma_{22} \end{cases} \tag{5.7}$$

As an example we report in the figure 5.15 a comparison between exact and LDFT results for the ground-state energy E_{gs}, NN bond order γ_{12} and charge transfer Δn in a Hubbard ring with $N = 14$ sites, and alternating Coulomb repulsions $U_1 = \overline{U} + \Delta U/2$ and $U_2 = \overline{U} - \Delta U/2$. The results indicate that the accuracy of LDFT is similar or better for site-dependent U_i than for the case where the Coulomb repulsions are assumed to be the same. Moreover, a detailed analysis reveals a much richer behavior. The interplay between kinetic energy and charge transfer due to the inhomogeneity of the potential (energy levels) and of the Coulomb interactions is far from trivial and deserves special attention. In the case with $\varepsilon/t = 0$, the ground state energy is maximum for $\Delta U = 0$, which correspond to a minimum of the NN bond order γ_{12}. The reduction of kinetic energy can be explained by the fact that when $\Delta U = \bar{U}$ one sub-lattice is not correlated and the other has a Coulomb integral $U = 2\bar{U}$ inducing a charge transfer between the two sub-lattices of the order of $\Delta n = 0.8 \rightarrow \gamma_{11} = 1.4 \;\; \gamma_{22} = 0.6$. Consequently, there is a minimization of the double occupations on sub-lattice $\mathcal{S}_2$ and a maximum of the kinetic energy due to the hole created on sub-lattice $\mathcal{S}_2$. The ground states for $\Delta U \neq 0$ is a CDW in order to optimize the kinetic energy and minimize the average double occupations on the less favorable sub-lattice.

The case $\varepsilon/t = 4$ is more interesting since for $\Delta U < 0$ one observe an interplay between ΔU, which excludes localization on sub-lattice $\mathcal{S}_1$ and the single-particle potential which favors the occupation on this sub-lattice. The consequence of this interplay are discussed in the following. Notice that for $\Delta U = 0$, the kinetic energy have a resonance at this point (see fig.5.8) since for $U \simeq \varepsilon$ the Coulomb repulsion on the doubly occupied sites on sub-lattice $\mathcal{S}_2$ compensates the energy difference between the two sub-lattices ($\varepsilon_1 = \varepsilon/2 = -\varepsilon_2 > 0$). This allows a nearly free-like motion of the γ_{11} electrons occupying sub-lattice $\mathcal{S}_1$, together with the extra $\gamma_{22} - 1$ electrons on sub-lattice $\mathcal{S}_2$ ($\gamma_{11} < \gamma_{22}$ for $\varepsilon > 0$). Consequently, the delocalization of the electrons is enhanced for $U \simeq \varepsilon$, yielding a maximum in γ_{12} as already discuss previously.
The ground-state energy decreases as ΔU increases. This can be understood as the result of the competition between ΔU, which excludes localization on sub-lattice $\mathcal{S}_1$, and the single-particle potential, which favors the occupation on this sub-lattice. When $\Delta U > 0$ both ΔU and ε/t favor occupations on the same sub-lattice. This phenomena is also seen on Δn. Consequently, the ground-state energy decreases and the charge transfer increases, the electrons populate the favorable sub-lattice. An interesting remark is that γ_{12} admits a maximum near that $\Delta U = 0$ but for $\Delta U < 0$. As discussed previously, for $\Delta U = 0$, $U_1 = U_2 = \varepsilon_1 = \varepsilon/2$, there is a nearly free-like motion between the two sub-lattices. By decreasing ΔU, the charge transfer also decreases allowing a more free-electron like motion and enhancing sensibly the kinetic energy. This phenomena is stopped when in one sub-lattice the Coulomb energy becomes too important and the electrons are localized. At the limit $\Delta U = -8$, it leads to an nearly homogeneous configuration, minimizing the

double occupations on the sub-lattice having $U_i = 8$. When $\Delta U > 0$ the localization on sub-lattice $\mathcal{S}_1$ becomes more favorable to reach a charge transfer $\Delta n = 1.75$ at $\Delta U = 8$ reducing automatically the kinetic energy and the ground state energy.

5.4 Applications to the attractive Hubbard model

As it was explained in Section 3.5, the Hubbard model with an attractive interaction is suitable to study the electronic pairing which, under some conditions (doping, low temperature), is at the origin of superconductivity. In the past year this approach has been studied on different systems by using various methods. One of the first studies used the quantum Monte Carlo method for a 2D Hubbard model [64]. In this work the authors argue that doping away from half-filling leads to superconductivity below a certain temperature T_C. Clearly other mechanisms can also accomplish this. For example, a next-nearest-neighbor hopping can also favor superconductivity [76] or a nearest-neighbor interaction V also leads to a superconducting transition at half band filling for $0 < |V| < 2t^2U$ and a phase separation at $V = 2t^2U$. Other works are devoted to comparing the BCS approximation with exact results for the attractive Hubbard model [65, 68, 70, 77]. They find that generally, the BCS approach is an excellent approximation for the Hubbard model ground state energy but not for the energy gap, in 1D finite [68] and infinite systems [65] as well as in 2D [70]. These studies have also revealed even-odd and super-even effects in the value of the charge gap as a function of the number of electron in finite structures.
It would be also interesting to study the effect of a diagonal disorder (different energy level shift for example) since without interactions these system are stabilized with CDWs. In a CDW-state the electrons are paired on the most favorable sub-lattice, and an attractive electronic interaction should, then, enhance this phenomenon. These studies are also motivated by the fact that most known superconductors present diagonal disorders as for example the cuprates [78]. In this section we present an extention of the global scaling approximation derived above to the attractive interaction in a bipartite Hubbard model. Secondly, we compare our results for representative finite and infinite one- and two-dimensions systems with available exact results (exact diagonalization, Bethe-*Ansatz*) and with the BCS mean field approximation.

Before looking if the scaling properties of the interaction-energy functional are preserved for attractive interactions, it appears important to study the representability domain of the single-particle density matrix. In Fig. 5.16 we present the NN bound order between two NN as a function of the electronic density in one sub-lattice. The curves, given only for $0 \leq \gamma_{11} \leq 1$, are symmetric with respect to the homogeneous case $\gamma_{11} = 1$ $[(\gamma_{11} + \gamma_{22})/2 = n = 1]$. They display the correlation between diagonal and off-diagonal elements of the density matrices γ_{ij}, as derived from the ground state of the model for different values of the parameters that define the system (i.e., the energy level difference $\Delta\varepsilon$ and the NN hopping t). These density matrices are known as pure-state interacting v-representable, or simply v-representable, by analogy with the DFT of the inhomogeneous electron gas. In the continuum theory the electron densities $\rho(\vec{r})$ derived from exact ground states are called interacting v-representable, since they stay in one-to-one correspondence with an external potential $v_{ext}(\vec{r})$ [1, 3, 4]. While the v-representable domain contains all the ground state γ_{ij}^{gs}, it is also important to investigate the properties of the more general

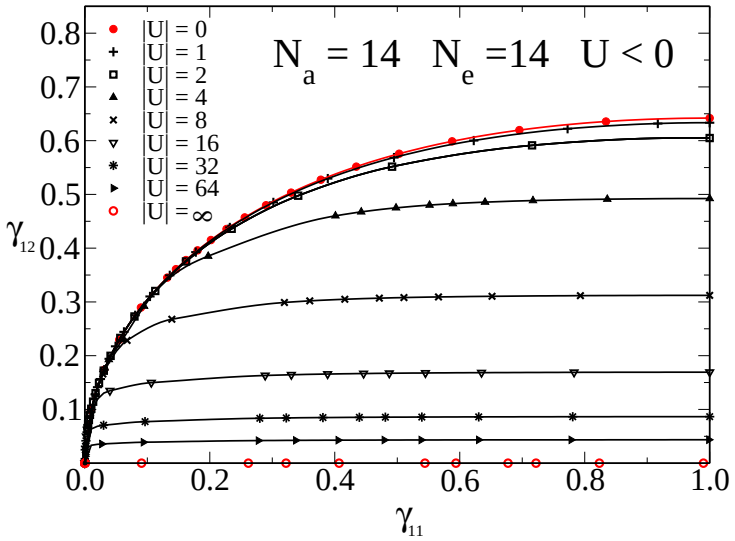

Figure 5.16: Representability domain of the 1D Hubbard chain having $N_a = 14$ sites and at half band filling. The red curve refers to the non correlated limit (full circles) and the strongly correlated limit (open circles). The dependence on the ground-state NN bond order γ_{12} as a function of the charge density γ_{11} on one sub-lattice is also shown for representative values of the strength of the local attractive interaction $U < 0$.

N-representable γ_{ij}, which constitute the domain of definition of Levy's functional $W[\gamma]$.

For each γ_{11}, or charge transfer $\Delta n = \gamma_{22} - \gamma_{11}$, the upper bound γ_{12}^0 for the NN γ_{12} corresponds to the largest possible value of the kinetic energy, which is achieved by the uncorrelated ground-state for the given Δn. Since the underlying electronic state is a single Slater determinant, the interaction energy is given by the Hartree-Fock value $W^0 = W[\gamma^0] = UN_a(\gamma_{11}^2 + \gamma_{22}^2)/8$, except possibly in cases with unusual degeneracies in the single-particle spectrum (e.g., $N_a = N_e = 4$ and $\Delta n = 0$). The uncorrelated γ_{12}^0 is largest for a homogeneous density distribution ($\Delta n = 0$) and decreases monotonically as the charge transfer increases. It vanishes in the limit where only one sub-lattice is occupied (see Fig. 5.16). This can be understood by recalling that in an uncorrelated state an increase of Δn is the result of an increasing difference $\Delta\varepsilon$ in the energy levels of the sub-lattices, which reduces in its turn the possibility for the electrons to delocalize. In the limit of complete charge transfer ($\gamma_{11} \to 0$) no charge fluctuations at all are possible.

For $\gamma_{12} < \gamma_{12}^0$, and a given Δn, the dimension of the subspace of accessible many-body states is larger and therefore the electrons can decrease the optimum value of the interaction W for a fixed γ_{ij} by increasing the number of double occupations ($U < 0$). The maximum value of the interaction energy per site is $W^\infty/U = N_e/2N_a$ for N_e even and $W^\infty/U = (Ne - 1)/2N_a$ for N_e odd. We shall denote by γ_{12}^∞ the largest possible value of γ_{12} compatible with the maximum number of double occupations W^∞/U. γ_{12}^∞ defines the lower bound for the v-representable γ_{ij} and corresponds to the the ground state of the model for $U \to -\infty$ [$W(\gamma_{12}^\infty) = W^\infty$, see Fig. 5.16]. Two different cases have to be taken into account, when the system has an even or an odd number of electrons. In the case of an even number of electron, when $U \to -\infty$, all electrons are paired

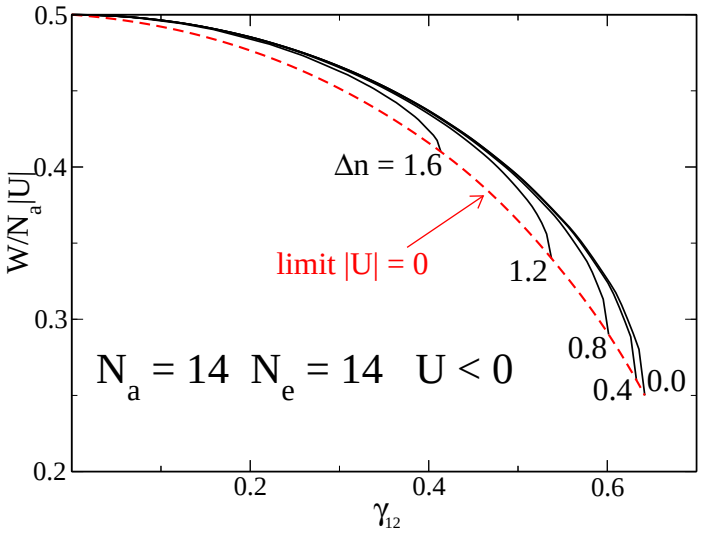

Figure 5.17: Exact correlation energy functional per site $W/N_a|U|$ as a function of the non-diagonal part of the density matrix γ_{12} for the 1D Hubbard chain having $N_a = 14$ sites at half band filling and for representative values of the charge transfer $\Delta n = \gamma_{22} - \gamma_{11}$. The red dashed line represents the average number of double occupations at the non-correlated limit.

implying that $\gamma_{ij}^{\infty} = 0$. In the other case, N_e odd, all electrons except one are paired ($W^{\infty}/U = (Ne-1)/2N_a$). This single electron is then free to move in the one particle potential provide by the bipartite potential. The largest possible value of γ_{12} compatible with the maximum number of double occupations is consequently the kinetic energy of a free electron in the lattice and equal to $\gamma_{ij}^{\infty} = \sqrt{\gamma_{11}(2-\gamma_{11})}/zN_a$ where z corresponds to the number of NN. Notice that this is a finite size effect since when $N_a \to \infty$, $\gamma_{ij}^{\infty} \to 0$, but it plays an important role for properties like the charge gap as we will discuss later. In order to extand the scaling approximation to attractive interaction, we should check whether the scaling properties described above for the Coulomb repulsion are still valid in this case. First of all, in Fig. 5.17 W is shown as a function of γ_{12} for representative values of $\Delta n = \gamma_{22} - \gamma_{11}$. Despite the strong dependence of W on Δn there are several important qualitative properties shared by all the curves:
(i) As already discussed, the domain of N representability of γ_{12} is bounded by the bond order γ_{12}^0 in the uncorrelated limit. γ_{12}^0 decreases monotonously as Δn increases, vanishing for $\Delta n = 2$. This is an important contribution to the Δn dependence of W which reflects the interplay between charge transfer and electron delocalization.
(ii) In the non-correlated limit, $W[\gamma_{12}^0, \Delta n] = W^0 = E_{HF}$ for all Δn, since the electronic state yielding the largest γ_{12} is a single Slater determinant. Moreover, one observes that $\partial W/\gamma_{12}$ diverges at $\gamma_{12} = \gamma_{12}^0$. This is a necessary condition in order for the ground-state density to satisfy $\gamma_{12}^{gs} < \gamma_{12}^0$ for arbitrarily small $U < 0$, as expected from perturbation theory.
(iii) Starting from γ_{12}^0, W increases with decreasing γ_{12}, reaching its largest possible value $W^{\infty} = 1/2$ ($N_e = 14$, even case) for $\gamma_{12} = \gamma_{12}^{\infty}$. The increase of W with decreasing γ_{12}

means that the increase of the interaction energy due to correlations is done at the expense of the kinetic energy or electron delocalization.
(iv) The strongly correlated γ_{12}^{∞} is 0 for even number of electrons or with odd number of electrons at the termodynamic limit $N_a \to \infty$. γ_{12}^{∞} shows a non-monotonous dependence on Δn if Ne is odd and N_a is finite ($\gamma_{ij}^{\infty} = \sqrt{\gamma_{11}(2-\gamma_{11})}/zN_a$).

In order to compare the functional dependence of W for different Δn and to analyze its scaling behavior, we focus on the v-representable domain $\gamma_{12}^{\infty} \leq \gamma_{12} \leq \gamma_{12}^{0}$ where W is not trivially constant. To this aim it is useful to bring the domains of representability for different N_a to a common range and to scale W with respect to the Hartree-Fock and strongly correlated values. We therefore consider $(W - W^{\infty})/(W^{0} - W^{\infty})$ as a function of $g_{12} = (\gamma_{12} - \gamma_{12}^{\infty})/(\gamma_{12}^{0} - \gamma_{12}^{\infty})$ as displayed in Fig. 5.18 ($W^{0} = E_{HF}$). In this form the results for different N_a appear as remarkably similar, showing that the largest part of the dependence of W on γ_{12} and Δn comes from the domain of representability of γ_{ij} and the limiting values for weak and strong correlations. Fig. 5.18 implies that the change in W associated to a given change in the degree of delocalization g_{12} can be regarded as nearly independent of the size of the system. As already discussed in Sec. 5.1 for the repulsive interaction, the very good scalability of W as a function of g_{12} is not obvious for different system sizes. In fact, if one considers $W(g_{12})$ for different charge transfers Δn, one observes more significant deviations. This is demonstrated in Fig. 5.19 where the results for a 1D ring with $N_a = 14$ sites are compared for different Δn. Qualitatively, the dependence of W on the degree of delocalization g_{12} is similar for different Δn. Notice, for instance, the behavior for weak and strong correlations ($g_{12} \approx 0$ or 1) and the overall shape in the crossover region. This shows that the scaling hypothesis works satisfactorily even for different Δn. However, the quantitative differences between the scaled W for various Δn are more significant than those found for different sizes (see Figs. 5.18 and 5.19). This is actually not very surprising, since the nature of the electronic correlations are expected to evolve as we move from purely metallic to strongly ionic-like bonds. It is therefore important to investigate systematically the functional dependence of W for different Δn in order to elucidate its scaling behavior and evaluate the possibilities of transferring it from simple to complex many-body problems. The band-filling dependence of W is also expected to present the same scaling properties as in the case of a repulsive interaction.
It has been shown that as in the case of a repulsive interaction, W can be appropriately scaled as a function of Δn and $g_{12} = (\gamma_{12} - \gamma_{12}^{\infty})/(\gamma_{12}^{0} - \gamma_{12}^{\infty})$, where γ_{12}^{0} (γ_{12}^{∞}) refers to the limit of weak (strong) electronic correlations. In other words, the change in W is associated to a given change in the degree of NN charge transfer and electron delocalization can be regarded as nearly independent of the system under study.

Following the derivation of the scaling *Ansatz* presented in Sec. 5.2 for positive U, the numerical studies presented above confirm the same scaling properties; then we propose that

$$\frac{W_{\rm sc} - W^{\infty}}{W^{0} - W^{\infty}} = \frac{W_2 - W_2^{\infty}}{W_2^{0} - W_2^{\infty}}, \tag{5.8}$$

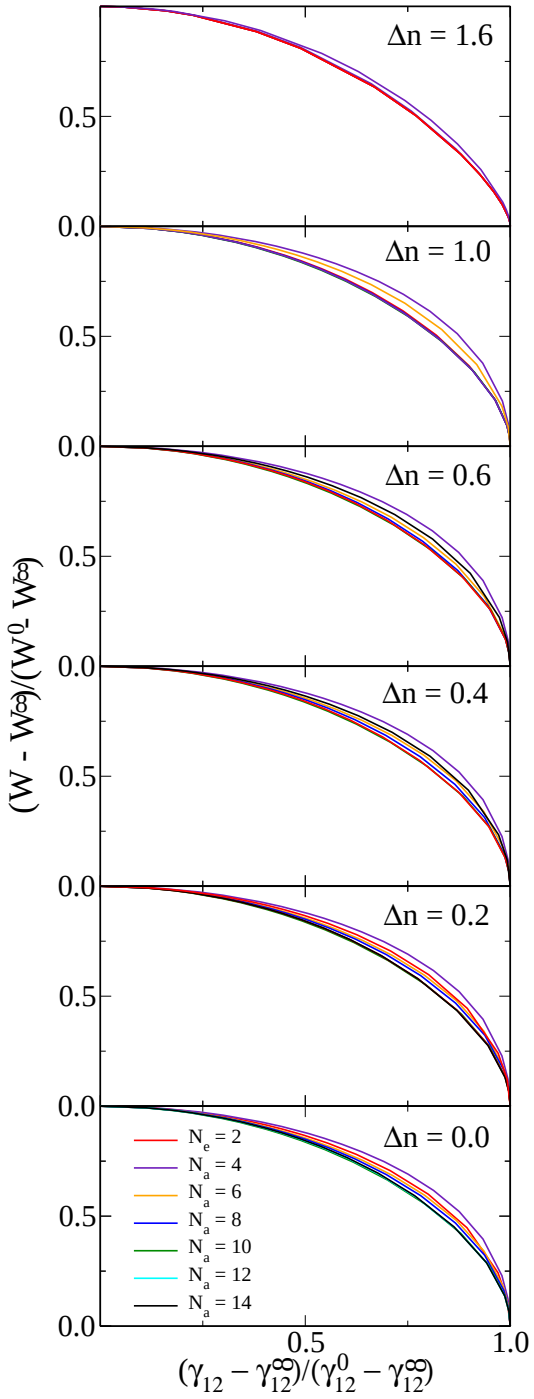

Figure 5.18: Scaled interaction energy W of the attractive 1D Hubbard model ($U < 0$) as a function of the degree of electron delocalization $g_{12} = (\gamma_{12} - \gamma_{12}^{\infty})/(\gamma_{12}^{0} - \gamma_{12}^{\infty})$. $W^0 = E_{HF}$ and γ_{12}^{0} refer to the uncorrelated limit ($U = 0$) while W^{∞} and γ_{12}^{∞} refer to the strongly correlated limit ($U/t \to -\infty$). Results are given for band filling $n = 1$, all even numbers of sites $N_a = 2$–14, and different charge transfers Δn.

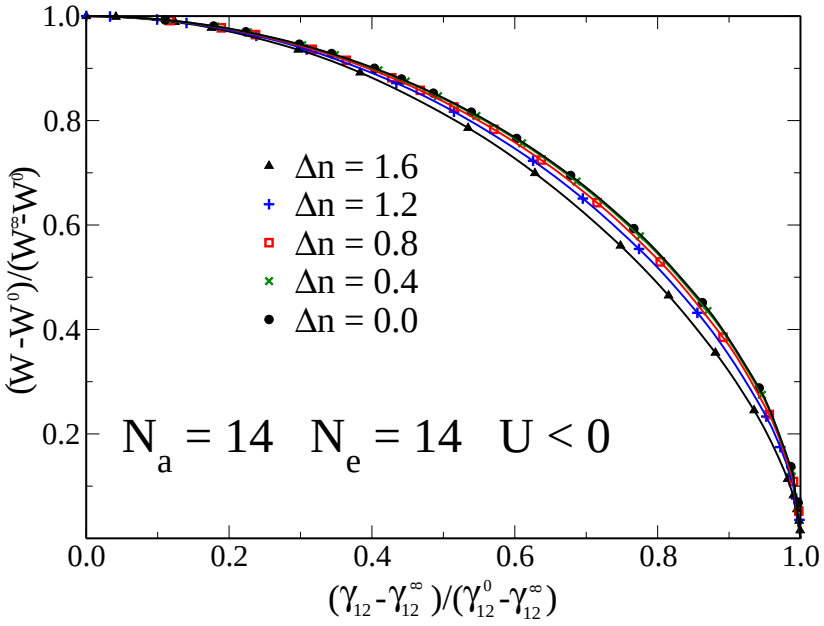

Figure 5.19: Charge transfer dependence of the the scaled interaction-energy functional W of the attractive 1D Hubbard model ($U < 0$). Results are given as a function of the degree of electron delocalization $g_{12} = (\gamma_{12} - \gamma_{12}^{\infty})/(\gamma_{12}^{0} - \gamma_{12}^{\infty})$ for $N_a = 14$, $n = 1$ and different charge transfers $\Delta n = 0.0$–1.6.

where the subindex 2 refers to the dimer. We can rewrite Eq. (5.8) in a compact form:

$$W_{\rm sc} = W^{\infty} + (W^{0} - W^{\infty})\frac{W_2 - W_2^{\infty}}{W_2^{0} - W_2^{\infty}}. \tag{5.9}$$

The exact dimer interaction-energy functional for $N_{\rm e} = 2$ for attractive interaction is given by

$$\frac{W_2}{UN_{\rm a}} = \begin{cases} 1 - \frac{\gamma_{12}^2}{2}\frac{1-\sqrt{1-(\Delta n/2)^2-\gamma_{12}^2}}{(\Delta n/2)^2+\gamma_{12}^2}, & \text{if } \gamma_{12}^{\infty} < \gamma_{12} < \gamma_{12}^{0} \\ n/2 - {\rm Mod}[Ne,2]/N_a, & \text{if } |\gamma_{12}| < \gamma_{12}^{\infty}. \end{cases} \tag{5.10}$$

Most of the properties of the interaction-energy functional reproduce several exact properties discussed above. In addition, some of them are similar to the one for a repulsive interaction [see Sec. 5.2].

For application we consider the same bipartite Hamiltonian [see Eq. (4.1)] except that $U < 0$. Representative systems are analyzed like a finite ring having $N_a = 14$ sites, from which finite size effects are studied. They result from the discrete nature of the one particle spectrum [see Fig 5.7]. In the case of repulsive Coulomb repulsion, finite size effects induce oscillations in the charge gap from $U = 0$ to finite U and we show that they are also present and accentuated in the case of an attractive interaction. We present also results concerning the thermodynamic limit ($N_a \to \infty$) in one and two dimensions.
Figures 5.20, 5.21 and 5.22 present the ground-state properties of, respectively, a 1D ring having $N_{\rm a} = 14$ sites, a one-dimensional infinite chain and a two-dimensional infinite

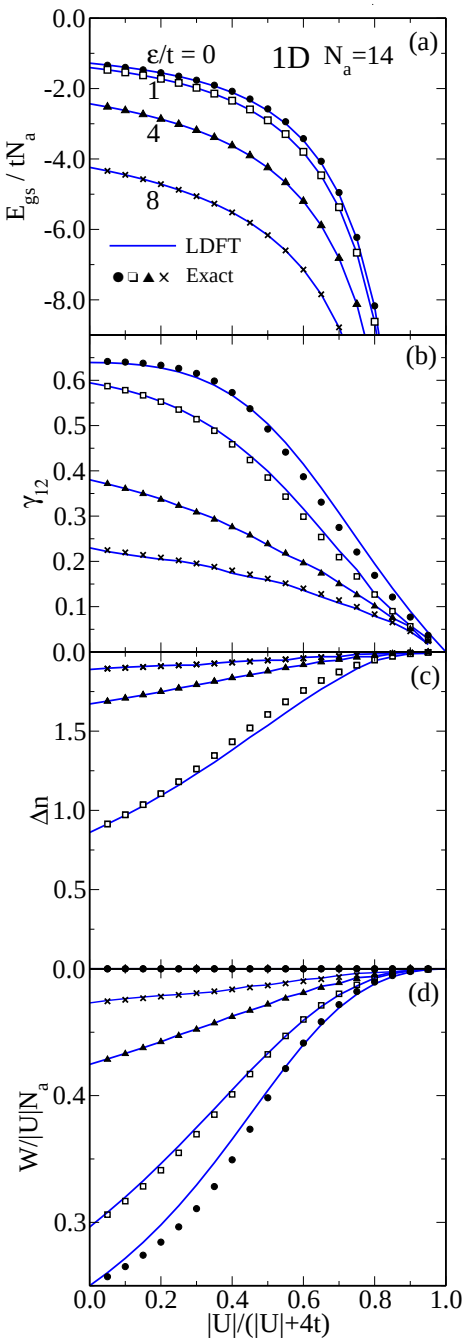

Figure 5.20: Ground-state properties of bipartite Hubbard rings having $U < 0$, $N_\mathrm{a} = 14$ sites and half band filling $n = 1$ as a function of the attractive interaction strength $|U|/t$. Different values of the energy level shift ε between the sub-lattices are considered as indicated in (a). Results are given for (a) ground-state energy E_gs, (b) NN bond order γ_{12}, (c) charge transfer $\Delta n = \gamma_{22} - \gamma_{11}$ and (d) average number of double occupations per site W/UN_a. The solid curves refer to LDFT using the scaling approximation W_sc [see Eq. (5.9)] while the symbols are the results of exact Lanczos diagonalizations.

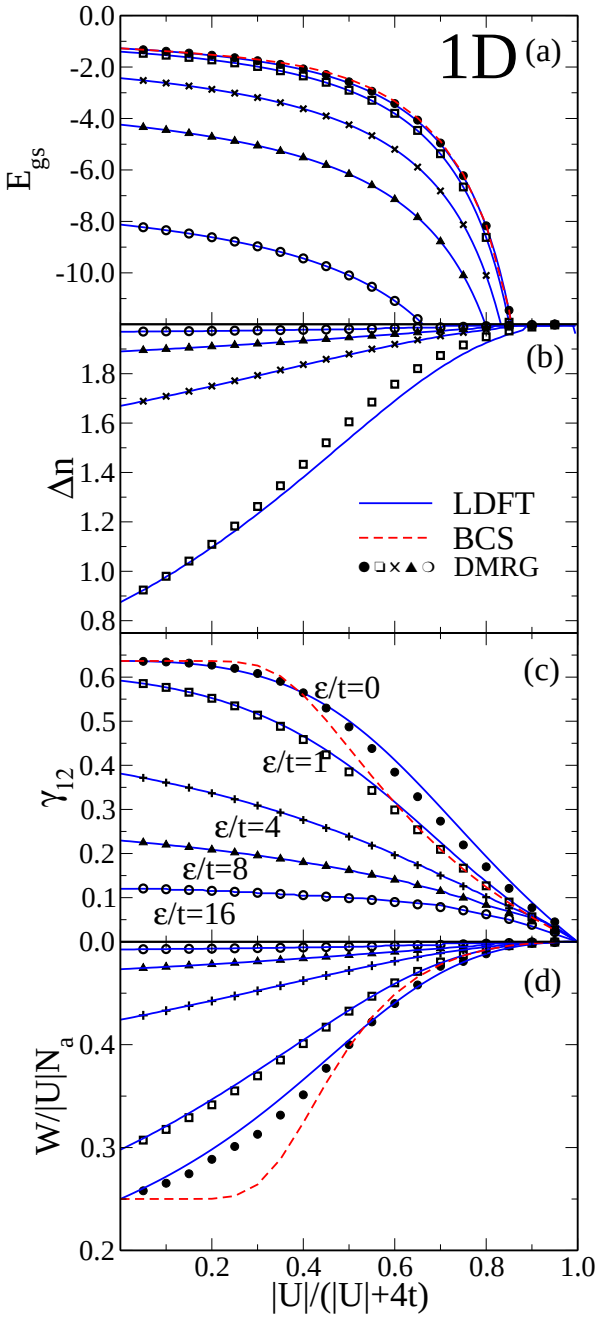

Figure 5.21: Ground-state properties of infinite bipartite Hubbard rings at half band filling $n = 1$ as a function of the attractive interaction strength $|U|/t$. Different values of the energy level shift ε between the sublattices are considered as indicated in (c). Results are given for (a) ground-state energy $E_{\rm gs}$, (b) NN bond order γ_{12}, (c) charge transfer $\Delta n = \gamma_{22} - \gamma_{11}$ and (d) average number of double occupations per site $W/UN_{\rm a}$. The solid curves refer to LDFT using the scaling approximation $W_{\rm sc}$ [see Eq. (5.9)], the symbols are the results of DMRG calculations, and the red dashed line corresponds to the BCS approximation for $\varepsilon/t = 0$.

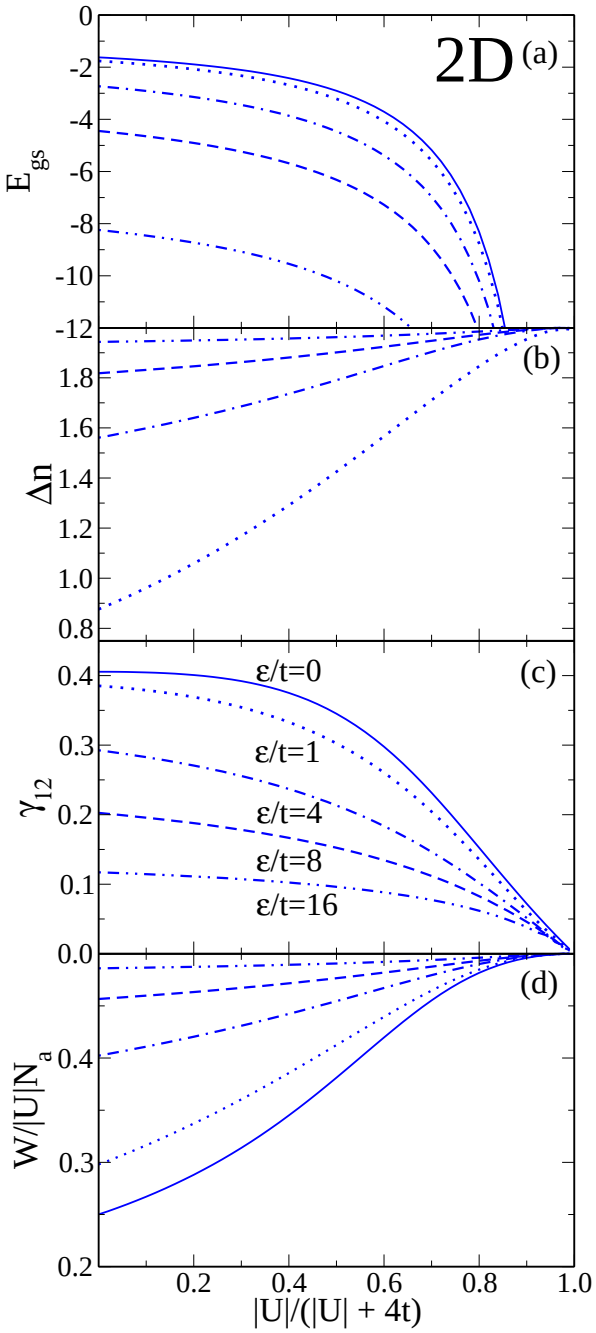

Figure 5.22: Ground-state properties of the attractive Hubbard model on a 2D square periodic lattice as a function of the attractive interaction strength $|U|/t$. The band filling is $n = 1$. Different values of the energy level shift ε between the sub-lattices are considered as indicated in (c). Results are given for (a) ground-state energy $E_{\rm gs}$, (b) NN bond order γ_{12}, (c) charge transfer $\Delta n = \gamma_{22} - \gamma_{11}$ and (d) average number of double occupations per site $W/UN_{\rm a}$. The curves refer to LDFT by using the scaling approximation $W_{\rm sc}$ [see Eq. (5.9)].

system as a function of the attractive interaction strength $|U|/t$. Different values of the energy level shift ε/t are considered at half band filling $n = 1$. First, we describe the general trend of the properties common to all the systems. First of all, for the homogeneous case ($\varepsilon/t = 0$ and $\Delta n = 0$) one observes a decrease of $E_{\rm gs}$ with increasing $|U|/t$ reaching $E_{\rm gs} = nU/2$ for $|U|/t \to \infty$, where electronic hopping vanishes and double occupations are maximum $W/|U|N_a = 1/2$. At the same time γ_{12} decreases and W increases monotonously with $|U|/t$ [see sub-figures (b) and (d)]. This picture is accentuated when the bipartite level shift ε is finite. In this case, as we go from weak to strong correlations, the system undergoes a qualitative change from a delocalized charge-density-wave (CDW) state ($\Delta n \simeq 0.9$–1.6 and $\gamma_{12} \simeq 0.3$–0.6) to a full localized charge-density-wave (CDW) state ($\Delta n = 2$ and $\gamma_{12} = 0$). Starting from the weakly correlated CDW state and increasing $|U|/t$, one observes an increase in Δn, since inhomogeneous charge distributions necessarily imply larger average double occupations [see sub-figures (c) and (d)]. The behavior of kinetic energy and bond order γ_{12} as a function of $|U|/t$, in contrast to the case where $U > 0$, is monotonous since the reduction of the NN bound order is made at the price of an increasing of double occupations on the most favorable lattice.
An important remark concerning the transition from a homogeneous distribution to a CDW is that an arbitrarily small value of ε/t implies this transition. Especially the charge transfer between the two sub-lattices will be more important as $|U|/t$ increases.
Concerning the comparison between LDFT and exact or numerical results [Fig. 5.20 with Lanczos diagonalization and Fig. 5.21 with DMRG] one observes, as with a repulsive interaction, that all the considered ground-state properties are very well reproduced by the scaled dimer *Ansatz*. This holds for all values of the energy level shift between the sub-lattices, not only close to the weakly and strongly correlated limits but also in the intermediate interaction region. Moreover, the fact that γ_{12}, Δn and W are all obtained with a high level of precision shows that the results for $E_{\rm gs}$ are not the consequence of a strong compensation of errors. It is also interesting to note that the accuracy is actually improved as the charge distribution becomes more inhomogeneous, i.e., as ε/t and the CDW are stronger. This is a particular advantage since at the strong interaction limit and with an arbitrarily small value of ε/t the electrons are fully localized on the most favorable lattice where the scaling approximation has a better accuracy. This seems reasonable, since large values of ε enhance the importance of single particle contributions to the energy and somehow tend to decouple the 1D chain in dimers, within which correlations are taken into account exactly. In Fig. 5.21, in the case $\varepsilon/t = 0$, we also compare our results with the BCS approximation [see Sec. 3.5.2]. The BCS results are obtained using a homogeneous finite lattice for simplicity, large enough for the properties to have converged to their bulk limit. In contrast to LDFT within the scaling approximation, the reasonably good agreement between DMRG and BCS is the result of error compensation between the kinetic and correlation energies. Especially, for small $|U|/t$ BCS theory predicts a really slow increase of W until $|U|/t \sim 1.5$ ($|U|/(|U| + 4t) \sim 0.27$), underestimating considerably the average number of double occupations. This is compensated in the ground state energy since the γ_{12} is also nearly constant until $|U|/t \sim 1.5$, overestimating the kinetic energy. The maximum of discrepancies in BCS occurs for the smaller contributions of the energy, in the small interaction regime for the average number of correlation energy and at the strong interaction regime for the kinetic energy. Notice that BCS predicts a good strongly correlated limit (all electrons paired). Nevertheless, if BCS gives a quite accurate ground-state energy, the error made on the different contributions can lead to a

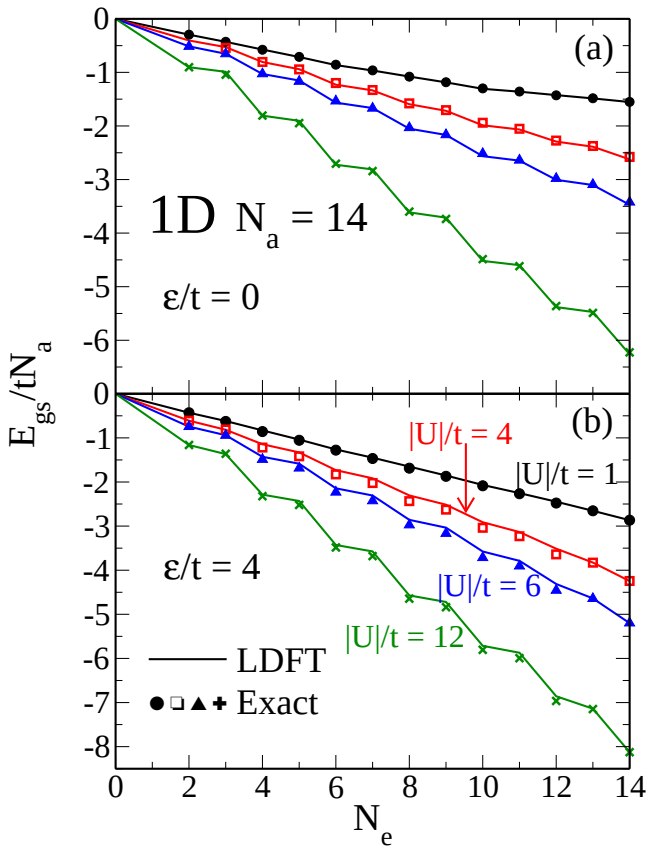

Figure 5.23: Band-filling dependence of the ground-state energy of 1D Hubbard rings having $U < 0$, $N_a = 14$ sites, and different bipartite potentials ε. The solid lines connecting discrete points refer to LDFT with the scaled dimer functional W_{sc}. The symbols correspond to exact numerical results. Representative values of the attractive interaction strength $|U|/t$ are considered as indicated.

bad description on more subtle properties as we see later on for the charge gap.

In Figs. 5.23, 5.24 and 5.25 we present the band-filling dependence of the ground-state energy E_{gs} of, respectively, a 1D ring having $N_a = 14$ sites, a one-dimensional infinite chain and a two-dimensional infinite system. Beside the finite size effect in Figs. 5.23 which will be discussed later on, the three figures present general similarity. E_{gs} decreases monotonously when the band filling increases for all value of $|U|/t$ and ε/t until $n = 1$. This trend is trivial in the noncorrelated case since by adding electrons, one fills one by one the one-particle states having a negative energy ($E(\vec{k}) = -2t(\cos(k_x)+\cos(k_y)+\cos(k_z))$). For finite values of the attractive interaction, the electrons are partially paired decreasing the energy ($U < 0$). Adding a bipartite potential also contributes to decreasing the energy since the electrons will form a pair on the most favorable sub-lattice. For a strong enough attractive interaction $|U|/t > 4$ and for finite size systems (see Fig. 5.23), the ground state energy oscillates since passing from an odd number to an even number of electron leads to an important reduction of the energy (creation of a pair) while when passing from an

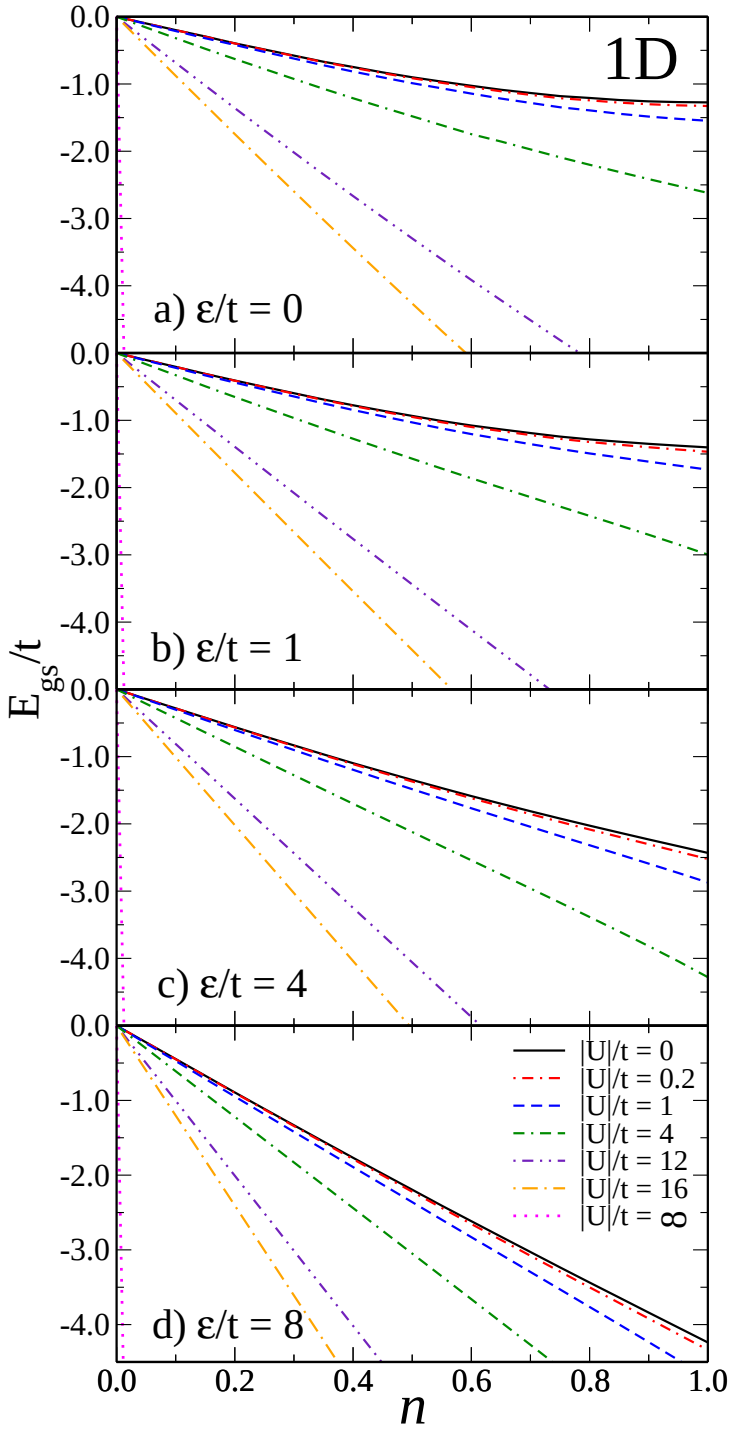

Figure 5.24: Band-filling dependence of the ground-state energy of infinite 1D Hubbard rings with attractive interaction ($U < 0$) and different bipartite potentials ε. The solid curves refer to LDFT with the scaled dimer functional W_{sc}, and the symbols to exact numerical results. Representative values of the attractive interaction strength $|U|/t$ are considered as indicated.

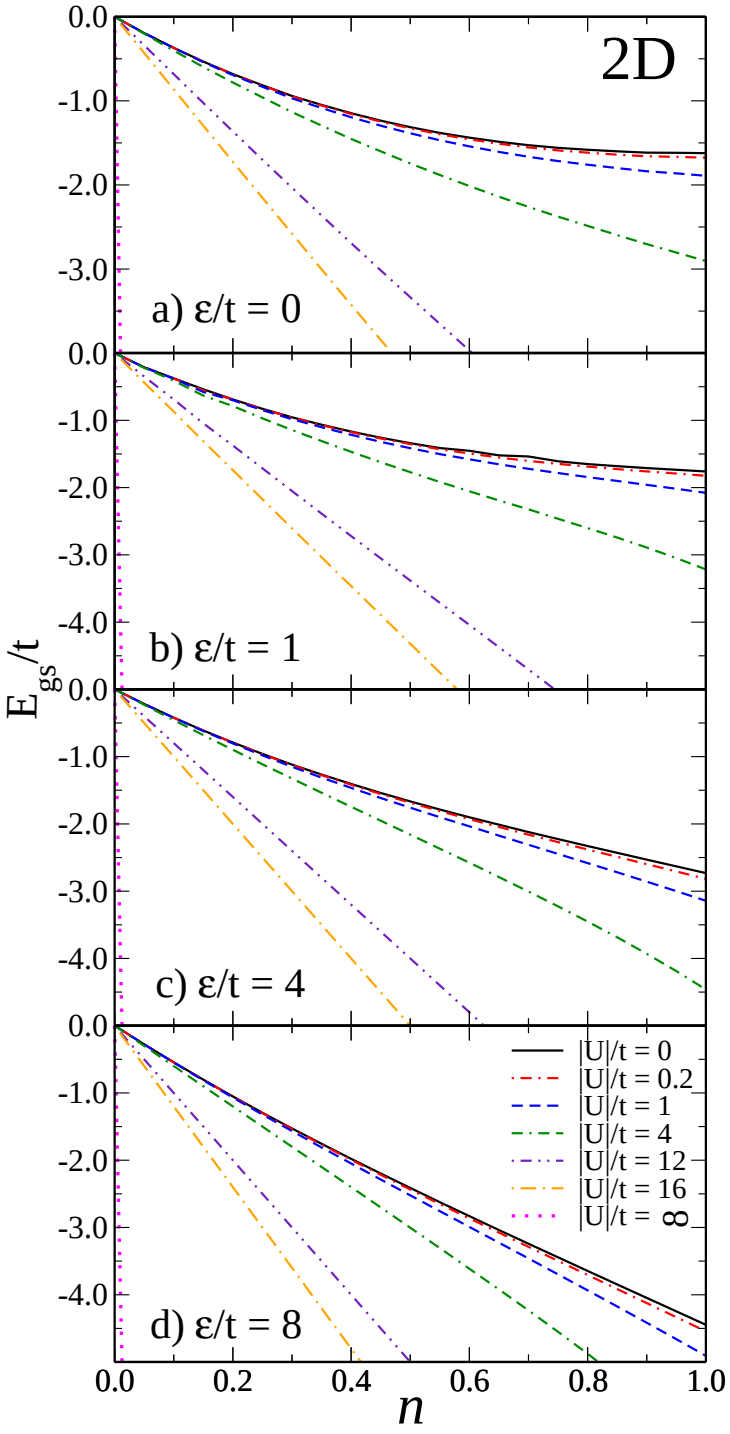

Figure 5.25: Band-filling dependence of the ground-state energy of the attractive 2D Hubbard model on an infinite 2D square lattice with different bipartite potentials ε. The solid curves refer to LDFT with the scaled dimer functional $W_{\rm sc}$, and the symbols to exact numerical results. Representative values of the attractive interaction strength $|U|/t$ are considered as indicated.

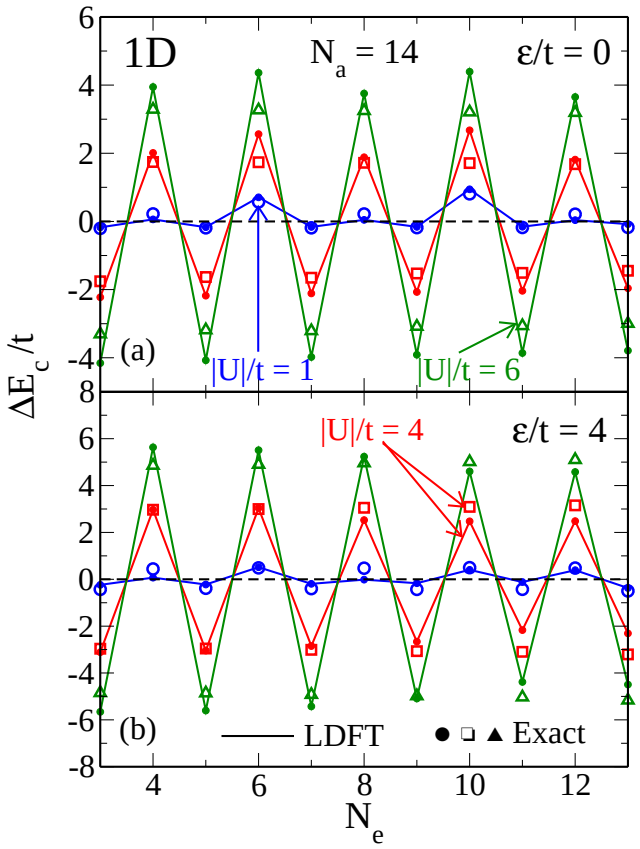

Figure 5.26: Charge gap $\Delta E_{\rm c} = E(N_{\rm e}+1) + E(N_{\rm e}-1) - 2E(N_{\rm e})$ as a function of the number of electrons N_e in 1D Hubbard rings having $N_{\rm a} = 14$ sites and different bipartite potentials ε. The solid lines connecting discrete points refer to LDFT with the scaled dimer functional and the symbols to exact Lanczos diagonalization. Representative values of the attractive interaction strength $|U|/t$ are considered. Results for $n = 1$ are given in Fig. 5.27.

even to an odd number of electrons only increases the kinetic energy which contributes less at this regime. These oscillations disappear at the thermodynamic limit ($N_a \to \infty$). These size effects are also responsible for the even-odd and super-even effects in the charge gap [68] as a function of the band-filling. To show these effects, we present in Fig. 5.26 the charge gap $\Delta E_{\rm c} = E(N_{\rm e}+1) + E(N_{\rm e}-1) - 2E(N_{\rm e})$ dependences on the band filling for a 1D Hubbard ring having $N_a = 14$ sites. Representative values of the attractive interaction $|U|/t$ are considered as well as two different values of the bipartite potential, in (a) $\varepsilon/t = 0$ and in (b) $\varepsilon/t = 4$. The first remark is that the gap for N_e odd is negative when the one for N_e even is positive producing oscillations. The amplitude of these oscillation increases as $|U|/t$ increases. The physics behind this behavior is understood in the sense that for a finite value of $|U|/t$, adding an electron to a system with an odd number of electrons makes the formation of a new (partial) pair possible. The added electron brings also a contribution which reduces the kinetic energy and we have $E(N_{\rm e}+1) < E(N_{\rm e})$. On the

other hand removing an electron from a system with an odd number of electrons does not destroy a pair since in this case the maximum number of pairs is $(N_e - 1)/2$; consequently only the kinetic energy is increased and $E(N_\mathrm{e}) < E(N_\mathrm{e} - 1)$. However, as we see in the non-correlated case in Fig. 5.10, the difference of the kinetic energy between adding and removing an electron is compensated leading to $\Delta E_\mathrm{c} < 0$ for finite values of $|U|/t$ and N_e odd. The same reason explains the positive gap in the case of N_e even, since removing an electron can (partially) destroy a pair and adding an electron only affects the kinetic energy. More subtle super-even effects for small values of $|U|/t$,which are consequences of the nature of the one-particle spectrum, are also observed (see blue line and symbol in Fig. 5.26). The charge gap for $N_e = 6$ and $N_e = 10$ is enhanced compared to other even numbers of electrons. This behavior disappears for $|U|/t > 4$. We can explain this phenomenon, which is also present in the case of a Coulomb repulsion (already explained in Sec. 5.3), by looking at the one-particle energy spectrum in Fig. 5.7. The effect of a one particle bipartite potential is to enhance the amplitude of the oscillation since it determines a most favorable sub-lattice where double occupations are promoted. The mechanism discussed above is consequently enhanced when the double occupations are more localized on a less energetic sub-lattice.
Again, the accuracy of LDFT with the scaling approximation to W is remarkable in all cases, and the maximum of discrepancies seems to appear for $N_e = 4m + 2$, m integer ≥ 1 and $|U|/t \geq 4$ where LDFT overestimates the gap. LDFT has the tendency to keep the super-even effect even for large $|U|/t$. This can be explained by the strong dependence of the correlation energy W_{sc} on the non-correlated value of the off-diagonal part of the density matrix γ_{12}. As previously, the accuracy is better within an external bipartite potential.

Figs. 5.27 and. 5.28 present the charge gap dependence on the attractive interaction strength $|U|/t$ for different systems at half band filling. The LDFT results are compared with exact calculations (exact diagonalization, Bethe *Ansatz*) and the BCS approximation. In both cases the dashed line represents the linear in $|U|/t$ asymptotic strongly correlated limit, the inset figure focuses on the charge gap dependence at the weakly correlated limit. General trends can be deduced from these two figures, like the monotonous increase of the charge gap as $|U|/t$ increases, in particular for $|U|/t > 8$; the increase is linear since all the electrons are already nearly paired and the nature of the ground states do not change. In the case of the finite ring having $N_a = 14$ sites, displayed in Fig. 5.27 and for $\varepsilon/t = 0$, the charge gap at the noncorrelated limit is finite due to finite size effects already discussed. An interesting point is the effect of the bipartite potential: for $\varepsilon = 4$ the gap increases from the weakly to the strongly correlated limit nearly linearly in $|U|/t$. In this case, the electrons are already paired on the most favorable sub-lattice at the non-correlated limit [$W/|U|N_a \sim 0.425$ and $\gamma_{22} \sim 1.85$ ($\Delta n \sim 1.70$), see Fig. 5.20].

At the thermodynamic limit $N_a \to \infty$, displayed in Fig. 5.28, we focus on the homogeneous case for one- and two-dimensional systems. For the one-dimensional case we compare our results with the BCS theory and the exact Bethe *Ansatz*. Generally LDFT provides a better approximation than the BCS theory except at the weakly correlated limit $|U|/t < 1.5$. Using the Bethe *Ansatz*, the charge gap at half band filling is given by:

$$\Delta E_\mathrm{c}^\mathrm{BA} = \frac{8t}{\pi} \sum_{m=1}^{\infty} \frac{1}{2m+1} K_1 \left(\frac{2\pi t}{|U|} (2m-1) \right), \tag{5.11}$$

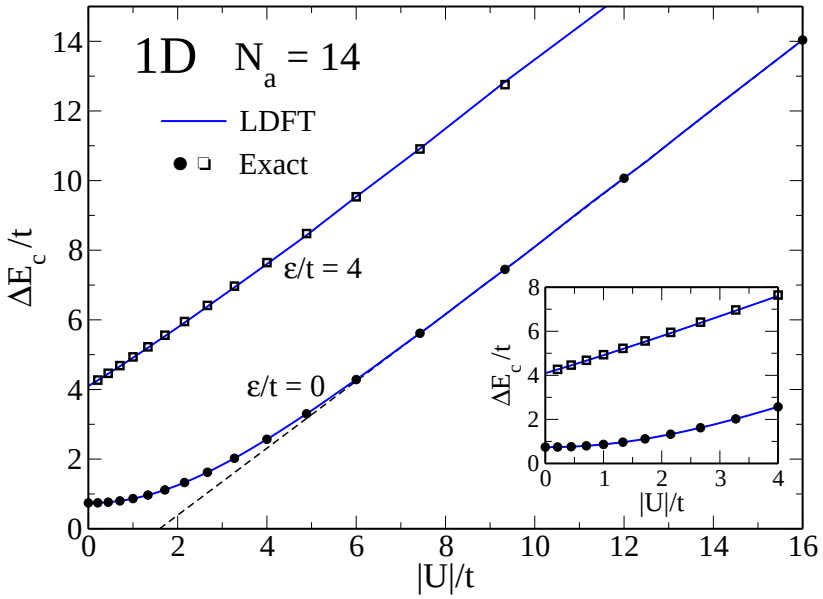

Figure 5.27: Charge gap $\Delta E_{\rm c} = E(N_{\rm e}+1) + E(N_{\rm e}-1) - 2E(N_{\rm e})$ as a function of the the attractive interaction strength $|U|/t$ in 1D Hubbard rings having $N_{\rm a} = 14$ sites at half band filling $n = 1$ for different values of the bipartite potentials ε. The solid blue curve corresponds to LDFT with the scaled dimer functional, and the symbols to exact Lanczos diagonalizations. The dashed black curve shows the asymptotic behavior of the charge gap for large values of $|U|/t$. In the inset small values of $|U|/t$ are highlighted.

where $K_1(x)$ is the first-order modified Bessel function. In the weak coupling regime this reduces to an exponential contribution

$$\Delta E_{\rm c}{}^{\rm BA}_{\rm weak} = \frac{4}{\pi}\sqrt{|U|t}\exp\left(\frac{-2\pi t}{|U|}\right). \tag{5.12}$$

On the other hand, the BCS gap at the weak coupling limit is given by [65]

$$\Delta E_{\rm c}{}^{\rm BCS}_{\rm weak} = 8t\exp\left(\frac{-2\pi t}{|U|}\right) \tag{5.13}$$

From Eq. (5.12) and (5.13) we see the same dependence in $|U|/t$ but a different pre-factor. For the homogenous system, the charge gap within the scaling approximation can be obtained at half band filling as [33]:

$$\begin{aligned}\Delta E_{\rm c}{}^{\rm LDFT} &= U\varepsilon_C(\gamma_{12}^{\rm LDFT}) + \left[\frac{U}{2\varepsilon_C(\gamma_{12}^{\rm LDFT})}\frac{(\gamma_{12}^{\rm LDFT}-\gamma_{12}^{\infty})^2}{(\gamma_{12}^{0}-\gamma_{12}^{\infty})^3}\frac{\partial\gamma_{12}^{0}}{\partial\gamma_{ii}}\right] \\ &\quad - \left[\frac{U}{2\varepsilon_C(\gamma_{12}^{\rm LDFT})}\left\{\frac{(\gamma_{12}^{\rm LDFT}-\gamma_{12}^{\infty})^2 - (\gamma_{12}^{\rm LDFT}-\gamma_{12}^{\infty})(\gamma_{12}^{0}-\gamma_{12}^{\infty})}{(\gamma_{12}^{0}-\gamma_{12}^{\infty})^3}\right\}\frac{\partial\gamma_{12}^{\infty}}{\partial\gamma_{ii}}\right]\end{aligned} \tag{5.14}$$

with $\gamma_{12}^{\rm LDFT} = \gamma_{12}^{\infty} + \frac{(\gamma_{12}^{0}-\gamma_{12}^{\infty})^2}{\sqrt{(\gamma_{12}^{0}-\gamma_{12}^{\infty})^2+(U/4zt)^2}}$ minimizing the energy using the scaling approxi-

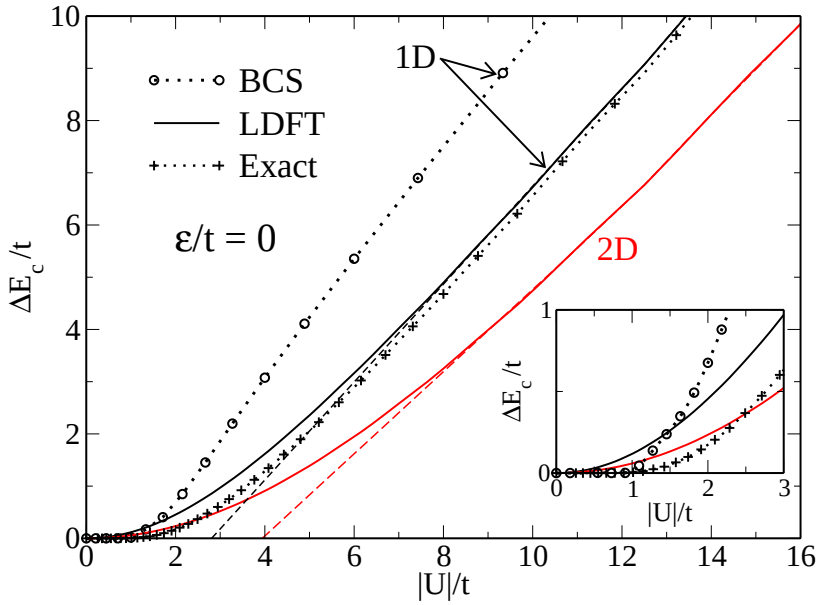

Figure 5.28: Charge gap $\Delta E_{\rm c} = E(N_{\rm e}+1) + E(N_{\rm e}-1) - 2E(N_{\rm e})$ as a function of the attractive interaction strength $|U|/t$ for the attractive Hubbard model in 1D (black) and 2D (red) periodic lattices. The band filling is $n = 1$ and $\varepsilon = 0$. The solid curves correspond to LDFT with the scaled dimer functional, the dotted curve with open circles to BCS (1D), the dotted curve with crosses to the exact Bethe-*Ansatz* solution (1D). Dashed curves show the asymptotic behavior of the charge gap for large values of $|U|/t$. In the inset small values of $|U|/t$ are highlighted.

mation and $W = (U/4)(1-\varepsilon_C)$ is the correlation energy with $\varepsilon_C = \sqrt{1-\left(\frac{\gamma_{12}^{\rm LDFT}-\gamma_{12}^{\infty}}{\gamma_{12}^{0}-\gamma_{12}^{\infty}}\right)^2}$. One finds at the weak correlation limit a quadratic behavior ($\Delta E_{\rm c}^{\rm LDFT}_{\rm weak} \propto (U/t)^2$) overestimating the charge gap. Nevertheless, LDFT captures the main physics of the charge gap in contrast to BCS, especially for $|U|/t \geq 4$. This can be related to the important errors in the kinetic and on the correlation energy done by the BCS approximation seen and discussed previously in Fig. 5.20.

5.5 Conclusion on the global scaling approximation

Based on investigations of the scalability and transferability of $W[\gamma]$, and on exact analytical results for the Hubbard dimer, we have proposed in this chapter a simple approximation to W, which takes advantage of its scaling behavior. In this way a unified description of the interplay between correlations and charge redistributions is achieved from weak to strong coupling and for all band fillings. Using this approximation, several important ground-state properties as well as the charge excitation gap of 1D and 2D lattices with repulsive and attractive interaction have been successfully determined as a function of the Coulomb repulsion strength and of the external bipartite potential.

The accuracy of the results confirm the pertinence of the scaling approximation and the transferability of the interaction-energy functional. Among the reasons for the success of the present scaled dimer approximation one should first of all mention the universality of the correlation-energy functional as stated by Hohenberg-Kohn's or Levy-Lieb's formulations. Moreover, the present approach has the asset of incorporating exact information on $W[\gamma]$ at the two most important limits of weak and strong correlations. These fundamental boundary conditions —somehow analogous to the sum rules of the local density approximation in the continuum— provide a useful guide for the development of the theory and are a further reason for the good performance of the method. The locality of the dominant interactions is in fact a characteristic of strongly correlated phenomena, which will be exploited more systematically in the forthcoming chapters. In this way it should be possible to improve the flexibility of the explicit approximations to $W[\gamma]$, thereby extending the range of applicability of LDFT. In particular, a local formulation of $W[\gamma]$ would be worthwhile. We have shown that the global scaling approximation offers the possibility to study a system with an inhomogeneous Coulomb integral. However, this approach is limited to bipartite lattices. A way to extend the applicability of the scaling *Ansatz* consists in developing an on-site formulation of the correlation energy functional $W[\gamma]$, offering the possibility to study a much larger variety of physical situations including disordered systems. This is the goal of the next chapter.

Chapter 6

A local approximation to $W[\gamma]$

Extending the work on homogenous systems, we have shown in the last chapter, that a good approximation to the correlation-energy functional (CEF) can be derived using global scaling properties. However, this approach is difficult to transfer to an arbitrary systems due to its non-local definition. In the present chapter we derive a local formulation for the CEF as a function of an universal degree of delocalization $\Gamma_{i\sigma}$ as given by Eq. (4.12). After proving the local scaling properties of the CEF, we derive the local scaling approximation (LSA) for ω_i in Sec. 6.1. In Sec. 6.2, applications of this generalization are presented for the metal-insulator transition in the bipartite Hubbard model (also known as ionic Hubbard model). The Hubbard chain with first and second nearest-neighbor hopping is considered in Sec. 6.3. Successes and limitations of this approach are discussed in Sec. 6.4.

6.1 Local *Ansatz* for $\omega_i[\gamma]$.

In this section we derive a local formulation of the interaction-energy functional, by using the definition of the average number of double occupations Eq. (4.12). A local formulation is a real advantage, since it allows a generalization of the CEF for all on-site interacting Hamiltonians. Furthermore, γ depends also implicitly on the size of the system, the band-filling and the charge distribution. An important consequence of these dependences is that γ_{ij} is bounded by a system-specific v-representability domain. Thus, for a given system, band-filling and charge distribution $\{\gamma_{ii}\}$, we must have $\gamma_{ij}^{\infty} \leq \gamma_{ij} \leq \gamma_{ij}^{0}$, where γ_{ij}^{∞} represents the maximum possible electronic delocalization with a minimum number of double occupations (at the strongly correlated limit) and γ_{ij}^{0} corresponds to the maximum of electronic delocalization without any restrictions (at the noncorrelated limit). It is therefore desirable to derive a dimensionless expression for the degree of electron delocalization (DED) which is independent of any external condition such as the size, geometry, band-filling and which could be transferred to any other system. Likewise, it is useful to consider a dimensionless degree of electronic correlation (DEC), since ω_i is bounded by ω_i^{∞} and ω_i^{0}, where ω_i^{∞} and ω_i^{0} refer respectively to the average number of double occupations at the strongly correlated and noncorrelated limits.
To be explicit, we focus first on the Hubbard dimer where the dimensionless DED and DEC appear quite naturally. In a dimer at half filling, the average number of double

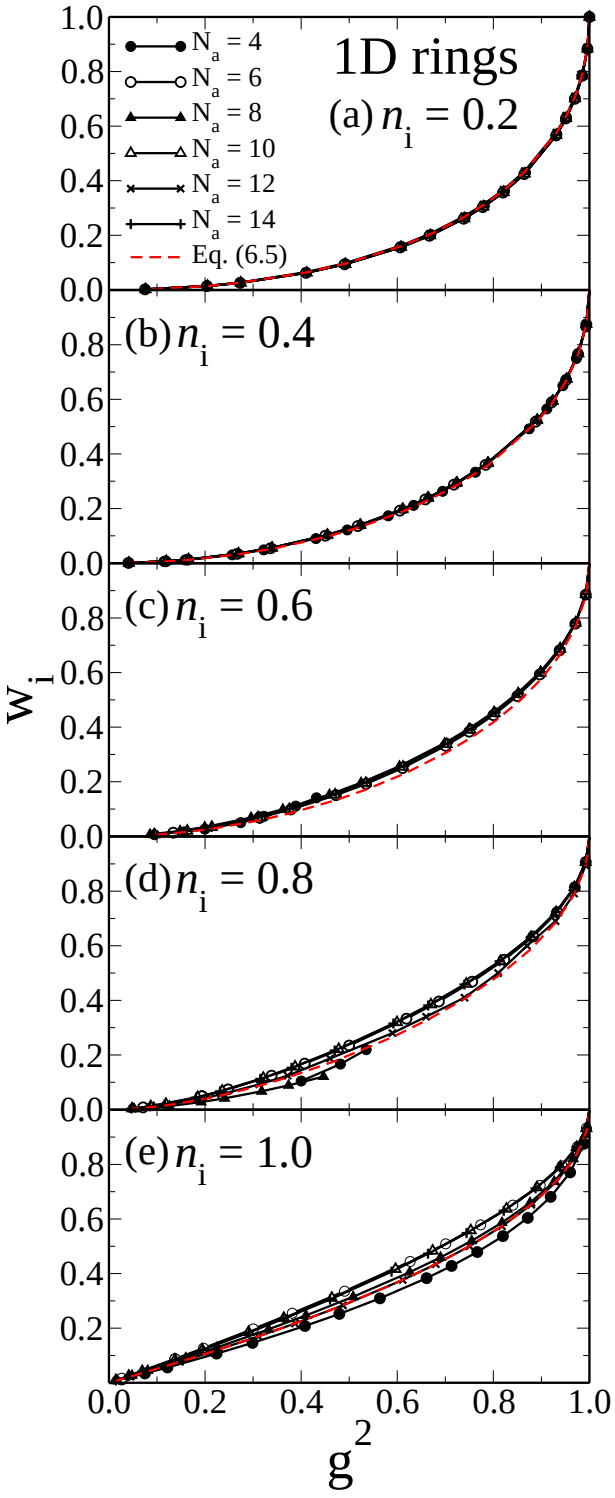

Figure 6.1: Transferability of the Dimension-less DEC w_i [Eq. (6.3)] as a function of the DED g [Eq. (6.6)] for different one dimensional bipartite rings ($N_a = 4-14$, symbols) and different number of free charges per site n_i. The black line with symbols refers to exact Lanczos diagonalization results and the red dashed line to Eq. (6.5).

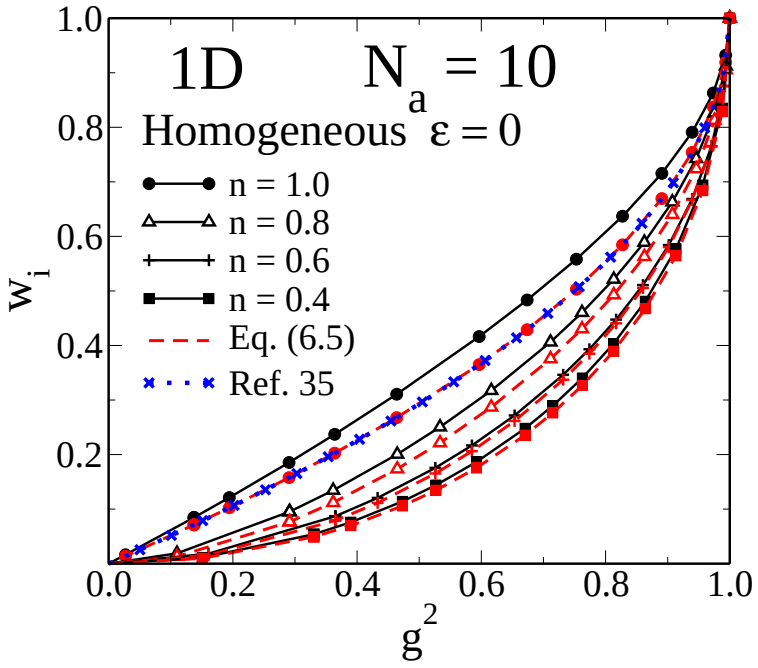

Figure 6.2: DEC w_i [Eq. (6.3)] as a function of the DED g [Eq. (6.6)] for a homogeneous ($\varepsilon = 0$ see [Eq. (4.1)]) 1D ring having $N_a = 10$ sites and for different band filling $n = N_e/N_a$. Symbols refer to different n, full line to exact diagonalization, dashed red line to the universal scaling approximations [Eq. (6.5)] and the dotted line to the simple scaling approach [34, 35, 36].

occupations defined in Eq. (4.12) is given by

$$\omega_i = \frac{1}{2}\left(\gamma_{ii} - \frac{\gamma_{12}^2}{2}\frac{1+\sqrt{\gamma_{ii}(2-\gamma_{ii})-\gamma_{12}^2}}{(1-\gamma_{ii})^2+\gamma_{12}^2}\right). \tag{6.1}$$

In this case, the v-representability domain is defined by the charge distribution $\{\gamma_{ii}\}$ ($0 \leq \gamma_{ii} \leq 2$) and by the maximum and minimum values of the off-diagonal γ_{12}. These are given respectively by

$$\begin{aligned} \gamma_{12}^0 &= \sqrt{\gamma_{ii}(2-\gamma_{ii})} \\ \gamma_{12}^\infty &= \begin{cases} \sqrt{2\gamma_{ii}(1-\gamma_{ii})} & \text{if} \quad \gamma_{\rm ii} \leq 1 \\ \sqrt{2(\gamma_{ii}-1)(2-\gamma_{ii})} & \text{if} \quad \gamma_{\rm ii} > 1 \end{cases} \end{aligned} \tag{6.2}$$

If one defines the DED g_i and DEC w_i on the site i as

$$g_i^2 = \frac{\gamma_{12}^2 - \gamma_{12}^{\infty\,2}}{\gamma_{12}^{0\;2} - \gamma_{12}^{\infty\,2}} \tag{6.3}$$

$$w_i = \frac{\omega_i - \omega_i^\infty}{\omega_i^0 - \omega_i^\infty}, \tag{6.4}$$

The Eq. (6.1) is simplified as a function of these dimensionless variables, so that, for a repulsive interaction ($U > 0$) we have

$$\mathrm{w}_i = \frac{(1-\chi_i)^2}{1-\delta_i\chi_i} \tag{6.5}$$

where $\chi_i = \sqrt{1-g_i^2}$ and $\delta_i = \min\{\gamma_{\mathrm{ii}}, 2-\gamma_{\mathrm{ii}}\}$. Notice that δ_i represents the "free available charge" taking into account the electron-hole symmetry. Note that Eq. (6.5) connects the DED, the DEC, and the "free available charge" without other explicit or implicit system-specific dependencies. Therefore, it is reasonable to assume that this relation is transferable to any other system with a properly extended definition of the DED g_i and DEC w_i. This is discussed in the following.
We have discussed in Sec. 4.5 that the ensemble-N-representability condition in real space introduces a dimensionless degree of delocalization $\Gamma^2_{i,\sigma}$ of a site i with its environment [see Eq. (4.24)]. At half filling and $S_z = 0$ this reads that $\Gamma^2_{i,\sigma} = \sum_{j\neq i} |\gamma_{ij,\sigma}|^2$. This can be viewed as a norm of the column vector i of the density matrix by taking out the square of the diagonal term γ^2_{ii}. It is then by definition invariant under any canonical transformation among the orbitals $j \neq i$. It has been shown previously that at half filling and for square lattice systems ($\gamma^\infty_{ij} = 0$), that the sum in $\Gamma^2_{i,\sigma}$ can be restricted only to the relevant non-diagonal terms for which $t_{ij} \neq 0$. A straightforward scaling *Ansatz* for the DED reads

$$g^2_{i,\sigma} = \frac{{\Gamma_{i,\sigma}}^2 - {\Gamma^\infty_{i,\sigma}}^2}{{\Gamma^0_{i,\sigma}}^2 - {\Gamma^\infty_{i,\sigma}}^2}. \tag{6.6}$$

In practice, for a Hubbard system with NN hoppings the only considered terms are the NN γ_{ij}: $\Gamma^2_{i,\sigma} = \sum_{j\,\mathrm{NN\,of}\,i} |\gamma_{ij,\sigma}|^2$. For a Hubbard system with up to next NN hoppings we consider the NN and next NN γ_{ij}: $\Gamma^2_{i,\sigma} = \sum_{j\,\mathrm{NN\,or\,nNN\,of}\,i} |\gamma_{ij,\sigma}|^2$. Since the DEC is defined independently for each site i, the previous definition of g_i [see Eq. (6.3)] can be applied for any site in an arbitrary environment. Accordingly, from Eq. (6.4), the average number of double occupations at site i in any system is given by

$$\omega^{sc}_i = \omega^\infty_i + \mathrm{w}_i[\gamma_{ii}, g^2_i](\omega^0_i - \omega^\infty_i), \tag{6.7}$$

where ω^∞_i and ω^0_i are simple functions of γ_{ii}. In most of the cases $\omega^\infty_i = \max[\gamma_{ii} - 1, 0]$ and $\omega^0_i = \gamma_{ii,\uparrow}\gamma_{ii,\downarrow} = \gamma^2_{ii}/4$. The set of Eqs. (6.5), (6.6), and (6.7) define the generalized local scaling approximation (LSA) of the on-site correlation energy for any system.
This LSA can be regarded as an effective medium theory in the sense that the effect of the rest of the system or environment on each site i is mapped into a single orbital of a site. The local contribution of site i to the interaction energy functional is then calculated on this reduced two-level system, which has the same charge density γ_{ii} at site i as the actual system under study, and a renormalized effective degree of electronic delocalization g.

In Fig. 6.1 we demonstrate the transferability of the relation between the local DEC and the local DED [see Eq. (6.5)] by considering different sizes of one dimensional bipartite Hubbard rings at half filling $n = 1$ and different charge densities δ_i (free charge) on the considered site i. Symbols refer to exact results obtained with the Lanczos diagonalization method [42] and the red dashed curves refer to the LSA Eq. (6.5). The results for w_i as a function of g_i for different sizes are remarkably similar, showing the pertinence and

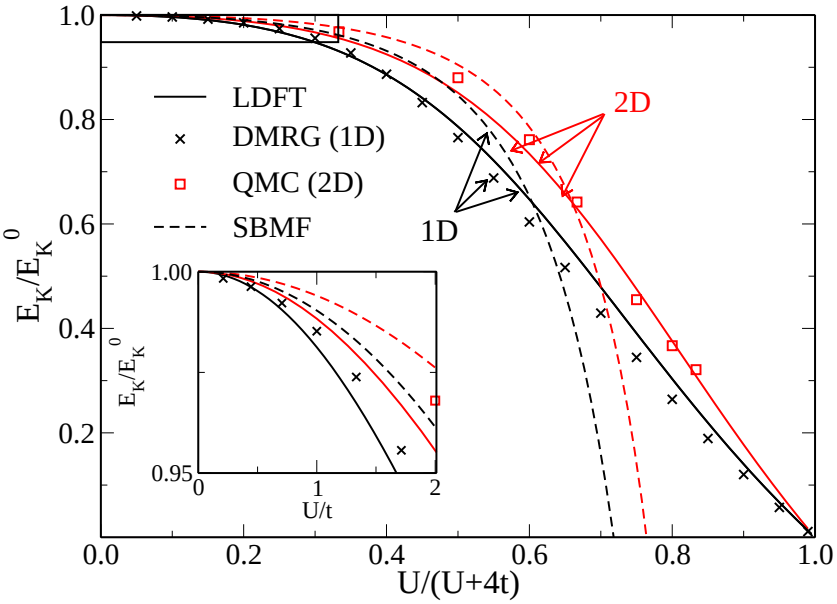

Figure 6.3: Renormalization of the kinetic energy E_K/E_K^0 for th one- (black) and two-dimensional (red) homogeneous Hubbard system. LDFT results (full line) are compared with slave boson mean field theory (SBMF, dashed line), DMRG (for 1D, cross) and QMC [79] (for 2D, square). The inset figure shows the weakly correlated limit of E_K/E_K^0 (region in rectangle in the figure).

transferability of Eq. (6.5).
Another important feature of this approximation is that it takes into account the charge density on the site γ_{ii}, thereby respecting the electron-hole symmetry. This contrasts with previous dimer scaling approximations [34, 36]. In Fig. 6.2 we show the dependence on the band filling n of the relation between w and g [Eq. (6.5)] for a homogeneous Hubbard ring with $N_a = 10$ sites. Full curves refer to exact results obtained with Lanczos diagonalization, the blue crossed curve to the homogeneous scaling approximation [34, 36], and the dashed red curves to Eq. (6.5). Since the LSA takes into account the specific charge density per site, even if the system is homogeneous, the accuracy is considerably enhanced as compared to this previous scaling approximation. Notice that at half filling, the LSA and the scaling approximation are equivalent.

As a first application of the LSA, which can be viewed as an effective medium theory, it is interesting to look at the effective renormalization of the kinetic energy E_K/E_K^0 or equivalently of the hopping integral t_{eff}/t, where E_K^0 is the kinetic energy at the noncorrelated limit. The results are displayed in Fig. 6.3 for homogenous one- and two-dimensional systems at half filling. LDFT within the LSA is compared with the slave-boson mean-field theory (SBMF) (see Sec. 3.3.2), with the DMRG method (1D) and with quantum Monte Carlo simulations (2D) [79].
Within a mean-field theory, the saddle point is calculated to minimize the energy, which

can be written as

$$\frac{E_{\rm gs}}{N_a} = -zqt\gamma_{12}^0 + U\langle\omega\rangle \tag{6.8}$$

where z is the coordination number. The renormalization of the hopping integral is defined by $t_{\rm eff} = qt$ and $\langle\omega\rangle$ represents the average number of double occupations per site. In this case, the renormalization of the hopping integral represents the reduction of the kinetic energy due to the electronic correlations. For a homogeneous system at half filling, the analytic solution of LDFT within the LSA minimization yields

$$q^{\rm LSA} = \frac{1}{\sqrt{1+(2U/D)^2}} \tag{6.9}$$

with $D = 8zt\gamma_{12}^0$ and

$$\langle\omega^{\rm LSA}\rangle = \frac{1}{4}\left(1 - \sqrt{1 - \frac{1}{1+(2U/D)^2}}\right). \tag{6.10}$$

On the other hand, in the spin-restricted slave-boson mean-field theory, one obtains at the saddle point:

$$q^{\rm SBMF} = 1 - \left(\frac{U}{D}\right)^2 \tag{6.11}$$

and

$$\langle\omega^{\rm SBMF}\rangle = \frac{1}{4}(1 - U/D) \tag{6.12}$$

where D is proportional to the kinetic energy of the noncorrelated system. The first remark is that the spin-restricted slave-boson approximation predicts that $t_{\rm eff}$ vanishes for a critical value of the Coulomb integral U_c. This would imply that the system undergoes a Mott-insulator transition ($t_{\rm eff}/t = 0$, $\omega_i = 0$) as it has been described in more detail in Sec. 3.3.2. In contrast, the exact solution and LDFT within LSA do not present such a transition since they predict an insulating behavior for an arbitrarily small value of U/t. The insulating behavior of these systems is discussed in more detail in the following section. Fig. 6.3 clearly demonstrates that LDFT is indeed far more accurate than the SBMF, especially for strong interactions. At the weakly correlated limit, displayed in the inset of Fig. 6.3, it is shown that the LSA underestimates the renormalization in contrast to SBMF which overestimates it. These differences can be explained by the fact that LSA of the correlation-energy functional depends explicitly on the renormalization of the hopping integral, while in SBMF theory the average double occupancy depends only on the ratio U/D.

6.2 From band insulator via metal to Mott insulator

In this section we present results of LDFT using the LSA for the bipartite Hubbard model, in the thermodynamic limit ($N_a \to \infty$). The model is given by

$$\hat{H} = \sum_{i,\sigma} \varepsilon_i \, \hat{n}_{i\sigma} + \sum_{\langle i,j\rangle\sigma} t_{ij}\hat{c}_{i\sigma}^\dagger \hat{c}_{j\sigma} + U\sum_i \hat{n}_{i\downarrow}\hat{n}_{i\uparrow}. \tag{6.13}$$

In the last chapter we have already discussed the physics of this model by focusing on finite clusters. Let us recall that in the past years considerable efforts have been devoted to analyzing the physics of this Hamiltonian, since it undergoes a transition from band to Mott insulator for a finite value of the bipartite potential. For some particular systems this transition is realized by passing through an intermediate metallic phase. Examples of this situation are the 2D square lattice, as shown by using quantum Monte Carlo methods [40], and the 2D Bethe lattice by using DMFT [80]. One-dimensional bipartite systems with NN hopping and the generalized ionic Hubbard model AB_n [81] do not present a metallic phase [82]. The latter only appears when one includes next NN hoppings [83].
An analysis of various limiting cases at half filling allows us to characterize the transitions, by using rigorous arguments. In fact, at the noncorrelated regime ($U/t = 0$) of the bipartite model an arbitrarily small value of the energy-shift level ε/t opens a gap of width ε/t in the one-particle density of states leading to a band-insulating behavior. In this limit, the Hamiltonian is diagonal in reciprocal space,

$$H = \sum_{\mathbf{k},\sigma} E_{\mathbf{k}} \hat{c}^{\dagger}_{\mathbf{k},\sigma} c_{\mathbf{k},\sigma} \tag{6.14}$$

where $E_{\mathbf{k}} = \pm\sqrt{\epsilon(\mathbf{k})^2 + (\varepsilon/2)^2}$, and $\epsilon(\mathbf{k})$ is the energy of a free-particle of wave vector $\mathbf{k}$. The sum runs over half of the Brillouin zone. The eigenenergies are split into two bands with an energy gap equal to ε separating them. Fig. 6.4 shows an example of the density of states at the noncorrelated limit of a two-dimensional square lattice in (a) the metallic phase $\varepsilon/t = 0$ and (b) the band insulator phase for $\varepsilon/t = 1$.
In the atomic regime, $t = 0$ (isolated atoms, no hopping integral), the picture is quite different. As long as $U < \varepsilon$, the system is a band insulator (with a gap $\Delta = \varepsilon - U$). In this case one sub-lattice $\mathcal{S}_2$ is fully occupied (i.e., $n_2 = \langle \hat{n}_i \rangle = 2$, for $i \in \mathcal{S}_2$) and the other one is empty ($n_1 = \langle \hat{n}_i \rangle = 0$, for $i \in \mathcal{S}_2$)). The gap $\Delta = (\varepsilon - U)$ decreases as U increases until at $U = \varepsilon$ the homogeneous singly occupied states ($n_1 = n_2 = 1$) and the inhomogeneous one ($n_2 = 2$ on $\mathcal{S}_2$) are degenerate. Finally, at large values of U, $U > \varepsilon$, we have a Mott insulator with a homogeneous electronic distribution on the system ($n_2 = n_1 = 1$) and a gap proportional to U.
Even though the solution of the ionic Hubbard model might sound trivial in the atomic regime, it clearly shows that the Coulomb repulsion is able to suppress the band-insulating gap. It is then understandable that due to electronic delocalization an intermediate metallic phase can appear during the band insulator Mott insulator transition.

In this section we want to apply LDFT using the LSA to this problem and compare the results with previous studies [40, 82]. For simplicity, LDFT results are obtained using finite 1D and 2D lattices, which are large enough so that the properties have converged to the thermodynamic limit. First, we present the ground-state properties, which are changing dramatically across the transition, second, we focus on the charge-gap analysis and draw the phase diagram of these systems. In particular, we discuss the contradiction in the phase diagram predicted in this work using LSA and in the previous study [40] for the 2D lattice. Figures 6.5 and 6.6 display ground-state properties of infinite Hubbard systems in one and two dimensions as a function of the Coulomb repulsion strength U/t. Different values of the energy level shift ε/t are considered at half filling $n = 1$. The behavior of the ground-state energy $E_{\rm gs}$, charge transfer $\Delta n = \gamma_{22} - \gamma_{11}$, and the NN bound order γ_{12} is very similar to the case of the 1D ring with $N_a = 14$ sites, which was presented in Fig. 5.8 and discussed in the previous chapter.

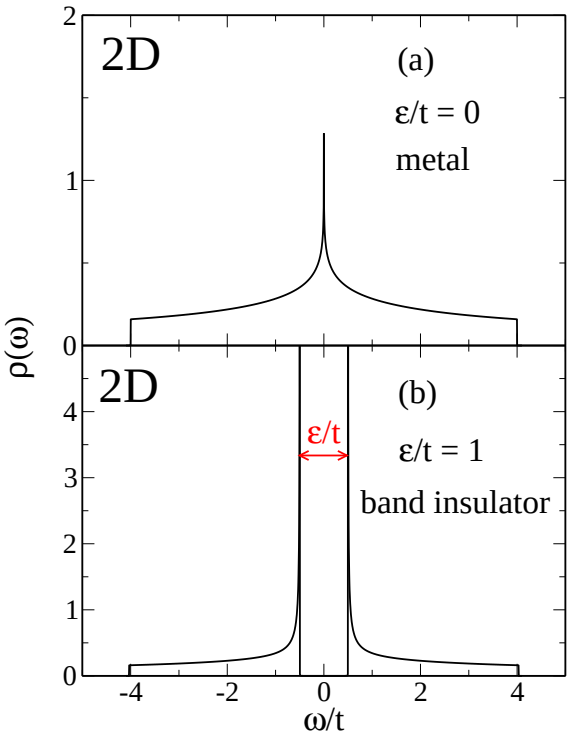

Figure 6.4: One-particle density of states $\rho(\omega)$ for the two dimensional noncorrelated bipartite Hubbard model ($U/t = 0$) at half filling ($N = 1$) for different values of the ionic potential ε/t. The insulating gap is clearly visible in (b) (band insulator $\varepsilon/t = 1$) while the metallic states $\varepsilon/t = 0$ show gapless excitations.

Here we also compare the ground-state energy of the homogeneous 2D system with available QMC [25] and VMC [84] results and note a good agreement with both of them. Indeed, this is already a meaningful success of the LSA, since the LDFT solution is much easier to obtain than the QMC calculations, which are numerically highly demanding.
Furthermore, the present local definition of the correlation-energy functional allows us to derive the average number of double occupations at each site [see sub-figure (d) of Figs. 6.5 and 6.6]. This contrasts with the previous approximation, which provides the global information on the system. In the homogeneous case, the average ω_i is evidently the same for all i, but for a finite value of ε/t an interesting small transfer of double occupations occurs. In fact, by increasing U/t ω_i decreases on the most filled sub-lattice [$\mathcal{S}_2$, negative values on sub-figure (d) of Figs. 6.5 and 6.6]. On the other hand, ω_1 has a non monotonous behavior, reaching a maximum value for a finite U/t. Starting from the noncorrelated limit, and increasing U/t, ω_1 increases slowly until it reaches a maximum value. Then it decreases more rapidly. This phenomenon is directly linked with the reduction of the charge transfer and favors the increase of γ_{12}. Furthermore, when U/t increases, ω_2 decreases on the most favorable sub-lattice $\mathcal{S}_2$ leading to a charge transfer. Consequently, the electronic density increases on the less favorable sub-lattice $\mathcal{S}_1$ as well as the double occupations and allows the enhancement of γ_{12}. Finally, when the Coulomb

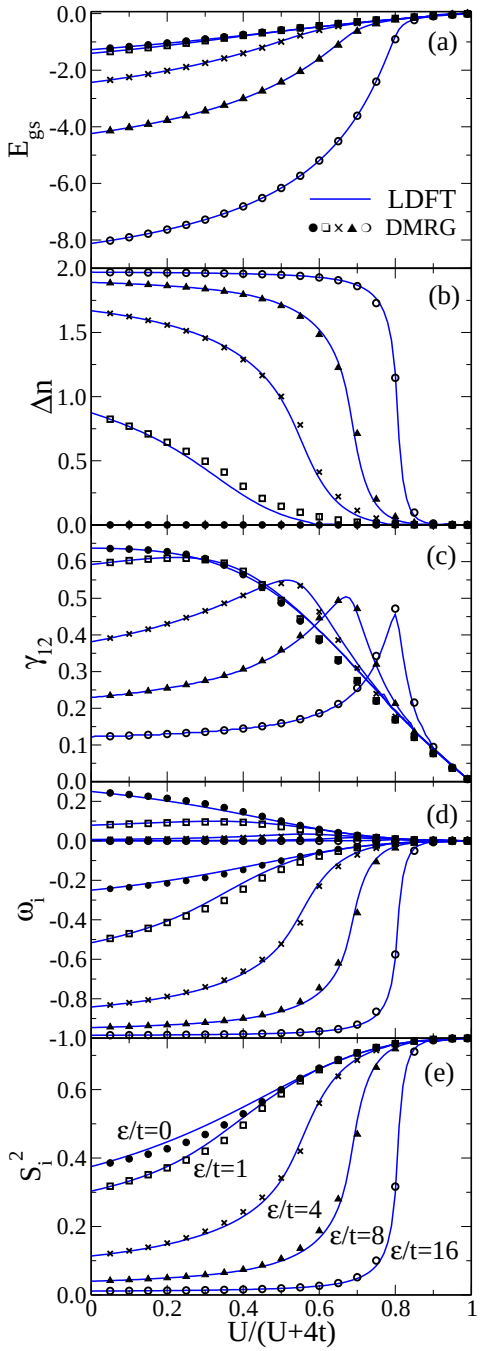

Figure 6.5: Ground-state properties of bipartite Hubbard chains at half filling as a function of the strength of the Coulomb repulsion U/t and for different values of the energy level shift ε/t. Presented, are in (a) the ground state energies E_{gs}, in (b) the charge transfer between the two sub-lattices Δn, in (c) the NN bound order γ_{12}, in (d) the interaction energy ω_i for the sub-lattice $\mathcal{S}_1$ (positive values) and $\mathcal{S}_2$ (negative values) and in (e) the local spin momentum S_i^2. Solid curves refer to LDFT within the LSA and symbols to DMRG.

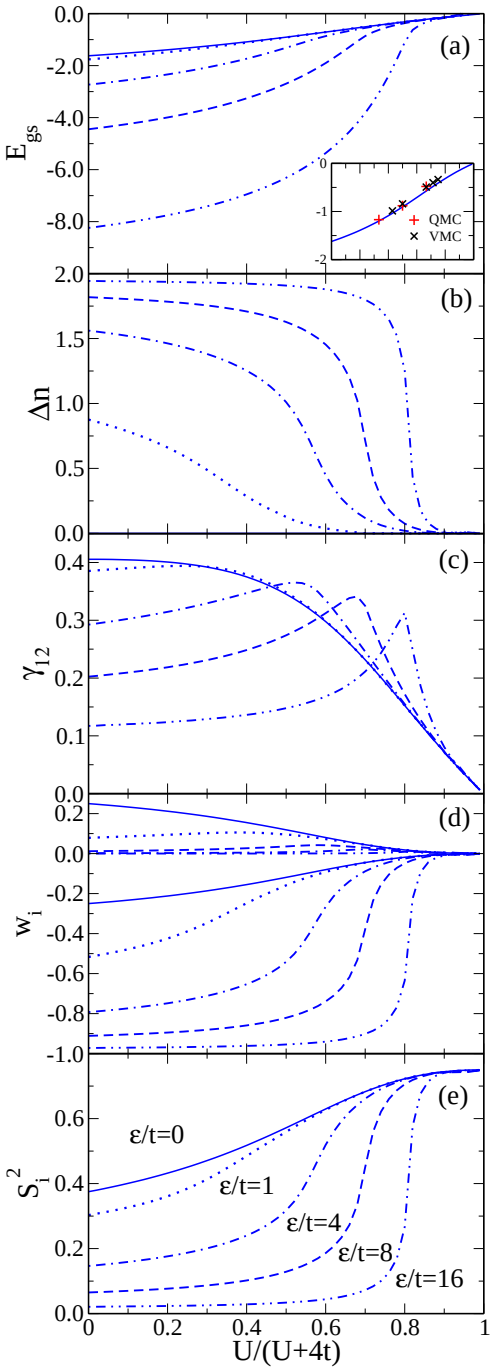

Figure 6.6: Ground-state properties of an infinite 2D bipartite Hubbard system at half filling as a function of the strength of the Coulomb repulsion U/t and for different values of the energy level shift ε/t. Presented, are in (a) the ground state energies E_{gs}, in (b) the charge transfer between the two sub-lattices Δn, in (c) the NN bound order γ_{12}, in (d) the interaction energy ω_i for the sub-lattice $\mathcal{S}_1$ (positive values) and $\mathcal{S}_2$ (negative values) and in (e) the local spin momentum S_i^2. Curves refer to LDFT within the LSA. In the inset in sub-figure (a) crosses refer to quantum Monte-Carlo [25] and variational Monte-Carlo [84] simulations.

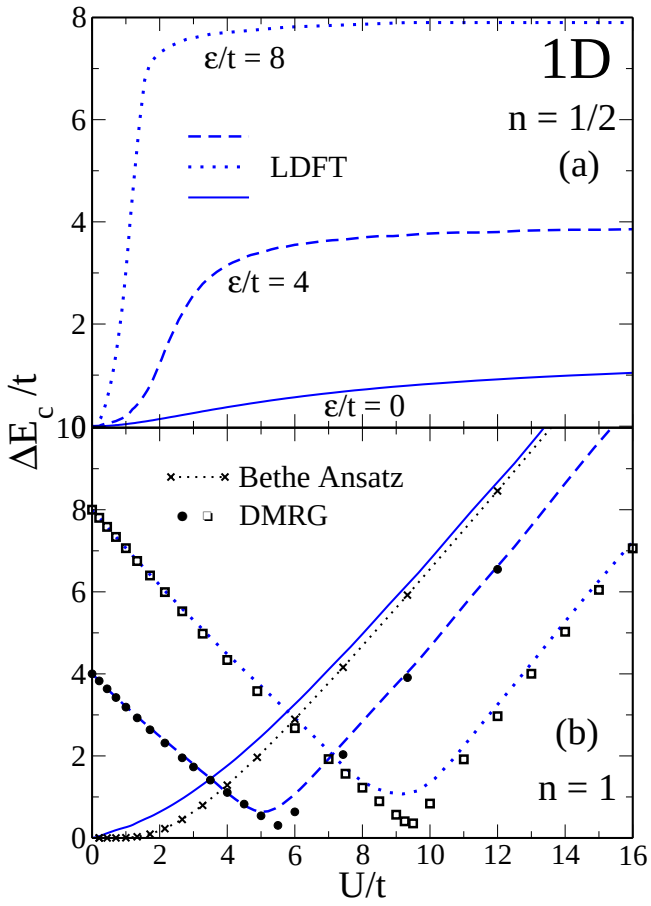

Figure 6.7: Charge gap $\Delta E_{\rm c}$ for a bipartite Hubbard chain at (a) quarter filling ($n = 1/2$) and (b) half band filling ($n = 1$). LDFT within the LSA results (curves) are presented for representative values of the energy shift level ε/t. They are compared with DMRG results (symbols) and with the Bethe *Ansatz* (dotted curve with crosses).

repulsion becomes too important, ω_1 decreases to reduce the interaction-energy.
The local magnetic moments $S_i^2 = \frac{3}{4}\langle(\hat{n}_{i\uparrow} - \hat{n}_{i\downarrow})^2\rangle = \frac{3}{4}\left(\gamma_{ii} - 2\langle\hat{n}_{i\uparrow}\hat{n}_{i\downarrow}\rangle\right)$ at the different sites i [see Figs. 6.5 (e) and 6.6 (e)] provide an alternative perspective of the electronic correlation and localization occurring as U/t increases. If one focuses on $S = 0$ states, S_i^2 can be directly interpreted as the variance of the local magnetic moment. In the case of half filling, even in the presence of an external potential, S_i is the same on the two sub-lattices due to electron-hole symmetry. This property is strictly respected by the LSA, as shown in Eq. (6.5). In this case, using Eqs. (6.7) and (6.5) one obtains $S_2^2 = \frac{3}{4}\left(\gamma_{22} - 2\omega_2\right) = \frac{3}{4}\left(2 - \gamma_{11} - 2\omega_2^{\infty} + 2\omega_1\right) = \frac{3}{4}\left(\gamma_{11} - 2\omega_1\right) = S_1^2$. In the uncorrelated limit $\hat{n}_{i\uparrow}\hat{n}_{i\downarrow} = \gamma_{ii}^2/4$ and therefore S_i^2 depends only the density distribution γ_{ii}. For example, for $n = 1$ one observes that S_i^2 decreases with increasing ε/t, namely, from $S_i^2 = 3/8$ for $\varepsilon/t = 0$ to $S_i^2 = 0$ for $\varepsilon/t = \infty$. In the latter case all electrons are paired on one sub-lattice ($U = 0$ and $n = 1$). If now the Coulomb repulsion is increased, one finds

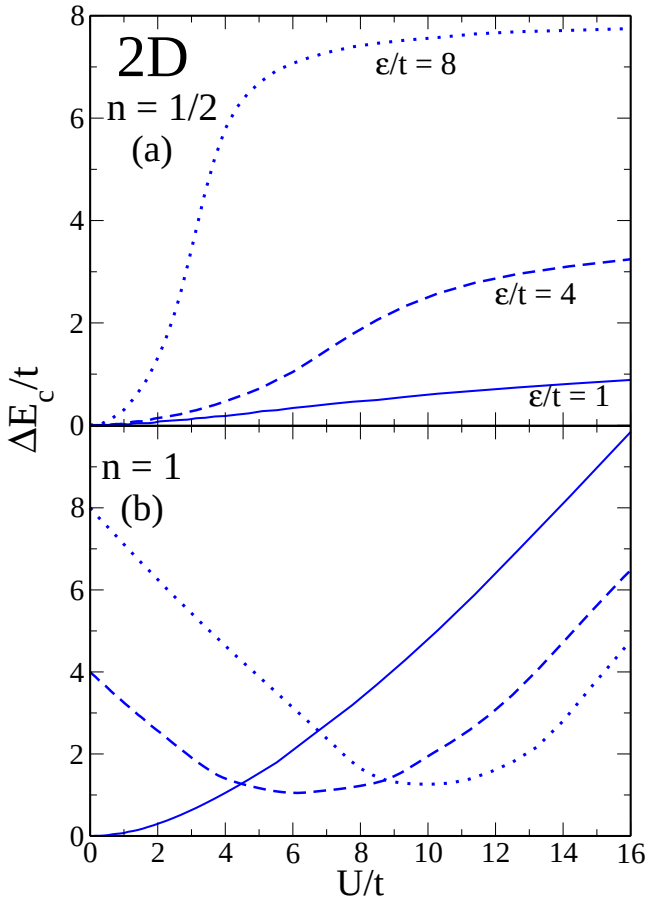

Figure 6.8: Charge gap ΔE_{c} for a two-dimensional bipartite Hubbard system at (a) quarter filling ($n = 1/2$) and (b) half band filling ($n = 1$). LDFT within the LSA results are presented for representative values of the energy level shift ε/t.

a reduction of charge fluctuations and thus an enhancement of S_i^2. Finally, for $U/t \gg 1$ and $U \gg \varepsilon$ the largest possible $S_i^2 = 3/4$ is reached, irrespectively of the value of ε/t. At this point all sites are singly occupied and the variance of S_i^2 is maximal ($S = 0$).
Figures 6.7 and 6.8 display the charge gap $\Delta E_{\mathrm{c}} = E(N_{\mathrm{e}} + 1) + E(N_{\mathrm{e}} - 1) - 2E(N_{\mathrm{e}})$ as a function of the repulsive interaction strength U/t for a one- and two-dimensional infinite system at quarter and half filling. Different representative values of the energy level shift ε/t are considered. At quarter filling and in the noncorrelated limit the gap is zero for any value of the bipartite potential ε/t, since the most favorable sub-lattice is not full. However, increasing the Coulomb repulsion opens a gap even for an arbitrarily small value of U/t. In the case of $\varepsilon/t \neq 0$, and starting from $U/t = 0$, the ground state corresponds to a delocalized charge-density wave, and the interplay between the kinetic energy and the potential energy determines the electronic density on the sub-lattices. Increasing U/t causes the double occupations to be energetically less favorable and leads to a decrease of the kinetic energy. At the same time the electrons become fully localized

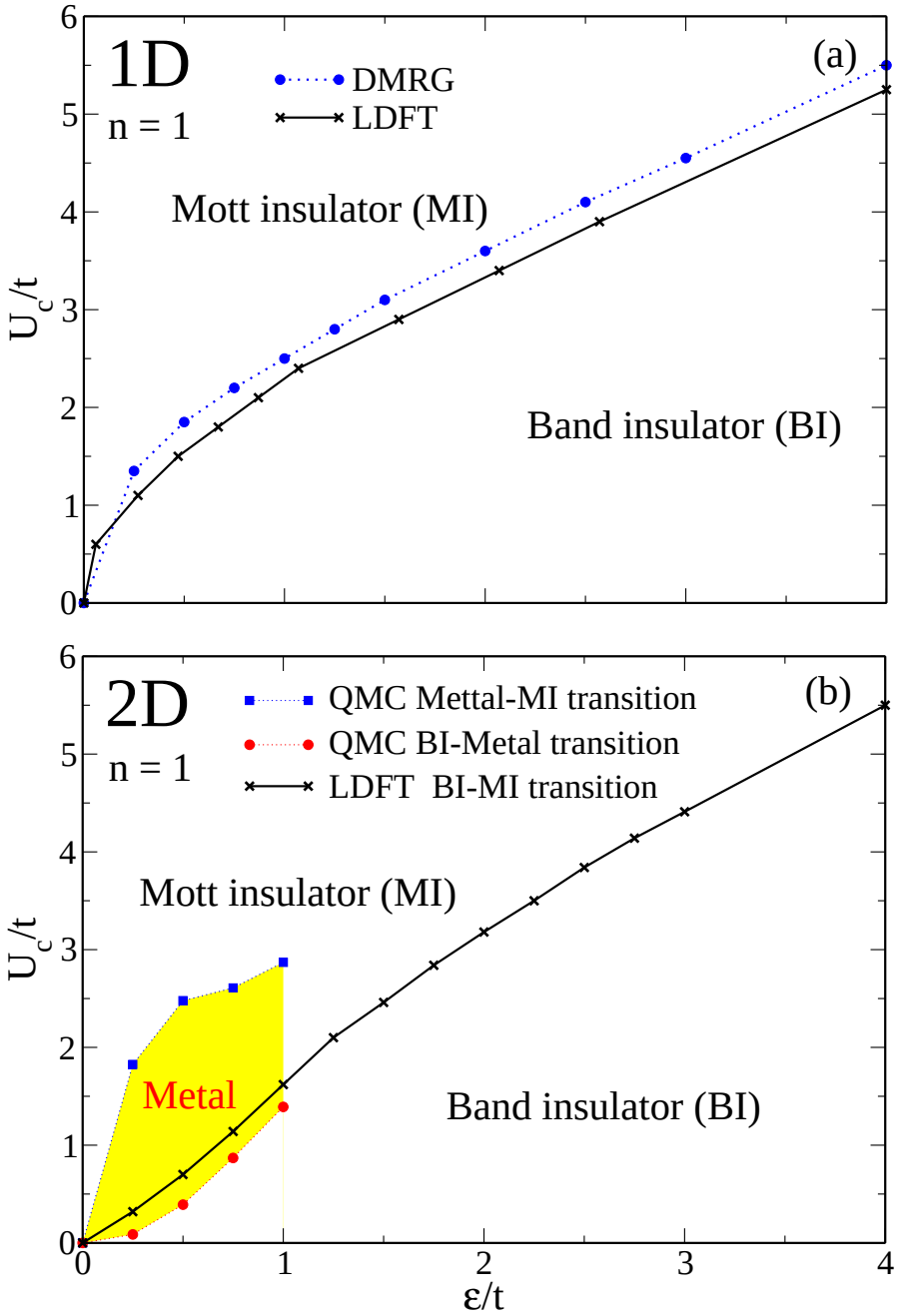

Figure 6.9: Phase diagram of the bipartite Hubbard model in (a) one dimension and (b) two dimensions at half filling ($n = 1$). The solid curve with crosses is the LDFT within LSA. In (a) the curve with dots represents the DMRG phase boundary. In (b) the dotted blue curve with squares and the dotted red curve with circles refers to quantum Monte Carlo calculations [40]. They indicate a metallic phase ($\Delta E_c = 0$) not found using the LSA to LDFT.

on the most favorable sub-lattice. Under these conditions, the addition of an electron occurs necessarily on the less favorable sub-lattice, since double occupation are highly unprobable. Consequently, this enhances the energy by about ε/t ($U/t \to +\infty$). The more important the energy of the charge transfer is, as compared to the kinetic energy, the faster the transfer happens. This explains the fact that in the 1D case the charge gap converges faster to its strongly correlated limit than in 2D since in two dimensions the hybridization is more important than in 1D (for instance for $\varepsilon/t = 8$, $\Delta E_{\rm c} = 7.9$ for $U/t \sim 6$ in 1D, and for $U/t \sim 12$ in 2D).
In the following, we focus on systems at half filling. As is already well known, in one- and two-dimensional systems there is no Mott transition at a finite value of U/t, for the homogeneous case ($\varepsilon/t = 0$). This means that for an arbitrarily small value of U/t the charge gap is already positive, and therefore, the system always exhibits an insulating behavior. At the non-interacting limit, and in the absence of ε/t, the system is metallic ($\Delta E_{\rm c} = 0$). However, a finite value of ε/t opens a gap in the one-particle spectrum and the system becomes a band insulator. On the other hand, at the strongly correlated limit, the charge gap increases linearly with U/t. The reason for this is that all electrons are localized and that adding an electron leads inevitably to a double occupation and to an energy increase of about U. Introducing inhomogeneities induces a non-monotonous behavior of the charge gap. At the noncorrelated limit the charge gap is already finite and takes a value of the order of ε/t. Remarkably, increasing the strength of the Coulomb repulsion U, $\Delta E_{\rm c}$ initially decreases nearly linearly, until it reaches a minimum for $U/t \simeq \varepsilon/t + 1$. Further increase of U implies that $\Delta E_{\rm c}$ increases nearly linearly in U/t. Starting from the noncorrelated limit, an increase in the strength of the interaction causes an increase of the kinetic energy [see Figs. 6.5 and 6.6] since for $U \simeq \varepsilon$ the Coulomb repulsion on the doubly occupied sites on sub-lattice $\mathcal{S}_2$ compensates the single-particle energy difference ε between the two sub-lattices. This allows a nearly free motion of the γ_{11} electrons occupying sub-lattice $\mathcal{S}_1$, together with the extra $\gamma_{22} - 1$ electrons on sub-lattice $\mathcal{S}_2$ ($\gamma_{11} < \gamma_{22}$ for $\varepsilon > 0$). Consequently, adding an electron on such a system is energetically less expensive due to the importance of the induced kinetic energy associated to its delocalization. At this point the system is nearly metallic, since the charge gap is weak. In fact, quantum Monte Carlo simulations predict a metallic phase in two dimensions [40] which is not observed in the LSA to LDFT. The minimum of the charge gap indicates a kind of critical point, namely, a band insulator (BI) to Mott insulator (MI) phase transition. In two dimensions, the minimum of the charge gap is smoother than in one dimension since in this case the hybridization is stronger (larger band-width). Finally, when the Coulomb repulsion becomes larger than both the kinetic energy and the charge-transfer energy ($U \sim \varepsilon + t$), the electrons become localized throughout the whole lattice, leading to a linear increase of the charge gap, as in the homogeneous case.
We compare LDFT results with the exact Bethe-*Ansatz* solution for the one-dimensional homogeneous case in Fig. 6.7. The strongly correlated limit is well reproduced by LDFT but at the weakly correlated limit the gap is overestimated. As was already discussed in the case of attractive interaction in Sec. 5.4, LSA predict also a quadratic increase in U/t of the gap at the weakly correlated limit. This is in contrast to the Bethe-*Ansatz* which predicts a gap which depends exponentially on $-t/U$. For the sake of comparison we also show, in Fig. 6.7, DMRG method predictions for finite values of the energy level shift ε/t. At the limit $U \gg \varepsilon$ and $U \ll \varepsilon$, LSA and DMRG results are in good agreement. However, near the critical point, some differences are present. First, the critical value U_c

for which the charge gap is minimal is slightly under-estimated in the LSA. For example for $\varepsilon/t = 4$, $U_c^{\mathrm{LDFT}} \simeq 5.2$ and $U_c^{\mathrm{DMRG}} \simeq 5.5$. The strongest differences between LSA and DMRG is the overestimation of the value of the charge gap near the critical point. In 2D (see Fig. 6.8) this overestimation implies that using the LSA, no metallic phase is found between the BI and the MI phase in contrast to QMC simulations. The overestimation of the charge gap done by using the LSA at the weakly correlated limit or at the BI-MI phase transition point results from the behavior of the charge gap of the dimer in a similar situation. For the dimer, the charge gap at the weakly correlated limit is quadratic in U/t and an significant gap at the BI-MI phase transition point (consequences of its discrete spectrum). Consequently, the LSA reproduces quantitatively this behavior for any system, since the dimer serves as the reference system to derive this approximation. Finally, to summarize, we present in Fig. 6.9 the phase diagram for (a) the one-dimensional and (b) the two dimensional bipartite Hubbard model. The solid black curves with crosses refer to the BI-MI phase transition predicted by LDFT within LSA. Note that in the atomic regime (isolated atoms, $t = 0$) the transition occurs for $\varepsilon = U$ since at this point the singly occupied states are degenerate with the inhomogeneous one ($n_2 = 2$ on $\mathcal{S}_2$). For the 1D case DMRG predictions are also plotted showing a good agreement between the two methods. For the 2D case we also show the results of QMC simulations [40] which predict a metallic phase between the BI and the MI ones. However, it is expected that the LSA provides qualitatively good results at the strongly correlated limit.

It has been shown that the LSA captures the main physics resulting of the interplay between electronic delocalization, charge distribution and Coulomb repulsion in the ionic Hubbard model. In particular, the important changes in the ground-state properties are well reproduced during the transition from a band insulator having a charge density wave to a Mott insulator where the charge is homogeneously localized in the systems. This the case for example of the ground-state energy, the NN bound order γ_{12}, the charge transfer between sub-lattices Δn, the correlation energy as well as the local spin momentum. This transition also occurs in the inhomogeneous dimer, and the changes in the ground-state properties appear remarkably transferable to any system through the LSA approximation. However, some discrepancies appear in the study of the charge gap at the weakly correlated limit and near the BI-MI phase transition point, where the LSA is significantly overestimating the charge gap. Moreover, these discrepancies are more pronounced in 2D than in 1D. One could argue that the fact that 1D systems are closer to the dimer than a 2D system implies a better description for the charge gap. The overestimation of the charge gap could be attributed to the nature of the reference system (the dimer) from which the LSA is derived. Possibilities to improve the charge gap at these limits are discussed at the end of this chapter.

6.3 The 1D Hubbard chain with second nearest neighbor hoppings

The success of LDFT within LSA to reproduce accurately most of the ground state properties, encourages us to explore more complicated physical systems. In the last section it was shown that the LSA captures the effects of an inhomogeneous charge distribution in a correlated system through the study of the ionic Hubbard model, specially in 1D systems. A particularly important extension is to consider magnetically frustrated systems.

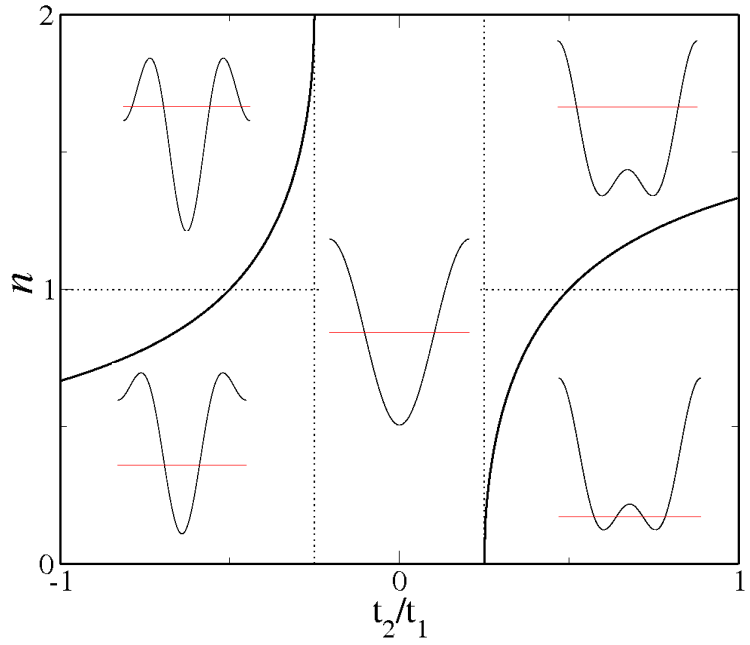

Figure 6.10: Phase diagram of a 1D Hubbard chain with first and second NN hopping in the noncorrelated limit ($U = 0$). The solid curves separate the two regimes (two or four Fermi points) and the inset figures illustrate the behavior of the dispersion relation [Eq. (6.17)] for the corresponding parameter range. The Fermi energy is represented by horizontal red lines.

In this sense the Hubbard chain with first and second NN hopping appears an ideal system to test LDFT. Indeed, a realistic description of materials often requires modifications of the simplest original Hubbard model. For example, to study quasi 1D organic conductor $(TMTSF_2)X$ (X=PF_6, ClO_4), the so-called Bechgaard salts [85], or other related systems like Copper oxide $Pr_2Ba_4Cu_7O_{15-\delta}$ [86], one needs to introduce second-nearest neighbor hoppings in order to describe the physics of such systems. In past years, this Hamiltonian has been intensively studied from a theoretical point of view [87, 88].
In this case the Hubbard Hamiltonian reads:

$$\hat{H} = \sum_{i,\sigma} t_1 \hat{c}^\dagger_{i,\sigma} \hat{c}_{i+1,\sigma} + \sum_{i,\sigma} t_2 \hat{c}^\dagger_{i,\sigma} \hat{c}_{i+2,\sigma} + U \sum_i \hat{n}_{i\downarrow} \hat{n}_{i\uparrow} \,, \tag{6.15}$$

where t_1 (t_2) is the hopping integral between first (second) NNs. As was described in the previous section, for a homogeneous chain with NN at half filling, electronic correlation leads to a finite charge excitation gap and thus insulating behavior for an arbitrarily small value of the Coulomb repulsion U/t. The introduction of next-nearest-neighbor hoppings could change this picture dramatically. It brings a sort of frustration to the spin degrees of freedom as well as some coupling between spin and charge degrees of freedom. In the strong coupling regime, the Hubbard model (6.15) can be developed perturbatively into a frustrated Heisenberg chain by using the Schrieffer-Wolf transformation (see Sec. 3.4).

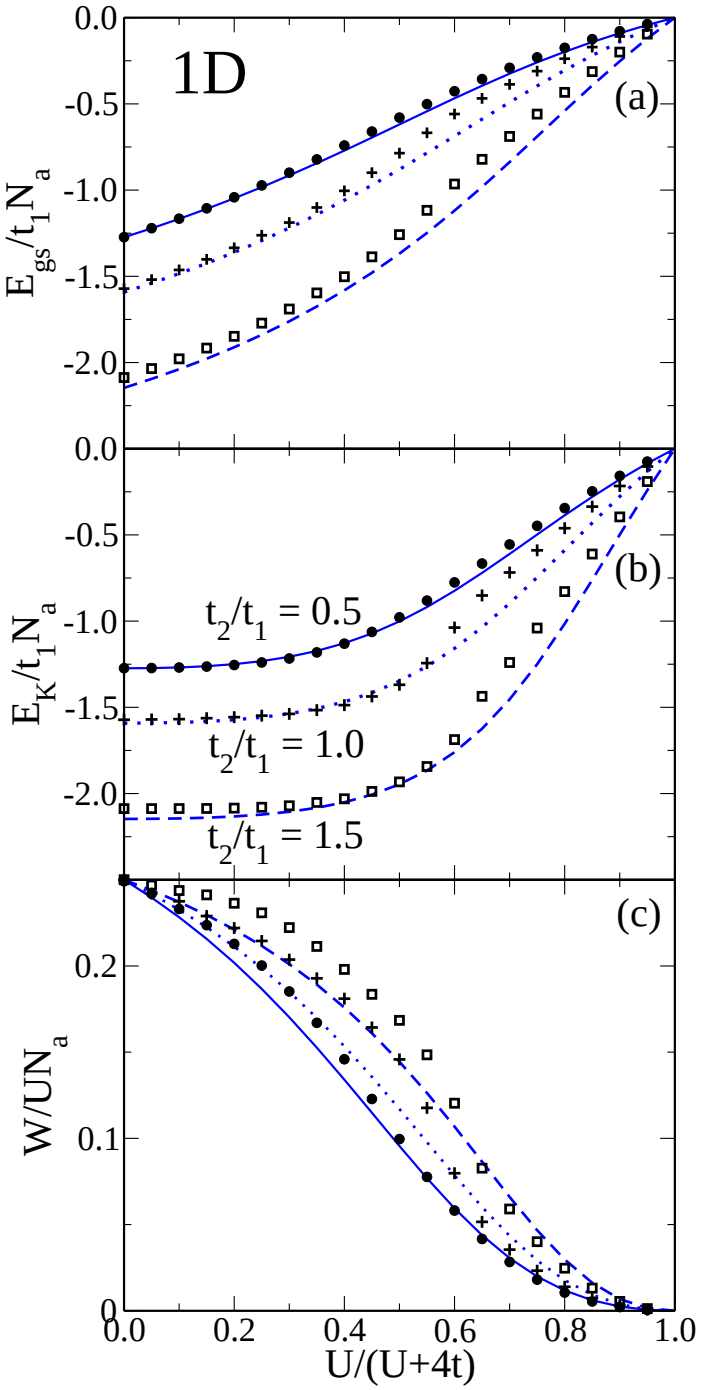

Figure 6.11: Ground-state properties of a Hubbard chain with nNN hopping at half filling as a function of the Coulomb repulsion strength U/t. Different values of the strength of the nNN hopping integral t_2/t_1 are considered as indicated in (b). Results are given for (a) ground-state energy $E_{\rm gs}$, (b) kinetic energy E_K and (c) average number of double occupations per site $W/UN_{\rm a}$. The solid curves refer to LDFT using the LSA approximation while the symbols are the DMRG results.

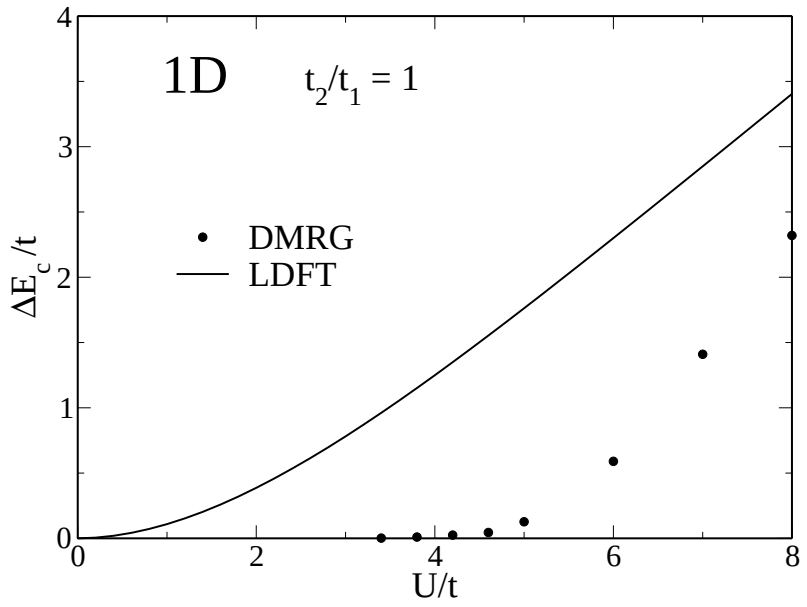

Figure 6.12: Charge gap $\Delta E_{\rm c}$ as a function of the Coulomb repulsion strength U/t in a Hubbard chain with nNN hopping having $t_2 = t_1 = 1$ and at half filling. The curves refer to LDFT within the LSA approximation and the symbols to DMRG calculations.

One then obtains

$$H = \sum_i J_1 S_i S_{i+1} + J_2 S_i S_{i+2} \tag{6.16}$$

where $J_1 = 4t_1^2/U$ and $J_2 = 4t_2^2/U$. Without the second NN hoppings and at half band filling, the ground state is known to be antiferromagnetic. However the second NN hoppings lead to a geometric frustration since the spin at one site cannot be aligned antiferromagnetically with both first and second neighbors. At weak coupling, the second NN hopping changes the band structure of the system, in particular the number of Fermi points (equivalent to the Fermi surface in 1D). At this limit the dispersion relation is given by

$$\epsilon(k) = -2t_1 \cos k - 2t_2 \cos 2k \tag{6.17}$$

where we have considered the lattice constant equal to one. The ground state phase diagram in this limit is displayed in Fig. 6.10. For $\mid t_2/t_1 \mid < \cos\left[(2-n)\pi/2\right]^2 / \sin\left[(2-n)\pi\right]^2$, the system has two Fermi points at $k = \pm n\pi/2$, and the properties of such a system are very similar to that for $t_2 = 0$. In the other case, for $\mid t_2/t_1 \mid > \cos\left[(2-n)\pi/2\right]^2 / \sin\left[(2-n)\pi\right]^2$, there is four Fermi points (two branches) $\pm k_{F1}$ and $\pm k_{F2}$ [88]. This leads, as we shall see later on, to important modifications of the properties, especially the charge gap.
In Fig. 6.11 the ground-state properties of a Hubbard chain with up to second NN hoppings are shown at half filling, as a function of the Coulomb repulsion strength U/t_1. Different values of the second NN hopping integral t_2 are considered. DMRG results are also displayed (symbols) in order to compare. First of all, one observes the well-known monotonous increase of $E_{\rm gs}$ with increasing U/t, reaching $E_{\rm gs} = 0$ for $U/t \to \infty$, where

both electronic hopping and double occupations vanish. By increasing t_2, the average number of double occupations (kinetic energy) decreases (increases) slowly. This can be explained by considering that the presence of the second NN increases the band width w of the system (for example $w/t_1 = 4$ for $t_2/t_1 = 0$ and $w/t_1 = 6.25$ for $t_2/t_1 = 1$). Consequently, one needs a larger value of U/t_1 to reduced by the same amount the average number of double occupations for a system with larger t_2/t_1. We find a relatively good agreement between the LDFT and DMRG predictions, in particular for small values of t_2. As t_2 increases, one observes some deviations in the average value of double occupations, even at the weakly correlated limit. For example $\Delta W/W \simeq 0.20$, for $t_2/t_1 = 1.0$ and $U/t_1 = 4$. In contrast, the kinetic energy is very well reproduced at the weak correlated limit. However, by increasing U/t, LSA becomes less accurate describing the kinetic energy, specially for cases where $t_2 \geq 1$.

Figure 6.12 shows the charge gap of a Hubbard chain with first and second NN hopping having $t_2 = t_1 = 1$ at half filling. In this case the 1D chain is actually a two leg triangular stripe. The comparison between LDFT and DMRG is qualitatively in disagreement. In fact, DMRG predicts a Mott transition for a critical value of the Coulomb repulsion strength $U_c/t = 3.2$ which is, around half the band width of the noncorrelated system $U_c \simeq w/2$ where $w = 6.25$ unlike LDFT which predicts a Mott insulator for any small value of the Coulomb repulsion.
For $U > 4$, LDFT predicts a quasi linear dependence in U when for DMRG, $\Delta E_{\rm c}$ is growing exponentially slowly after U_c and then increases linearly for $U/t > 6$.

The one dimensional chain with first and second NN hoppings appears more difficult to reproduce for the LSA than systems with only NN hoppings. The deviations observed in the ground-state properties and the more serious failure in the description of the charge gap are due to the nature of the reference system at the basis of the LSA. For instance in the dimer geometric frustrations do not exist. This fact is responsible for the discrepancies between DMRG and LSA kinetic energy for moderate hopping ratio $t_2/t_1 \geq 0.5$ in the strongly correlated limit ($U/t > 4$). Moreover, at half filling, the nature of the noncorrelated ground-state are qualitatively different in a dimer and in a chain with $t_2/t_1 > 0.5$, since in the former the lowest single-particle state is the even ($k = 0$-like) state while in the latter the minimum in the dispersion relations occurs for a non-zero k (see Fig. 6.10). Consequently at the weakly correlated limit and for $t_2/t_1 > 0.5$ the average number of double occupancies predicted by the LSA is less accurate. In addition, the dimer is an insulator for any finite value of U/t, making it evident that it cannot be a good reference system to describe a metal-insulator transition at a finite value of U/t.

6.4 Discussion

In the two previous sections, it has been shown that LDFT within the LSA approximation for the correlation-energy functional predicts quite accurately the ground-state properties of on-site correlated systems, even in the presence of inhomogeneities in the external potential or first and second NN hoppings. However, we saw that at half filling it always predicts an insulator for any arbitrarily small value of the Coulomb repulsion. In the case of one- and two-dimensional homogeneous square lattices this is in accordance with other numerical or exact solutions, but the charge gap is still overestimated at the weakly-correlated limit. Adding inhomogeneities, as for example in the bipartite ionic Hubbard

model, one also observes that the charge gap is still overestimated in our calculations near the critical point where a BI-metal-MI phase transition predicted by QMC calculations occurs. In fact, this implies that LDFT within LSA does not predict a metallic phase in two dimensions as it was obtained in QMC simulations. In the case of the chain with nNN hopping it is now well known that a Mott transition occurs and that the system is metallic up to a finite critical value of the Coulomb repulsion. Also in these cases the LSA to LDFT results always overestimate the charge gap, predicting an insulator for all non vanishing values of U.

In this context it is worth noting that the charge gap is a very subtle property. For example, at the weakly correlated limit, perturbation theory predicts a power-law decay of the kinetic energy (or of the NN bond-order) as a function of the correlation energy in the case of a NN hopping system. Moreover, in Hartree-Fock approximation, the charge gap is always zero, which implies a metallic phase even for $U/t \to \infty$. Improving the LSA functional in order to reproduce correctly the weakly correlated limit of the charge gap still remain a challenge for theory. Different ways can be considered such as combining the LSA functional, which is very performant at the strongly correlated limit, with another functional which could be derived from perturbation theory. The latter should allow to increase the accuracy in the weakly correlated limit.

However, as was already pointed out, most of the discrepancies observed using the LSA result from the nature of the reference system basis of this approximation, namely the inhomogeneous dimer. In fact, the low-dimensionality and the non-frustrated nature of the dimer inferred in the LSA functional explains that it can not reproduce effects of a large band width or magnetic frustration. In this sense, it could be very interesting to study the transferability of a functional derived from a high-dimensional system. In particular, one should be able to obtain a functional of the infinite-dimensional Hubbard model ($d \to \infty$) where exact results are known (for example from DMFT which is exact at the $d \to \infty$ limit [23]). Moreover, the $d \to \infty$ limit of the Hubbard model is very relevant since it presents remarkable similarity with 2D and 3D systems. In addition, one can imagine the construction of a hybrid functional as an interpolation of the LSA and a $d \to \infty$ functionals. Such a combination could reproduce more accurately the properties of systems in intermediate dimensions.

Another possibility consists in computing $W[\gamma]$ for a bigger system of finite size, by performing a cluster-expansion either in real- or reciprocal-space, in order to take into account at least the short range dependence of the correlation-energy functional. This of course implies a more important computational effort but it should include the spatial dependence of the correlation-energy functional. This is the challenge to which we try to provide a solution in the next chapter. As we shall see, the nature of the cluster embedding plays a major role in describing correctly properties involving exited states.

Chapter 7

Renormalized cluster expansion of the interaction-energy functional

During the previous chapters we have built up approximations to the correlation-energy functional $W[\{\gamma_{ij}\}]$ based on a scaling hypothesis in which the Hubbard dimer plays the role of the reference system. We have shown that major ground-state properties are correctly described within these approximations, and that the relative errors are in the worst case around 20%. In particular, the LSA approximation can be applied to any spin independent on-site correlated system but excludes in principle applications to systems having inter-orbital correlations. However, in order to reproduce realistic systems, and in particular the ones including $3d$- or $4f$-elements, it is in general necessary to consider multi-band model Hamiltonians. These models include in general inter-orbital interaction as for example the exchange interaction between orbitals which is at the origin of Hund's rules. In addition, in many physical systems, spatial charge fluctuations are not negligible and could for example be the source of frustrations. In this case, it has been shown that a functional derived from the dimer could not correctly describe these effects. Generally, frustration effect are important at the strongly correlated limit, where it has been shown that the Hubbard systems can be mapped on a spin Hamiltonian like the tJ or Heisenberg model. These systems are physically interesting since a lot of materials display frustrated lattices (triangular, Honey-comb, etc...). In order to approach these systems correctly, one needs to take into account short-range charge and spin fluctuations.

The aim of this chapter is to present a more general and potentially more accurate approximation of $W[\gamma]$ which can be applied to spin dependent systems with inter-orbital interaction and which is able to describe short-range charge and spin fluctuations. For simplicity, we focus first on the simple Hubbard model. As we shall see the formalism used to derive the approximation of $W[\gamma]$ is spin dependent and can be straightforwardly extended to systems having also inter-site interactions or multiple bands.

The main idea is to split the Hamiltonian in three parts, one acting on a defined cluster, one on the rest of the system (the environment) and the last contribution is the interaction between the cluster and the environment. We intend to map the cluster-environment contribution to an effective Hamiltonian acting only within the cluster, and then uncouple the cluster from the environment. This effective Hamiltonian is constrained, by using a set of Lagrange parameters, such that it have a given ground state density matrix γ. The correlation-energy functional $W[\gamma]$, is then obtained by diagonalizing the effective

Hamiltonian and by minimizing its energy.

7.1 Single-site approximation

In order to explain the approximations made in the cluster expansion, it is helpful to start with the simplest cluster: a single site. Given an arbitrary Hubbard system one can define a local basis $\{|\varphi_c^\alpha\rangle\} = \{|0\rangle, |\uparrow\rangle, |\downarrow\rangle, |\uparrow\downarrow\rangle\}$, for any site i, obtained with the four possible configurations, namely, empty, singly occupied or doubly occupied site. If we now split the system into a cluster, here a site, and the environment, we can rewrite the ground state $|\Psi\rangle$ as

$$|\Psi\rangle = \sum_{\alpha=1}^{4} \sum_{\mu} c_{\alpha,\mu} \; |\varphi_c^\alpha\rangle \otimes | \; \varphi_E^\mu\rangle, \tag{7.1}$$

where $\{|\varphi_E^\mu\rangle\}$ is a generic many-body basis of the environment and $\alpha = 0, \uparrow, \downarrow$, and $\uparrow\downarrow$ denotes the configurations of the cluster c, in this case the site i.
Let us now assume that the site i and the environment are uncoupled which is true in the atomic limit $t = 0$. In this case, the ground state of the total system is written as $| \; \Psi\rangle = | \; \psi_c\rangle \otimes \; | \; \psi_E\rangle$, where $|\psi_c\rangle = \sum_{\alpha=1}^{4} a_\alpha \; |\varphi_c^\alpha\rangle$ involves only the cluster degrees of freedom and $|\psi_E\rangle = \sum_\mu b_\mu \; |\varphi_E^\mu\rangle$ only the environment. Strictly speaking, this is not true since one should instead write $|\Psi\rangle = \sum_{\alpha=1}^{4} \sum_\mu c_{\alpha,\mu} \; |\varphi_c^\alpha\rangle \otimes | \; \varphi_E^\mu\rangle$. For example in the limit $U \to 0$ the ground-state is known to be very delocalized. However, we shall see that this approximation gives good results even at this limit. This is not a trivial approximation since we consider that the probability amplitude of states of the cluster's local basis $\{| \; \varphi_c^\alpha\rangle\}$ are uncoupled from the rest of the environment, i.e, $c_{\alpha,\mu} = a_\alpha b_\mu$.

The one-particle density matrix elements $\gamma_{i\beta,\sigma} = \langle \Psi \mid \hat{c}_{i,\sigma}^\dagger \hat{c}_{\beta,\sigma} \mid \Psi \rangle$ between the site i representing the cluster and all its z_i connected sites can then be expressed as:

$$\gamma_{ii,\sigma} = a_2^2 + a_{1\sigma}^2 \tag{7.2}$$

and

$$\sum_{\beta=1}^{z_i} \gamma_{i\beta,\sigma} = \xi a_0^* a_{1\sigma} + \xi' a_{1\bar{\sigma}}^* a_2, \tag{7.3}$$

where ξ and ξ' provide the overlap with the environment,

$$\begin{aligned} \xi &= \sum_{\beta=1}^{z_i} \sum_{\varphi_E^\mu} \sum_{\varphi_E^\nu} \langle \varphi_E^{\mu,Ne-1} \mid \hat{c}_{\beta,\sigma} \mid \varphi_E^{\nu,Ne} \rangle \\ \xi' &= \sum_{\beta=1}^{z_i} \sum_{\varphi_E^\mu} \sum_{\varphi_E^\nu} \langle \varphi_E^{\mu,Ne-2} \mid \hat{c}_{\beta,\sigma} \mid \varphi_E^{\nu,Ne-1} \rangle \end{aligned} \tag{7.4}$$

and $\{\varphi_l^{\mu,X}\}$ is a basis for the environment having X electrons. ξ (ξ') corresponds to removing an electron from the environment when the system is empty (singly occupied). Given the previous equations of the coefficients ξ and ξ', then the average number of double occupations, i.e., the on-site correlation energy functional

$$\omega_i[\gamma] = a_2^2 \tag{7.5}$$

can be obtained by expressing a_2 as a function of γ_{ii} and γ_{ij} by using the system of equations (7.2) and (7.3) with the normalization constraint

$$a_0^2 + a_{1\uparrow}^2 + a_{1\downarrow}^2 + a_2^2 = 1. \tag{7.6}$$

The challenge is therefore to find an approximation for ξ and ξ' such that

$$\xi a_0^* a_{1\sigma} + \xi' a_{1\bar{\sigma}}^* a_2 = \langle \Psi \mid \hat{c}_{i,\sigma}^\dagger \hat{c}_{j,\sigma} \mid \Psi \rangle \tag{7.7}$$

for the coupled system. As a preliminary step, if we consider that the environment is very large (at the thermodynamic limit) so that it has an infinite number of electrons, one can consider that $\xi = \xi'$. In addition, since the Hamiltonian can be chosen to be real, we consider the coefficients a_α real too. In the following, we propose two different strategies to approximate ξ.

7.1.1 Self-consistent approach

Considering that the system is homogeneous and translationally invariant, such that $\gamma_{i\beta,\sigma} = \gamma_{12,\sigma}$ and that $a_\alpha^i = a_\alpha^\beta$ for all sites i and β. One obtains

$$\xi = z_i(a_0 a_{1\sigma} + a_{1\bar{\sigma}} a_2). \tag{7.8}$$

leading to

$$\gamma_{12,\sigma} = a_0^2 a_{1\sigma}^2 + a_{1\bar{\sigma}}^2 a_2^2 + 2a_0 a_{1\sigma} a_{1\bar{\sigma}} a_2. \tag{7.9}$$

Both sides of the previous equation have to be normalized. For instance, at the noncorrelated limit and at half-band filling ($a_0^2 = a_{1\uparrow}^2 = a_{1\downarrow}^2 = a_2^2 = 1/4$) one finds that $\gamma_{12,\sigma} = 1/4$. Moreover, this should correspond to the limit of $\gamma_{12,\sigma}/\gamma_{12,\sigma}^0 = 1$ where $\gamma_{12,\sigma}^0$ is the noncorrelated value of $\gamma_{12,\sigma}$. In order to reproduce this limit correctly, one has to renormalize the $\gamma_{12,\sigma}$ with $\gamma_{12,\sigma}^0$ but also $a_0^2 a_{1\sigma}^2 + a_{1\bar{\sigma}}^2 a_2^2 + 2a_0 a_{1\sigma} a_{1\bar{\sigma}} a_2$. Indeed Eqs. (7.3) and (7.8) can be interpreted as a scalar product between vectors which need to be normalized. In fact, the ratio $-1 \leq \gamma_{12,\sigma}/\gamma_{12,\sigma}^0 \leq 1$ is actually the cosine of the angle between these vectors. One obtains

$$\begin{aligned} \frac{\gamma_{12,\sigma}}{\gamma_{12,\sigma}^0} &= \xi (a_0^2 + a_{1\sigma}^2)^{-1/2} (a_0 a_{1\sigma} + a_{1\bar{\sigma}} a_2)(a_2^2 + a_{1\bar{\sigma}}^2)^{-1/2} \\ \xi &= (a_0^2 + a_{1\sigma}^2)^{-1/2} (a_0 a_{1\sigma}^* + a_{1\bar{\sigma}} a_2^*)(a_2^2 + a_{1\bar{\sigma}}^2)^{-1/2}, \end{aligned} \tag{7.10}$$

so that Eq. (7.3) can be rewritten as

$$\frac{\gamma_{12,\sigma}}{\gamma_{12,\sigma}^0} = \frac{a_0^2 a_{1\sigma}^2 + a_{1\bar{\sigma}}^2 a_2^2 + 2a_0 a_{1\sigma} a_{1\bar{\sigma}} a_2}{(a_0^2 + a_{1\sigma}^2)(a_2^2 + a_{1\bar{\sigma}}^2)}. \tag{7.11}$$

It is interesting to note that these equations are analogous to the slave-boson theory (see Sec. 3.3.2 and Ref. [22]). At half-band filling, one finds $\omega_i = \frac{1}{4}\left(1 - \sqrt{1-q}\right)$ with $q = \gamma_{12,\sigma}/\gamma_{12,\sigma}^0$, and consequently the total energy of the system [see Eq. (4.8)] is minimized for

$$q = 1 - \left(\frac{U}{8zt\gamma_{12}^0}\right)^2. \tag{7.12}$$

Finally, the single-site local functional is given by

$$\omega_i = \frac{1}{4}\left(1 - \frac{U}{8zt\gamma_{12}^0}\right). \tag{7.13}$$

7.1.2 Scaling approach

The other strategy to approximate ξ is to derive it by considering that the environment has a metallic behavior, i.e., the environment can always exchange an electron with the cluster without any energy restriction. This implies that the coefficient ξ does not depend on the variation of the density matrix and then it can be deduced from equation (7.3) at the noncorrelated limit. Consequently, one obtains

$$\xi = \frac{\sum_{\beta=1}^{z_j} \gamma^0_{i\beta,\sigma}}{\langle \hat{c}_i^\dagger \rangle^0}, \tag{7.14}$$

where $\langle \hat{c}_i^\dagger \rangle^0$ represents the rate of adding an electron on the cluster or equivalently to the environment at the noncorrelated limit. Then, if the environment can always exchange an electron with the cluster without any energy restriction this rate is equal to one and $\xi = \sum_{\beta=1}^{z_j} \gamma^0_{ij,\sigma}$. For a translationally invariant model with nearest-neighbor hopping, Eq. (7.14) and the system of equations [(7.2), (7.3), (7.6), and (7.14)], yield the relation between the average number of double occupation per site $\omega_i = a_2^2$, the charge density γ_{ii}, and the NN bound order γ_{12}. One obtains

$$\omega_i = \frac{1}{2}\left[\gamma_{ii} - \frac{\gamma^2_{12,\sigma}}{2{\gamma^0_{ij,\sigma}}^2} \frac{1 + \sqrt{\gamma_{ii}(2-\gamma_{ii}) - (\gamma_{12,\sigma}/\gamma^0_{12,\sigma})^2}}{(1-\gamma_{ii})^2 + (\gamma_{12,\sigma}/\gamma^0_{12,\sigma})^2}\right]. \tag{7.15}$$

This equation is very similar to the local scaling approximation [Eq. (6.7)], the only difference being that in this case the degree of electronic delocalization is scaled only with respect to the noncorrelated limit, i.e., $g_i^2 = (\gamma_{12,\sigma}/\gamma^0_{12,\sigma})^2$.

Note that the self-consistent approach requires that the studied Hamiltonian is homogeneous, i.e., all sites are equivalent. This condition is not necessary in the scaling approach. The latter just needs the knowledge of the noncorrelated density matrix $\gamma^0_{ij,\sigma}$ at the noncorrelated limit. Another important advantage is that the formulation is spin dependent and can then be applied to spin polarized systems.

7.2 General formulation of the density-matrix renormalized cluster expansion

In this section we generalize the scheme proposed in the previous section to a cluster of N_c sites, in order to include into the correlation-functional the effects of spatial spin and charge fluctuations. For simplicity, we consider here only the simple Hubbard Hamiltonian but the generalization to systems with inter-site correlation is straightforward. The idea is to start from the Levy-Lieb definition of the interaction energy functional and to derive an effective local Hamiltonian for the cluster. The interaction energy functional is written as

$$W[\{\gamma_{ij}\}] = \min_{\Psi\to\{\gamma_{ij}\}} \langle \Psi[\{\gamma_{ij}\}] | \sum_i U_i \hat{n}_{i\uparrow}\hat{n}_{i\downarrow} | \Psi[\{\gamma_{ij}\}]\rangle, \tag{7.16}$$

which can be rewritten by using the Lagrangian formalism, as

$$\mathcal{L} = \langle\Psi| \sum_i U_i \hat{n}_{i\uparrow}\hat{n}_{i\downarrow} |\Psi\rangle - \sum_{i,j,\sigma} \lambda_{i,j,\sigma} \left(\langle\Psi| \hat{c}^\dagger_{i,\sigma}\hat{c}_{j,\sigma} |\Psi\rangle - \gamma_{ij,\sigma} \right) - \varepsilon \left(\langle\Psi|\Psi\rangle - 1 \right), \tag{7.17}$$

where λ_{ij} and ε are Lagrange multipliers to conserve the fixed density matrix and the normalization of the state vector $|\Psi\rangle$. The Lagrange equations are given by

$$\left(\sum_i U_i \hat{n}_{i\uparrow}\hat{n}_{i\downarrow} - \sum_{i,j,\sigma} \lambda_{i,j,\sigma}\hat{c}^\dagger_{i,\sigma}\hat{c}_{j,\sigma}\right)|\Psi\rangle = \varepsilon|\Psi\rangle, \tag{7.18}$$

$$\langle\Psi|\hat{c}^\dagger_{i,\sigma}\hat{c}_{j,\sigma}|\Psi\rangle = \gamma_{ij,\sigma}, \tag{7.19}$$

and

$$\langle\Psi|\Psi\rangle = 1. \tag{7.20}$$

The challenge is to approximate the solution of this set of equations Eq. (7.18) corresponds to an eigenvalue problem, with an effective corresponding Hamiltonian

$$\hat{H}[\lambda] = \sum_i U_i \hat{n}_{i\uparrow}\hat{n}_{i\downarrow} - \sum_{i,j,\sigma} \lambda_{i,j,\sigma}\hat{c}^\dagger_{i,\sigma}\hat{c}_{j,\sigma} \tag{7.21}$$

that is a function of the Lagrange parameters $\lambda_{i,j,\sigma}$. These are determined by the conditions Eq. (7.19) and (7.20). We want to split the Hamiltonian Eq. (7.21) into two parts, one acting on the cluster and the other on the rest of the system or environment. However, the operator $\hat{H}[\lambda]$ cannot be separated since the kinetic operator can not be considered as the sum of two independent contributions acting on separate noninteracting portions of the system. Nevertheless, in the following, we will show that the information which gets lost by calculating $W[\gamma_{ij}]$ locally, corresponds to long range charge fluctuations, which are less significant in the strongly correlated limit. In addition, we shall see that this approximation gives good results even for $U = 0$. Given a site i of the system we want to determine $\langle\hat{n}_{i\uparrow}\hat{n}_{i\downarrow}[\gamma]\rangle = \partial W[\gamma]/\partial U_i$. We can then define a cluster surrounding the site i and split the Hamiltonian Eq. (7.18) into three parts $H = H_c + H_E + H_{cE}$, where the first part acts only on the sites belonging to the cluster, the second on those belonging to the rest of the system (the environment) and the third part contains the interaction between cluster and environment sites:

$$\hat{H}_c = \sum_i U_i \hat{n}_{i\uparrow}\hat{n}_{i\downarrow} - \sum_{i,j,\sigma} \lambda_{i,j,\sigma}\hat{c}^\dagger_{i,\sigma}\hat{c}_{j,\sigma} + h.c., \tag{7.22}$$

$$\hat{H}_E = \sum_\beta U_\beta \hat{n}_{\beta,\uparrow}\hat{n}_{\beta\downarrow} - \sum_{\beta,\delta,\sigma} \lambda_{\beta,\delta,\sigma}\hat{c}^\dagger_{\beta,\sigma}\hat{c}_{\delta,\sigma} \ + h.c., \tag{7.23}$$

and

$$\hat{H}_{cE} = -\sum_{j,\beta,\sigma} \lambda_{j,\beta,\sigma}\hat{c}^\dagger_{j,\sigma}\hat{c}_{\beta,\sigma} + h.c., \tag{7.24}$$

where the indices i, j run over cluster sites and the indices β and δ over the environment sites.
The challenge is then to derive an effective Hamiltonian $\tilde{H}[\lambda]$ acting only on the cluster that takes into account the effect of the environment. One of the problems in order to accomplish this goal is essentially due to the anti-commutative nature of fermionic

operators which induces a phase effect. H_{cE} is the term which contains the cluster-environment interaction. It can be rewritten as

$$\begin{aligned}\hat{H}_{cE} &= -\sum_{j,\beta,\sigma} \lambda_{j,\beta,\sigma} \hat{c}^{\dagger}_{j,\sigma} \hat{c}_{\beta,\sigma} + h.c. \\ &= -\sum_{j,\sigma} \hat{c}^{\dagger}_{j,\sigma} \sum_{\beta} \lambda_{j,\beta,\sigma} \hat{c}_{\beta,\sigma} + h.c. \\ &= -\sum_{j,\sigma} \lambda_{j,\sigma} \left(\hat{c}_{j,\sigma} \hat{\Xi}^{\dagger}_{j,\sigma} + \hat{c}^{\dagger}_{j,\sigma} \hat{\Xi}_{j,\sigma} \right), \end{aligned} \tag{7.25}$$

where

$$\hat{\Xi}^{\dagger}_{j,\sigma} = \frac{1}{\lambda_{j,\sigma}} \sum_{\beta=1}^{z_j} \lambda_{j\beta,\sigma} \hat{c}^{\dagger}_{\beta,\sigma} \quad \text{and} \quad \hat{\Xi}_{j,\sigma} = \frac{1}{\lambda_{j,\sigma}} \sum_{\beta=1}^{z_j} \lambda_{j\beta,\sigma} \hat{c}_{\beta,\sigma}. \tag{7.26}$$

Here z_j is the coordination number between j and its neighbors β in the environment. One would like to map the effect of $\hat{H}_{cE}$ as an effective Hamiltonian acting within the cluster. The simplest idea to do so is to replace $\hat{\Xi}_{j,\sigma}$ by its average value $\xi_{j,\sigma} = \left\langle \hat{\Xi}_{j,\sigma} \right\rangle$ and to neglect only fluctuations around its mean value. Nevertheless, one quickly realizes that such a transformation is not invariant under a unitary transformation among the single particle basis of the cluster. Consider for example the case where j is the first element of the basis, then the transition induced by $\xi_{j,\sigma} \hat{c}^{\dagger}_{j}$ or $\xi_{j,\sigma} \hat{c}_{j,\sigma}$ would have the same phase independently of the many-body state of the cluster since no anticommutation is needed in order to restore normal ordering. It is clear then, that this would not hold if j is the second or any other element of the basis. In order to solve this problem one needs to replace $\hat{\Xi}_{j,\sigma}$ by an *operator* $\hat{\xi}_{j,\sigma}$ acting within the cluster, which is proportional to the average value $\xi_{j,\sigma} = \left\langle \hat{\Xi}_{j,\sigma} \right\rangle$ but yields the same phase for all states in the many-body basis of the cluster. In this way the effect of the environment preserves the important property of being invariant with respect to any unitary transformations among the many-body states. In other words, the operator $\hat{\xi}_{j,\sigma}$ is a scalar equal to $\xi_{j,\sigma} = \left\langle \hat{\Xi}_{j,\sigma} \right\rangle$ within each subspace of the cluster. Note that this is the only reasonable choice for $\hat{\xi}_{j,\sigma}$, since the only matrix commuting with all unitary transformations is a scalar matrix. Formally, one can define $\hat{\xi}_{j,\sigma}$ such that it anticommutess with all $\hat{c}_i$ for $i < j$, commute with all $\hat{c}_i$ for $j > i$ and $\hat{\xi}_{j,\sigma}|\text{vac}\rangle = \xi_{j,\sigma}|\text{vac}\rangle$. Note that $\xi_{j,\sigma} = \left\langle \hat{\Xi}_{j,\sigma} \right\rangle = \left\langle \hat{\Xi}^{\dagger}_{j,\sigma} \right\rangle$ since in equilibrium the rate to create or annihilate an electron on one site must be the same.
With this approximation the cluster and the environment are uncoupled and can thus be treated separately. We then rewrite the set of equations defining the correlation-energy functional of the cluster [Eqs. (7.18), (7.19) and (7.20)] such that for i, j in the cluster we have

$$\left(\sum_i U_i \hat{n}_{i\uparrow} \hat{n}_{i\downarrow} - \sum_{i,j,\sigma} \lambda_{i,j,\sigma} \hat{c}^{\dagger}_{i,\sigma} \hat{c}_{j,\sigma} + \sum_{i,\sigma} \lambda_{i,\sigma} \left(\hat{\xi}^{\dagger}_{i,\sigma} \hat{c}_{i,\sigma} + \hat{c}^{\dagger}_{i,\sigma} \hat{\xi}_{i,\sigma} \right) \right) |\psi_c\rangle = \varepsilon |\psi_c\rangle, \tag{7.27}$$

The eigenvalue problem (7.27) corresponds to an effective Hamiltonian acting only on the local basis of the cluster

$$\tilde{H}[\lambda] = \sum_i U_i \hat{n}_{i\uparrow}\hat{n}_{i\downarrow} - \sum_{i,j,\sigma} \lambda_{i,j,\sigma} \hat{c}^\dagger_{i,\sigma}\hat{c}_{j,\sigma} - \sum_{i,\sigma} \lambda_{i,\sigma} \left(\hat{\xi}^\dagger_{i,\sigma}\hat{c}_{i,\sigma} + \hat{c}^\dagger_{i,\sigma}\hat{\xi}_{i,\sigma} \right). \tag{7.28}$$

The Lagrange parameters $\lambda_{i,j,\sigma}$ and $\lambda_{i,\sigma}$ ensure that the ground-state of (7.28) respects the condition of the density matrix given by

$$\langle \psi_c | \hat{c}^\dagger_{i,\sigma}\hat{c}_{j,\sigma} | \psi_c \rangle = \gamma_{ij,\sigma}, \tag{7.29}$$

and

$$\langle \psi_c | \hat{\xi}_{j,\sigma}\hat{c}^\dagger_{j,\sigma} | \psi_c \rangle = \sum_{\beta=1}^{z_j} \gamma_{j\beta,\sigma}, \tag{7.30}$$

where β is a site of the environment that is connected to j. Notice that only the relevant terms of the density matrix need to be considered (i.e., for which $t_{ij} \neq 0$). Finally the last condition imposes that

$$\langle \psi_c | \psi_c \rangle = 1 \tag{7.31}$$

As in the single-site-cluster case, we propose two ways of determining $\xi_{j,\sigma}$. To this aim, we focus on the homogeneous and translationally invariant Hubbard model with only NN hoppings. From Eq. (7.30) we have that

$$\sum_{\beta=1}^{z_j} \gamma_{j\beta,\sigma} = z_j \gamma_{12,\sigma} = \xi_{j,\sigma} \left\langle \frac{\hat{\xi}^\dagger_{j,\sigma}}{\xi_{j,\sigma}} \hat{c}_{j,\sigma} \right\rangle. \tag{7.32}$$

Moreover, if all sites are equivalent, we can write that

$$\xi_{j,\sigma} = z_j \left\langle \frac{\hat{\xi}_{j,\sigma}}{\xi_{j,\sigma}} \hat{c}^\dagger_{j,\sigma} \right\rangle \tag{7.33}$$

which leads to

$$\xi^2_{j,\sigma} = z_j^2 \gamma_{12,\sigma}. \tag{7.34}$$

This equation establishes the proportionality between $\xi^2_{j,\sigma}$ and $\gamma_{12,\sigma}$. However, to ensure that the noncorrelated limit is correctly reproduced, one has to renormalize this relation. Actually, we must have $(\xi^0_{j,\sigma})^2 = z_j^2 \gamma^0_{12,\sigma}$. Thus one obtains

$$\xi^2_{j,\sigma} = \frac{\gamma_{12,\sigma} {\xi^0_{j,\sigma}}^2}{\gamma^0_{12,\sigma}}, \tag{7.35}$$

where $\gamma^0_{12,\sigma}$ is the noncorrelated value of the NN bond order and $\xi^0_{j,\sigma}$ is the noncorrelated value of the rate on the site j. $\xi^0_{j,\sigma}$ is calculated numerically solving the set of equations (7.27), (7.29) and (7.31) with $U_j = 0$ for all sites and respecting the noncorrelated density matrix in the cluster γ^0_{ij}. Without the embedding, the cluster cannot have the same density matrix γ^0_{ij} as the system that we want to study. $\xi^0_{j,\sigma}$ is then the strength of

the embedding effect needed at $U = 0$ to reproduce γ^0_{ij} in the cluster. We will refer to this approach as self-consistent embedding (SCE).

A simpler and more general way to approximate $\xi_{i,\sigma}$, is obtained by following the scaling approach of the one-site cluster. The idea is to approximate the strength of the environment as independent of the variations of the density matrix. In other words, the environment can always exchange an electron with the system without any restrictions. $\xi_{i,\sigma}$ can be then calculated at the noncorrelated limit. From Eq. (7.30) we have

$$\xi_{j,\sigma} = \frac{\sum_{\beta=1}^{z_j} \gamma^0_{j\beta,\sigma}}{\left\langle \frac{\hat{\xi}^\dagger_{j,\sigma}}{\xi_{j,\sigma}} \hat{c}_{j,\sigma} \right\rangle^0}. \tag{7.36}$$

The uncorrelated , $\left\langle \frac{\hat{\xi}^\dagger_{j,\sigma}}{\xi_{j,\sigma}} \hat{c}_{j,\sigma} \right\rangle^0 = \xi^0_{j,\sigma}$ is calculated as for the SCE numerically by solving the set of equations (7.27), (7.29) and (7.31) with $U_j = 0$ for all sites and by respecting the noncorrelated density matrix in the cluster γ^0_{ij}. Notice that in contrast to the one-site cluster, $\xi^0_{j,\sigma}$ is in general not equal to one since $\hat{\xi}_{j,\sigma}$ takes into account effects of fermionic anticommutation. We will refer to this approach as scaling embedding (SE).

Finally, when the set of equations (7.27), (7.29) and (7.31) is solved numerically for the ground state, the correlation functional per site is obtained by calculating $\omega_i[\gamma] = \langle \psi_c | \hat{n}_{i\uparrow} \hat{n}_{i\downarrow} | \psi_c \rangle$ in the center of the cluster in order to minimize boundary effects.

Notice that as for the case of the one-site cluster, the scaling approach to the embedding coefficient $\xi_{j,\sigma}$ does not require any particular property of the Hamiltonian. In addition, this method can be directly applied to spin-polarized systems. The extension of the method to inter-site correlation in the cluster is straightforward by adding this contribution in $\hat{H}_c$. The process to split the cluster to the environment is unchanged, and the interaction functional is computed in the same way as for $\omega_i[\gamma]$.

7.3 Applications to the Hubbard model: size convergence

In order to study the accuracy of the method we propose to treat the simplest case, namely the homogeneous Hubbard model with NN hopping:

$$\hat{H} = \sum_{\langle i,j \rangle \sigma} t_{ij} \hat{c}^\dagger_{i\sigma} \hat{c}_{j\sigma} + U \sum_i \hat{n}_{i\downarrow} \hat{n}_{i\uparrow}, \tag{7.37}$$

We focus first on the one-dimensional case for which exact results are available. We start by showing the relative error on the ground state energy of a 1D infinite chain at half-band filling considered as a function of the Coulomb repulsion strength and the cluster size N_c (see Fig. 7.1). We employ the two above-mentioned approximations to treat the environment, and display the results in (a) for the scaling embedding (SE) and in (b) the self-consistent embedding (SCE). Results are presented only for clusters with an odd number of sites but a similar accuracy is also found for even cluster sizes. The accuracy systematically increases by increasing N_c, particularly at the strongly correlated limit. These remarkable results show the relevance of the method used to derive the effective Hamiltonian $\tilde{H}[\lambda]$ given in Eq. (7.28). For a NN system, the effective contribution of the

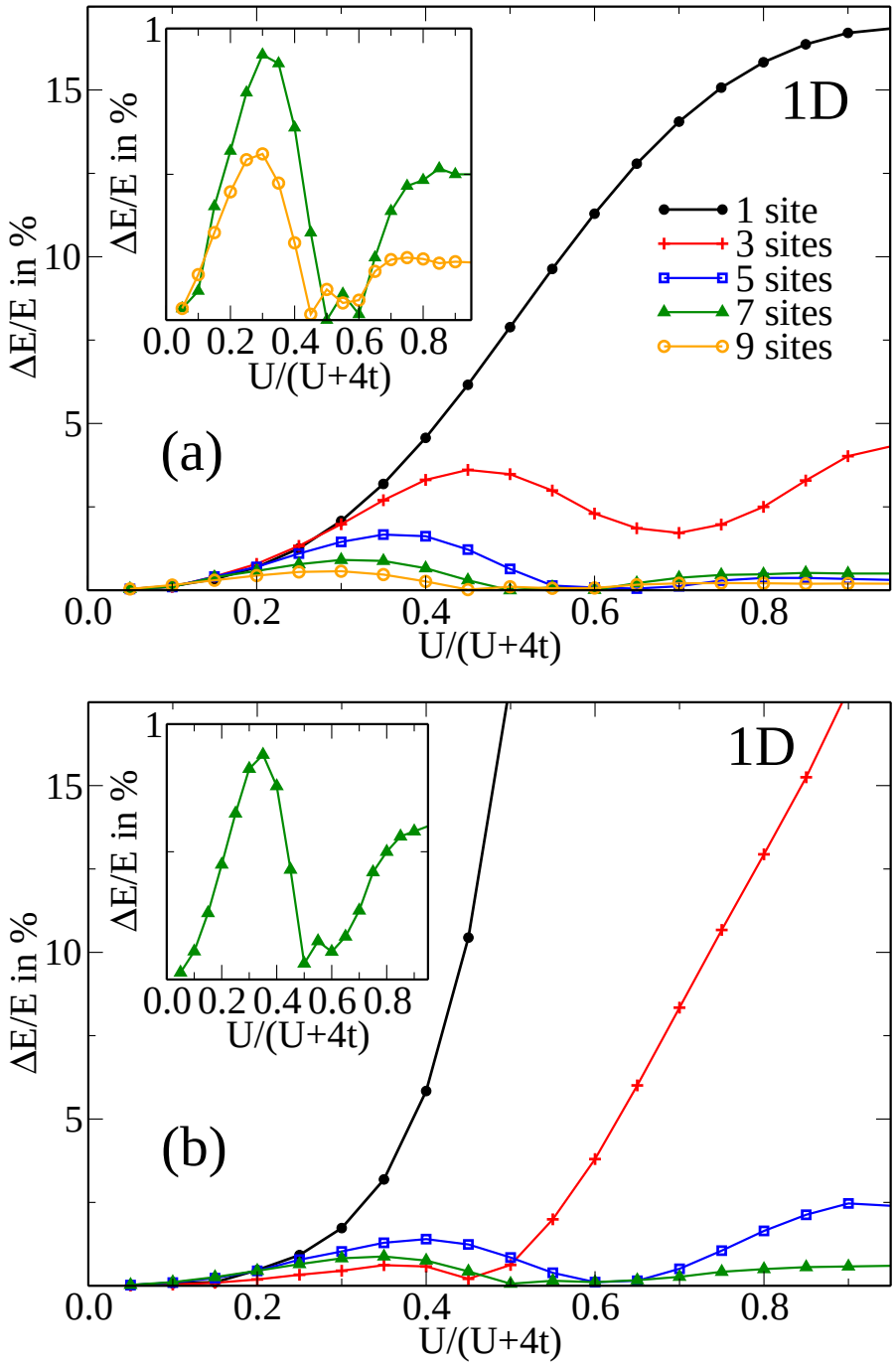

Figure 7.1: Relative error $\Delta E/E$ of the renormalized cluster expansion on the ground-state energy of a homogeneous infinite chain at half-band filling. The exact results are obtained from the Bethe *Ansatz* solution. $\Delta E/E$ is given as a function of the Coulomb repulsion strength and for different cluster sizes N_c. The environment is approximated following (a) the SE and (b) the SCE.

environment acts only at the boundary of the cluster so that its effect decreases as increases N_c. In addition, a larger cluster takes into account a larger range of the spatial charge fluctuations (up to the size of the cluster). This explains the important improvement of the accuracy at the strongly correlated limit, since at this limit only short range charge fluctuations are relevant. Notice that the $U = 0$ case is exact since the embedding was renormalized in order to recover this limit. However, the finite cluster-expansion yields very modest or no improvement for the limit where $U \to 0$ since here the delocalized nature of the single particle state cannot be recovered in a finite cluster.
The two approaches for the cluster embedding lead to very different behavior of the relative error. First of all for the one-site case, the SE is much better that the SCE, especially in the strong coupling regime. This is mainly due to the fact that the SCE embedding predicts a finite value U_c of the strength of the Coulomb repulsion corresponding to vanishing double occupation and consequently vanishing kinetic energy ($E_{\rm gs} = 0$ for $U \geq U_c$). By increasing N_c, the relative error is systematically reduced, and for $N_c = 7$ the results of the two embeddings are qualitatively equivalent. This can be explained by the fact that the embedding acts at the boundary of the cluster. Consequently, for a large enough cluster, the different embeddings have very similar effects at the center of the cluster where $\omega_i[\gamma]$ is obtained.

In Fig. 7.2 we show results for the Lagrange multiplier $\lambda = \lambda_{ij}$ in the middle of the cluster. These Lagrange multipliers ensure that to the ground state of the effective cluster Hamiltonian (7.28) corresponds a given density matrix γ. In other words, λ represents the renormalization of the hopping integral due to the embedding. At the limit of an infinite cluster ($N_c \to \infty$) the effect of the embedding at the boundary of the cluster does not affect anymore its center. Then, $\lambda = t = 1$ for all values of U/t since all short and long range charge and spin fluctuations would be included with the cluster. At half-band filling and in the atomic limit ($U \gg t$), when $\gamma_{ij} = 0$, all sites are uncoupled, then the cluster expansion is exact and one expects no hopping renormalization, i.e. $\lambda/t = 1$. In this sense, λ/t is a good measure of the effect introduced by the finite size of the cluster or equivalently by the effect of the environment. Therefore, we expect that λ/t increases when the cluster size increases and that it converges to 1 for $N_c \to \infty$. Indeed, for both approximations of the embedding, λ/t increases when N_c increases. The only exception is the SCE approximation for $N_c = 2$, which we will discuss later. Moreover, as the Coulomb repulsion strength U/t increases, it converges more rapidly to its atomic limit $\lambda/t = 1$ (see for example for $U/t = 12$, $\lambda/t \geq 0.99$ for $N_c \geq 7$ in both case) and in particular for $U/t \geq 4$. In fact, for large values of U/t, only short-range charge fluctuations are relevant and they are mainly captured within the cluster expansion. In the case of the SCE, $\lambda/t = 0$ for $N_c = 2$ and $U/t = 12$. This has to be related with the one-site and the SCE approximation which predicts a Mott transition for $U_c \simeq 10.2$ in one dimension. In this case the slave boson theory predicts $\gamma_{12} = 0$ and $\omega_i = 0$. Then, to obtain $\gamma_{12} = 0$, one requires that $\lambda/t = 0$. Furthermore, in one dimension and for any finite value of U/t, the system is an insulator, $\gamma_{ij} \neq 0$ in contrast to the slave boson theory. This explains why a value $\lambda/t \neq 1$ is obtained for $N_c = 3$ whereas LDFT predicts $\gamma_{12} = 0.205$.
The value of λ/t can be considered as a convergence criterion indicating for which cluster size the correlation-energy functional is converged, but it can also help in choosing the most accurate approximation for the embedding. For instance at weak coupling (see for example $U/t = 1$) and for small cluster size ($N_c < 5$) the SCE leads to higher values of λ/t and a better accuracy of the ground-state energy than the SE.

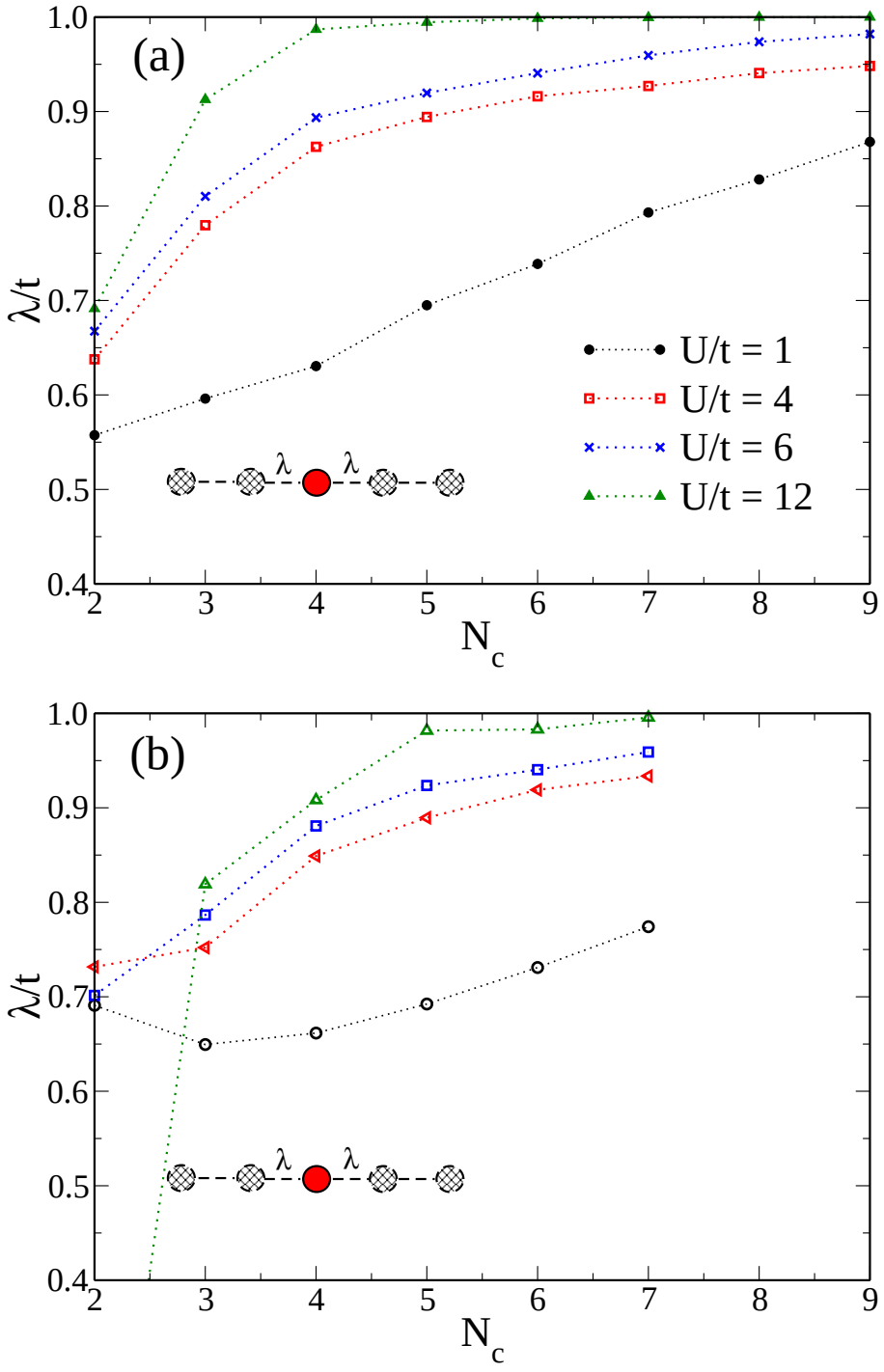

Figure 7.2: Cluster size dependence of the Lagrange parameter λ_{ij} constraining γ_{ij} at the center of the cluster and representing the renormalization of the hopping integral. Results are shown for a homogeneous infinite chain at half-band filling. Representative values of the Coulomb repulsion U/t are considered. The environment effects are approximated by (a) the SE and (b) the SCE. The lines connecting the points are a guide to the eyes.

Table 7.1: Ground state energy per site $E_{\rm gs}/N_a t$ of a two-dimensional infinite Hubbard system at half filling for different values of the Coulomb repulsion strength. Results of LDFT using the cluster expansion with $N_c = 1$ and $N_c = 9$ and the SE approximation are compared with predictions of other standard many-body methods as quantum Monte-Carlo (QMC), variational Monte-Carlo (VMC) and modified random phase approximation (MRPA).

U/t	2	3	4	6	8	10	12	16
QMC [25]	-1.17		-0.88		-0.48			
QMC [79]			-0.864					
VMC [84]		-0.987	-0.841	-0.629	-0.493	-0.401	-0.336	
MRPA [89]	-1.173		-0.850		-0.522		-0.361	-0.282
LDFT 9 sites	-1.176		-0.849	-0.646	-0.518		-0.368	-0.284
LDFT 1 site	-1.201	-1.032	-0.905	-0.709	-0.588	-0.499	-0.410	-0.916

In Table 7.1 we compare for the 2D homogeneous Hubbard model LDFT results with the correlation energy obtained from a cluster made up of one and nine sites and using the SE with available quantum Monte Carlo (QMC) [25, 79], variational Monte Carlo (VMC) [84] and modified random phase approximation (MRPA) [89]. LDFT with a one-site cluster results are qualitatively equivalent to the ones obtained with other methods, with a tendency to overestimate the ground-state energy. The cluster expansion corrects most of this overestimation showing the excellent accuracy of the method.

It was shown in this chapter, that the cluster expansion method predicts with high accuracy the ground-state properties of correlated systems, and in particular for large values of U/t. In addition, the accuracy increases systematically when the size of the considered cluster increases. However, at the weak coupling limit, the cluster expansion yields very modest or no improvement due to the delocalized nature of the ground-state at this limit, which cannot be captured on a finite-size cluster. The reason of this failure is due to the fact that we perform the cluster expansion in real space focusing only on short-range charge and spin fluctuations, which play a major role for large values of U/t. However, it should be possible to develop a similar cluster expansion in the reciprocal space, devoted to reproducing with very high accuracy the effects of the electronic interaction for small values of U/t. Nevertheless, in this case, the approximation will be less accurate at the strongly correlated limit.

The results presented for the simple Hubbard model in one and two dimensions are in fact very promising, since the method is general and can be applied to study much more complex systems. In this sense, it would be very interesting to apply it to systems with broken spin symmetry, to the periodic Anderson model, or to a multi-band Hamiltonian. In particular, the present cluster approach seems well adapted to studying $3d$ and $4f$ elements since the dominant correlations are intra-atomic and the d- and f-orbitals are localized so that U/t is large.

A limitation of this method concerns the charge gap ΔE_c. Indeed, using any of the proposed embedding approximations, the charge gap is not well reproduced for all values of U/t. First of all, in the case a the single-site cluster, using the SE the charge gap is zero for any value of U/t. Moreover, the SCE predicts, for any system at half filling, a Mott transition at a finite critical value of U/t. In fact, this transition is known to take place at half filling only for systems with NN hopping and for dimensions higher or equal to three. In addition, in this case, the SCE overestimates considerably the critical value of U/t for the onset of the Mott phase and predicts no kinetic energy ($\gamma_{12} = 0$) and no double occupancy which is far from true. By increasing the size of the cluster, the prediction of the charge gaps are improved only for large values of U/t. In both cases, the system is metallic up to an overestimated threshold value of U/t and then becomes an insulator. However, for $N_c \geq 5$, at large U/t, by using both SE and SCE approaches the value of the charge gap is very well reproduced and has its correct value for $U/t \to \infty$ where $\Delta E_c = U - 2w$ with w the band width of the system. The poor predictions at the weakly correlated limit result, once again, from the real space nature of the cluster expansion, which cannot take properly into account long-range charge fluctuations. As already mentioned, a similar cluster expansion in the reciprocal space could improve the quality of the predictions concerning the charge gap at the weakly-correlated limit.

Chapter 8

Summary and Outlook

LDFT is in principle applicable to any lattice Hamiltonian, since there exists a functional relation and an associated variational principle between the ground-state energy and the ground-state density matrix γ. Consequently, the ground-state energy of a many-body system can be obtained through minimization over all physical density matrices. However, this process requires the knowledge of an unknown quantity, the interaction-energy functional. The main challenge of the theory consists then, in deriving an accurate approximation for this unknown.

Previous formulations of the interaction-energy functional were limited to the homogeneous Hubbard model and were hardly transferable to other lattice Hamiltonians. These previous studies have shown the remarkable scaling properties of the correlation-energy functional (CEF) when it is expressed as a function of a universal degree of delocalization, that is scaled between the non-correlated and strongly correlated limits. Using these properties, an analytical approximation of the CEF was derived and applied to several homogeneous systems. The success of such a simple approach was the motivation of this thesis in order to further develop and extend the applicability of LDFT to more realistic problems including broken symmetry charge-density distributions, as often found in oxides, band-insulators, finite clusters or magnetic materials.

First, we have presented a systematic study of the functional dependence of W of the bipartite Hubbard model as a function the NN density-matrix element γ_{12} and charge transfer $\Delta n = \gamma_{22} - \gamma_{11}$. Rigorous numerical results have been obtained from exact Lanczos diagonalization on finite clusters with periodic boundary conditions. The functional dependence of W has been analyzed by varying the degree of charge transfer and electron delocalization between the sub-lattices, as well as the number of sites N_a and the band filling $n = N_e/N_a$. It has been shown that W can be appropriately scaled as a function of Δn and $g_{12} = (\gamma_{12} - \gamma_{12}^{\infty})/(\gamma_{12}^{0} - \gamma_{12}^{\infty})$, where γ_{12}^{0} (γ_{12}^{∞}) refers to the weak (strong) limit of electronic correlations. In other words, the change in W associated to a given change in the degree of NN charge transfer and electron delocalization can be regarded as almost independent of the system under study. This pseudouniversal behavior of the scaled interaction energy functional provides a unified description of correlations from weak to strong coupling regimes. Moreover, it encourages transferring the results from clusters to infinite systems with different lattice geometries.

Based on these investigations of the scalability and transferability of $W[\gamma]$, and on exact analytical results for the Hubbard dimer, we have proposed a simple approximation

to W, which takes advantage of its scaling behavior. In this way a unified description of the interplay between correlations and charge redistributions is achieved, from weak to strong coupling, and for all band fillings. Using this approximation, several important ground-state properties, as well as the charge excitation gap of 1D and 2D lattices, have been determined successfully as a function of the Coulomb repulsion strength and of the external bipartite potential.

The accuracy of the results confirms the pertinence of the scaling approximation and the transferability of the interaction-energy functional. Among the reasons for the success of the present scaled dimer approximation one should first of all mention the universality of the correlation-energy functional as stated by Hohenberg-Kohn's or Levy-Lieb's formulations. Moreover, the present approach has the asset of incorporating exact information on $W[\gamma]$ at the two most important limits of weak and strong correlations. These fundamental boundary conditions —somehow analogous to the sum rules of the local density approximation in the continuum— provide a useful guide for the development of the theory and are a further reason for the good performance of the method.

Motivated by the interest to apply the present scaling approximation to other types of interactions, we have considered the attractive Hubbard model, where the nature of the electronic correlations and the resulting properties of the functional $W[\gamma]$ are fundamentally different. The same holds for the conditions of v-representability of γ_{ij}, which depends on the explicit form of the Hamiltonian. However, the notion of N-representability, which involves the whole Hilbert space of the system, only depends on the number of sites and electrons. For $U < 0$, W corresponds to the maximum number of double occupations for a given γ_{ij}. As for the repulsive case, the scalability of the correlation functional has been shown. Then, based on the exact solution of the attractive Hubbard dimer, a scaling functional was derived and applied to clusters and infinite systems. It has been shown that LDFT within the scaling approximation reproduces also very accurately the properties of the attractive inhomogeneous Hubbard Hamiltonian when it is compared with the exact results (Bethe-Ansatz), and accurate numerical methods such as DMRG. It improves considerably standard approximations such as the BCS theory.

The locality of the dominant interactions and correlations is in fact a characteristic of strongly correlated phenomena, which could be exploited more systematically. In this work we have shown that is possible to obtain a local formulation of the scaling approximation of the correlation energy, namely, the local scaling approximation (LSA), which improves the flexibility of the explicit approximations to $W[\gamma]$. Moreover, the LSA can be applied to any on-site correlated Hamiltonian. In this thesis we have focused on the Hubbard model with translational invariance to compare and predict new results using the LSA. However, it would be interesting to study in the framework of LDFT within the LSA other systems as for example the Anderson impurity model, disordered systems, or one-dimensional case since LDFT reproduces accurately both the ground states properties and the phase diagram. However, in two dimensions, the ground-state properties are well reproduced, but the LSA does not predict the metallic phase occurring along the transition. The metal-insulator transition was also studied in the one-dimensional chain with nearest neighbor hopping. Once again, the ground-state results are satisfactory but the local scaling approximation fails to reproduce the Mott transition occurring at finite U/t. These facts highlight the importance of accurately treating the weakly correlated limit in the scaling functional. Some possibilities of improvements have been discussed. In particular, we should mention the importance of the properties of the inhomogeneous Hubbard dimer,

which is the basis of the scaling approximation. For instance, the quadratic dependence in $(U/t)^2$ of the charge gap of the dimer at the weakly-correlated limit is transferred to any system through the LSA. In other words, some discrepancies observed in ground-state properties obtained by using the LSA result from differences between the studied system and the dimer. In this sense, it would be most interesting to study the transferability of the CEF based on other systems. In particular, the case of the Hubbard model in infinite dimensions ($d \to \infty$) could be a good candidate, since accurates solution are known. Moreover the $d \to \infty$ Hubbard model presents many similarities with 2D and 3D systems. Maybe it would be possible to construct a hybrid approximation of the CEF based on an interpolation of the functionals derived from the Hubbard dimer and the limit of infinite dimensions.

In Chap. 7 we have developed a general method to approximate $W[\gamma]$ based on the idea of a renormalized cluster expansion. In this approach we have split the Hamiltonian into three parts, one acting on a finite cluster, one on the rest of the system (the environment) and the last one representing the interaction between the cluster and the environment. The latter and more subtle contribution has been mapped on to an effective Hamiltonian acting only within the cluster. In this way a decoupling of the cluster and the environment is achieved. This Hamiltonian is constrained, by using Lagrange parameters, in order that its ground-state is associated to a given density matrix γ. The correlation-energy functional is then obtained by diagonalizing the effective Hamiltonian. The results presented for the simple homogeneous Hubbard model with NN hoppings are most promising, since it has been shown that the accuracy of the ground state energy is systematically increased by increasing the size of the cluster, in particular at the strongly correlated limit. For example, we have shown that in one dimension, within a cluster having $N_c = 7$ sites, the relative error on the ground state energy is at most one percent. However, in the weakly correlated limit the cluster expansion does not particularly increase the accuracy, since the ground-state is very delocalized at this limit and the long-range charge fluctuations cannot be captured by a finite cluster. This fact explains also that the charge gap at the weakly correlated limit is not well reproduced in contrast to the strongly correlated limit, where the charge gap is already recovered with good accuracy for a cluster larger or equal to $N_c = 5$ sites. It has been pointed out that a possible remedy to the problem at the weakly correlated limit, one could derive a similar cluster expansion in reciprocal space. In this way one expects that long-range charge fluctuations should be described more accurately at the expense of the short-range ones. This could result in a very good description of the weakly correlated limit, but probably in a less accurate one for large values of U/t. It is important to note that the method is very general, in particular, the formalism is spin dependent, so that a direct application to systems with broken spin symmetry can be performed. In addition, we mention that the extension to inter-site correlations is rather straightforward. This constitutes a promising basis for future developments, since it allows investigation of more realistic systems like multi-band Hamiltonians, describing the physics of complex systems, for example materials including d- of f-valence orbitals.

In order to summarize, in this work we have considerably extended the scope of LDFT to nearly any lattice Hamiltonian. A variety of novel applications of the theory in condensed matter and material sciences are thereby opened. Extensions to finite temperatures and time-dependent Hamiltonians constitute two remarkable challenges for the future

Bibliography

[1] P. Hohenberg and W. Kohn, Phys. Rev. **136**, B864 (1964).

[2] W. Kohn and L.J. Sham, Phys. Rev. **140**, A1133 (1965).

[3] R.G. Parr and W. Yang, *Density-Functional Theory of Atoms and Molecules* (Clarendon, Oxford, 1989);

[4] R.M. Dreizler and E.K.U. Gross, *Density Functional Theory* (Springer, Berlin, 1990) and references therein.

[5] K. Capelle, *A bird's-Eye View of Density-Functional Theory*, arXiv:cond-mat/0211443v5

[6] D.C. Langreth and M.J. Mehl, Phys. Rev. B **28**, 1809 (1983); A.D. Becke, Phys. Rev. A **38**, 3098 (1988); J.P. Perdew, K. Burke and M. Ernzerhof, Phys. Rev. Lett. **77**, 3865 (1996) and references therein.

[7] R. O. Jones, O. Gunnarson, Rev. Mod. Phys. **61**, 689 (1989)

[8] C. S. Wang and B. M. Klein, Phys. Rev. B **24**, 3393 (1981)

[9] L. J. Sham and M. Schlüter, Phys. Rev. Lett. **51**, 1888 (1983)

[10] J. P. Perdew and M. Levy, Phys. Rev. Lett. **51**, 1884 (1983)

[11] K. Terakura, T. Oguchi, A. R. Williams and J. Kuebler , Phys. Rev. B **37**, 2239 (1984)

[12] G. A. Sawatzky and J. W. Allen, Phys. Rev. Lett. **53**, 2239 (1984)

[13] A. Zunger, J. P. Perdew and G. L. Oliver, Solid Sate Commun. **34**, 1033 (1977)

[14] See, for instance, P. Fulde, *Electron Correlations in Molecules and Solids* (Springer, Berlin, 1991); N.H. March, *Electron Correlation in Molecules and Condensed Phases* (Plenum, New York, 1996); G.D. Mahan, *Many-Particle Physics* (Kluver, New York, 2000).

[15] E. Dagotto, Rev. Mod. Phys. **66**, 763 (1994); A. Georges, G. Kotliar, W. Krauth, and M.J. Rozenberg, *ibid.* **68**, 13 (1996); M. Imada, A. Fujimori, and Y. Tokura, *ibid.* **70**, 1039 (1998).

[16] J. Hubbard, Proc. R. Soc. London **A276**, 238 (1963); **A281**, 401 (1964); J. Kanamori, Prog. Theo. Phys. **30**, 275 (1963); M.C. Gutzwiller, Phys. Rev. Lett. **10**, 159 (1963).

[17] P. W. Anderson, Phys. Rev. **124**, 41 (1961).

[18] E.H. Lieb and F.Y. Wu, Phys. Rev. Lett. **20**, 1445 (1968);

[19] Y. Nagaoka, Solid State Commun. **3**, 409 (1965).

[20] E.H. Lieb, Phys. Rev. Lett. **62**, 1201 (1989);

[21] M. Potthoff, M. Aichhorn, and C. Dahnken, Phys. Rev. Lett. **91**, 206402, (2003); M. Balzer, W. Hanke, and M. Potthoff, Phys. Rev. B **77**, 045133 (2008); M. Potthoff, Adv. Solid State Phys. **45**, 135 (2005)

[22] G. Kotliar and A. E. Ruckenstein, Phys. Rev. Lett. **57**, 1362 (1986)

[23] A. Georges, G. Kotliar, W. Krauth, and M. L. Rev. Mod. Phys. **68**, 13, (1996)

[24] S. R. White, Phys. Rev. Lett. **69**, 2863 (1992); Phys. Rev. B **84**, 10345 (1993).

[25] J. E. Hirsch, Phys. Rev. B **31**, 4403 (1985)

[26] V. I. Anisimov, J. Zaanen, and O. K. Andersen, Phys. Rev. B **44**, 943 (1991).

[27] V. I. Anisimov, A. I. Poteryaev, M. A. Korotin, A. O. Anokhin, and G. Kotliar, J. Phys.: Condens. Matter **9**, 7359 (1997); A. I. Lichtenstein and M. I. Katsnelson, Phys. Rev. B **57**, 6884 (1998); G. Kotliar, S. Y. Savrasov, K. Haule, V. S. Oudovenko, O. Parcollet, and C. A. Marianetti, Rev. Mod. Phys. **78**, 865 (2006).

[28] O. Gunnarsson and K. Schönhammer, Phys. Rev. Lett. **56**, 1968 (1986); A. Svane and O. Gunnarsson, Phys. Rev. B **37**, 9919 (1988); K. Schönhammer, O. Gunnarsson and R.M. Noack, *ibid.* **52**, 2504 (1995).

[29] A. Schindlmayr and R.W. Godby, Phys. Rev. B **51**, 10427 (1995).

[30] A.E. Carlsson, Phys. Rev. B **56**, 12058 (1997); R.G. Hennig and A.E. Carlsson, *ibid* **63**, 115116 (2001).

[31] N.A. Lima, M.F. Silva, L. N. Oliveira and K. Capelle, Phys. Rev. Lett. **90**, 146402 (2003).

[32] C. Verdozzi, Phys. Rev. Lett. **101**, 166401 (2008).

[33] R. López-Sandoval, *Théorie de la fonctionalle de la matrice densité pour des Hamiltoniens modèles*, Thèse de l'université Paul Sabatier Toulouse III (2000)

[34] R. López-Sandoval and G.M. Pastor, Phys. Rev. B **61**, 1764 (2000).

[35] R. López-Sandoval and G.M. Pastor, Phys. Rev. B **66**, 155118 (2002).

[36] R. López-Sandoval and G.M. Pastor, Phys. Rev. B **67**, 035115 (2003).

[37] R. López-Sandoval and G.M. Pastor, Phys. Rev. B **69**, 085101 (2004).

[38] W. Töws, *Entwicklung und Anwendung der Dichtematrix-Funktional-Theory für das Anderson-Modell*, Diplomarbeit, Universität Kassel, Germany (2009).

[39] G. M. Pastor, R. Hirsch and B. Mühlschlegel, Phys. Rev. Lett. **72**, 3879, (1994); G. M. Pastor, R. Hirsch and B. Mühlschlegel, Phys. Rev. B **53**, 10382 (1996)

[40] K. Bouadim, N. Paris, F. Hébert, G. G. Batrouni, and R. T. Scalettar, Phys. Rev. B **76**, 085112 (2007)

[41] E. Sigmund and K. A. Müller, *Phase separation in Cuprate Superconductors*, (Spinger, Heidelberg, 1994)

[42] C. Lanczos, J. Res. Nat. Bur. Stand. **45**, 255 (1950); B. N. Parlett, *The symmetric eigenvalue problem* (Prentice Hall, Engelwood Cliffs, 1980).

[43] L. H. Thomas, Proc. Camb. Phys. Soc. **23**, 542 (1927).

[44] E. Fermi, Rend. Accad. Lince, **6**, 602 (1927).

[45] M. Levy, Proc. Natl. Acad. Sci. U.S.A. **76**, 6062 (1979).

[46] E. H. Lieb, Int. J. Quantum Chem. **24**, 243, (1983)

[47] H. English and R. English, Physica, **121A**, 253 (1983)

[48] L. Hedin and B. I. Lundqvit, J. Phys. C:Solid Sate Phys., **4**, 2064 (1971)

[49] M. P. Tosi, R. H. Land, K. S. Singwi and A. Sjölander, Phys. Rev. B **1**, 1044 (1970)

[50] U. von Bart and L. Hedin, J. Phys., **5**, 1629, (1972)

[51] A. Svane and O. Gunnarsson, Phys. Rev. B **37**, 9919 (1988)

[52] A. Svane and O. Gunnarsson, Europhys. Lett. **7**, 171 (1988)

[53] J. Zaanen, O. K. Andersen and V. I. Anisimov, Phys. Rev. B **44**, 943 (1991)

[54] M. T. Czyżyk and G. A. Sawatzky, Phys. Rev. B **49**,14221 (1991)

[55] M. C. Gutzwiller, Phys. Rev. Lett. **10**, 159 (1963)

[56] J. Kanamori, Prog. Theor. Phys. **30**, 275 (1963)

[57] H. Tasaki, Phys. Rev. B **40**, 9192 (1989).

[58] H. Bethe. Z. Physik, **71**, 205 (1931).

[59] see for instance M. Gaudin *Modèles exactement résolus*, Les Editions de Physique (1995); F. H. L. Essler, H. Frahm, F. Göhmann, A. Klümper and V. E. Korepin, *The One-Dimensional Hubbard Model* , Cambridge University Press (2005)

[60] H. Shiba, Phys. Rev. B **6**, 930 (1972).

[61] M. Saubanère and G. M. Pastor, unpublished

[62] J. R. Schrieffer and P. A. Wolf, Phys. Rev. **149**, 491, (1966)

[63] C. Gros, R. Joynt and T. M. Rice, Phys. Rev. B **36**, 381, (1987); A. Teubel, E. Kolley and W. Kolley, J. Phys. A **23**, 837, (1990)

[64] R. T. Scalettar, E. Y. Loh, J. E. Gubernatis, A. Moreo, S. R. White, D. J. Scalapino, R. L. Sugar and E. Dagotto, Phys. Rev. Lett. **62**, 1407 (1989)

[65] F. Marsiglio, Phys. Rev. B **55**, 575, (1997)

[66] R. D. Parks, *Superconductivity*, Marcel Dekker, INC., (1969)

[67] J. Bardeen, L. N. Cooper, and J. R. Schrieffer Phys. Rev. **106**, 162 (1957); J. Bardeen, L. N. Cooper, and J. R. Schrieffer Phys. Rev. **108**, 1175 (1957)

[68] K. Tanakana and F. Marsiglio, Phys. Rev. B **60**, 3508, (1999)

[69] See, for exemple, J. R. Schrieffer *Theory of Superconductivity*, Benjamin, (1964); P. G. de Gennes *Superconductivity of Metals and Alloys*, Benjamin, (1966); M. Tinkham *Introduction to superconductivity* McGraw-Hill, Inc, (1975); P.A.Martin, F.Rohen *Problème à N-corps et champs quantiques* Presse ploytechniques et universitaires romandes, (1990)

[70] N. Salwen, S. A. Sheets, and S. R. Cotanch Phys. Rev. B **70**, 064511, (2004)

[71] T.L. Gilbert, Phys. Rev. B **12**, 2111 (1975). For more recent studies see, for example, S. Goedecker and C.J. Umrigar, Phys. Rev. Lett. **81**, 866 (1998) and references therein.

[72] S.M. Valone, J. Chem. Phys. **73**, 1344 (1980); **73**, 4653 (1980).

[73] R. López-Sandoval and G.M. Pastor, unpublished.

[74] M. Saubanère and G. M. Pastor, Phys. Rev. B **79**, 235101 (2009).

[75] E. H. Lieb, Phys. Rev. Lett. **62**, 1201 (1989).

[76] J. E. Hirsch and D. J. Scalapino, Phys. Rev. Lett. **56**, 2732 (1986)

[77] J.-H. Hu, J.-J. Wang, G. Xianlong, M. Okumura, R. Igarashi, S. Yamada, and M. Machida, Phys. Rev. B **82**, 014202, (2010)

[78] V. B. Shenoy, Phys. Rev. B **78**, 134503, (2008)

[79] S. R. White, D. J. Scalapino, R. L. Sugar, E. Y. Loh, J. E. Gubernatis and R. T. Scalettar, Phys. Rev. B **40**, 506 (1989).

[80] A. Garg, H. R. Krishnamurthy, and M. Renderia, Phys. Rev. Lett. **97**, 046403 (2006)

[81] M. E. Torio, A. A. Aligia, G. I. Japaridze, and B. Normand, Phys. Rev. B **73**, 115109 (2006)

[82] S. R. Manmana, V. Meden, R. M. Noak, and K. Schönhammer, Phys. Rev. B **70**, 155115 (2004)

[83] G. I. Japaridze, R. Hayn, P. Lombardo, and E. Müller-Hartmann, Phys. Rev. B **75**, 245122 (2007)

[84] H. Yokohama and H. Shiba, J. Phys. Soc. Jpn., B **56**, 3582 (1987)

[85] D. Jérome, A. Mazaud, M. Ribault, and K. Bechgaard, J. Phys. Lett. **41**, L95 (1980); K. Bechgaard, K. Carneiro, M. Olsen, F. B. Rasmussen and C. S. Jacobsen, Phys. Rev. Lett. **46**, 852 (1981)

[86] M. Matsukawa, Y. Yamada, M. Chiba, H. Ogasawara, T. Shibata, A. Matsushita, and Y. Takano, Physica C **411**, 101 (2004)

[87] S. Daul, R. M. Noak, Phys. Rev. B **61**, 245122, (2000); G. I. Japaridze, R. M. Noak, D. Baeriswyl, and L. Tincani, Rev. B **76**, 115118, (2007)

[88] S. Nishimoto, K. Sano, and Y. Otha Rev. B **77**, 085119, (2008);

[89] K. S. Singwi, M. P. Tosi, R. H. Land, and A. Sjölander, Phys. Rev. **176**, 589 (1968)

Veröffentlichungen - List of publications

- *Scaling and transferability of the interaction-energy functional of the inhomogeneous Hubbard model*, Matthieu Saubanère and G. M. Pastor, Phys. Rev. B **79**, 235101 (2009)

- *Electronic and magnetic properties of Co and Ni impurities in Cu wires: First-principles investigation of local moment formation in one dimension*, Matthieu Saubanère, J. L. Ricardo-Chávez, and G. M. Pastor, Phys. Rev. B **82**, 054436 (2010)

- *First principles theoretical study of complex magnetic order in transition-metal nanowires*, M. Saubanère, M. Tanveer, P. Ruiz-Díaz, and G. M. Pastor, Phys. Status Solidi B, **247**, 2610-2620 (2010)

- *Density-matrix functional study of the Hubbard model on one- and two-dimensional bipartite lattices*, Matthieu Saubanère and G. M. Pastor, accepted Phys. Rev. B (2011)

Erklärung

Hiermit versichere ich, daß ich die vorliegende Dissertation selbständig und ohne unerlaubte Hilfe angefertigt und andere als die in der Dissertation angegebenen Hilsmittel nicht benutzt habe. Alle Stellen, die wörtlich oder sinngemäß aus veröffentlixhten oder unveröffentlichten Schriften entnommen sind, habe ich als solche kenntlich gemacht. Zusätzlich versichere ich, daß Kein Teil dieser Arbeit in einem anderen Promotions- oder Habilitationsverfahren verwendet worden ist.

Juli 2011, Kassel

Matthieu Saubanère